Durability of Segmental Retaining Wall Blocks: Final Report

PUBLICATION NO. FHWA-HRT-07-021

APRIL 2007

U.S. Department of Transportation
Federal Highway Administration

Research, Development, and Technology
Turner-Fairbank Highway Research Center
6300 Georgetown Pike
McLean, VA 22101-2296

Foreword

Segmental retaining wall (SRW) systems are used commonly and successfully in a range of applications, including highway projects. Their popularity can be attributed to a combination of reduced construction costs, versatility, aesthetic appearance, and ease of installation. Despite these inherent advantages, there have been some reported problems with durability of SRW blocks in cold climates susceptible to freeze-thaw cycles. The premature deterioration of some SRW blocks has led to stricter performance specifications, and in some cases, the restricted use of these walls by some State Highway Agencies.

In response to these concerns, the Federal Highway Administration (FHWA) initiated the Transportation Pool Funded research project, TPF-5(026), "Durability of Segmental Retaining Wall Blocks." The primary objectives of this project were to determine the cause and extent of SRW block distress and to provide recommendations on the pertinent test methods and specifications to ensure the long-term durability of SRW blocks in highway applications. The report also provides some guidance on producing durable SRW blocks.

Through this research project, it has been confirmed that the vast majority of SRW blocks have performed well and continue to perform well, even in cold climates and when exposed to deicing salts. However, this project also identified cases where SRW blocks showed significant deterioration in both field applications and laboratory evaluations. The factors that most affect frost resistance were identified, and modifications to the standard test methods ASTM C 1262 and specification ASTM C 1372 have been developed for proposed revisions.

Gary L. Henderson
Director, Office of Infrastructure
Research and Development

Notice

Quality Assurance Statement

The Federal Highway Administration (FHWA) provides high-quality information to serve Government, industry, and the public in a manner that promotes public understanding. Standards and policies are used to ensure and maximize the quality, objectivity, utility, and integrity of its information. FHWA periodically reviews quality issues and adjusts its programs and processes to ensure continuous quality improvement.

Technical Report Documentation Page

1. Report No.	2. Government Accession No.	3. Recipient's Catalog No.
FHWA HRT-07-021		

4. Title and Subtitle	5. Report Date
Durability of Segmental Retaining Wall Blocks: Final Report	April 2007
	6. Performing Organization Code

7. Author(s)	8. Performing Organization Report No.
Cesar Chan, Kenneth C. Hover, Kevin J. Folliard, Randall M. Hance, and David Trejo	

9. Performing Organization Name and Address	10. Work Unit No.
Concrete Durability Center The University of Texas at Austin 10100 Burnet Road, Bldg. 18B, Austin, TX 78712	11. Contract or Grant No. DTFH61-01-02-R-00078

12. Sponsoring Agency Name and Address	13. Type of Report and Period Covered
Office of Infrastructure Research and Development Federal Highway Administration 6300 Georgetown Pike McLean, VA 22101-2296	Final Report
	14. Sponsoring Agency Code

15. Supplementary Notes

Contracting Officer's Technical Representative (COTR): Michael Adams, HRDI-06

16. Abstract

Segmental retaining wall (SRW) systems are commonly and successfully used in a range of applications, including highway projects. Their popularity can be attributed to a combination of reduced construction costs, versatility, aesthetic appearance, ease of installation, and an increasing number of proprietary designs available in the market. Despite these inherent advantages, there have been some reported problems with durability of SRW blocks in cold climates. The deterioration of some SRW installations in State highway agency (SHA) applications has resulted in concern over the long-term performance of SRW systems and has led to stricter specifications and, in some cases, restrictions on future use of SRW systems.

In response to these concerns, a Federal Highway Administration (FHWA)-funded research project was initiated to determine the cause and extent of SRW block distress, to identify and recommend test methods for improving durability of SRW systems, and to recommend specifications for SHAs to ensure long-term durability and performance of SRW systems in highway applications. This report summarizes the key findings of this project and provides guidance on producing durable SRW blocks to ensure long-term performance of SRW systems in highway applications.

17. Key Words	18. Distribution Statement
Segmental retaining wall; SRW; freeze-thaw; salt distress; SRW blocks; frost resistance	No restrictions. This document is available to the public through the National Technical Information Service, Springfield, VA 22161

19. Security Classif. (of this report)	20. Security Classif. (of this page)	21. No. of Pages	22. Price
Unclassified	Unclassified	271	

SI* (MODERN METRIC) CONVERSION FACTORS

APPROXIMATE CONVERSIONS TO SI UNITS

Symbol	When You Know	Multiply By	To Find	Symbol
		LENGTH		
in	inches	25.4	millimeters	mm
ft	feet	0.305	meters	m
yd	yards	0.914	meters	m
mi	miles	1.61	kilometers	km
		AREA		
in^2	square inches	645.2	square millimeters	mm^2
ft^2	square feet	0.093	square meters	m^2
yd^2	square yard	0.836	square meters	m^2
ac	acres	0.405	hectares	ha
mi^2	square miles	2.59	square kilometers	km^2
		VOLUME		
fl oz	fluid ounces	29.57	milliliters	mL
gal	gallons	3.785	liters	L
ft^3	cubic feet	0.028	cubic meters	m^3
yd^3	cubic yards	0.765	cubic meters	m^3
		NOTE: volumes greater than 1000 L shall be shown in m^3		
		MASS		
oz	ounces	28.35	grams	g
lb	pounds	0.454	kilograms	kg
T	short tons (2000 lb)	0.907	megagrams (or "metric ton")	Mg (or "t")
		TEMPERATURE (exact degrees)		
^oF	Fahrenheit	5 (F-32)/9 or (F-32)/1.8	Celsius	^oC
		ILLUMINATION		
fc	foot-candles	10.76	lux	lx
fl	foot-Lamberts	3.426	$candela/m^2$	cd/m^2
		FORCE and PRESSURE or STRESS		
lbf	poundforce	4.45	newtons	N
lbf/in^2	poundforce per square inch	6.89	kilopascals	kPa

APPROXIMATE CONVERSIONS FROM SI UNITS

Symbol	When You Know	Multiply By	To Find	Symbol
		LENGTH		
mm	millimeters	0.039	inches	in
m	meters	3.28	feet	ft
m	meters	1.09	yards	yd
km	kilometers	0.621	miles	mi
		AREA		
mm^2	square millimeters	0.0016	square inches	in^2
m^2	square meters	10.764	square feet	ft^2
m^2	square meters	1.195	square yards	yd^2
ha	hectares	2.47	acres	ac
km^2	square kilometers	0.386	square miles	mi^2
		VOLUME		
mL	milliliters	0.034	fluid ounces	fl oz
L	liters	0.264	gallons	gal
m^3	cubic meters	35.314	cubic feet	ft^3
m^3	cubic meters	1.307	cubic yards	yd^3
		MASS		
g	grams	0.035	ounces	oz
kg	kilograms	2.202	pounds	lb
Mg (or "t")	megagrams (or "metric ton")	1.103	short tons (2000 lb)	T
		TEMPERATURE (exact degrees)		
^oC	Celsius	1.8C+32	Fahrenheit	^oF
		ILLUMINATION		
lx	lux	0.0929	foot-candles	fc
cd/m^2	$candela/m^2$	0.2919	foot-Lamberts	fl
		FORCE and PRESSURE or STRESS		
N	newtons	0.225	poundforce	lbf
kPa	kilopascals	0.145	poundforce per square inch	lbf/in^2

*SI is the symbol for the International System of Units. Appropriate rounding should be made to comply with Section 4 of ASTM E380.
(Revised March 2003)

TABLE OF CONTENTS

CHAPTER 1: INTRODUCTION AND SCOPE 1

1.1 OVERVIEW 1

1.2 SRW SYSTEMS 1

1.3 RESEARCH BACKGROUND AND SCOPE 5

1.4 ORGANIZATION OF REPORT 8

CHAPTER 2: LITERATURE REVIEW 11

2.1 INTRODUCTION 11

2.2 FROST DAMAGE IN CONCRETE 11

2.2.1 Mechanisms of Frost Damage in Concrete 11

2.2.2 The Role of Deicing Salts in Frost Damage 16

2.3 FREEZE-THAW DURABILITY OF DRY-MIXED CONCRETE PRODUCTS 18

2.3.1 Introduction 18

2.3.2 Mechanisms of Freeze-Thaw Damage in Dry-Mixed Concretes 19

2.3.3 The Role of Salts in Frost Damage in Dry-Mixed Concretes 20

2.3.4 Role of Air and Compaction Voids 21

2.3.4.1 Air Void Characteristics in Low-Slump Concretes (Whiting, 1985) 21
2.3.4.2 Frost and Salt Scaling Resistance of RCC (Marchand et al., 1990) 22
2.3.4.3 Air Entrainment in No-Slump Mixes (Marchand et al., 1998) 22
2.3.4.4 Air Entrainment in Dry Masonry Concrete (Hazrati and Kerkar, 2000) 23
2.3.4.5 Other Studies (Pigeon and Pleau, 1995 and SEM, 2001) 24
2.3.4.6 Summary of Studies on Air Entrainment and Compaction Voids 24

2.4 SUMMARY 25

CHAPTER 3: FIELD EVALUATION OF SRW BLOCKS 27

3.1 INTRODUCTION 27

3.2 FIELD EVALUATIONS OF SRWS IN WISCONSIN AND MINNESOTA 27

3.2.1 Types of Distress Observed in SRW blocks 27

3.2.2 Laboratory Evaluation of SRW Blocks Procured From Inservice Walls 35

3.2.2.1 Test Methods for SRW Blocks Procured From Inservice Walls 37
3.2.2.2 Test Results for SRW Blocks Procured From Inservice Walls 38

3.3 SUMMARY 40

CHAPTER 4: LABORATORY EVALUATIONS 41

4.1 OVERVIEW 41

4.2 SAMPLING CONSIDERATIONS FOR SRW BLOCKS 42

4.2.1 Current Sampling Guidelines 45

4.2.2 Spatial Variability of Material Properties 46

4.2.2.1 Within-Manufacturer Variability 46
4.2.2.2 Between-Manufacturer Variability 49
4.2.3 Split Face Delamination 56
4.2.4 Recommendations for Sampling 60
4.2.4.1 Sampling of SRW Units 61
4.2.4.2 Extracting Specimens From SRW Units 62
4.2.4.3 General Laboratory Practice 67
4.2.4.4 Other Research 70
4.3 VARIABILITY IN FREEZE-THAW EQUIPMENT USED IN ASTM C 1262 (2003) 70
4.3.1 Comparison Between Different Freezers 72
4.3.1.1 Chest Freezer 76
4.3.1.2 Walk-in Environmental Chamber 79
4.3.1.3 Cabinet Freezer 84
4.3.1.4 Recommendations To Reduce Freezer Internal Variability 91
4.4 CHARACTERISTICS OF THE FREEZE-THAW CYCLE 93
4.4.1 Significance of Freeze-Thaw Cycle 95
4.4.2 The Cooling Curve 101
4.4.2.1 Ice Formation and Rates 101
4.4.2.2 Changes in Concentration for Saline Solution 105
4.4.2.3 Damage Point 107
4.4.2.4 Connection to Freeze-Thaw Test Specimens 113
4.4.2.5 Rates of Temperature Change 126
4.4.3 Other Aspects Relevant to the ASTM C 1262 (2003) Test Method 128
4.4.3.1 Concept of Frozen Solid 128
4.4.3.2 Temperature Tolerance 129
4.4.3.3 Cooling Rates and Target Cold Soak Temperatures 129
4.4.3.4 Degree of Saturation 135
4.4.3.5 Warming Rate 136
4.4.4 Summary—Implications for ASTM C 1262 (2003) 136
4.5 SYNOPSIS OF NCMA STUDY 138
4.5.1 Variability Test Series 138
4.5.2 Performance Criteria (PC) Test Series 139
4.5.3 Significance of NCMA Project Findings 139
4.6 FROST DURABILITY INDICES FOR SRW UNITS 139
4.6.1 Background 140
4.6.2 Databases of SRW Block Freeze-Thaw Performance and Material Properties 141
4.6.3 Synthesis of Data 143
4.6.4 Discussion of ASTM C 1262 (2003) (in Water) Results 145
4.6.5 Discussion of ASTM C 1262 (2003) (in 3 percent NaCl solution) Results 163
4.6.6 Summary 164

4.7 SYNOPSIS OF STUDY ON EFFECTS OF ALTERNATIVE DEICING SALTS ON SRW BLOCK DURABILITY 164

4.8 RESEARCH ON DEVELOPMENT OF MORE REALISTIC FREEZE-THAW TEST FOR SRW BLOCKS 166

4.8.1 Phase I Investigation 167

4.8.2 Phase II Investigation 174

4.8.3 Summary 184

4.9 OTHER RESEARCH 185

4.10 SUMMARY 185

CHAPTER 5: CONCLUSIONS AND RECOMMENDATIONS FOR FUTURE WORK 187

5.1 INTRODUCTION 187

5.2 CONCLUSIONS—FIELD PERFORMANCE AND DURABILITY OF SRW BLOCKS 187

5.3 CONCLUSIONS—SRW MATERIAL CHARACTERIZATION AND SAMPLING 187

5.4 CONCLUSIONS—FROST DURABILITY OF SRW UNITS 189

5.5 CONCLUSIONS—GENERAL FREEZE-THAW TESTING AND PROCESSES 195

5.6 CONCLUSIONS—ASTM C 1262 (2003) TESTING AND SPECIMEN PERFORMANCE 197

5.7 RECOMMENDATIONS—ASTM C 1262 (2003) TESTING FOR SRW UNITS 202

5.8 RECOMMENDATIONS—FUTURE RESEARCH 202

5.8.1 SRW Material Characterization—Between-Unit Variability 202

5.8.2 Frost Durability of SRW Units—Frost Index 202

5.8.3 Dilation Tests for SRW Specimens 203

5.8.4 Acoustic Emission Testing 203

5.8.5 Effect of Freeze-Thaw Cycle on Specimen Performance 203

5.8.6 Effect of Specimen Preconditioning 204

5.8.6.1 Effect of Pretest Exposure 204

5.8.6.2 Effect of Saturating Specimens Prior to Freeze-Thaw Testing 204

5.8.7 Significance of Mass Loss and 1 Percent Limit on Different Grades of SRW Mixes 204

5.8.8 Partial Versus Full Immersion of Specimens 205

5.8.9 Database of Mass Loss Prediction Constants 205

5.8.10 Efficacy of Silane or Other Coatings/Sealants in Mitigating Damage for Inservice SRW Blocks. 205

5.8.11 Freeze-Thaw Performance—Field and Laboratory Correlation Based on Critical Moisture. 205

APPENDIX A: NEWLY PROPOSED VERSIONS OFASTM C 1262 (2003)—FREEZE-THAW TEST FOR SRW BLOCKS) 207

ANNEX: RECOMMENDED PROCEDURE FOR SURVEY OF INTERNAL TEMPERATURE DISTRIBUTION OF FREEZE-THAW CHAMBER 228

APPENDIX B: NEWLY PROPOSED VERSION OF ASTM C 1372 (2003)— SPECIFICATIONS FOR SRW BLOCKS..... 241

REFERENCES..... 249

LIST OF FIGURES

Figure 1. Drawing. Conventional forms of SRW construction (NCMA, 2005a). 2
Figure 2. Drawing. Soil reinforced forms of SRW construction (NCMA, 2005a). 2
Figure 3. Drawings. Sample sizes and shapes of SRW units for SRW systems (Bathurst, 1993). 2
Figure 4. Photos. Example applications of SRW systems. 3
Figure 5. Photo. View of mix during production of SRW units at block plant. 4
Figure 6. Photo. SRW unit immediately after compaction and demolding. 4
Figure 7. Photos. Comparison of internal structures between SRW and ordinary concretes. 4
Figure 8. Photo. Condition of SRW in Ithaca, NY. 5
Figure 9. Map. State highway agency requirements for freeze-thaw durability of SRW blocks (Thomas et al., 2003). 8
Figure 10. Diagram. Powers' rendition of an air bubble and its "sphere of influence" (Powers, 1949). 12
Figure 11. Photo. Demolding of SRW units during production. 18
Figure 12. Photo. Typical deterioration of SRW blocks with scaling most pronounced for cap units. 28
Figure 13. Photo. Severely damaged cap units on otherwise healthy wall. 28
Figure 14. Photo. Effects of drainage and salt exposure from parking lot above SRW. 30
Figure 15. Photo. Deteriorated SRW blocks closest to roadway (bottom of photo) and undamaged SRW blocks farthest from roadway. 30
Figure 16. Photo. Severe damage of SRW blocks in direct path of drainage from bridge overpass above. 30
Figure 17. Photo. Deterioration of SRW blocks due to exposure to fertilizers from adjacent golf course. 32
Figure 18. Photo. Cap block experiencing scaling of front face and macrocracking towards the back of the blocks. 33
Figure 19. Photo. Deterioration of exposed vertical surfaces of SRW blocks. 34
Figure 20. Photo. Another example of deterioration of exposed horizontal surfaces of SRW blocks. 35
Figure 21. Photo. Blocks obtained from SRW in Wisconsin (WI-2). 36

Figure 22. Photo. Blocks obtained from SRW in Wisconsin (WI-4). 37
Figure 23. Photo. Blocks obtained from SRW in Minnesota (MN-4). 37
Figure 24. Graph. ASTM C 1262 test results for blocks obtained from Wisconsin SRW (WI-2), with samples tested in water. 39
Figure 25. Photo. Internal structure of block from Wisconsin SRW (WI-4), showing large compaction voids and low cement paste content. 39
Figure 26. Photo. Typical chloride concentrations for SRW blocks exhibiting poor field performance (data for WI-2 and WI-4, SRWs from Wisconsin). 40
Figure 27. Diagram. Concentration groups for the evaluation of ASTM C 1262 test method. 42
Figure 28. Photo. Units immediately after demolding. 43
Figure 29. Photo. Units prior to entering curing chamber. 43
Figure 30. Photo. Splitting of conjoined units. 43
Figure 31. Photo. Split face of units. 43
Figure 32. Photos. Definition of terms: SRW units (or blocks). 44
Figure 33. Drawing and photo. Definition of terms: test specimens (or coupons). 44
Figure 34. Photo. Possible exposure condition of units in winter weather. 46
Figure 35. Photo. Percentages in spatial distribution of absorption in large wall unit. 47
Figure 36. Drawing. Distribution of absorption in large wall unit. 47
Figure 37. Photo. Percentages in spatial distribution of absorption in small wall unit. 48
Figure 38. Drawing. Distribution of absorption in small wall unit. 48
Figure 39. Drawings. Simple random versus stratified random sampling from the face of an SRW unit. 49
Figure 40. Drawing and photos. Sampling of test specimens from SRW units from different manufacturers. 51
Figure 41. Graphs. Spatial distributions of ASTM C 642 boiled absorption on split face of SRW units (values shown represent mass of absorbed water as percent of mass of oven-dried specimen). 53
Figure 42. Graphs. Spatial distributions of volumetric paste content. 54
Figure 43. Graphs. Spatial distributions of volumetric compaction void content. 55
Figure 44. Photo. Sample A of split face delaminations on SRW units. 56
Figure 45. Photo. Sample B of split face delaminations on SRW units. 56

Figure 46. Drawings and photo. Suspected cause of split face delaminations. 57
Figure 47. Photo. Breaking off of split face delamination due to ice “jacking” action in field SRW units. 58
Figure 48. Photo. Detached split face delamination under frost conditions in field SRW units. 58
Figure 49. Photo. Freeze-thaw damage on SRW unit in field. 59
Figure 50. Photos. Section through region containing split face delamination. 60
Figure 51. Drawing. Sampling of SRW units from pallet. 62
Figure 52. Drawings. Extraction of freeze-thaw specimens from SRW unit. 63
Figure 53. Drawing. Extraction of specimens shorter than the unit height (view into back face). 64
Figure 54. Drawing. Extraction of specimens from middle layer. 64
Figure 55. Drawing. Solid unit showing recommended sampling locations (red dashed lines). 66
Figure 56. Photo. Sample of solid unit. 66
Figure 57. Photo. Second sample of solid unit. 66
Figure 58. Drawing. Hollow unit showing recommended sampling locations (red dashed lines). 67
Figure 59. Photo. Sample of hollow unit. 67
Figure 60. Photo. Second sample of hollow unit. 67
Figure 61. Photo. Defects along edges of SRW units. 68
Figure 62. Photo. Scratched surface. 68
Figure 63. Photo. Example of sound surface. 68
Figure 64. Drawing. Recommended clearance from edges. 69
Figure 65. Photo. Specimen before washing, following saw-cutting. 70
Figure 66. Photo. Specimen after washing, following saw-cutting. 70
Figure 67. Graph. ASTM C 1262 (2003) freeze-thaw cycle—definitions. 72
Figure 68. Photo. Closed chest freezer used in study. 73
Figure 69. Photo. Open chest freezer. 73
Figure 70. Photo. Walk-in freezer used in the study. 74
Figure 71. Photo. View of inside of walk-in freezer. 74

Figure 72. Drawing. Environmental chamber of walk-in freezer. 74
Figure 73. Photo. Cabinet freezer, closed. 75
Figure 74. Photo and drawing. Inside of cabinet freezer. 75
Figure 75. Photo. View of chest freezer with wooden frame and six specimens. 76
Figure 76. Graph. Internal temperature variations in chest freezer loaded with six specimens—T-t response. 78
Figure 77. Graph. Internal temperature variations in chest freezer loaded with six specimens—standard deviation-time response. 78
Figure 78. Photo. View of walk-in chamber with thermocouples on shelving units and suspended from ceiling. 80
Figure 79. Graph. Internal temperature variations in walk-in chamber loaded with 60 specimens—T-t response. 81
Figure 80. Graph. Internal temperature variations in walk-in chamber loaded with 60 specimens—standard deviation-time response 81
Figure 81. Graph. Average temperatures in walk-in chamber with varying quantities of specimens (values shown are number of specimens). 83
Figure 82. Photos and drawings. View of thermocouple (TC) placement in cabinet freezer instrument to tests. 85
Figure 83. Photo. View of thermocouple (TC) placement with specimens in cabinet. 85
Figure 84. Graph. Internal temperature variations in cabinet freezer loaded with 28 specimens—T-t response. 86
Figure 85. Graph. Internal temperature variations in cabinet freezer loaded with 28 specimens—standard deviation-time response. 87
Figure 86. Drawing. Individual temperature locations (front view of freezer, plan view of each shelf). 89
Figure 87. Drawing. Temperature mapping in cabinet freezer (side view of the freezer cabin)..... 89
Figure 88. Graph. Average temperatures in cabinet freezer with varying quantities of specimens (values shown are number of specimens). 90
Figure 89. Graph. T-t curves for freezer air, water surrounding specimen and specimen..... 94
Figure 90. Photo. Water surrounding specimen and specimen (as graphed in figure 89). 94

Figure 91. Photo. Temperature-monitored glass vials used to characterize freeze-thaw cycles and impact on water and saline solutions. 95
Figure 92. Drawing. Location of thermocouples. 95
Figure 93. Photo. Vials in freezer. 95
Figure 94. Photo. Broken vials. 95
Figure 95. Photo. View of typical specimen in test set A in cabinet freezer and walk-in freezer (NCMA study). 96
Figure 96. Photo. View of open container with specimen. 96
Figure 97 Graph. Comparative performance of specimens in test set A in cabinet freezer (darker lines) and specimens in walk-in freezer (lighter lines)—percent mass loss. 97
Figure 98. Graph. Comparative performance of specimens in test set A in cabinet freezer (darker lines) and specimens in walk-in freezer (lighter lines)—relative dynamic modulus. 97
Figure 99. Graph. Cooling curves comparison for typical cycles in the two freezers. 99
Figure 100. Graph. Rates of temperature change for curves in figure 99—temperature. 99
Figure 102. Graph. Rates of temperature change for curves in figure 99—solution. 100
Figure 103. Graph. Cooling curves and FP-t curves for plain water. 103
Figure 104. Graph. Cooling curves and FP-t curves for 3 percent NaCl solution. 103
Figure 105. Graph. Cooling curves and rate of ice formation curves for water. 104
Figure 106. Graph. Cooling curves and rate of ice formation curves for 3 percent NaCl solution. 104
Figure 107. Graph. Plots of FP as function of temperature. 105
Figure 108. Graph. Changes in NaCl concentration in unfrozen solution. 106
Figure 109. Graph. Rates of ice formation and concentration changes for initial 3 percent NaCl solution. 106
Figure 110. Photo and drawing. Circuit resistance for detecting expansion damage in freezing vials. 107
Figure 111. Photo. Strain gage for detecting expansion damage in freezing vials. 107
Figure 112. Drawing and photo. Direct observation for detecting expansion damage in freezing vials. 108

Figure 113. Graph. Results of water-filled unconfined vial in circular resistance test. 109
Figure 114. Photo. Water-filled unconfined vial. 109
Figure 115. Graph. Results of water half-filled unconfined vial in circular resistance test. 109
Figure 116. Photo. Water half-filled unconfined vial. 109
Figure 117. Graph. Results from water-filled, mortar-confined vial in circular resistance test. 109
Figure 118. Photo. Water-filled, mortar-confined vial. 109
Figure 119. Graph. Results of strain gage method—plain water. 110
Figure 120. Photo. Vial after test. 110
Figure 121. Graph. Results of strain gage method— 3 percent NaCl solution. 110
Figure 122. Photo. Vial after test. 110
Figure 123. Graph and photos. Results for direct observation method of damage detection (for water). 111
Figure 124. Graph and photos. Results for direct observation method of damage detection (for 3 percent NaCl). 112
Figure 125. Drawing. Location of thermocouples (S_1, S_2, S_3) embedded in SRW specimen 113
Figure 126. Drawing. Location of thermocouples (A_f, A_m) and in water (W_u, W_a). 113
Figure 127. Photo. Container used to hold SRW blocks 113
Figure 128. Photo. Varying container sizes. 113
Figure 129. Graph. Cooling curves for SRW mix A and B. 114
Figure 130. Photo. SRW mix A. 114
Figure 131. Photo. SRW mix B. 114
Figure 132. Graph. Specimen cooling curves for different volumes of surrounding water (reproduced from Hance, 2005). 116
Figure 133. Graph. Simple approach to estimate length of freezing plateau. 116
Figure 134. Graph Specimen cooling curves for different container sizes (reproduced from Hance, 2005). 118
Figure 135. Graph. Cooling curves for varying specimen quantities in the walk-in chamber—freezer air. 120
Figure 136. Graph. Cooling curves for varying specimen quantities in the walk-in chamber—specimen cooling curves. 120

Figure 137. Photo. View of chest freezer used for single-location repeatability tests..... 122
Figure 138. Photo. View of chest freezer interior. The circled portion indicates the location of the instrumented specimen. 122
Figure 139. Graph. Freezer air and specimen cooling curves for seven cycles. 123
Figure 140. Graph. Comparison of specimen cooling curve in 2 different freezers (chest freezer with 6 specimens, walk-in freezer with 40 specimens). 124
Figure 141. Graph. Relationship between size of pores and freezing point from Pigeon and Pleau (1995). 125
Figure 142. Graph. Relationship between size of pores and freezing point from Marchand et al. (1995). 125
Figure 143. Graph. Rates of temperature change for specimen and surrounding water. 127
Figure 144. Photo. Specimen after 4.5-hour cold soak in walk-in freezer appears frozen solid. 129
Figure 145. Photo. Second specimen, also after 4.5-hour cold soak in walk-in freezer, shows wet spots as indicated in the circled areas. 129
Figure 146. Graph. Results of cooling in chest freezer..... 131
Figure 147. Photo. Half-filled vial after cooling in chest freezer. 131
Figure 148. Graph. Results of cooling in walk-in freezer..... 131
Figure 149. Photo. Half-filled vial after cooling in walk-in freezer. 131
Figure 150. Photo. Half-full vial after 30 minutes of exposure in the chest freezer. 132
Figure 151. Photo. Half-full vial after 40 minutes of exposure in the chest freezer. 132
Figure 152. Diagram. ASTM C 666 (ASTM 2004), Procedure A specified T-t exposure of control specimen. 134
Figure 153. Graph. Comparison between cooling curves specified in European test methods and ASTM C 1262 (2003) specimens. 135
Figure 154. Drawing. ASTM C 1262 (2003) partially immersed specimen. 135
Figure 155. Drawing. Definition of compaction void in ASTM C 457 (2004) testing. 142
Figure 156. Graph. Relating mass loss to material property for a given SRW unit type. 143
Figure 157. Graph. Mass loss versus material property for each of the SRW units evaluated using centroids. 144

Figure 158. Graph. Mass loss versus material property for each of the SRW units evaluated using boundary points. 145
Figure 159. Graph. ASTM C 140 compressive strength. Data representation by boundary points. 148
Figure 160. Graph. ASTM C 140 compressive strength. Data representation by centroids. 148
Figure 161. Graph. ASTM C 140 24-hour water absorption. Data representation by boundary points. 149
Figure 162. Graph. ASTM C 140 24-hour water absorption. Data representation by centroids. 149
Figure 163.Graph. ASTM C 140 Unit weight. Data representation by boundary points. 150
Figure 164. Graph. ASTM C 140 Unit weight. Data representation by centroids. 150
Figure 165. Graph. NCMA index. Data representation by boundary points. 151
Figure 166. Graph. NCMA index. Data representation by centroids. 151
Figure 167. Graph. ASTM C 642 Boiled absorption. Data representation by boundary points. 152
Figure 168. Graph. ASTM C 642. Bottom graph. Data representation by centroids. 152
Figure 169. Graph. ASTM C 642. Volume of permeable voids. Data representation by boundary points. 153
Figure 170. Graph. ASTM C 642 Volume of permeable voids. Data representation by centroids. 153
Figure 171. Graph. Saturation coefficient. Data representation by boundary points. 154
Figure 172. Graph. Saturation coefficient. Data representation by centroids. 154
Figure 173. Graph. Total air and compaction voids content. Data representation by boundary points. 155
Figure 174. Graph. Total air and compaction voids content. Data representation by centroids. 155
Figure 175. Graph. Paste content. Data representation by boundary points. 156
Figure 176. Graph. Paste content. Data representation by centroids. 156
Figure 177. Graph. Paste-to-total-void ratio. Data representation by boundary points. 157
Figure 178. Graph. Paste-to-total-voids ratio. Data representation by centroids. 157

Figure 179. Graph. ASTM C 457 Specific surface. Data representation by boundary points. 158
Figure 180. Graph. ASTM C 457 Specific surface. Data representation by centroids. 158
Figure 181. Graph. ASTM C 457 spacing factor. Data representation by boundary points. 159
Figure 182. Graph. ASTM C 457 Spacing factor. Data representation by centroids. 159
Figure 183. Graph. Specific surface/total void content. Data representation by boundary points. 160
Figure 184. Graph. Specific surface/total void content. Data representation by centroids. 160
Figure 185. Graph. Evaluation of data points for mass loss less than 5 percent only. 161
Figure 186. Graph. Mass loss in 3 percent NaCl solution versus paste-to-total-voids ratio. Data representation by boundary points. 163
Figure 187. Graph. Mass loss in 3 percent NaCl solution versus paste-to-total-voids ratio. Data representation by centroids. 164
Figure 188. Graph. Average ASTM C 1262 (2003) mass loss for all salt solutions evaluated. 166
Figure 189. Drawing. Exposure chamber. 168
Figure 190. Photo. Freeze-thaw test setup showing SRW blocks. 169
Figure 191. Photo. Smaller SRW block testing in Phase I. 170
Figure 192. Graph. Percent weight change for samples from test 1 (ramp rate of 0.33 °C/min (0.6 °F/min) with 1-hour hold time, sprayed with water). 171
Figure 193. Graph. Percent weight change for samples from test 2 (ramp rate of 0.18 °C/min (0.3 °F/min) with 1-hour hold time, sprayed with 3 percent NaCl). 171
Figure 194. Graph. Percent weight change for samples from test 3 (ramp rate of 0.33 °C/min (0.6 °F/min) with 1-hour hold time, sprayed with 3 percent NaCl). 172
Figure 195. Graph. Percent weight change for samples from test 4 (ramp rate of 0.55 °C/min (1.0 °F/min) with 2 hour hold time, sprayed 3 percent NaCl). 172
Figure 196. Photo. Typical cracking and spalling from freeze-thaw damage from test 1. 173

Figure 197. Photos. Freeze-thaw deterioration over 40 cycles from Test 4: a. after 10 cycles, b. after 20 cycles, c. after 30 cycles, and d. after 40 cycles. 174
Figure 198. Photo. SRW block from manufacturer A. 175
Figure 199. Photo. SRW block from manufacturer B. 176
Figure 200. Photo. SRW block from manufacturer C. 176
Figure 201. Photo. Typical stacking for larger SRW blocks tested in Phase II. 177
Figure 202. Graph. Typical block temperature data from Phase II investigation. 178
Figure 203. Photo. SHA-approved block from manufacturer A (water exposure). 179
Figure 204. Photo. SHA-approved block from manufacturer A (3 percent NaCl solution exposure). 179
Figure 205. Photo. Non-SHA-approved cap from manufacturer A (water exposure). 179
Figure 206. Photo. Surface of non-SHA-approved block from manufacturer A (3 percent NaCl solution). 179
Figure 207. Graph. Percent weight change as a function of freeze-thaw exposure cycles for SHA-approved SRW blocks exposed to NaCl solution—from manufacturer A. 180
Figure 208. Graph. Percent weight change as a function of freeze-thaw exposure cycles for SHA-approved SRW blocks exposed to water—from manufacturer A. 180
Figure 209. Graph. Percent weight change versus freeze-thaw exposures for non-SHA-approved SRW blocks from manufacturer A exposed to NaCl solution (positive values indicate weight loss). 180
Figure 210. Photo. SHA-approved block from manufacturer B (NaCl Solution). 181
Figure 211. Graph. Percent weight change for manufacturer B SRW blocks exposed to NaCl solution resulting from freeze-thaw cycling for SHA-approved blocks. 181
Figure 212. Graph. Percent weight change for manufacturer B SRW blocks exposed to NaCl solution resulting from freeze-thaw cycling for non-SHA-approved blocks. 181
Figure 213. Photo. SHA-approved C block exposed to fresh water. 182
Figure 214. Photo. SHA-approved C block exposed to 3 percent NaCl solution. 182

Figure 215. Graph. Percent weight change resulting from freeze-thaw cycling of SRW blocks exposed to NaCl solution for SHA-approved blocks—from manufacturer C..... 182
Figure 216. Graph. Percent weight change resulting from freeze-thaw cycling of SRW blocks exposed to NaCl solution for non-SHA-approved blocks—from manufacturer C..... 182
Figure 217.Graph. Percent weight change resulting from freeze-thaw cycling of SRW blocks from manufacturer C. Blocks exposed to water for SHA-approved blocks. 183
Figure 218. Graph. Percent weight change resulting from freeze-thaw cycling of SRW blocks from manufacturer C. Blocks exposed to water for non-SHA-approved blocks. 183
Figure 219. Graph. Compaction void content versus paste content for all SRW mixes evaluated. 189
Figure 220. Graph. Mass loss versus cycles. 190
Figure 221. Photo. Comparison of water versus saline tests on wall unit after 100 cycles in water. Specimens were from a single manufacturer. 191
Figure 222. Photo. Comparison of water versus saline test on wall unit after 60 cycles in saline. Specimens were from a single manufacturer..... 191
Figure 223. Graph. Dependence of mass loss prediction constant “a” on paste content (Hance, 2005)..... 192
Figure 224. Graph. Relationship between mass loss after 100 cycles in water and paste-to-total air and compaction void ratio. 193

LIST OF TABLES

Table 1. Blocks from in situ SRWs obtained for laboratory evaluation. 36
Table 2. Characteristics of the various freezers investigated (from Hance, 2005). 76
Table 3. Temperature variations inside a chest freezer..... 79
Table 4. Temperature variations inside the walk-in freezer loaded with 60 specimens. 82
Table 5. Temperature variations inside the walk-in freezer loaded with varying specimen quantities. 84
Table 6. Temperature variations inside the cabinet freezer loaded with 28 specimens. 87
Table 7. Temperature variations inside the cabinet freezer loaded with varying specimen quantities. 91
Table 8. Comparison of cycle parameters between cabinet and walk-in freezers. 101
Table 9. Measured differences for conditions of varying volumes of surrounding water. 117
Table 10. Measured differences for conditions of varying container sizes. 118
Table 11. Measured differences for conditions of varying specimen quantities. 121
Table 12. Comparison of cooling curve characteristics for half-full vials in different freezers. 133
Table 13. Comparison of specimen cooling rates for cooling curves of section 4.4.2.3 133
Table 14. Scope of ASTM C 1262 (2003) test program. 141
Table 15. Standard test methods and material properties evaluated for SRW units. 142
Table 16. Ranking of material properties using different types of analyses. 161
Table 17. Threshold values of material properties determined from figures 159 to 184..... 162
Table 18. Phase I experimental program. 169
Table 19. Experimental plan showing number of blocks tested in Phase II. 175
Table 20. Chloride diffusion coefficients for larger SRW block samples. 183
Table 21. Comparison of cold soak requirement in freeze-thaw test methods 196
Table A.1 R values for t_{trial} 237

CHAPTER 1: INTRODUCTION AND SCOPE

1.1 OVERVIEW

Segmental retaining wall (SRW) systems are commonly and successfully used in a range of applications, including highway projects. Their popularity can be attributed to a combination of reduced construction costs, versatility, aesthetic appearance, ease of installation, and an increasing number of proprietary designs available in the market. Despite these inherent advantages, there have been some reported problems with durability of SRW blocks in cold climates. The deterioration of some SRW installations in State highway agency (SHA) applications has resulted in concern over the long-term performance of SRW systems and has led to stricter specifications and, in some cases, restrictions on future use of SRW systems.

In response to these concerns, an FHWA-funded research project was initiated to determine the cause and extent of SRW block distress, to identify and recommend test methods for improving durability of SRW systems, and to recommend specifications for SHAs to ensure long-term durability and performance of SRW systems in highway applications. This report summarizes the key findings of this project and provides guidance on producing durable SRW blocks to ensure long-term performance of SRW systems in highway applications.

The remainder of this chapter provides a brief overview of SRW systems, highlights some of the key technical aspects associated with SRW blocks, and describes broadly the scope of the SRW block deterioration problem at the time that this research project was launched. Lastly, this chapter provides a brief summary of the organization of the remaining chapters in this report.

1.2 SRW SYSTEMS

SRW systems have become increasingly popular in the past decade for earth retention and landscaping applications. These systems, consisting of dry-stacked (mortarless) concrete masonry units, can be used either as conventional gravity structures or as part of a reinforced soil system in conjunction with horizontal layers of soil reinforcement (figures 1, 2, and 3). Wall heights can range anywhere from 200 mm (millimeters) (8 inches) to 6 (meters) m (20 feet (ft)) depending on the specific application as shown in figure 4.

SRW units are manufactured in concrete block plants at typically dry consistencies using low water contents and/or low overall paste contents to achieve a stiff consistency for compaction into molds and to allow almost immediate demolding (figures 5 and 6).

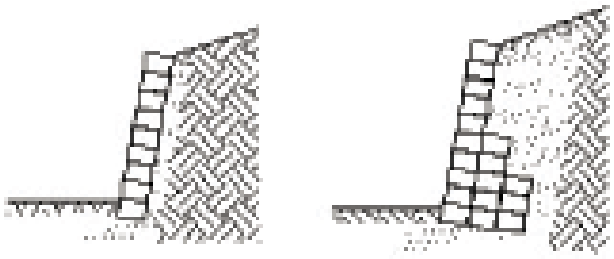

Figure 1. Drawing. Conventional forms of SRW construction (NCMA, 2005a).

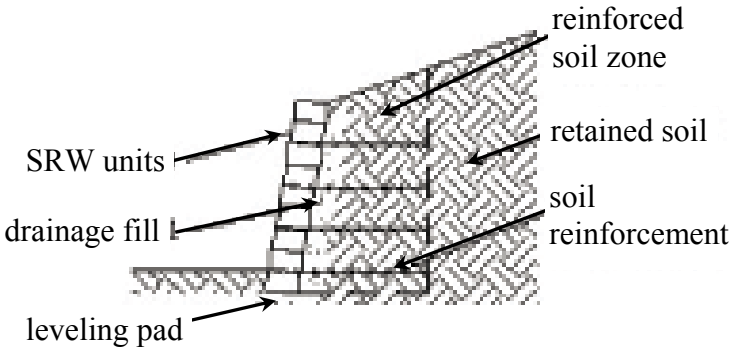

Figure 2. Drawing. Soil reinforced forms of SRW construction (NCMA, 2005a).

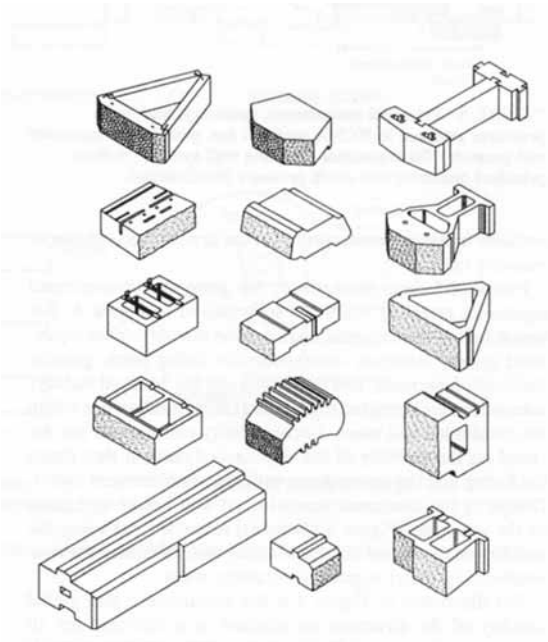

Figure 3. Drawings. Sample sizes and shapes of SRW units for SRW systems (Bathurst, 1993).

a. Highway.

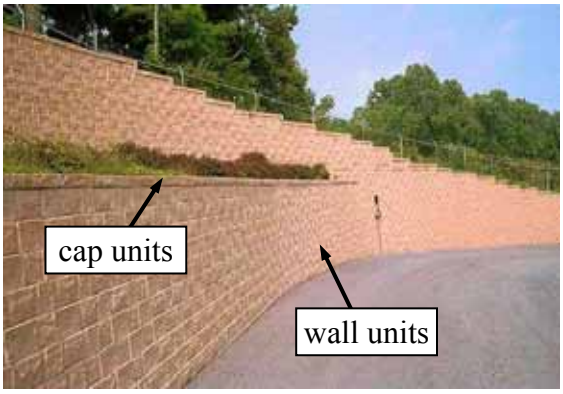

b. Parking lots.

c. Commercial centers.

d. Parks.

e. Landscaping.

f. Residential.

Figure 4. Photos. Example applications of SRW systems.

Figure 5. Photo. View of mix during production of SRW units at block plant.

Figure 6. Photo. SRW unit immediately after compaction and demolding.

Due to the low paste contents of SRW units, a material characterized by a network of irregularly shaped voids is produced, as depicted in figure 7, in which the internal structures of ordinary and SRW concretes are contrasted. These voids are termed "compaction voids" since they are formed during the compaction process, and their role in the durability of SRW units is still not fully understood (Pigeon and Pleau, 1995). From the data obtained under this FSRW project, the volume fraction of compaction voids can account for up to 25 percent of the total volume of concrete. As comparison, the air void content of air-entrained concretes is approximately in the range of 4–8 percent by volume (Kosmatka and Panarese, 1994).

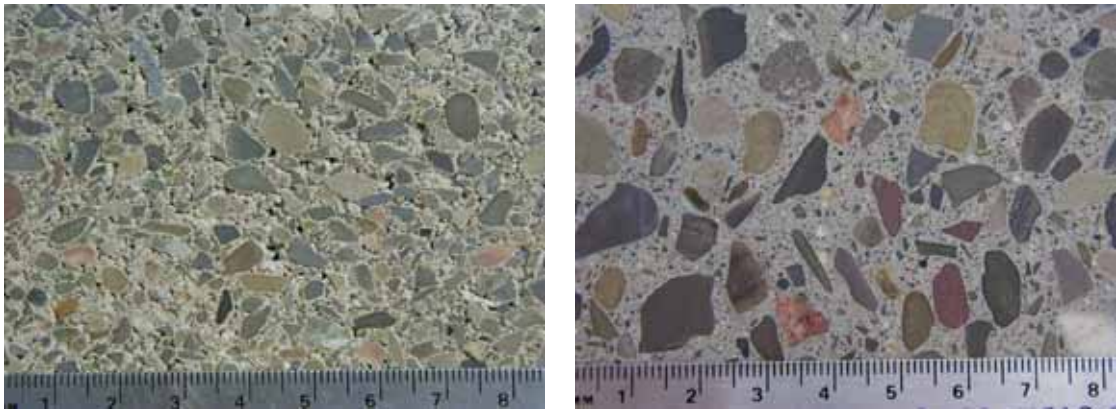

a. SRW mix (note compaction voids). b. Ordinary concrete.

Figure 7. Photos. Comparison of internal structures between SRW and ordinary concretes.

Presently, in the United States, the material performance of SRW units is evaluated based on the following standards (NCMA, 2002):

- ASTM C 1372, Standard Specification for Segmental Retaining Wall Units (ASTM C 1372, 2003).
- ASTM C 140, Standard Test Methods for Sampling and Testing Concrete Masonry Units and Related Units (ASTM C 140, 2000).

- ASTM C 1262, Standard Test Method for Evaluating the Freeze-Thaw Durability of Manufactured Concrete Masonry Units and Related Concrete Units (ASTM C 1262, 2003).

ASTM C 1372 specifies dimensional tolerances, compressive strength, absorption, and density of the material, as well as freeze-thaw durability. ASTM C 140 is actually a masonry standard covering test procedures for dimension measurement, compressive strength, absorption, and density, while ASTM C 1262 covers procedures for freeze-thaw durability testing of SRW units.

1.3 RESEARCH BACKGROUND AND SCOPE

Although SRW manufacturing technology has improved in recent years and durable units can be produced, there have been reported cases of deterioration of SRW units in the field. This is particularly the case in cold regions where frost exposure in combination with deicing salts can severely damage the units (Thomas, 2003). An example of a damaged SRW is shown in figure 8.

Figure 8. Photo. Condition of SRW in Ithaca, NY.

In May 2000 a survey of SRW performance was released to selected cold weather States and responses were obtained from Illinois, Iowa, Kansas, Michigan, Minnesota, Missouri, New York, Wisconsin, and Wyoming. All States have minimum strength and maximum absorption regulations, and Iowa, , Michigan, Minnesota, New York, and Wisconsin all require freeze/thaw testing according to ASTM C 1262 (ASTM 2003) (described in detail throughout this report). Illinois requires 100 cycles conducted according to ASTM C 666 “Standard Test Method for Resistance of Concrete to Rapid Freezing and Thawing” (2004) a requirement that producers have had difficulty meeting due to the severity of the test. Illinois, Kansas, Minnesota, Missouri,

Wisconsin, and Wyoming all have regulated wall sizes and/or design requirements based on durability concerns with SRWs. Minnesota and Wisconsin have set the most rigorous requirements based on the severity of the problem and the volume of walls that have been constructed.

In recent years, both Minnesota and Wisconsin Departments of Transportation (Mn/DOT and WisDOT respectively) have conducted extensive field surveys to assess the level of damage to in service SRWs. In July of 2001 a report was released by Mn/DOT detailing the condition of 104 SRWs (Embacher et al., 2001). Only walls built before 1994 were examined, with an emphasis on walls located at the same intersection facing different directions and constructed during the same year. Privately owned walls identified by industry representatives were also investigated. Each wall was assigned a distress rating between 0 and 5, with 0 indicating the worst distress, and 5 indicating no visible distress. Only 7 percent of the walls examined were classified as poor to very poor, but it was found that over 50 percent of the walls exhibited freeze-thaw damage. Walls located at parking lots or close to the roadway exhibited the most damage, due to increased amounts of snow accumulation and water runoff, therefore allowing for greater saturation, and exposure to deicing salts. Walls exposed to fertilizer also exhibited more damage, due to phosphates in the fertilizers behaving in a manner similar to that of deicing salts.

In the summer of 2000 WisDOT randomly surveyed 87 walls throughout the State. Walls were between 1 and 15 years old with the majority of walls being between 5and 10 years old. A database was created with photographs of each wall and specific rating and wall details for each wall. Walls were rated based on the distress manual developed in the Mn/DOT wall survey. A total of 18 walls (roughly 20 percent of those surveyed) displayed freeze-thaw distress, with 8 showing low severity, 6 showing medium severity, and 4 showing high severity. It was concluded that even though a lower percentage of Wisconsin walls displayed damage than in Minnesota, freeze-thaw durability is still a major issue and should be examined in more detail.

The distress shown by existing walls has resulted in more rigorous requirements for the construction of walls in many States as can be seen in figure 6. Minnesota and Wisconsin have been the most aggressive in setting guidelines for freeze-thaw requirements of SRWs. After March 1, 2001, Mn/DOT required all walls to conform to a strict list of requirements (Mn/DOT, 2001), as follows. No walls are allowed in locations where they will be directly supporting roadways or bridge abutments. Walls greater than 1.2 m (4 ft.) in height have no restriction on location on roadways with traffic volumes less than 5,000 annual average daily traffic (AADT), for roadways with traffic volume between 5,000 and 20,000 AADT, the wall must be greater than 6.0 m (20 ft.) beyond the outside shoulder or gutter line, and for roadways with traffic volume greater than 20,000 AADT, the walls must be located greater than 9.1 m (30 ft.) beyond the outside shoulder or gutter line. The maximum allowed wall height is 3.0 m (10 ft.), and it is assumed an additional 0.6 m (2 ft.) will be buried below ground.

All blocks being placed in Minnesota must conform to ASTM C 1372 (2003), and have a minimum compressive strength of 38 megapascals (MPa) (5,500 pounds per square inch (psi)) for any individual unit, and 40 MPa (5,800 psi) for an average of three units. Walls must also exhibit a weight loss for each of 5 specimens at the conclusion of 90 cycles of not less than 1 percent, or 4 out of 5 specimens at the conclusion of 100 cycles of not less than 1.5 percent when

subject to ASTM C 1262 (2003) testing in 3 percent saline solution. The specifications are the same for cap units except they need only be subject to 40 and 50 cycles as opposed to 90 and 100 cycles. One sample of every 5,000 units of continuous production should be tested in accordance to ASTM C 140 (2000) with the exception that coupons must be tested, and tests on full size units are not allowed.

WisDOT allows only six block manufacturers to create the facing of SRWs (WisDOT, 2000). Blocks shall exhibit a minimum compressive strength of 34 MPa (5,000 psi) and a maximum of 6 percent absorption when subject to ASTM C 140 (2000) testing. Walls must also exhibit a weight loss for each of 5 specimens at the conclusion of 40 cycles of not less than 1 percent, or 4 out of 5 specimens at the conclusion of 50 cycles of not less than 1.5 percent, when subject to ASTM C 1262 (2003) testing in 3 percent saline solution. All tests shall be conducted by a WisDOT approved independent testing laboratory for each lot of 5,000 blocks.

Some measures are also being taken by State departments of transportation (DOTs) to reduce further damage to inservice walls that have already shown freeze/thaw distress as shown in Figure 9. The most common technique being used is the application of silane or siloxane coatings. The purpose of these coatings is to try to keep moisture from penetrating the surface of SRWs and therefore, reduce future damage. The long-term effects of sealers are still unknown, and in lab settings, these types of coatings have shown mixed results. Sealers have proved to be useful in reducing deicer salt scaling on insufficiently air-entrained conventional concrete, but the protection is limited over time (Hazrati, 1993). On surfaces with adequate salt-scaling resistance, Hazrati (1993) observed that sealers actually increase the amount of salt scaling damage.

In response to the concerns raised above regarding frost resistance of SRW blocks, a pooled fund project was initiated in 2003 by the Federal Highway Administration, under which The University of Texas at Austin (UT), Cornell University and Texas A&M University engaged in a research project on SRW durability. The objectives of this research were to determine the mechanisms responsible for the deterioration of SRW units in the field, identify variables that contribute to the durability of these units, and provide recommendations for the production of durable units and for the protection of existing SRWs.

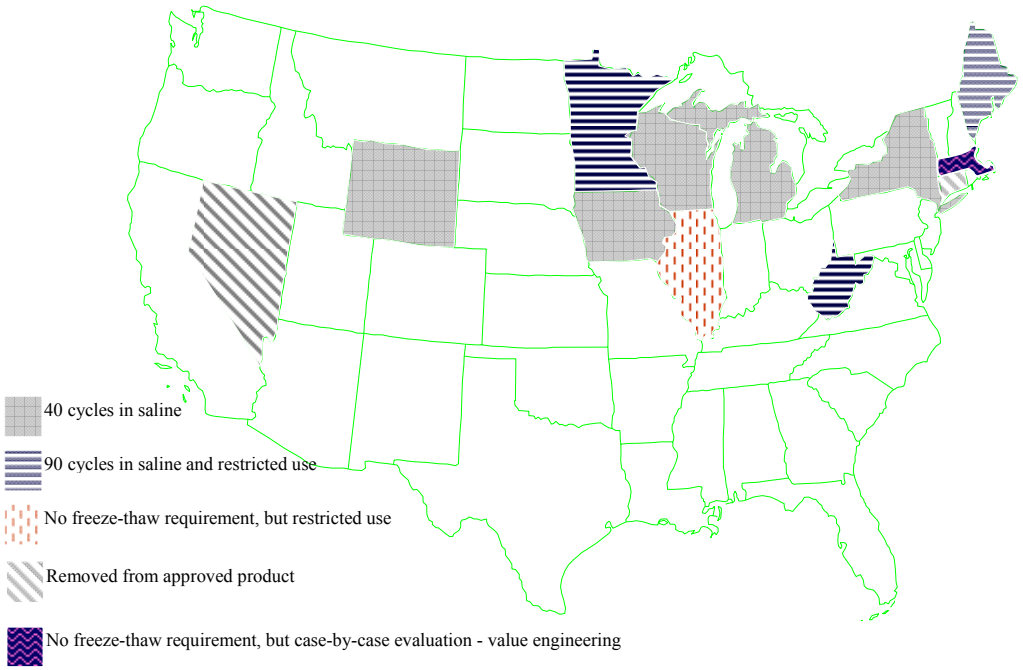

Figure 9. Map. State highway agency requirements for freeze-thaw durability of SRW blocks (Thomas et al., 2003).

1.4 ORGANIZATION OF REPORT

The remainder of this report presents the key findings from FHWA Project No. DTFH61-02-R-00078. This final project report draws from several documents generated under this project, including:

- Chan, C., *Freeze-Thaw Durability and ASTM C 1262 Testing of Segmental Retaining Wall (SRW) Units*, Ph.D. Dissertation, Cornell University, 2006.
- Hance, R., *Studies of the Frost-Resistance of Segmental Retaining Wall Units*, Master of Science thesis, Cornell University, 2005.
- Haisler, J., *Freeze-Thaw Durability of Segmental Retaining Wall Blocks,* Master of Science thesis, The University of Texas at Austin, 2004.
- Chan, C., Hover, K.C. and Folliard, K. J., "Spatial Variations in Material Properties of Segmental Retaining Wall (SRW) Units, Part I: Observed Variations," *Journal of ASTM International, Civil Engineering and Building Materials*, February 2005 (2005a).
- Chan, C., Hover, K.C. and Folliard, K. J., "Spatial Variations in Material Properties of Segmental Retaining Wall (SRW) Units, Part II: Sampling Considerations for Absorption Tests," *Journal of ASTM International, Civil Engineering and Building Materials*, February 2005 (2005b).
- Chan, C., Hover, K.C., and Folliard, K.J., "Performance of Segmental Retaining Wall (SRW) Units: from Laboratory to Field," *Construction Materials, Proceedings of*

CONMAT 05 and Mindess Symposium (eds. N. Banthia, T. Uomoto, A. Bentur and S.P. Shah), Vancouver, Canada, Aug. 21-24, 2005 (2005c).

- Chan, C., Hover, K.C., Folliard, K.J. and Trejo, D., "Frost Durability Indices of Segmental Retaining Wall (SRW) Units," manuscript submitted to *ACI Materials Journal*, November 2005 (2005d).

The remainder of this report is organized into the following chapters:

Chapter 2 contains a brief literature review on freeze-thaw damage, with a primary emphasis on SRW block durability.

Chapter 3 summarizes field evaluations of SRW systems conducted under this project, with emphasis on SRWs used in highway applications in Minnesota and Wisconsin.

Chapter 4 describes a comprehensive laboratory research program focusing on frost resistance of SRW blocks. The work includes detailed studies on sampling issues, freeze-thaw test methods, impact of salts on damage, and efforts to develop a more realistic approach to test full SRW blocks under simulated exposure conditions. The main focus of the chapter is on refining and improving ASTM C 1262 to make it more reliable, reproducible, and user friendly.

Chapter 5 summarizes the key findings of this research project and provides guidance on how to specify and test SRW blocks to ensure long-term durability.

Appendixes A and B contains newly proposed versions of ASTM C 1262 (freeze-thaw testing of SRW blocks) and ASTM C 1372 (standard specifications for SRW blocks), based on the key findings from this research project. These appendixes are intended to serve as stand-alone products that can readily be considered for adoption by SHAs and the American Association of State Highway and Transportation Officials (AASHTO).

CHAPTER 2: LITERATURE REVIEW

2.1 INTRODUCTION

This chapter provides a brief summary of literature to date related to frost resistance of SRW blocks. For conciseness, only an abridged version of a much more comprehensive review by Chan (2006) is presented herein, and readers are directed towards Chan's review (in his 2006 Ph.D. dissertation) for more detailed coverage of freeze-thaw mechanisms (for both conventional concrete and SRWs), including issues related to salt scaling and associated damage. The next section of this chapter briefly discusses some of the more recent literature related to frost damage and salt scaling for conventional concrete, followed by a more thorough summary of published literature on the frost (and salt) resistance of SRW blocks and other dry-cast cementitious materials. Through these discussions, it should be quite clear that the mechanisms of frost damage and salt scaling in conventional concrete are quite complex and not fully understood, and furthermore, that very little is known about freezing and thawing of SRW blocks. This review of available literature confirms the importance and need for research on the frost resistance of SRW blocks, the results of which are discussed in chapter 4.

2.2 FROST DAMAGE IN CONCRETE

2.2.1 Mechanisms of Frost Damage in Concrete

Powers (1949) was one of the first researchers to focus in detail on the mechanisms of frost action and damage in concrete. Powers proposed that the expansion of water during freezing (9 percent volume expansion on freezing) in critically saturated capillary pores forces unfrozen water away from the freezing sites. This displaced water must travel under pressure through the cement paste, and as a result, destructive stresses can occur depending on the amount of resistance to this flow. The role of air voids is to provide "escape" boundaries where the flowing water can escape and freeze without causing damage. Because this theory was based on the flow of water through a permeable cement paste, Darcy's law was employed to model the process. Powers considered a single air bubble and the part of the paste within the bubble's "sphere of influence," shown as a shell in figure 10. This portion of paste contains capillary pores which expel unfrozen water into the air bubble during freezing. Hence, the shell thickness (L) would represent the maximum distance that water must travel before reaching the air void boundary. From Powers' analysis, it was determined that the maximum shell thickness (L_{max}) above which hydraulic pressures generated by the flow of water is enough to cause cracking of the paste was given by:

$$\frac{L_{max}^{3}}{r_b} + \frac{3L_{max}^{3}}{2} = \frac{1}{0.03\,\eta}\,\frac{KT}{UR} \qquad \text{Equation 1}$$

where r_b = radius of bubble
η = coefficient of viscosity
K = coefficient of permeability of the paste
T = tensile strength of the paste

U = quantity of water that freezes per degree drop in temperature
R = freezing rate

It is seen here that increasing the viscosity of the liquid, increasing the freezing rate, decreasing the permeability of the paste or decreasing the strength of paste are more critical as any of these conditions require smaller L_{max} values (i.e., shorter path lengths).

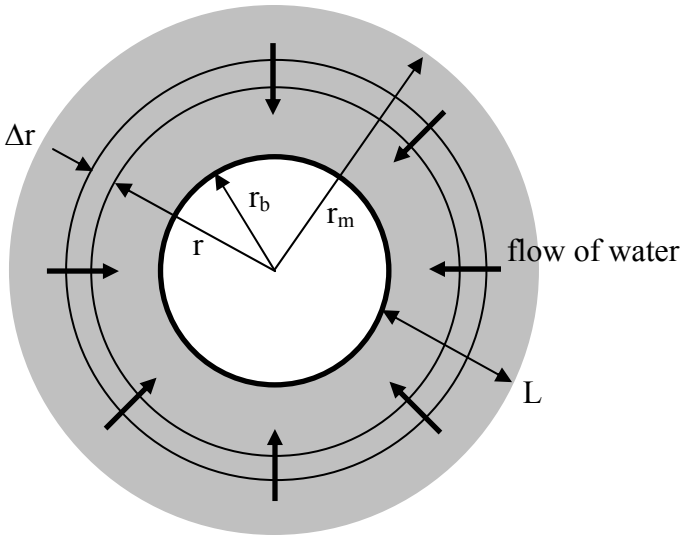

Figure 10. Diagram. Powers' rendition of an air bubble and its "sphere of influence" (Powers, 1949).

The above theory was, however, developed for a single bubble with its own sphere of influence. To extend this analysis to real paste systems comprised of an assortment of bubble sizes, Powers developed a hypothetical model consisting of equal sized spherical bubbles and derived an expression to estimate the average value of L for all air voids in the paste. This average value was termed the Spacing Factor ($\bar{L}$), which represents the approximate half-distance between two adjacent air voids. Two expressions of the Spacing Factor were derived based on the relative proportion of paste to air voids. The equations for $\bar{L}$ hence determined were eventually adopted by ASTM C 457 (2004) as a standard method to characterize the air void system in hardened concrete. The full set of equations can be found either in Powers (1949) or ASTM C 457 (ASTM 2004).

Moreover, Powers used experimental data available at the time for a variety of concretes with the intention of estimating the maximum permissible spacing factors for freeze-thaw durable concretes. These concrete mixes had air concretes of about 3 percent, specific surfaces (α) of about 600 square inches/cubic inches and were subjected to freezing rates of [Tf = 9/5 * Tc + 32] degrees Celsius per hour (°C/hr)] (20 degrees Fahrenheit per hour (°F/hr)). Powers determined that the Spacing Factors among the mixes capable of withstanding the imposed freezing conditions were about 0.254 mm (0.010 inch) or less. This value of the spacing factor was in general agreement with the values of L_{max} computed for the various cement pastes mentioned earlier.

The main advantage of this theory is that it demonstrates the importance of the spacing of air voids in the paste's resistance to freezing and thawing. This theory is also the only one that establishes mathematical relationships between the paste properties, the freezing rate and the spacing of air voids, and how these relate to internal pressures (Pigeon and Pleau, 1995). As will be seen in the next parts however, subsequent to the development of the Hydraulic Pressure Theory, there has been growing experimental evidence that water actually travels towards freezing sites rather than away from them. As a result, doubts have been cast on the actual mechanisms and assumptions entailed by the 1949 Powers' paper. The concepts and equations developed in it are nevertheless still widely used today to evaluate and compare different air void systems.

In the years following the development of the Hydraulic Pressure Theory, Powers, in conjunction with Helmuth, made several important realizations regarding the possible mechanisms taking place during freezing of pastes (Powers and Helmuth, 1953). These new insights, which advanced the understanding of frost damage, were also supported by experimental evidence. The two main aspects suggested by these authors concerned the following:

1. Not all evaporable water in the pores of the paste is freezable. Powers explained that the quantity of ice formed is generally much smaller than the quantity that is thermodynamically freezable at the given temperature. For instance, he quoted other references where it was shown that at −15 °C (5 °F), approximately one-half of the water in pores large enough to be frozen at this temperature remained unfrozen. He attributed this to various reasons. One suggested cause was that due to surface tension, water in the capillary pores would tend to supercool unless it is seeded by an ice crystal on which it can nucleate. At the same time, water in gel pores cannot freeze above –78 °C (108 °F) because it is adsorbed to the surfaces of the calcium-silicate-hydrate (CSH). In fact, at each given temperature below the normal freezing point of water, there are certain pore sizes below which freezing of its water cannot occur. As a result, in a saturated paste, there would always be a fraction of water that is unfrozen, and most of this is likely contained in the smaller pores (including gel pores).
2. Pore water is not pure and contains dissolved chemicals such as alkalis. Ice formation in this solution is accompanied by an increase in the concentration of dissolved chemicals in the unfrozen water. Consequently, concentration differences exist throughout the paste between regions where ice has formed and regions with no ice.

As a result of the above phenomena, a new hypothesis for frost mechanisms and frost damage of pastes was developed as follows. As temperature drops below the normal freezing point of water, ice starts forming in a number of capillary pores while water in gel pores remains unfrozen. The lower free energy (or chemical potential) of ice in the larger pores compared to liquid water in the smaller pores creates a thermodynamically imbalanced condition. This can only be brought back to equilibrium by the flow of liquid water to the ice formation sites. The growth of ice in these larger pores can create enough pressures to damage the paste. Powers referred to these pressures as crystal pressures (Powers, 1975). In addition, the growing chemical concentration of the unfrozen water in the larger pores compared to that in the smaller pores produces a concentration gradient between these two regions. This can also only be balanced by the osmotic flow of liquid water from gel to capillary pores (osmotic pressures). As a consequence, large internal stresses can be generated in the paste due to osmotic pressures from this flow of water.

Powers, however, indicated that there is no fundamental difference between the two cases, and they could be simply refereed to as osmotic pressures (Powers, 1975).

It is also noted from these processes that dilution of the unfrozen solution in the capillary pores is possible due to the continued flow of water into the pores. The lower concentration of this solution hence elevates its melting point, thereby promoting more ice formation. Thus, the above described mechanisms become amplified. Furthermore, if the temperature continues to decrease, smaller and smaller pores become prone to freezing and the above phenomena become more pronounced over the entire paste volume.

Powers described experimental observations which agreed with the above mechanisms. It was noted that non-air-entrained pastes would undergo continued dilation while the temperature remained constant. Air-entrained pastes, however, exhibited shrinkage during freezing. Moreover, in other experiments, it was shown that a slightly desiccated non-air-entrained paste would shrink during cooling shortly after the start of freezing, but it would then expand sharply after some low temperature had been passed. These phenomena were explainable considering the mechanisms just described: the paste tends to shrink as water is drawn from the smaller to the larger pores, but would then tend to expand after the capillary voids are filled with water which freezes and expands (Cordon, 1966). These observations could, however, not have been explained using concepts from the Hydraulic Pressure Theory. It is further noted that these length-change observations of freezing concrete specimens have also become the basis for the standard test method, ASTM C 671 “Critical Dilation Test” (ASTM, 2002), which uses length change measurements to compare the frost durability of different concrete mixtures.

As far as air voids are concerned, their role here is to compete with the capillary pores for the flowing water. These air bubbles have more room to allow ice formation, and if spaced sufficiently close together, the air bubbles provide escape routes for the flowing water and alleviate pressure buildup.

Following the early works of Powers (1949) and Powers and Helmuth (1953), a substantial amount of work has been undertaken to advance the understanding of freezing mechanisms and frost damage in porous materials, especially concrete. While hydraulic pressure and osmotic pressure mechanisms are still brought up in various references to explain frost damage, it is evident that other processes may be significant. The application of thermodynamic principles has been vital to elucidate many of these processes. For instance, the expressions relating freeze-point depression to pore size and the Kelvin equation describing capillary condensation in pores have shed light on freezing behavior in various pore sizes (Penttala, 1998). These concepts have set the groundwork for much of the subsequent research on frost processes. Also, the use of low temperature calorimetry has provided a useful way to track ice formation and ice melting. This technique has allowed observing changes in ice formation with changes in the paste microstructure. For instance, it was shown that increasing water-cement ratios and repeated freeze-thaw cycles raise the temperatures at first-freeze (i.e., ice first forms at a warmer temperature). However, more mature pastes and higher cooling rates lower the temperatures at first-freeze. Ice formation was also detected at temperatures down to about −20°C (68 °F) corresponding to freezing of smaller pores. From such tests, the hysteretic nature of freezing and thawing was also elucidated.

As far as frost mechanisms in the paste microstructure are concerned, there is a range of hypotheses proposed in the reviewed literature to explain the various stages occurring during freezing and thawing of pastes and concretes. Kaufmann (2002) provided a qualitative sequential description of these mechanisms. As temperatures drop below the freezing point of bulk water, ice first forms in the larger pores or on the exterior surfaces of concrete. Most of the water in large pores does not interact with the pore walls and is thus held like bulk water. Rapid cooling rates may also induce large hydraulic pressures. Then, as the temperature is further reduced, it is generally agreed that water in smaller pores migrates to larger pores due to the thermodynamic imbalance existing between the unfrozen water in smaller pores compared to the ice in larger pores. This was the basis of the findings in Powers and Helmuth (1953) in which differing length-change trends were also observed in non-air-entrained and air-entrained pastes. While non-air-entrained pastes dilated on freezing, air-entrained pastes shrank on freezing. These results were also confirmed by Penttala (1998). The driving pressures causing this migration of water were determined to be around 1.22 MPa/°C (34.2 MPa/°F) in gel pores (Setzer, 1999) and 1.3 MPa/°C (34.3 MPa/°F) (Scherer and Valenza, 2005). As seen, a few degrees Celsius of undercooling can cause sufficient driving pressures for the redistribution of water in the pore system.

Scherer and Valenza (2005) then pointed out that as the ice in larger pores grow (by "draining" water in smaller pores), this ice eventually exerts crystallization pressures on the pore walls. This pressure is a function of the shape and curvatures in the pores in question as well as the contact angle between ice and pore wall. Scherer attributed this crystallization pressure as being responsible for damage in the material. The amount of pressure generated in the pores has been determined theoretically by Scherer and Valenza (2005) and experimentally by Penttala (1998) who calculated pore pressures based on test chamber relative humidity. In both cases, pore pressures can reach several MPas at several degrees Centigrade below normal freezing point (e.g., at around −5 °C (23 °F)). However, as Scherer pointed out, the calculated pressure applies to one pore only and high stress in a single pore is not likely to crack or fail a material because the volume affected by the stress is too small. Gross material damage is not expected until the crystals propagate through the pore space.

The concept of crusting (Scherer, 1993) and entrapped water (Chatterji, 1999a and 1999b) has not been mentioned frequently in the literature. It deserves attention due to the magnitude of stresses that can be developed under these circumstances. This situation can arise when rapid cooling rates prevail, when a wide range of pore sizes are present (Scherer, 1993), or when dissolved substances continually depress the freezing point of the solution (Scherer, 2005). High pressures in trapped capillary water due to rapid cooling rates was also mentioned in Harnik et al. (1980). The pressures generated in these conditions can reach up to 13.5 MPa/°C (56.3 MPa/°F).

The closed-model container by Fagerlund (1995) which is related to the entrapped water concept revealed that very little freezable water is required to cause damage. As a reminder, the maximum tolerable contents of freezable water values were estimated to be 5 percent of the cement volume at −5 °C (23 °F), 2 percent at −10 °C (50 °F) and 0.7 percent at −20 °C (68 °F). As mentioned before, this model is highly conservative due to the assumption that all water is contained inside the sphere. However, in separate calculations, Fagerlund also demonstrated that

substantial amounts of freezable water can potentially exist in pastes, even those that are considered dense such as those with low water-cement ratio. As such, there is always a potential for freeze-thaw damage as long as water is available. It should also be noted that pastes subjected to freeze-thaw cycles have the potential to acquire more water with each cycle due to the micropump effect (Setzer, 1999). This water uptake has been observed experimentally by various researchers who concluded that the uptake caused by freezing and thawing can be even higher than the uptake from capillary absorption alone. Thus, the degree of saturation in the paste gradually increases. It would therefore not be surprising to observe durable behavior in cement pastes during early freeze-thaw cycles but then observe increasingly higher vulnerability with increased number of cycles.

2.2.2 The Role of Deicing Salts in Frost Damage

The above discussions have focused on classical and modern theories on frost damage in concrete; however, these discussions have not yet delved into the role and importance of deicing salts on deterioration in cold climates. It is well established that the presence of deicing salts in concrete can greatly affect its freeze-thaw durability. Harnik et al. (1980) pointed out that concretes generally exhibit lower resistance to the combined effects of frost and salts compared to frost alone. The reasons for the poorer performance in the presence of salts are not fully understood. It is nevertheless recognized that the presence of salts in solution has three fundamental effects: it lowers the vapor pressure of the solution, it depresses the freezing point of the solution (Pigeon and Pleau, 1995), and it increases the viscosity of the solution. These effects are likely responsible, at least in part, for the more severe damage to concrete. Moreover, from a phenomenological standpoint, it has been shown that salts are most damaging to concrete surfaces at concentrations of about 3 to 4 percent depending on the particular deicer (Verbeck and Klieger, 1957).

Various theories have been proposed to explain the deleterious effects of salts. These have been presented in Harnik et al. (1980) and in Pigeon and Pleau (1995) and are summarized here.

Amplification of Osmotic Pressures
The presence of deicing salts can give rise to local concentration gradients causing an osmotic imbalance. The resulting osmotic pressures would amplify those already existing due to ice-water thermodynamic imbalance (according to Powers and Helmuth's osmotic pressure theory). Salts on the surface of concrete would also enhance the vapor pressure differential between surface ice and supercooled pore water. Based on Litvan's desorption theory, the pore water would thus have a greater tendency to migrate out of the concrete. In both cases, osmotic pressures are most likely increased.

Degree of Saturation
The presence of salts in solution lowers the equilibrium vapor pressure of the solution. As a result, water molecules in the vicinity of the solution have a greater tendency to migrate towards the solution compared to pure water. This is the basis for the hygroscopicity of saline solutions. The degree of saturation in the concrete is thus increased.

Supercooling
Due to the depression of freezing point, ice crystals do not form on the surface of concrete at temperatures near 0 °C thereby causing supercooling of the pore water. When this water eventually freezes, the phase transition effects are more destructive than in normal freezing. Harnik et al. (1980) experimentally demonstrated that large supercoolings lead to faster propagation of the ice front and thus greater hydraulic pressures.

Thermal Shock
When salts melt ice on the surface of concrete, the endothermic phase transition can draw up large amounts of heat, primarily from the concrete itself. The sudden extraction of heat can cause shock-like cooling with consequent high tensile stresses at the concrete surface. These tensile stresses may be large enough to rupture the outer layers of the concrete.

Layer-by-Layer Effect
The presence of salts lowers the freezing point of the solution. If the salt concentration is non-uniform in concrete, there would also be non-uniform freezing throughout the concrete. These various regions would thus have different dilation properties from which stresses can develop. Variations in dilation could arise from differences in ice formation or from contraction of the paste (if protected by air voids).

Salt Crystallization
Salt crystal growth in large pores in concrete can occur if the salt solution becomes supersaturated. Supersaturation can arise due to evaporation of water from the solution, transport of salt ions from smaller pores toward salt crystals in larger pores, freeze concentration of the salt solution, or solution reaching eutectic conditions. The continued growth of salt crystals in pores can exert sufficient pressures on the pore walls to cause damage.

The above-described mechanisms can account at least in part for the severity of damage caused by salt solutions (i.e., any of the above or combination of the above may be responsible for the damage). It is also noted that due to the depressed freezing point of solutions, salts are beneficial to concrete by delaying ice formation. The countering of positive effects (i.e., delayed ice formation) and negative effects (described above) may be the reason behind the pessimum salt concentrations observed by Verbeck and Klieger (1957) (about 3 to 4 percent). At high concentrations, the positive effects could outweigh the damage potential of the salts, while at low concentrations, the effect of the salts may not be significant. Regardless of the damage mechanisms, it has been demonstrated that air entrainment can significantly improve the deicing scaling resistance of concrete (Pigeon and Pleau, 1995).

2.3 FREEZE-THAW DURABILITY OF DRY-MIXED CONCRETE PRODUCTS

2.3.1 Introduction

SRW units are generally considered a type of dry-mixed concrete product. Other types of dry-mixed concrete products may include concrete masonry units, concrete pavers, and roller compacted concretes. Pigeon and Pleau (1995, p. 206) define dry concretes as "*[concretes] in which the amount of water or cement paste in the mix is significantly lower than that in normal concretes.*" In these mixtures, the amount of water is carefully controlled because the stiffness of the mix plays an important role in the placement process. For instance, SRW units are demolded immediately after they are compacted, and thus a high stiffness is required for the unit to retain its shape after demolding (figure 11).

Figure 11. Photo. Demolding of SRW units during production.

Due to the low paste content of dry concretes, the void spaces between aggregate particles cannot be filled completely. Consequently, a network of irregularly shaped voids is created as was previously shown in figure 7, which compares the internal structures of ordinary and SRW concretes. These voids are termed "compaction voids" since they are formed during the compaction process (Pigeon and Pleau, 1995). The role of these voids in frost durability of dry concretes is still uncertain as will be described in the following sections. It is interesting to note that dry-mix shotcrete which also contains low water-cement ratios and is compacted pneumatically, has a very low volume of compaction voids. The cement content in shotcretes is in the range of 400 to 500 kilograms per cubed meter (kg/m^3) (674 to 843 lbs/yd^3), as batched (Morgan, 1995), which is higher than the 250 to 380 kg/m^3 (421 to 641 lbs/yd^3)for frost resistant dry-mixed concretes (see following sections). Pigeon and Pleau (1995) also explain that due to the low water-cement ratio in dry concretes, there is less mixing and dispersion of cement grains.

The presence of unhydrated cement particles may influence the frost durability of dry concretes (MacDonald et al., 1999).

The literature on SRW frost durability is fairly limited to date, because SRW construction has only become popular in recent years, and frost-related problems have only surfaced recently (SEM, 2001). There is a larger body of literature for other more established dry concrete products such as the ones mentioned earlier. Hence, this section of the literature survey examines frost-related research work performed on various types of dry-mixed concrete products.

2.3.2 Mechanisms of Freeze-Thaw Damage in Dry-Mixed Concretes

The theories of ice formation mechanisms and frost-induced damage presented in sections 2.2.1 and 2.2.2 were developed primarily for conventional structural concretes. For these concretes, ice was generally presumed to form in capillary voids, and the role of the larger air voids was to provide escape boundaries where ice could freely grow. Whether these mechanisms apply similarly to dry-mixed concretes is unresolved, largely because of the different microstructure exhibited by dry-mixed concretes compared to conventional concretes.

Detailed surveys of existing literature on frost durability of dry-mixed concretes are covered in Haisler (2004), Hance (2005) and SEM (2001). Since the body of literature on this subject is not extensive compared to ordinary concretes, there is a fair amount of overlap in these reviews comprising approximately 25 separate investigations on various types of dry-mixed concrete products. A summary of the findings is presented here.

The reviewed literature covered a wide range of dry-mixed concrete products, focusing primarily on the influence of mix composition and material properties on the frost durability of these materials. Among the various types of concrete products investigated were roller-compacted concretes (RCC), concrete masonry units, concrete paving units and SRW units that were evaluated using a variety of freeze-thaw test methods. For instance, in some studies, RCC specimens were evaluated using ASTM C 666 (2004), Procedure A methods (2004). This method involves rapid freezing and thawing of specimens fully submerged in water. In other investigations, SRW units were evaluated using ASTM C 1262 methods (2003), which involves freezing and thawing of specimens partially immersed in water. Other investigations may have involved testing concrete masonry units using ASTM C 672 methods (2004), which also involves freezing partially immersed specimens. The freezing times are, however, much longer (20 ± 1 hour), compared to that required in ASTM C 1262 (2004). As a result, it is not surprising that a fairly large range of results, observations, and performance criteria have been garnered from these investigations.

Although the reviewed literature does not point to a single frost damage mechanism in dry concretes or to a single frost durability predicting parameter, there is some general agreement with respect to certain factors affecting frost resistance. Higher compressive strengths, lower water-cement ratios, and lower absorptions have generally been observed to decrease freeze-thaw vulnerability. Specific values of these parameters depended largely on the specific material tested and the freeze-thaw method employed. For example, a minimum compressive strength of 21 MPa (3,040 psi) was suggested for concrete masonry units under “severe” exposure, while minimum compressive strengths of 50 MPa (7,250 psi) had been suggested for “durable”

concrete paving blocks. For these same paving blocks, a water-cement ratio below approximately 0.30 was required for frost durability. In a separate study on concrete pavers, minimum compressive strengths in the range of 55 to 67 MPa (8,000 to 9,700 psi), with accompanying absorption of less than 4 percent by mass, were recommended for frost durable material. In other studies on SRW units, it was shown that units displaying water absorption lower than 176 kg/m^3 had better likelihood of meeting the ASTM C 1372 (2001) freeze-thaw criterion of 1 percent maximum mass loss. In this same study, units with compressive strength higher than 62 MPa (9,000 psi) were also more likely to meet this 1 percent maximum mass loss criterion. Despite observing general trends in the durability of dry concrete products with respect to the above-described material properties, both Haisler (2004) and Hance (2005) concurred that these properties were weakly correlated to frost durability. As such, the adequacy of any of these properties as a reliable predictor of freeze-thaw performance is questionable. From their reviewed literature, these authors did find, however, that cement content was an important parameter for frost durability. Recommended minimum values ranged from 252 to 395 kg/m^3.

In the literature reviewed by SEM (2001), other factors were also investigated for their relevance to frost durability. As far as mix composition is concerned, conflicting results have been reported. While binder type and water-binder ratio were reported to be of little influence on the frost resistance of concrete pavers, the use of mineral admixtures (e.g., silica fume) was found to improve frost durability of concrete masonry units. Aggregate selection and proper curing were also mentioned as being important for the frost resistance of dry concretes. In particular, it has been reported that for SRW units, larger quantities of unhydrated cement particles existed in frost susceptible units compared to more durable units. As a result, the degree of hydration (as influenced by curing methods) was reported to be critical for SRW units.

2.3.3 The Role of Salts in Frost Damage in Dry-Mixed Concretes

In their survey of literature on frost durability of dry concretes, SEM (2001) also covered several studies related to the deicing salt scaling resistance of these concretes. This compilation by SEM comprised five separate investigations covering concrete pavers, concrete masonry units and SRW units. One of the key points identified in this survey was the fact that manufacturing processes can strongly affect the scaling resistance of paving blocks. In one study, it was noted that "it was extremely difficult to accurately evaluate the durability of the paving blocks since all productions were plagued by large variations in the properties of the paving blocks." In a similar study, it was noted that special care should be taken to "adequately consolidate" all pavers since their performance could be "strongly affected by the casting operations."

Regarding correlations to other properties, it was noted from one study that the scaling resistance of paving blocks correlated well with capillary water absorption, but less so with compressive and flexural strengths. However, in another study, no useful correlations were found to exist between the durability of the specimens and parameters such as compressive strength, dynamic modulus of elasticity, and water absorption. Other investigations also pointed toward the importance of specifying minimum cement contents that were determined to be in the range of 320 to 380 kg/m^3 to ensure durable paving units. For these same units, an average compressive strength of 65 MPa (9,400 psi), an average tensile strength of 6 MPa (870 psi), a mean unit weight of about 2275 kg/m^3 and a mean water absorption of 4 percent were typical of durable units. This same study indicated that the cement-aggregate ratio strongly influenced the frost

durability, although no values of this parameter were provided. Moreover, a maximum water-cement ratio of 0.35 was demonstrated to be a common quality among durable units.

2.3.4 Role of Air and Compaction Voids

In ordinary concretes, it is well-established that the presence of microscopic, discrete, and well-dispersed air voids helps reduce the damage caused by repeated cycles of freezing and thawing. In the case of dry-mixed concrete products however, the use of mixture designs differing from those of ordinary concretes, and the batching, casting, and curing methods produce a material that exhibits a fairly dissimilar microstructure compared to that in ordinary concretes. As a result of this, two issues arise:

- Difficulty in developing an air void system in dry-mixed concrete products.
- The role of air and compaction voids with respect to frost protection.

This section briefly reviews several recent studies and investigations which address these two issues. It will be shown that conflicting results arise and that there are no simple answers to the above issues.

2.3.4.1 Air Void Characteristics in Low-Slump Concretes (Whiting, 1985)

Whiting investigated the air void characteristics in fresh and hardened low-slump dense concretes (LSDC) which were used as overlays for highway bridge decks. This type of concrete nominally incorporates cement contents of approximately 490 kg/m^3, water-cement ratios of 0.30 to 0.32 by weight and air contents of 6.5 ± 1.0 percent. These mixes require vigorous vibration either by vibration or rodding for its consolidation. Although the cement content at about 250 to 400 kg/m^3 is higher than that in dry-concrete products, it is difficult to entrain air voids into the stiff LSDC mixture. Hence, Whiting's study focused on two objectives: establishing dosages of various air-entraining admixtures required to achieve specified air contents in the freshly mixed LSDC, and investigating the air void system of LSDC mixes meeting the specified air content.

With respect to entraining air voids, Whiting found that using neutralized vinsol resin and alkyl-benzyl sulfonate-type air entraining agents, large dosages were required to achieve the specified air contents (6 ± ½ percent) in LSDC. The required dosages of these admixtures were up to 10 times higher than that required in ordinary concretes. Once reaching its target value, the air content became less sensitive to changes in the admixture dosage. On the other hand, attempts to use other types of air entraining admixtures (alkali-stabilized, saponified natural wood resin and an organic acid salt consisting of tall-oil derivatives) were not successful in achieving the target air content, regardless of dosage.

Hardened concrete air void parameters were examined for mixes meeting the specified 6 ± ½ percent in the fresh state. For these mixes, void frequencies larger than 10 per inch, specific surfaces exceeding 39 mm^2/mm^3 (1,000 square inch/cubed inch) and spacing factors, below 125 microns (μm) (0.005 inch) were consistently obtained. The specific type of air entraining admixture used did not appear to affect these results (for mixes achieving 6 ± ½ percent air content). Whiting also reported that these mixes exhibited hardened air contents that were

approximately 1 to 2 percent lower than those measured in the fresh state. The size distribution of these air voids was also found to be finer compared to that in ordinary concretes.

2.3.4.2 Frost and Salt Scaling Resistance of RCC (Marchand et al., 1990)

Marchand et al. (1990) conducted an investigation of the frost durability and characteristics of the air void system of RCC. A total of 20 RCC loads were produced in a field test site encompassing the following variables in mix composition:

- Binder type including ASTM Type I, ASTM Type III and silica fume addition.
- Water-cement ratios of 0.27, 0.33 and 0.35.
- Cement contents in the range of 12 to 16 percent.

For the air-entrained mixes, an aqueous solution of neutralized sulfonated hydrocarbon was used as air-entraining admixture. This was added at twice the manufacturer recommended dosage, and a total mixing time of 5 minutes was maintained. For all mixes, ASTM C 666 (Procedure A, ASTM 2004) rapid freeze-thaw tests, ASTM C 672 (2004) salt scaling tests and ASTM C 457 (2004) hardened concrete air void analyses were conducted.

Marchand et al. found that the addition of an air-entraining admixture did not assist in the entrainment of air bubbles, even with higher than normal dosages. Most of the voids found were of the compaction type. It is not clear from this paper, however, how air voids and compaction voids are distinguished from one another. Large variations in total air content were determined, from as low as 2 to 3 percent to as high as 10 percent. Values of the specific surface for most mixes were lower than 25 mm^{-1}, while spacing factors were generally found to be less than 250 μm (0.010 inch). Marchand questioned the validity of applying ASTM C 457 (2004) parameters to this type of concrete, in light of the irregular shape of compaction voids observed.

As far as frost resistance is concerned, all RCC samples tested withstood 300 cycles of freezing and thawing in water without any significant deterioration. Consequently, Marchand suggested that some compaction voids may act as air voids, but that this positive influence of compaction voids should not be relied upon too heavily. The deicing salt scaling resistance of the RCC mixes was found to be poor. Reasons provided for this include interconnected compaction voids which favor saturation of the concrete, nonhomogeneity of the paste, and lack of air bubbles. From these results, Marchand also suggested that it is possible that the well-established relationship between spacing factor and freeze-thaw durability in conventional concretes does not apply to RCC.

2.3.4.3 Air Entrainment in No-Slump Mixes (Marchand et al., 1998)

In a separate laboratory study, Marchand et al. examined 21 different zero-slump concrete mixtures for their air-entrainment characteristics and hardened air void parameters. In all mixes, the cement content was fixed at 13 percent of the total mass of dry materials and the water-cement ratio maintained at 0.37. Two types of mixers were used: a counter-current pan mixer and a revolving drum mixer. Four types of air-entraining agents were used: synthetic detergent, neutralized sulfonated hydrocarbon salt, vinsol resin, and vegetable oil extract. These were added at dosages of 1 to 4 milliliters per kilogram (ml/kg) (1.5 to 6.1 fl oz/100 lbs of cement, which in

some cases represented more than 10 times the manufacturer recommended dosage. These mixes were evaluated by ASTM C 457 Modified Point Count method (ASTM 2004), pressure saturation tests (to measure the volume of capillary voids and the amount of non-connected voids) and scanning electron microscopy.

With respect to ASTM C 457 (2004) air void analysis, distinction was made between spherical air voids and compaction voids. It was determined that the spherical air void content was generally low (less than about 1.5 percent). Mixes exhibiting higher spherical air void content corresponded to those mixed in the pan mixer and employing synthetic detergent or vegetable oil extract at 4 ml/kg of cement. The total air content of the mixes was quite variable, ranging from 5.4 to 10.8 percent (by volume). The authors concluded that entraining air bubbles in no-slump mixes is difficult due to low water content in the mix. Even so, air entrainment is not impossible, depending on the type of mixer and air-entraining agent used. Scanning electron microscopy observations revealed the presence of microscopic bubbles (less than 50 μm (0.002 inch)) in the air-entrained mixes. The role of these microscopic bubbles in providing frost resistance to the concrete remained uncertain. As far as absorption was concerned, the capillary absorption was found to be generally below 5 percent despite the presence of compaction voids. Pressure saturation test results revealed that a certain percentage (3 to 4 percent) of voids were nonconnected. Hence, the authors suggested that part of the nonconnected voids could act as air bubbles during freezing.

2.3.4.4 Air Entrainment in Dry Masonry Concrete (Hazrati and Kerkar, 2000)

Hazrati and Kerkar studied the freeze-thaw durability of concrete masonry units containing an integral water repellent admixture and a "novel freeze-thaw admixture." Several mixes were produced in which the cement-aggregate ratio ranged between 11 to 18 percent, and the dosage of the above-mentioned admixtures was varied. These mixes were evaluated using the following test methods: ASTM C 1262 (2003) freeze-thaw durability in water and in 3 percent sodium chloride (NaCl) solution, ASTM C 140 (2000) compressive strength, water absorption and unit weight and ASTM C 457 (2004) Modified Point Count method.

From the freeze-thaw tests, it was generally observed that mixes containing only the integral water repellent admixture exhibited early deterioration, regardless of the cement content. Samples tested in water surpassed a 1 percent mass loss after about 30 cycles, while samples tested in saline solution showed substantial mass loss (>5 percent) after only 10 or less cycles. However, when the "novel freeze-thaw admixture" was added, the mixes showed much improved durability. The samples tested in water exhibited mass loss less than 1 percent even after 120 cycles, while samples tested in saline solution displayed less than 1 percent mass loss even after 80 cycles. With respect to air void systems, Hazrati and Kerkar reported spacing factors of 450 to 550 μm (0.018 to 0.022 inch) for non-air-entrained mixes and 200 to 300 μm (0.008 to 0.011 inch) for air-entrained mixes. From this the authors suggested maximum spacing factors of 300 μm (0.011 inch) for frost resistance in water and 200 μm (0.008 inch) for frost resistance in saline solution. Image analysis on fluorescent impregnated thin sections revealed that the degree of hydration in mixes containing only a water repellent admixture was below 50 percent. On the other hand, mixes containing the "novel freeze-thaw admixture" displayed degrees of hydration of about 70 percent. Specimen age or curing methods were not provided in this reference.

From their results and observations, the authors concluded that the "novel freeze-thaw admixture" significantly improved frost resistance in water and in saline. The beneficial effect of using this admixture was even greater than that of increasing cement content alone. This benefit was likely a result of entraining air voids into the concrete and dispersing cement grains to allow further hydration. With respect to the lower durability found in mixes with water repellent admixture, Hazrati and Kerkar (2000) suggested that "conditions that reduce permeability without drastically decreasing the porosity could be detrimental to the freeze-thaw durability of cement based materials."

2.3.4.5 Other Studies (Pigeon and Pleau, 1995 and SEM, 2001)

Pigeon and Pleau (1995) provided a brief compilation on the work done by several other researchers on the issue of air entrainment in dry concretes. They cited three separate studies in which it has been possible to introduce air bubbles to such concretes. In one study on RCC, the batching sequence had to be altered by first mixing the cement, water, air entraining agent and a portion of the aggregate. Once mixing had been carried out long enough to allow air voids to form, the rest of the aggregates were added. In the other two studies, high-energy mixers consisting of rotating blades were employed to obtain air entrainment in the mix.

SEM (2001) also covered several other investigations related to frost protection in dry concrete mixtures. With respect to RCC tested according to ASTM C 666 (Procedure A, Rapid Freezing and Thawing in Water, ASTM 2004), one study showed that the addition of air-entraining agents had a positive effect on frost durability, although there was no significant influence from the particular type of agent used. In another study, it was concluded that the frost durability of RCC was directly related to the air void spacing factor, with a maximum suggested value of 250 μm (0.010 inch). This same study also suggested showed that non air-entrained RCC could be to a certain degree resistant to frost. Hence, it was concluded that compaction voids could offer similar frost protection to concrete as entrained air voids.

2.3.4.6 Summary of Studies on Air Entrainment and Compaction Voids

In general, it is apparent that issues relating to air entrainment and frost protection are distinct for dry-mixed concretes compared to ordinary concretes. In ordinary concretes, the use of air entrainment has been shown to improve frost resistance and deicing-salt scaling resistance. The necessity of air voids for frost protection in dry concretes is still contested, however. The issue of air entrainment itself has led to conflicting views. While some studies showed that air entrainment is extremely difficult to achieve regardless of the dosage of admixture used, other studies showed that air entrainment was possible under certain conditions. It appears that the specific type of air-entraining agent used, the mix composition, the type of mixer used and perhaps even the batching and mixing procedures employed played important roles in determining the success in entraining air voids. At the other end of the spectrum, Hazrati and Kerkar (2000) showed that with nominal amounts of a "novel freeze-thaw admixture," good air void systems could be achieved and frost durable masonry units were obtained.

The roles of air and compaction voids in providing frost protection to dry concretes still remain unexplained. Marchand et al. (1998) reported that while some field and laboratory investigations

tended to indicate that some compaction voids can act as air voids and offer frost protection, other reports have demonstrated that non-air-entrained, no-slump concretes are vulnerable to frost damage. The connectivity of these compaction voids has been cited as being a critical parameter, since some researchers suggested that isolated compaction voids may act as air voids. On the other hand, connected voids can increase saturation and exacerbate frost damage.
The validity of ASTM C 457 (ASTM 2004)parameters in characterizing the void system of dry concretes has also been questioned by several authors. This is because the equations in ASTM C 457 (ASTM 2004) were developed assuming spherical voids uniformly dispersed in the cement paste. This hypothetical void shape and spatial distribution is even less valid in dry-mixed concrete than in conventional concrete. In dry-mixed concretes, interconnected compaction voids may dominate. Consequently, the relationships developed between spacing factor and freeze-thaw durability for conventional concretes may not be valid for dry concretes. Hence, it has been suggested that the actual role of compaction voids during freeze-thaw conditions must be first understood before establishing any relationships between ASTM C 457 (ASTM 2004) parameters and frost durability in dry concretes.

2.4 SUMMARY

This chapter summarized some of the main published works to date on the frost durability of conventional concrete, SRW blocks, and other dry-mixed concrete products. Through this discussion, it is quite evident that the mechanisms of frost damage and salt scaling are not completely understood for conventional concrete, and this understanding is even less when considering SRW blocks and other dry-cast products. Lack of understanding with regard to SRW block durability can be attributed to several factors, including the relative newness of the SRW market (compared to conventional concrete), the unique nature of SRW block microstructure, and the general lack of scientific publications on the topic. Based on this review, the need for comprehensive research on the frost resistance of SRW blocks is quite evident, and the efforts detailed in the rest of this report aim at addressing these needs.

CHAPTER 3: FIELD EVALUATION OF SRW BLOCKS

3.1 INTRODUCTION

As described in section 1.3, the discovery of various deteriorated SRW blocks (from freeze-thaw damage) in highway applications led to concerns within the SHA community, resulting in tighter specifications, and in some cases, restrictions on new SRW construction. These concerns also resulted in the initiation of the FHWA-funded research described in this report. As part of the current project, the research team discussed this durability issue with various SHAs and also visited SRW installations throughout North America to inspect for frost/salt damage. The overwhelming majority of SRWs visited during the course of this project are performing very well, even in cold climates. However, there are some SRWs that are performing very poorly in cold climates, and the observed deterioration can be quite severe. The observed damage, without exception, was found in SRW blocks that were exposed to deicing salts (or fertilizer runoff) and numerous freeze-thaw cycles.

This chapter highlights the key findings from the most comprehensive field survey initiated under the project, which was conducted in cooperation with SHA engineers from Wisconsin and Minnesota in August 2003. The remainder of this chapter describes this field evaluation, provides a summary of the conditions of the SRWs that were inspected, and describes testing performed on SRW blocks procured from selected SRW installations.

3.2 FIELD EVALUATIONS OF SRWS IN WISCONSIN AND MINNESOTA

Overall, seven different in service walls were examined in Wisconsin, and seven were examined in Minnesota. These walls were all located near Madison, WI or St. Paul, MN, and the walls to be viewed were selected based on feedback from members of the SHAs in Wisconsin and Minnesota. Walls were selected based on location, exposure conditions, and distress levels. Of the walls visited, five in Wisconsin and seven in Minnesota showed significant freeze-thaw damage. This is not an indicator of the condition of the walls in general for either State, as most of these walls were chosen because the presence of damage had been previously recognized. This does, however, give insight as to how damage is occurring and at what locations.

The research team was able to locate and photograph existing walls and document their level of damage, as well as identify walls from which to obtain samples for future laboratory testing. The research team was also able to obtain feedback from DOT members regarding the state of existing walls and construction and repair methods currently being used. In addition, various other SRWs (e.g., county or city installations, commercial properties, etc.) were informally inspected during this field study, with the same general trend in behavior—that is, most of the SRWs are performing as expected, but a minority of the walls show the same type of distress as seen in highway applications for SRWs located where deicing salts or fertilizers are applied.

3.2.1 Types of Distress Observed in SRW blocks

For the blocks showing significant deterioration, the most common distress manifested itself in scaling of the exposed surface (front and/or top). Figure 12 shows a typical example of this

deterioration, which tended to be most prevalent closest to the roadway or where exposed to direct/indirect runoff of deicing salts from above (e.g., from bridge or pavement at higher elevation). Distress was also typically most pronounced for cap units (i.e., top block on SRW), as illustrated in figures 12 and 13. Discussions on the key role that exposure to deicing salts plays in SRW block deterioration are presented next, along with further discussion on the unique nature and behavior of cap blocks.

Figure 12. Photo. Typical deterioration of SRW blocks with scaling most pronounced for cap units.

Figure 13. Photo. Severely damaged cap units on otherwise healthy wall.

For a given SRW installation, the blocks with the most direct exposure to moisture, and especially salts, tended to exhibit the most distress. Walls located below, or at the edge of parking lots consistently showed the same pattern of heavily deteriorated blocks located directly in the path of drainage, while other blocks located not in the drainage path showed little or no

freeze-thaw damage. The moisture draining over these particular walls would likely be very strong in salt content due to the application of salt on the parking lot being pushed to the edge of the lot and accumulating in snow piles that eventually will melt, creating saline solution draining over the wall. Blocks exposed to saline solution have shown consistently worse freeze-thaw durability when compared to those exposed to pure water in a laboratory setting, as discussed in chapter 4. Figure 14 shows that the damage at areas of water and salt runoff from a parking lot can be so severe that whole portions of the wall can lose their serviceability. Interestingly, portions of the wall not directly in the path of drainage showed little sign of freeze-thaw damage.

Another example of microclimate or exposure-related distress can be seen in figure 15 in which a large multiwall SRW installation adjacent to a freeway exhibited excellent performance away from and above the roadway, but the blocks closest to the roadway (and hence salt spray) showed significant distress. This is an interesting case where the both wall sections (upper and lower) were constructed from the same SRW blocks, but only the lower wall section (lower portion of figure 15), which was about 2.5 m (8 ft) from the roadway, exhibited distress. There was heavy cracking in the cap block units of this wall and moderate damage to the body of the wall. One last example of the vivid effects of microclimate or exposure conditions can be seen in figure 16, in which a wall located beneath a bridge overpass shows very severe damage only in the section of wall that receives direct runoff from the overpass. Sections either sheltered from the elements by the overpass or located a “safe” distance from the direct runoff were in good shape.

Figure 14. Photo. Effects of drainage and salt exposure from parking lot above SRW.

Figure 15. Photo. Deteriorated SRW blocks closest to roadway (bottom of photo) and undamaged SRW blocks farthest from roadway.

Figure 16. Photo. Severe damage of SRW blocks in direct path of drainage from bridge overpass above.

The idea of salt spray action leading to further deterioration of the walls has been thought of as the main issue in freeze-thaw durability for some time. Although the exposure to saline solution from road salts being sprayed against the wall is a more severe exposure condition than pure water, the effects of salt spray were not as noticeable as other exposure conditions such as drainage, which can lead to a higher degree of saturation of the blocks. This is especially the case when the poor drainage allows saltwater (from deicing salts) to penetrate into the blocks. The reason salt spray may not be of as much concern as poor drainage could be due to walls salt sprayed not actually being exposed to as much moisture and salt as walls receiving exposure due to poor drainage. Although some salt will reach the wall through snow plowed adjacent to the wall, this snow could actually protect the wall from any additional road salt being sprayed onto the wall. There is also the possibility that the areas which are located in the spray zone are protected from going through as many freeze-thaw cycles as other sections of the wall because the areas in the spray zone are subjected to large piles of snow during freezing months. These piles of snow next to the wall may actually provide insulation for the wall, causing it to go through fewer freeze-thaw cycles than the portion of the wall where snow piles are not present. The role of salt spray and the exact amount of moisture and salt it imparts upon a given wall is still unclear. However, what is evident is that the presence of salt, whether from salt spray or runoff, is required for serious deterioration to occur. This observation also validates the need for laboratory-based testing using saline solutions.

The examples in figures 12 through 16 clearly show that exposure to deicing salts (typically NaCl or lately magnesium chloride ($MgCl_2$) for highways), coupled with freezing and thawing cycles, can lead to distress for certain SRW blocks. An interesting observation made during this field survey was that other chemicals, particularly fertilizers, can have a similar detrimental effect on SRW blocks. Walls exposed to drainage from areas such as golf courses also showed severe damage when compared to walls exposed only to water. The blocks that were directly exposed to the runoff of water containing large amounts of chemicals (phosphates or nitrates) from fertilizer were heavily distressed when compared to blocks on the same wall not exposed to fertilizer. As is the case with saltwater, water with significant amounts of these chemicals has proven to be highly detrimental to the freeze-thaw durability of SRW blocks when compared to those exposed only to water in a laboratory environment. Figure 17 shows a wall severely damaged due to exposure to runoff high in phosphates from an adjacent golf course. It is obvious that a large number of the blocks show complete deterioration, and adjacent blocks show severe cracking on the top face.

Figure 17. Photo. Deterioration of SRW blocks due to exposure to fertilizers from adjacent golf course.

As stated previously, the most common form of distress observed in SRW blocks was the progressive and sometimes severe loss of mass, which was worst for cap units and when blocks suffered from poor drainage or direct exposure to salts. However, in a smaller number of cases, macrocracking was observed. For example, in the wall shown in figure 18, large cracks were located near the back, formed-face of the wall, perhaps indicating heavy internal damage, which leads to microcracking and finally large cracks that reach the surface of the block. Although this type of cracking was most evident in cap blocks, there were some cases where relatively large cracks appeared in noncap blocks, with this type of distress typically accompanying the more common scaling and significant mass loss shown in figures 12 through 16. This may indicate that, like conventional concrete, damage to SRW blocks due to freezing and thawing in the presence of deicing salts can lead to both surface scaling and internal damage caused by freezing water.

Figure 18. Photo. Cap block experiencing scaling of front face and macrocracking towards the back of the blocks.

In reviewing the various types of distress in SRW blocks and the influencing parameters, it is evident that the cap blocks consistently displayed more freeze-thaw damage than the blocks from the body of the wall. It is not clear whether this is solely a result of the top course of blocks being exposed to much worse conditions or if the cap blocks themselves are that much more susceptible to freeze-thaw damage. It is likely that both of these factors play into the cap blocks receiving more damage, but more research on why cap blocks behave differently than the wall blocks is needed. Once the cap units are significantly damaged, it is much easier for the damage to progress below to the next row of blocks as there is now a direct path for water and saline solutions. Cap blocks are typically cast separately from the blocks used for the main body of the wall. Cap units may contain a different mix design than the wall blocks, have a different geometry, and receive different levels of compaction (mainly due to size and shape of block). Many of the cap blocks are rectangular and much shorter than the blocks used for the body of the wall. The cap units typically have less stringent freeze-thaw requirements when compared to the wall block, which is mainly a function of ease of replacement of damaged cap blocks when compared to wall blocks.

Although cap blocks tend to show the most distress, freeze-thaw durability problems are not limited to these top blocks. There are cases where the main blocks also suffer from deterioration, especially when exposure conditions are severe. This is especially the case when walls are constructed at an angle (as opposed to vertical), with blocks staggered in a stair step fashion.

This can lead to exposure to excessive moisture (and salts) due to ponding of water or snow and an increase in the ingress of water into the block. The added amount of moisture can cause blocks with exposed surfaces to have an area of weakness near the exposed horizontal surface and/or have overall worse freeze-thaw performance throughout the block. Although the presence of staggered blocks can lead to more frost damage for those blocks with inherent poor frost resistance, blocks that are durable with regard to frost resistance are generally not impacted by this block configuration.

Figure 19 shows a wall that is staggered much like a set of stairs. On this particular wall, approximately 25 mm (0.98 inch) of the top face of each block was exposed, and this exposed area showed considerably more damage than the other sections of the block. The exposed horizontal section of the blocks exhibited major cracking and some signs of scaling. On many of the lips of the wall in Figure 19, the top layer (approximately 6–13 mm (0.24–051 inch)) had been degraded or could be physically removed using little force, due to horizontal cracks reaching the vertical surface of the block. The front, vertically aligned faces of the blocks on this wall did not show significant freeze-thaw damage, reaffirming the idea that the exposed horizontal surface can be harmful from a freeze-thaw durability standpoint for those blocks that are not inherently resistance to freezing and thawing damage.

Figure 19. Photo. Deterioration of exposed vertical surfaces of SRW blocks.

Other walls, like the one shown in figure 20, make use of block geometries that tend to result in part of the horizontal top surface being exposed. The exposed portion of the block, where water or snow would be allowed to accumulate shows much worse damage on the exposed surface compared to the front facing of the block. The wall in figure 20 had cracks on the top layer that reached the top surface and front face of the block, causing portions of the block to chip. Scaling was also present, mainly at the corner of the block where the exposed horizontal face meets the exposed vertical face of the block. This pattern of much worse damage on an exposed horizontal face can also be seen in cap units, as mentioned previously. It should be noted that the block geometry and wall design shown in figure 20 perform well in the vast majority of applications. It

is only when using nondurable SRW blocks in particularly aggressive environments (exposure to salts) that the exposed horizontal surface can exacerbate distress.

Figure 20. Photo. Another example of deterioration of exposed horizontal surfaces of SRW blocks.

Inspecting inservice walls exhibiting freeze-thaw damage allowed the research team to look at a wide range of the factors involved in the issue. Although the performance of a wall is influenced primarily by the properties of the blocks (e.g., frost and salt resistance) being used, other issues can affect the freeze-thaw performance of walls. The exposure conditions, block geometry, and wall configuration can play key roles in the performance of SRWs, and these issues should not be overlooked when designing new SRW installations. These issues are beyond the scope of this project, which focuses exclusively on the inherent frost and salt scaling resistance of SRW blocks, but discussions were provided on the relevance of each of the above issues for completeness. In addition to visually inspecting the various SRWs in Wisconsin and Minnesota, the research team also procured SRW blocks from selected walls for subsequent evaluation in the laboratory, as described next.

3.2.2 Laboratory Evaluation of SRW Blocks Procured From Inservice Walls

SRW blocks were obtained from three SRWs for laboratory evaluation. These walls were chosen for sampling because of ease of access to the walls and differing distress levels. Blocks were obtained and tested from one wall in Minnesota and two walls in Wisconsin, as shown in table 1. The Wisconsin samples obtained included two blocks from a wall (WI-2) where the distress levels within the wall varied between very poor and very good (figure 21). One of these blocks was exhibiting severe distress and was part of the original wall construction; the other was a block that had replaced a block that had deteriorated to the point that replacement was necessary. Another Wisconsin wall (WI-4, shown in figure 22), which was in quite poor overall conditions, was selected for sampling, and a block exhibiting severe distress from this wall was obtained for testing. One block exhibiting severe distress was taken from the Minnesota SRW, which could be classified as being in very poor condition as a whole (figure 23).

Table 1. Blocks from in situ SRWs obtained for laboratory evaluation.

Wall ID	Block Location Within Wall	Block Condition	ASTM C 1262 Samples
WI-2-2	Second row, edge of wall under drainage	Good	3 saline, 3 water
WI-2-3	Third row, edge of wall under drainage	Poor	3 saline, 3 water
WI-4	Top row, edge of wall at drainage path	Poor	3 saline
MN-4	Top row, edge of wall at drainage path	Poor	4 saline

Figure 21. Photo. Blocks obtained from SRW in Wisconsin (WI-2).

Figure 22. Photo. Blocks obtained from SRW in Wisconsin (WI-4).

Figure 23. Photo. Blocks obtained from SRW in Minnesota (MN-4).

3.2.2.1 Test Methods for SRW Blocks Procured From Inservice Walls

Upon receipt of the SRW blocks, they were saw-cut for freeze-thaw testing (ASTM C 1262, (2003) tested in water/and or 3 percent NaCl solution) microstructural analysis. Two of the samples were also profile grinded to determine the concentration of chlorides as a function of distance from the front block surface. For the ASTM C 1262 (2003) tests, after 24 hours of testing, additional water or saline solution was added to containers if the fluid level had dropped (due to absorption) below a depth of 12.7 mm (5 inches). Mass loss of specimens was recorded

at regular intervals during the test (note that tests were conducted until either significant mass loss was measured (greater than 20 percent) or 100 cycles were reached. Much more detailed information on the specifics of ASTM C 1262 (2003) is provided in chapter 4.

Microscopic air-void analysis was conducted on the SRW units described previously according to the procedures of ASTM C 457, "Standard Test Method for Microscopical Determination of Parameters of the Air-Void System in Hardened Concrete, Procedure B—Modified Point-Count Method" (2004). One of the challenges in conducting air-void analysis of SRW concrete was caused by the presence of the irregularly shaped and possibly interconnected compaction voids. As a first approximation, a compaction void is simply defined as a void in which less than three-fourths of its boundary is a paste-void interface, while an air void is defined as a void in which more than three-fourths of its boundary is a paste-void interface. As such, it is not necessary for a void to be completely surrounded by paste to be classified an air-void. This arbitrary definition was based on the fact that in ordinary concretes, certain air bubbles (entrapped or entrained) are not entirely surrounded by paste and may be partly bounded by an aggregate particle or by another air bubble. However, when using this definition in the examination of SRW units, any spherical shaped bubble completely surrounded by paste would be considered an air-void (as in the classical model for entrained air bubbles) and largely connected voids would be considered compaction voids. More discussion on SRW microstructure and air-void characteristics is provided in chapter 4.

Chloride penetration analysis was conducted on field samples WI-4 and WI-5. A strip from the middle of the test unit spanning from the front face to the rear was examined and powder mortar samples were retrieved at various depths from the front face of the sample using a profile grinder. The mortar dust was collected using a vacuum pump and an aerosol filter system. The standard test method for measuring the total chloride content in mortar or concrete using the specific ion probe was used to identify the chloride thresholds at various depths from the face of the samples. This test method is based on a chloride test method developed by the Strategic Highway Research Program 1992 (SHRP-S/FR-92-110 1992). The specific ion electrode was calibrated using a set of predetermined concentrations of NaCl solutions prior to testing the SRW dust samples. Readings were taken for each calibration solution and a linear regression was performed.

3.2.2.2 Test Results for SRW Blocks Procured From Inservice Walls

All of the block samples obtained from in situ SRWs performed poorly in ASTM C 1262 (2003) when tested in 3 percent NaCl solution, with each sample exhibiting complete deterioration (e.g., 100 percent mass loss) before reaching 10 freeze-thaw cycles. This behavior is not surprising, given the generally poor field performance of the SRWs from which the blocks were taken. The durability of selected blocks tested under ASTM C 1262 (2003) using water (instead of saline) was also not good, as shown in figure 24. All of the WI-2 samples suffered at least 1 percent mass loss by about 75 cycles, and mass loss was severe soon after passing this typical threshold value for mass loss.

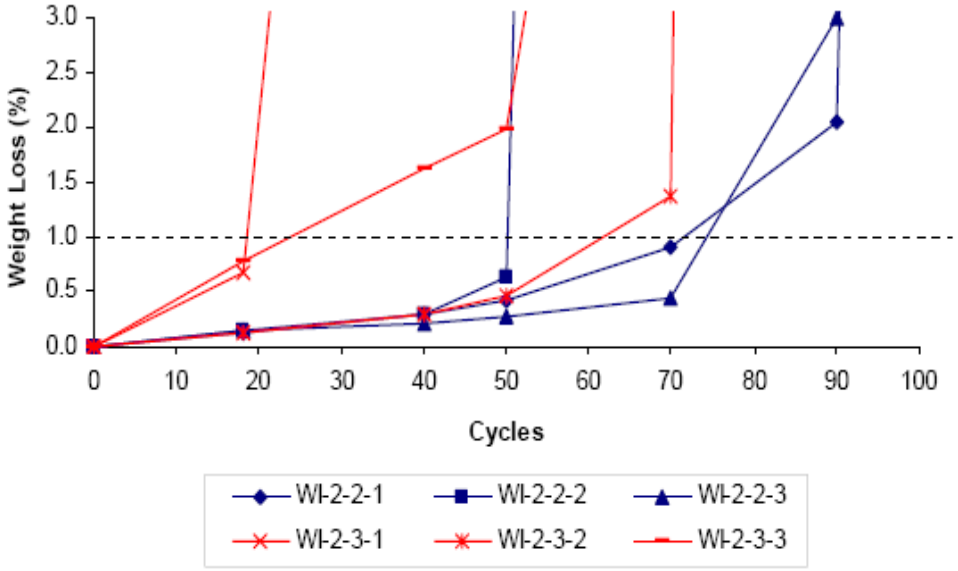

Figure 24. Graph. ASTM C 1262 test results for blocks obtained from Wisconsin SRW (WI-2), with samples tested in water.

Microscopic analyses of all of the field units indicated internal characteristics similar to those of other nondurable blocks studied in detail in chapter 4. All the blocks displayed regions with large compaction voids and low paste contents, which contributed to the poor performance under ASTM C 1262 (2003) testing (in saline and for some, in water). Examples of the typical microstructure of these poorly performing SRW blocks is shown in figure 25.

Figure 25. Photo. Internal structure of block from Wisconsin SRW (WI-4), showing large compaction voids and low cement paste content.

The results of chloride profiling on SRW blocks exhibiting distress in highway applications clearly show that chloride contents are extremely high (compared to conventional concrete), and

based on the literature review (chapter 2) and laboratory program (chapter 4), it is not surprising that blocks with this type of microstructure performed poorly when exposed to freeze-thaw cycles. Typical results of chloride profiling are shown in figure 26, in which it can be seen that the chloride levels are extremely high, especially in the outer 10–15 mm (0.39–0.59 inch) of the blocks (that is, the first 10–15 mm (0.39–0.59 inch) from the front face of the blocks). Such high salt concentrations are expected to adversely affect block performance based on the various mechanisms described in chapter 2 (e.g., freezing point depression, increased osmotic pressure, salt crystallization, etc.).

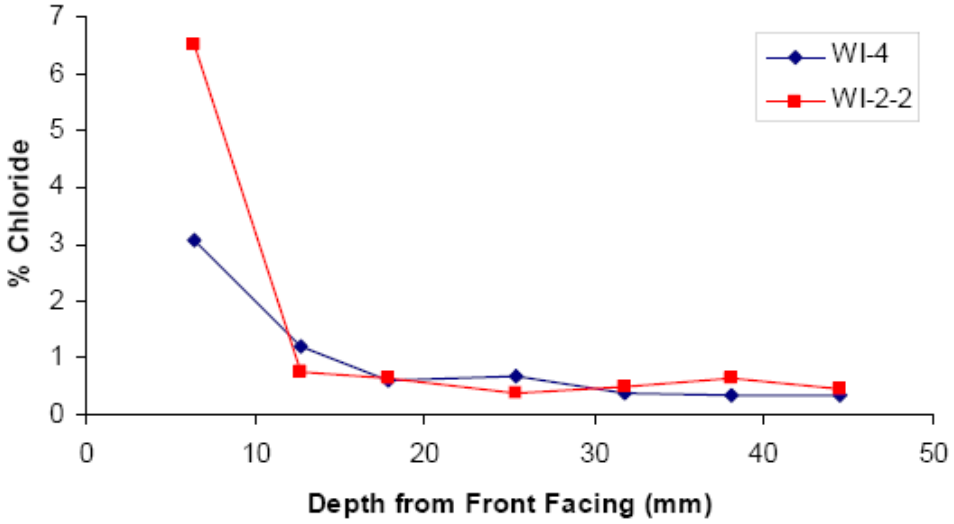

1 mm = 0.039 inch

Figure 26. Photo. Typical chloride concentrations for SRW blocks exhibiting poor field performance (data for WI-2 and WI-4, SRWs from Wisconsin).

3.3 SUMMARY

This chapter summarized some of the key findings from field evaluations of SRWs in Minnesota and Wisconsin. The overall findings are consistent with other visual observations from SRW installations in other cold weather regions—that is, most SRWs have performed very well, with very little sign of frost damage or salt distress. However, this chapter clearly shows that there are some cases where durability-related problems with SRWs are quite severe, confirming the need for research to address the problem. These field evaluations clearly show that exposure to both moisture (e.g., rain or snow) and salts is a prerequisite to damage, strongly suggesting that any attempt to assess durability in the laboratory should include saline solutions as part of the testing regime. Although the type and amount of distress observed in some SRW installations is quite troublesome, it is reassuring that SRW blocks can and are currently being produced that seem to be quite resistant to both freezing and thawing cycles and salt exposure. Thus, the challenge is identifying which types of SRW blocks will be most durable, based on accelerated laboratory testing, and being able to specify test methods that will discern good from poorly performing blocks. The laboratory program described in the next chapter focused on this challenge and provides guidance on how best to assure long-term durability of SRWs, even in severe environments.

CHAPTER 4: LABORATORY EVALUATIONS

4.1 OVERVIEW

This chapter summarizes a comprehensive laboratory evaluation focusing on the frost resistance (with and without salts) of SRW blocks. The chapter is based upon the research described in Chan (2006), Hance (2005), and Haisler (2004), as well as the other technical documents produced under this FHWA project (see section 1.4). Because of the extensive amount of laboratory work performed in this project, efforts have been made to synthesize the key research and to present only the most important and relevant results with an eye toward which ones can or should be implemented into accelerated test methods and specifications to ensure long-term durability of SRW blocks in aggressive, cold environments.

Much of the research described in this chapter is related to ASTM C 1262 (2003), which was the most commonly used test method for assessing freeze-thaw durability of SRW blocks when this project was initiated. Because this method was being used and/or specified by a number of SHAs, including those States that reported durability problems associated with SRWs, the decision was made from the onset of this project to focus on refining and improving reliability and reproducibility of the test. To elaborate on this point, it should be noted that ASTM C 1262 (2003) test had received significant criticism from end users due to concerns over the repeatability of test results, even within one set of samples from the same lot of SRW blocks. There were also questions as to the actual relation between the test results and field exposure conditions and performance. Given the shortage of previous published research on this general topic (frost resistance of SRW blocks) and on this specific issue (test methods to predict field performance), fundamental research was initiated to improve the understanding of the distress mechanisms associated with SRW blocks and in properly testing potential SRW blocks for use in aggressive environments. Figure 27 shows the overall scope of research that was performed on the various aspects of ASTM C 1262 (2003), with the basic information on each of the areas of concentration. It is not feasible to discuss in detail all of these aspects of the research program; figure 27 provides the reader with the overall scope of the efforts launched under this project. It should also be noted that some of the research focusing on damage assessment methods was performed in a separate research project funded by National Concrete Masonry Association (NCMA), but this work was performed by essentially the same research team as the FHWA project, and the work was done parallel to the research described in this project report. Only a brief synopsis of these NCMA-funded efforts is presented herein.

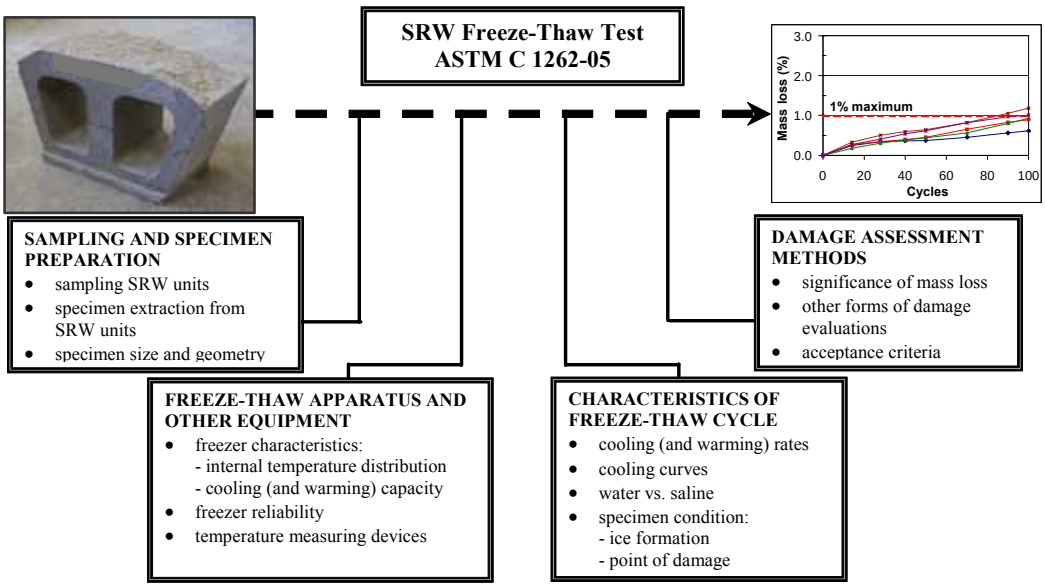

Figure 27. Diagram. Concentration groups for the evaluation of ASTM C 1262 test method.

The remainder of this chapter is organized as follows:

- Sampling of SRW blocks for laboratory evaluation, including studies on spatial variations of properties within SRW units. *Goal was to provide better guidance on prudent sampling and testing of SRW units.*
- Issues related to ASTM C 1262 (2003), including variability in exposure conditions within chamber, temperature control and monitoring, and relation between testing regime and damage mechanisms. *Goal was to provide better guidance on testing methodology to improve repeatability and to better capture mechanisms that relate to field performance.*
- Evaluation of SRW properties that best relate to frost resistance in the laboratory and field. *Goal was to develop frost indices that can be used to predict durability, based in part on key SRW block properties.*
- Role of various deicing salts (and other compounds) on durability of SRW blocks. *Goal was to compare damage observed in SRW blocks when exposed to common deicing salts, other salts found in nature (e.g., sodium sulfate), or fertilizers.*
- Evaluation of full-scale approach to testing full SRW blocks in simulated exposure conditions. *Goal was to determine if more realistic testing conditions in the laboratory would better relate to actual distress mechanisms and manifestations in the field.*

4.2 SAMPLING CONSIDERATIONS FOR SRW BLOCKS

One of the initial steps in the freeze-thaw testing of SRW units involves extracting test specimens from representative units. These steps are covered in sections 6 and 7 of the ASTM C 1262 (2003) standard. The specific manner in which a laboratory technician selects the units and

extracts test specimens from them may influence the outcome of test results, as will be described in this section.

Before proceeding further, a brief overview of the manufacturing process is provided. SRW units are manufactured in block plants typically by compacting (while simultaneously vibrating) concrete mixes into steel molds, followed by immediate removal of the molds. The shaped units are subsequently conveyed to curing chambers maintained at elevated temperatures and humidity where the units are kept for a certain time period (which may be variable) before being withdrawn. In one plant visited in early 2004, residence time of SRW units in the curing chamber was understood to last anywhere from 1 to 3 days, depending on production schedule. In many cases, units are cast as sets of conjoined pairs, which are then split in the middle to produce a natural-looking or "split face" fractured surface. Following splitting, the units are stacked on pallets and stored in a nonstandard manner. These steps are illustrated in figures 28 through 31. From this description and in reference to figure 32, the following locations on the units are identified for the solid and hollow units shown in the figure:

- Front face (split face): natural-looking fractured surface that is used as the exterior face of the wall.
- Back face: surface opposite and parallel to split face.

Figure 28. Photo. Units immediately after demolding.

Figure 29. Photo. Units prior to entering curing chamber.

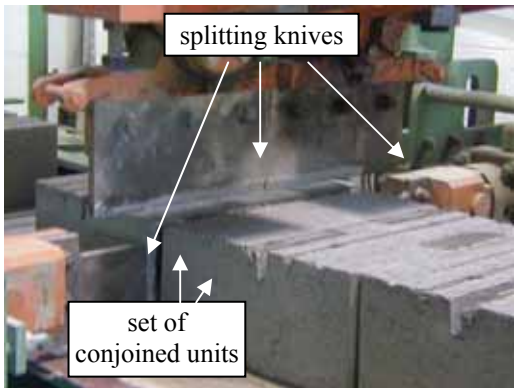

Figure 30. Photo. Splitting of conjoined units.

Figure 31. Photo. Split face of units.

Also shown is the height, H, of the units for which 200 mm (8 inches) and 150 mm (6 inches) are common dimensions. For the rest of this report, the term unit will be used to refer to a whole block as produced in manufacturing plants, as shown in figures 32 and 33. Specimens or coupons are typically cut from the units for testing such as ASTM C 140 (2000) tests for compressive strength, absorption and density and ASTM C 1262 (2003) freeze-thaw tests. ASTM C 1262 (2003) uses the words specimens and coupons interchangeably, as does this report.

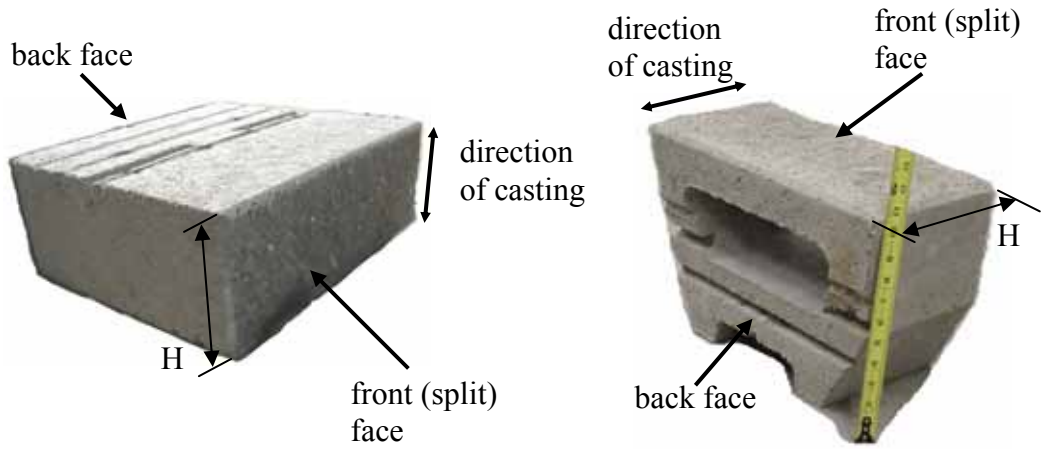

Figure 32. Photos. Definition of terms: SRW units (or blocks).

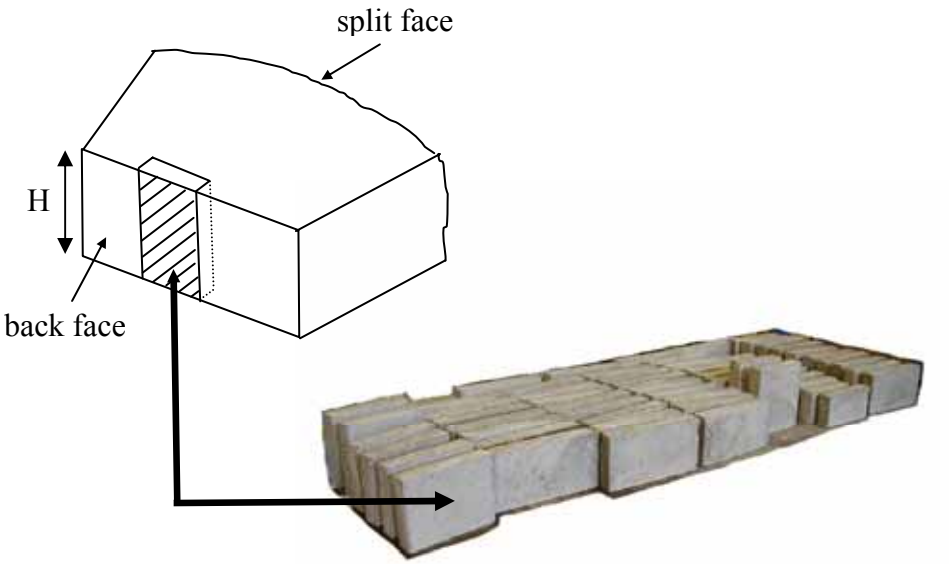

Figure 33. Drawing and photo. Definition of terms: test specimens (or coupons).

4.2.1 Current Sampling Guidelines

In the procurement of test specimens from SRW units, there are two levels of sampling. The first is sampling of SRW units from lots (defined below) and the second is extraction of test specimens from individual units. This research project did not investigate the first level of sampling in detail; however, some general comments are provided. As for sampling units from lots, section 6 of ASTM C 1262 (2003) states the following:

> Clause 6.1:
> "Select whole units representative of the lot from which they are selected. The units shall be free from visible cracks or structural defects."
>
> Clause 6.2
> "Select five units for freezing and thawing tests."

Meanwhile, ASTM C 140 (2000) defines "lot" as follows (Clause 4.1.2):

> Any number of concrete masonry units of any configuration or dimension manufactured by the producer using the same materials, concrete mix design, manufacturing process, and curing method

While this clause provides a generalized statement of what a "lot" encompasses, various details of this definition still remain unclear. The length of production time (1 year, 1 month, one project or one batch) during which "the same materials, concrete mix design, manufacturing process, and curing method" were used is not clear. The manner in which units are to be selected from the lot also remains vague. For example, are units to be randomly sampled as they come out of the production line, or are units to be sampled from pallets during storage at the block plant or at a jobsite? ASTM C 140 (2000) includes curing method as one characteristic of a lot, but it does not necessarily imply curing time or duration. Production plant logistics play a role in determining how long SRW units are kept in the curing chamber. This is critical because the overall quality of concrete varies with early-age curing; and whether units are cured for 1 day or 3 days plus curing conditions (temperature and relative humidity) impact the quality of the material. Furthermore, depending on ambient weather conditions, the storage condition of the SRW units is critical, as illustrated by the picture in figure 34. Units sampled from within a pallet that is shrink-wrapped may be of different quality than ones from unprotected pallets, as shown in this figure.

When extracting test specimens from SRW units, ASTM C 1262 (2003) requires "saw-cutting solid coupons (test specimens) from full sized units" (Clause 7.1), and for units with exposed nonplanar surface which could be split, fluted or ribbed, the coupon should be cut "from another flat molded surface" (Clause 7.1.1). Aside from these statements, there is no further indication of where or how these specimens should be sampled within parent units. As will be discussed in the next sections, material properties within SRW units vary systematically with location, and thus a simple random scheme for specimen extraction (whereby specimens are extracted from random locations over a unit) may not work. An alternate method known as stratified random sampling is shown to reduce variability. The challenge in sampling equally applies to ASTM C 1262 (2003) specimens extracted for freeze-thaw testing or ASTM C 140 (2000) specimens extracted for material property determination.

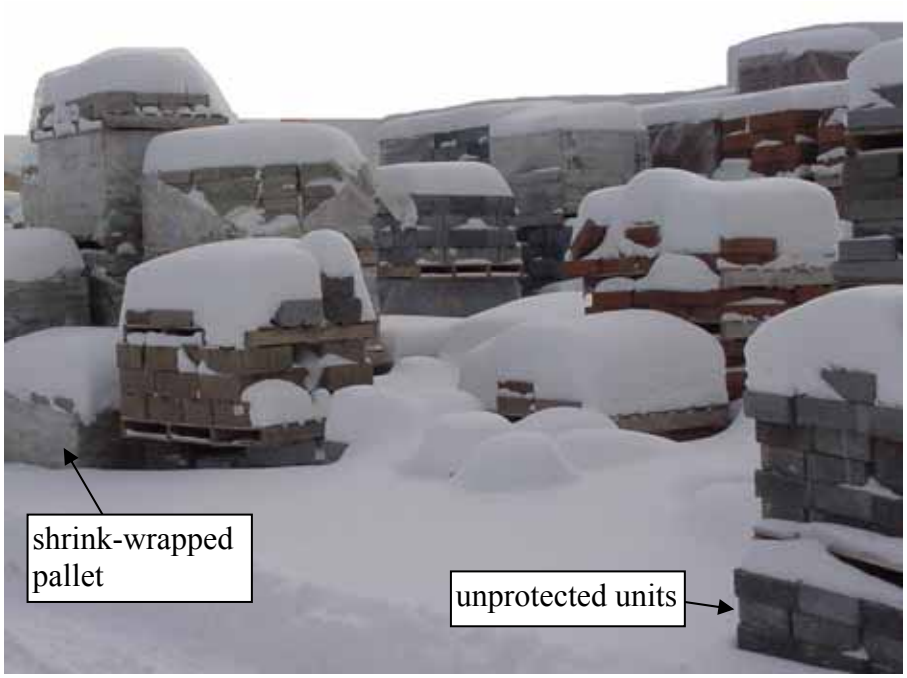

Figure 34. Photo. Possible exposure condition of units in winter weather.

Two different philosophies with respect to sampling are possible depending on the intended purpose of the tests. These are:

- Tests to evaluate the performance of as-manufactured units for comparison of mixture designs, manufacturing methods or quality of raw materials.
- Tests to evaluate the performance of units to be installed in projects.

In the first case, it may be desired to sample whole units and extract specimens from these units in such manner that variability between test specimens is reduced. Ways in which this can be achieved are described in this chapter. For site acceptance of units, however, it is more sensible to sample units that are most vulnerable (i.e., of lowest quality among the population of units) and to extract specimens from the most vulnerable locations within the unit. The following sections describe how quality varies over a unit and how knowledge of this variation helps with the decision on choosing samples from units.

4.2.2 Spatial Variability of Material Properties

4.2.2.1 Within-Manufacturer Variability

Studies were conducted to investigate spatial variation in selected material properties in SRW units obtained from a single block manufacturer (Chan et al., 2005a and b). These units are depicted in figures 35 through 38. Figures 35 and 36 were referred to as large wall unit, and figures 37 and 38 were referred to as small wall unit. Specimens from each of these types of SRW units were extracted in the manner shown in the figures and tested for flexural strength to ASTM C 78 (ASTM 2002), flexural elastic modulus, 24-hour absorption to ASTM C 140

(2000), and boiled absorption to ASTM C 642 (ASTM 2002). An example of the spatial distribution in the 24-hour water absorption observed in these units is shown in figures 35 through 38. The values shown in this figure are average values across each of the rows of specimens shown (i.e., four specimens per row in the front face of large wall units, two to three specimens per row in the back face of large wall units, and two to three specimens per row in the small wall units). Three units were tested for each type of wall unit (large or small), and each of these units showed similar patterns in the measured properties, as follows:

- Along the casting direction, material at the bottom layer of a block (i.e., material first deposited during casting) displayed the lowest absorptions out of all sampling locations on that particular face (front or back face). On the other hand, material in the middle layer displayed the highest absorptions of all sampling locations on that particular face. Material in the top layer exhibited absorption values that were intermediate to those of the bottom and middle layers.
- Along a direction from the front (split) face towards the back face, values of water absorption exhibited a decreasing trend away from the front face. This trend was evident in small wall units where specimens taken from nearest to the front face exhibited the highest absorption values, specimens on the back face exhibited the lowest values, and specimens in between exhibited intermediate values. In the case of large wall units, this trend was also evident from the lower overall absorption of back face specimens compared to front face specimens.

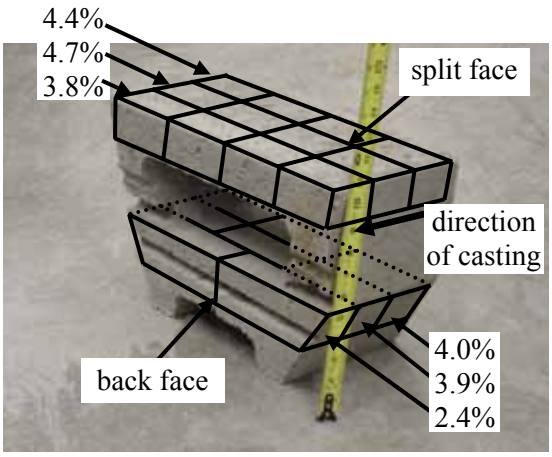

Figure 35. Photo. Percentages in spatial distribution of absorption in large wall unit.

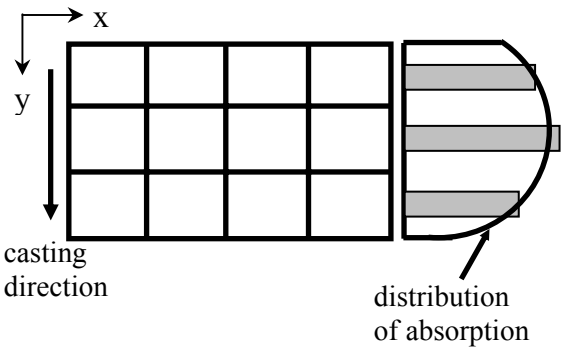

Figure 36. Drawing. Distribution of absorption in large wall unit.

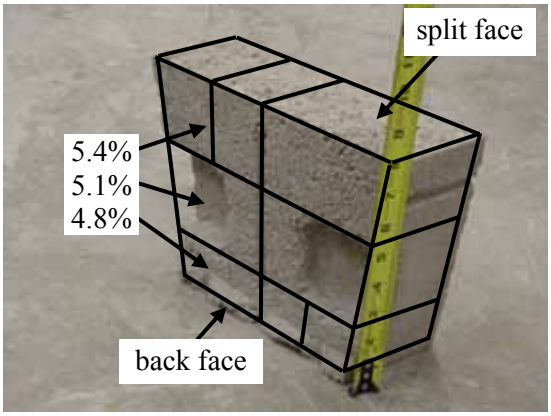

Figure 37. Photo. Percentages in spatial distribution of absorption in small wall unit.

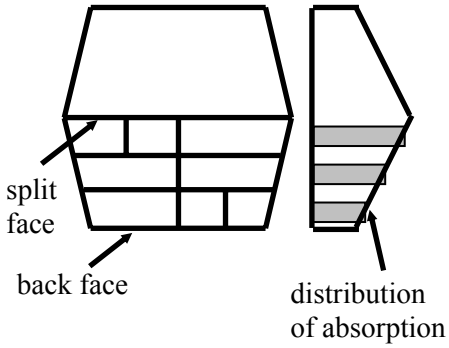

Figure 38. Drawing. Distribution of absorption in small wall unit.

Flexural strength and flexural elastic modulus, followed the same trend, although inverse of absorption (i.e., locations exhibiting lower absorptions displayed higher flexural strength and flexural elastic modulus, while locations exhibiting higher absorptions displayed lower flexural strength and flexural elastic modulus). These patterns altogether suggested that the material in the middle layer on the front face was likely of lowest quality (highest absorption and lowest flexural strengths and moduli) in the unit, while material in the back face was likely of higher quality (Chan et al., 2005a). A general linear model (GLM) analysis (Ott 1993) was also performed on the absorption data to verify the statistical significance of trends at the 95 percent confidence level (Chan et al., 2005b). This model confirmed a parabolic distribution of absorption along the casting direction (along the y-axis shown in the figure with maximum absorption in the middle layer), and a linear distribution of absorption in a direction from front to back face (with maximum absorption at the front face and minimum at the back face). These distributions are depicted in figures 35 through 38. No statistically significant distributions were detected along the x-axis.

Systematic spatial variations of properties in the SRW units tested suggest that the specific method of sampling alone can lead to disparate test results. For instance, on the front face of the large wall unit shown in figures 35 and 36, water absorption values of specimens in the middle layer were 24 percent higher than those in the bottom layer; while on the back face, water absorption values of specimens in the middle layer were up to 60 percent higher than those in the bottom layer. This indicates that extraction of test specimens from random locations without consideration of the forms of distribution augments test variability. To reduce apparent variability due to the spatial distributions of properties, an alternate sampling scheme known as stratified random sampling (as opposed to simple random sampling) can be employed (Chan et al., 2005b). The difference between these two methods is shown in figure 39 for sampling from 12 possible locations on the face of an SRW unit. In simple random sampling, replicate specimens in a test set are randomly extracted from the various locations, tested for a particular material property and their results averaged. On the other hand, in stratified random sampling, specimen sampling is carried out in a more systematic manner reflecting the expected distribution of properties (Lohr, 1999). For the types of distribution observed here, an equal

number of specimens is extracted from each of the rows or strata (three shown in Figure 39) to form the test set. Other size test sets consisting two or five specimens can also be selected under stratified random sampling, but the computation of average value of the measured property for the test set needs to be adjusted accordingly. Details on this calculation are covered in Chan et al. (2005b). This technique yields results that are more representative of the overall unit and is shown to reduce the apparent variability in test results. For the population of front face specimens, it is demonstrated that test variability (as measured by coefficients of variation) is reduced by approximately one-third when using stratified random sampling as opposed to Simple Random.

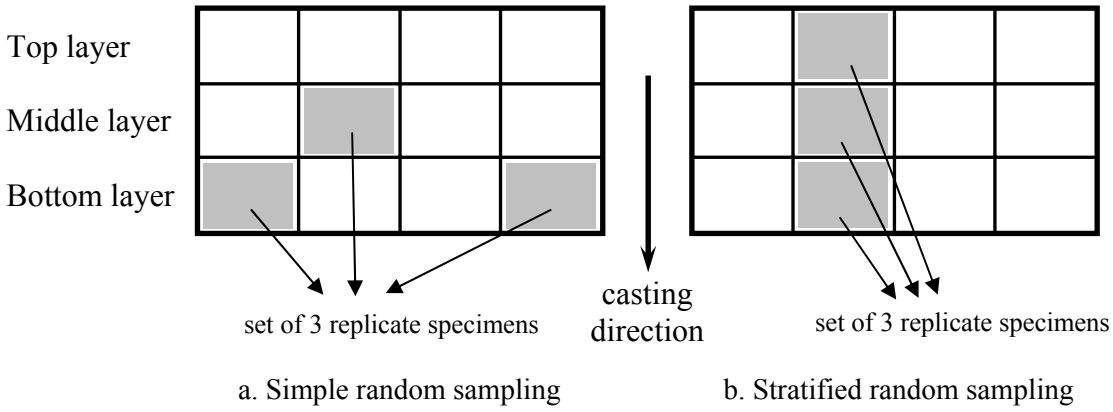

Figure 39. Drawings. Simple random versus stratified random sampling from the face of an SRW unit.

It should be emphasized that stratified random sampling yields results that are more representative of the entire SRW unit and with lower variability. This approach may not be applicable in cases where the quality of the entire SRW unit (i.e., at every location on the unit) needs to comply with minimum quality standards, such as ASTM C 1372 (2003) for compressive strength, absorption, and density. In these cases, sampling from the middle layers is preferred because material in this layer is typically of lowest quality in a given face of the unit. Compliance with specifications of this middle layer thus increases the likelihood that the unit overall is satisfactory.

4.2.2.2 Between-Manufacturer Variability

The studies described in the previous section focused on systematic spatial variations in material properties in SRW units from a single, residential-grade manufacturer. Further investigations were conducted to determine whether similar trends also existed in SRW units from other manufacturers producing commercial grade units. SRW units from four major block manufacturers (identified as Manufacturers A, B, C and D) were also evaluated for systematic spatial distributions of properties. Complete details and results of this investigation on spatial variability are provided in Chan et al. (2006c). A brief discussion is presented here.
Each of the four participating manufacturers were asked to provide two grades of SRW units:

- Units that complied with local DOT specifications.
- Units that did not necessarily satisfy DOT specifications but considered satisfactory for typical commercial use (non-DOT).

DOT units generally possessed denser internal structure with higher paste volume and lower compaction void volume, and freeze-thaw durability compliant with ASTM C 1372 (2003) or State specifications. On the other hand, most non-DOT units had a leaner internal structure and contained larger volume of compaction voids. The various types of SRW units were then labeled as follows: A-D (for Manufacturer A, DOT unit), A-N (for Manufacturer A, non-DOT unit), B-D, B-N, C-D, C-N, D-D and D-N. Mixture designs, production methods or curing, and storage details of these units were not available. Similar block samples from each manufacturer were also tested using ASTM C 1262 (2003) (in water and saline), and these results will be discussed later in this chapter.

For these units, only the front (split) faces were evaluated, and specimens were extracted at approximately 25 to 50 mm (0.98 inch to 1.96 inch) from the split surface, as shown in figure 40a. As in the previous studies, three layers along the casting direction were also considered. Figure 40b shows the features on the side faces of the SRW units that were used as position references to identify the exact locations of specimen extraction. These side faces were referred to as either lipped/grooved (containing intentional indentations, ledges, or both), and flush side (consisting of a smooth surface with no features).

Material properties evaluated in these SRW units included the following:

ASTM C 140 tests
- 24-hour absorption.
- Oven-dry density.

ASTM C 642 tests
- Boiled absorption.
- Volume of permeable voids.
- Specific gravity after immersion and boiling 24-hour absorption.

ASTM C 457 tests
- Air void content.
- Compaction void content.
- Paste content.
- Specific surface.
- Spacing factor.

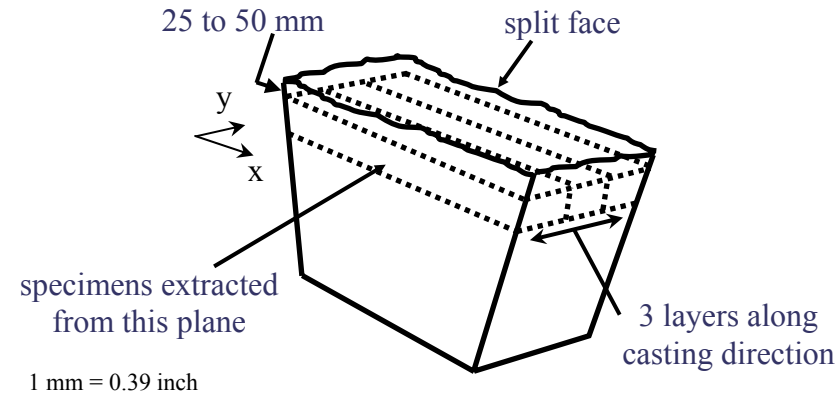

a. Location of test specimens.

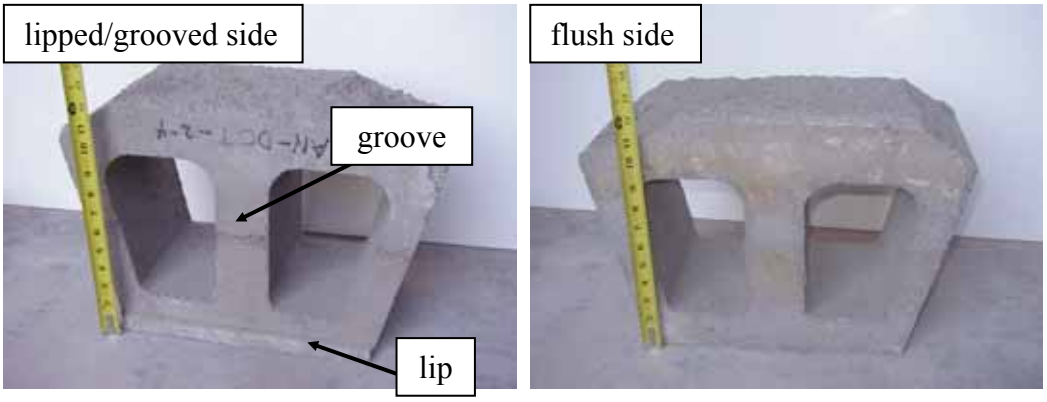

b. Lipped/grooved side of SRW units evaluated. c. Flush side of SRW units evaluated.

Figure 40. Drawing and photos. Sampling of test specimens from SRW units from different manufacturers.

Examples of the spatial distribution exhibited by some of these properties are shown in figure 41 for ASTM C 642 (2002) boiled absorption, figure 42 for volumetric paste content, and figure 43 for volumetric compaction void content. The values shown in these figures represent the average absorption value of specimens in each of the layers shown (typically three to four specimens per layer). As with the SRW units described in section 4.2.2.1, variations in the measured values of these properties could arise depending on where samples were extracted from. For example, for unit C-D, samples taken from the middle layer showed 23 percent higher boiled absorption, 3 percent lower paste contents, and 63 percent higher compaction void contents compared to samples extracted near the lipped/grooved side. Also, as with the SRW units described in the previous section, the middle layer showed highest absorption of all sampled locations on this particular face.

A perhaps more significant observation was the consistency in the locations where maximum or minimum values occurred for various properties. As demonstrated in figures 41, 42, and 43, boiled absorption was generally highest in the middle layer of the units, which is also where paste volume was generally lowest and compaction void volume highest. Oven-dried density was also lowest in this layer (Chan et al., 2006c). Although these observed relationships in the properties were as expected, the consistency in the locations where maximum values occurred

indicated that the above distributions were not random, but systematic in nature. These trends occurred similarly for all manufacturers and SRW unit grades evaluated, suggesting that these distributions in properties were likely tied to the manufacture of SRW units. As before, stratified random sampling methods would be more applicable for these units compared to simple random sampling.

From the preceding sections, it is evident that spatial distributions of material properties in SRW units were systematic in nature, and their statistical significance was demonstrated for units from a single manufacturer. While it is suspected that these distributions are related to manufacturing processes such as compaction and curing (Chan et al. 2005a), the existence of these patterns lead to several consequences. First, from a mix qualification standpoint, there may be units of lower quality compared to the ones tested here where sampling location could make the difference between compliance and noncompliance. For example, if the overall average water absorption of a given unit was hypothetically right on the specification limit for this property, specimens extracted from the middle layers would be found noncompliant, while specimens extracted from the outer layers would be found compliant. Second, due to spatial distributions of properties, the interpretation of material variability, operator variability or test method variability will be affected by sampling location. For the units described here, a laboratory technician who consistently chose to sample from the middle layers would obtain different results from a technician who consistently chose to sample from the outer (top and bottom) layers. Finally, the observed spatial patterns in various material properties such as absorption, flexural strength, compaction void content, and density imply that other properties such as permeability and freeze-thaw durability will vary from location to location within an SRW unit.

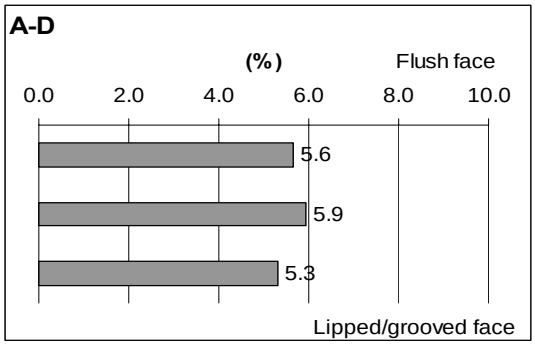

a. A-D Blocks

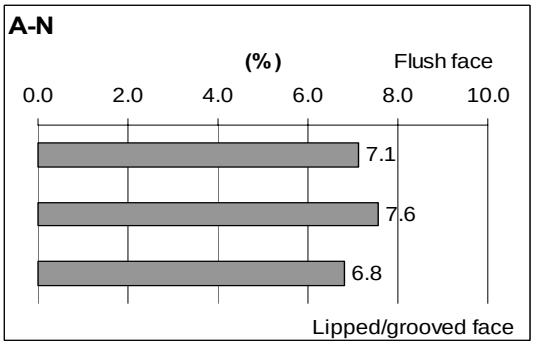

b. A-N Blocks

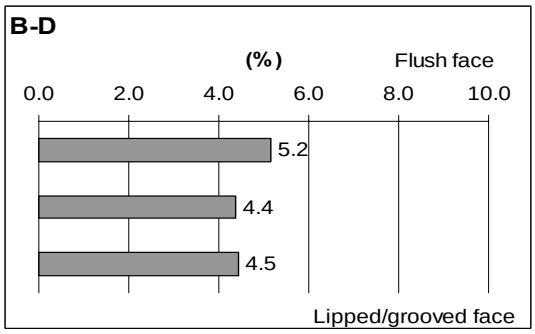

c. B-D Blocks

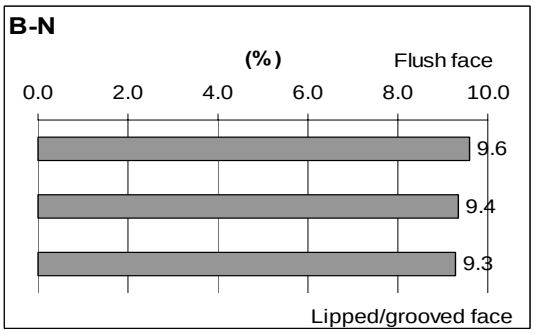

d. B-N Blocks

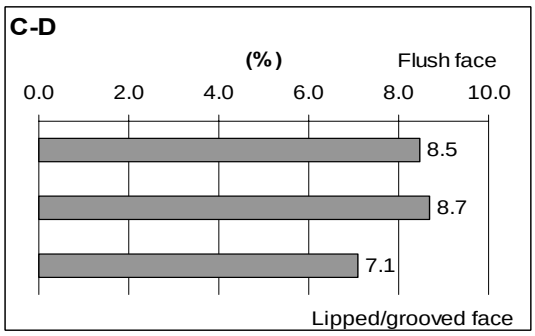

e. C-D Blocks

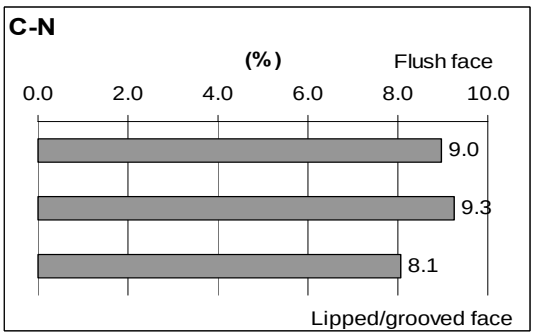

f. C-N Blocks

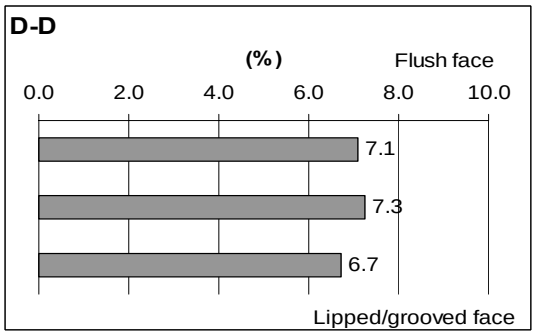

g. D-D Blocks

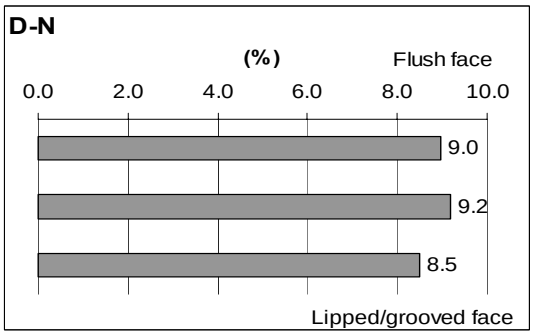

h. D-N Blocks

Figure 41. Graphs. Spatial distributions of ASTM C 642 boiled absorption on split face of SRW units (values shown represent mass of absorbed water as percent of mass of oven-dried specimen).

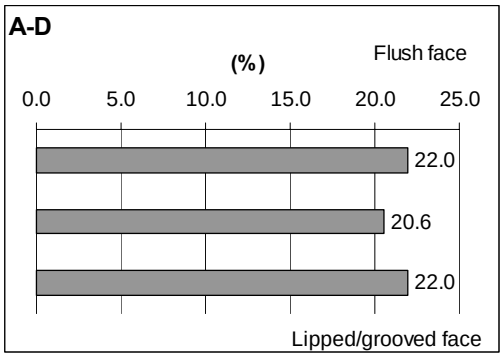

a. A-D Blocks

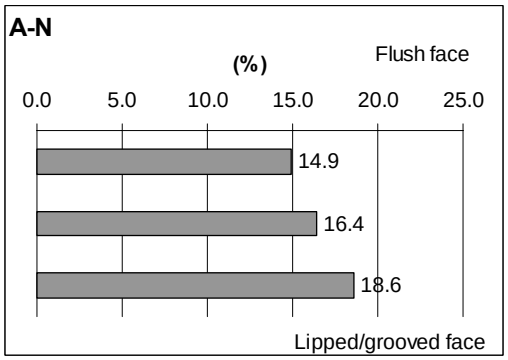

b. A-N Blocks

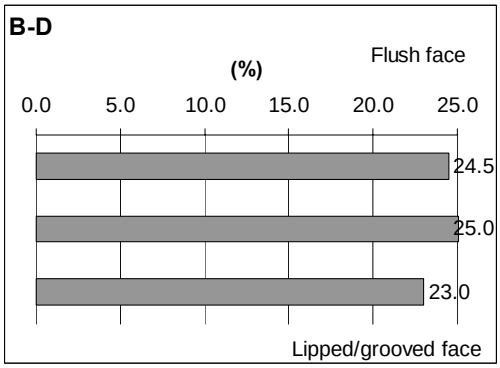

c. B-D Blocks

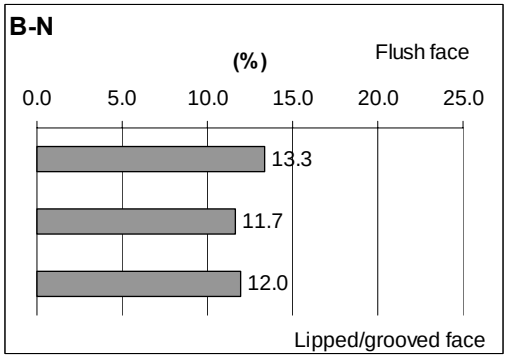

d. B-N Blocks

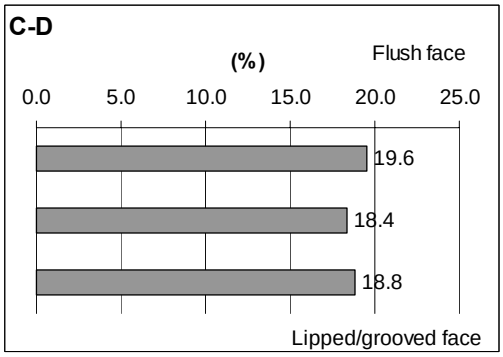

e. C-D Blocks

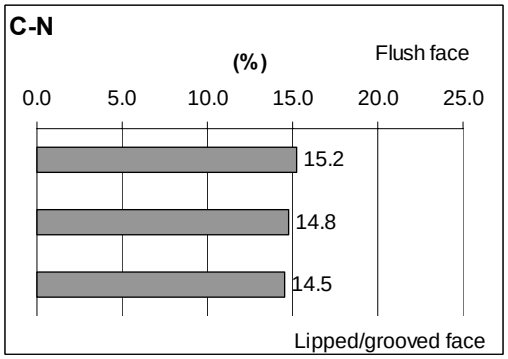

f. C-N Blocks

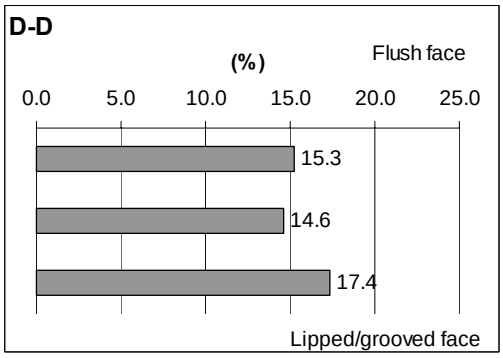

g. D-D Blocks

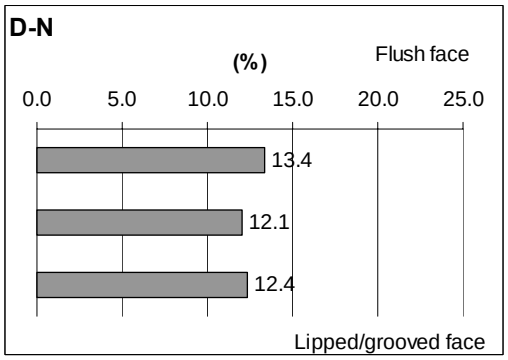

h. D-N Blocks

Figure 42. Graphs. Spatial distributions of volumetric paste content.

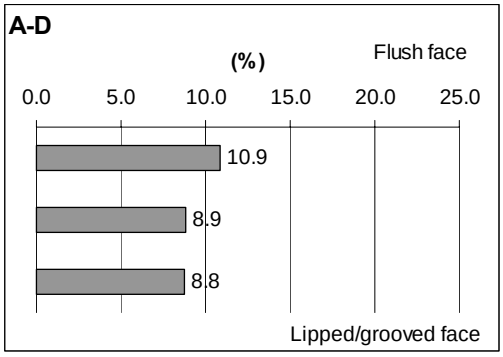

a. A-D Blocks

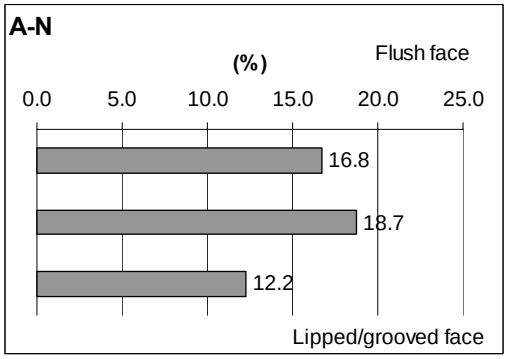

b. A-N Blocks

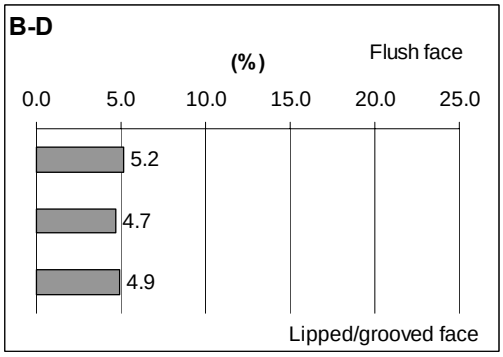

c. B-D Blocks

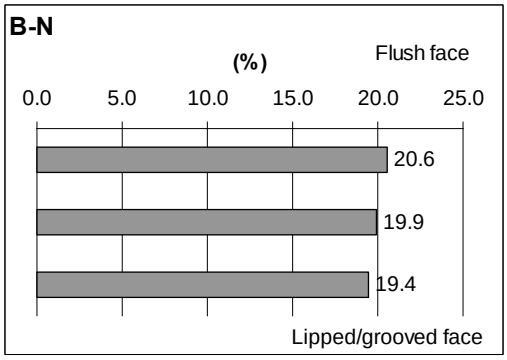

d. B-N Blocks

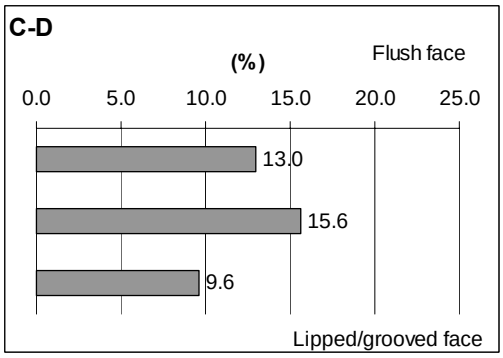

e. C-D Blocks

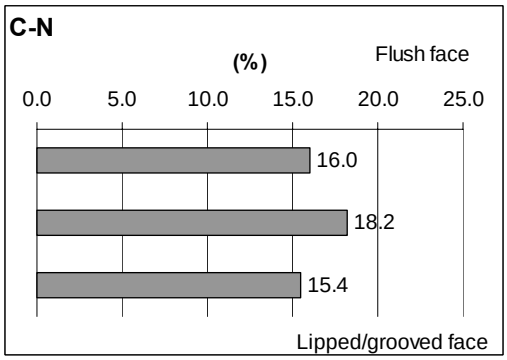

f. C-N Blocks

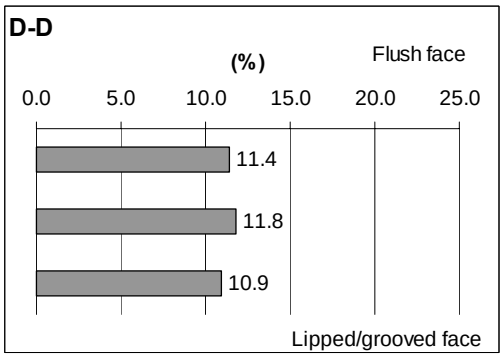

g. D-D Blocks

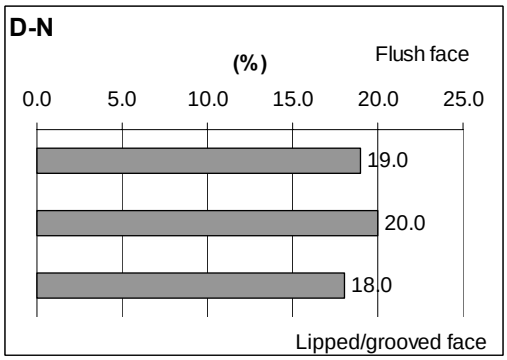

h. D-N Blocks

Figure 43. Graphs. Spatial distributions of volumetric compaction void content.

4.2.3 Split Face Delamination

One advantage of SRW systems rests on the aesthetic appearance offered by the front split surface of the SRW units. A closer look at this surface, however, often reveals thin delaminations or cracked sections of varying sizes, as shown in figures 44 and 45. These cracked sections are referred to here as split face delaminations. Chan et al. (2006a) discuss the possible origins of these delaminations, as well as the significance these may have on the evaluation of SRW unit condition both in the field and in the laboratory. As for their cause, it is suspected that split face delaminations are created in the manufacturing of SRW units during the splitting process. As shown earlier in figures 28 through 31, splitting of conjoined units is accomplished by pressing steel knife edges at the preformed notch location to be split and forcing the units to crack at this plane. Cracks emanating from the edges of the units may merge as they approach one another, as shown in figure 46a, leaving behind fractured sections in the split plane. This interaction between approaching cracks was simulated using a linear elastic fracture mechanics model (using the software FRANC2D, Cornell University, 2002) shown in figure 46b. The fractured sections left behind after crack merging are believed to constitute split face delaminations. Further support to this suggested mechanism was obtained from visual observations at a local manufacturing plant. Figure 46c shows a view of the split face of one unit immediately after being split, where a detached split face delamination is seen.

Figure 44. Photo. Sample A of split face delaminations on SRW units.

Figure 45. Photo. Sample B of split face delaminations on SRW units.

During field inspection, split face delaminations can mislead an inspector to attribute this feature as environmental damage or deterioration of the SRW unit. This confusion is enhanced by the fact that such features occur at the split surface of SRW units, which is also the surface in direct contact with the environment. During actual freezing conditions, water can seep into the space between the delamination and the SRW unit and expand upon freezing, thereby "jacking" the delaminated piece out of position (figure 47). Figure 48 shows a detached delamination under frost conditions. This mechanism may thus be interpreted as being frost-related damage during routine field inspection. One way that split face delaminations can be distinguished from other forms of damage is by the nature of the cracked and/or broken off residues. As shown in the previous sections, delaminated pieces tend to be thin and slender sections on the SRW split surface. On the other hand, frost degradation typically consists of crumbly material which appears in addition to cracking in the units, as shown in figure 49. Another point of distinction

involves the quantity of fractured material. While split face delaminations tend to occur as single and isolated pieces, frost damaged material usually appears as more than one broken piece.

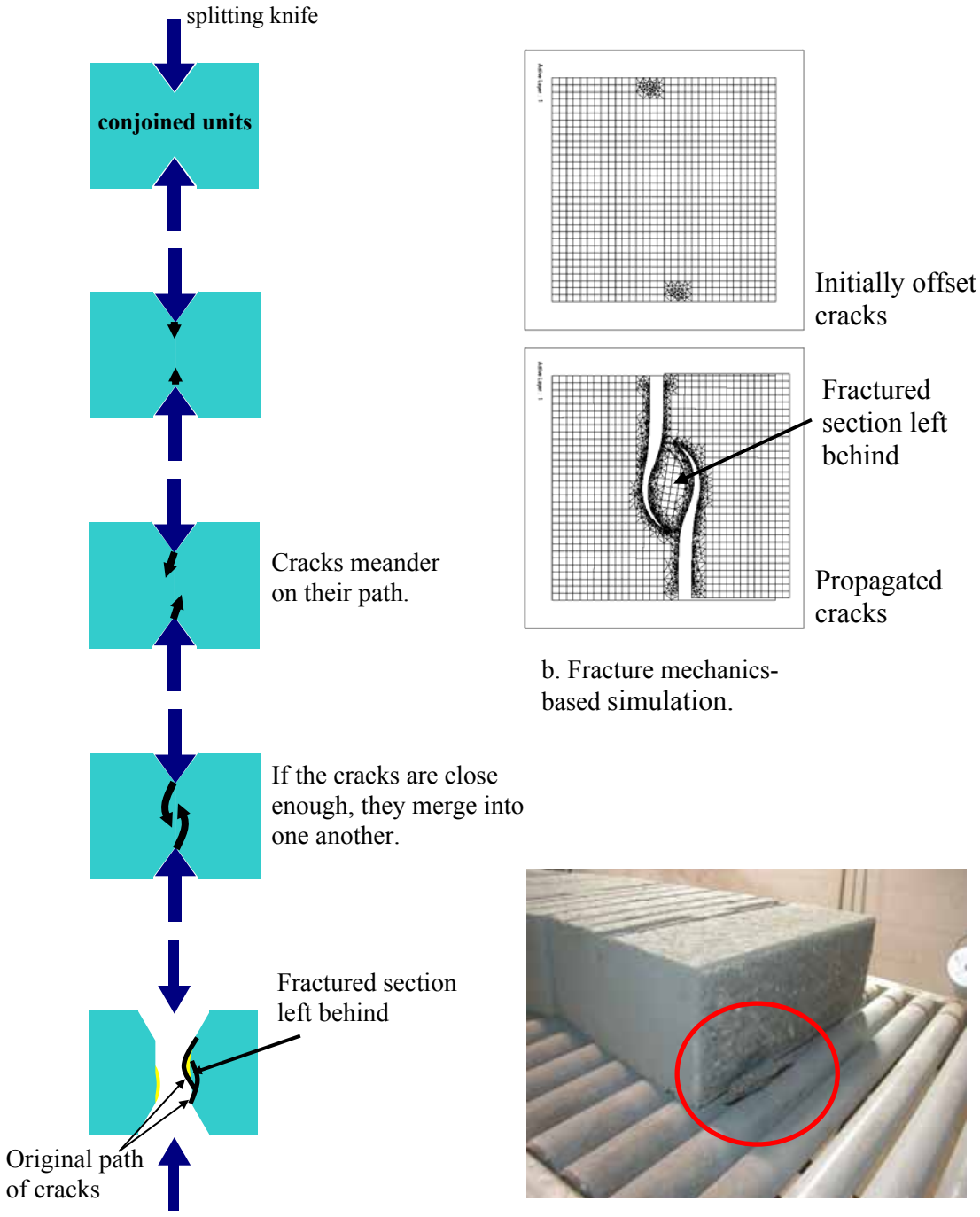

a. Splitting process.

b. Fracture mechanics-based simulation.

c. Observations at block plant.

Figure 46. Drawings and photo. Suspected cause of split face delaminations.

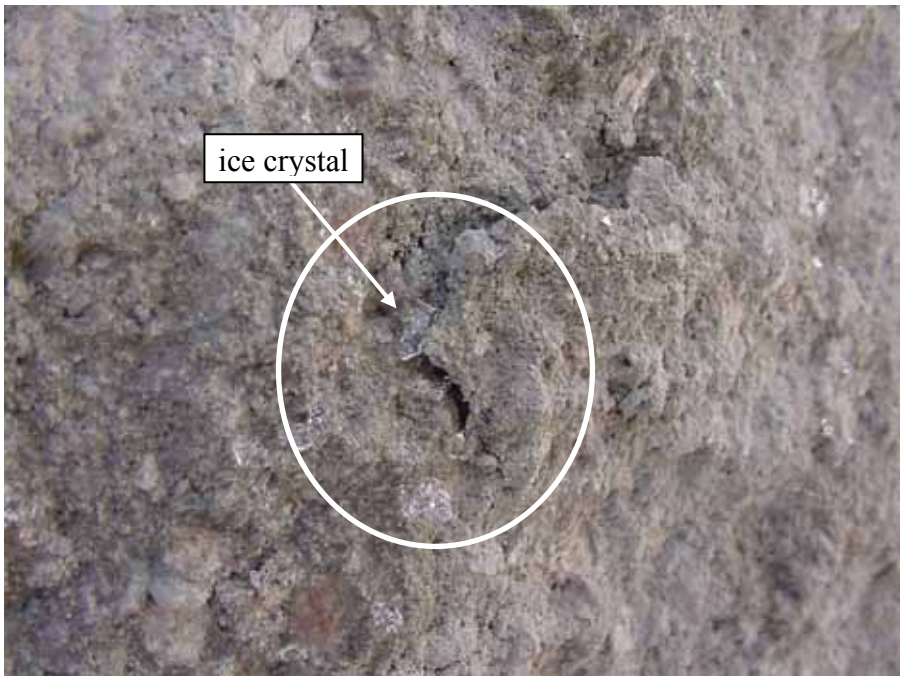

Figure 47. Photo. Breaking off of split face delamination due to ice "jacking" action in field SRW units.

Figure 48. Photo. Detached split face delamination under frost conditions in field SRW units.

Figure 49. Photo. Freeze-thaw damage on SRW unit in field.

As for testing SRW units in the laboratory, perhaps the most critical issue with split face delaminations concerns the inclusion of these loose pieces in test specimens. While these delaminations are commonly observed on the surface of units as thin shallow pieces, it is not improbable that the cracks penetrate deeper into the units. Figure 50 shows a section through the split face of an SRW unit that was shipped directly from a manufacturer to Cornell without previous exposure in the field. The size of the cracked section is approximately 130 mm long (5.12 inches) and up to 20 mm deep (0.79 inch), and it is also possible that microcracks exist in the vicinity of the main crack shown. The concern is that, if a laboratory technician extracted specimens from the split face region of a unit containing these delaminations, results from tests (e.g., strength, absorption, freeze-thaw resistance) conducted on these specimens will be misleading. To prevent this, the technician must thoroughly inspect test specimens for cracks or loose pieces prior to testing them. If loose pieces are only prevalent on the specimen surface, these pieces can pried off; however, if the specimen is cracked, the cracked portions must be trimmed off from the specimen by saw-cutting; otherwise the test specimen should be discarded and another one extracted from the parent unit. An alternate and more reliable solution is to entirely avoid extracting samples from the split face region and sample from a different surface such as those shown by the dashed lines in figure 50a. Avoiding the extraction of specimens from the split face is currently a requirement in ASTM C 1262 (2003) as mentioned in section 4.2.1 of this chapter.

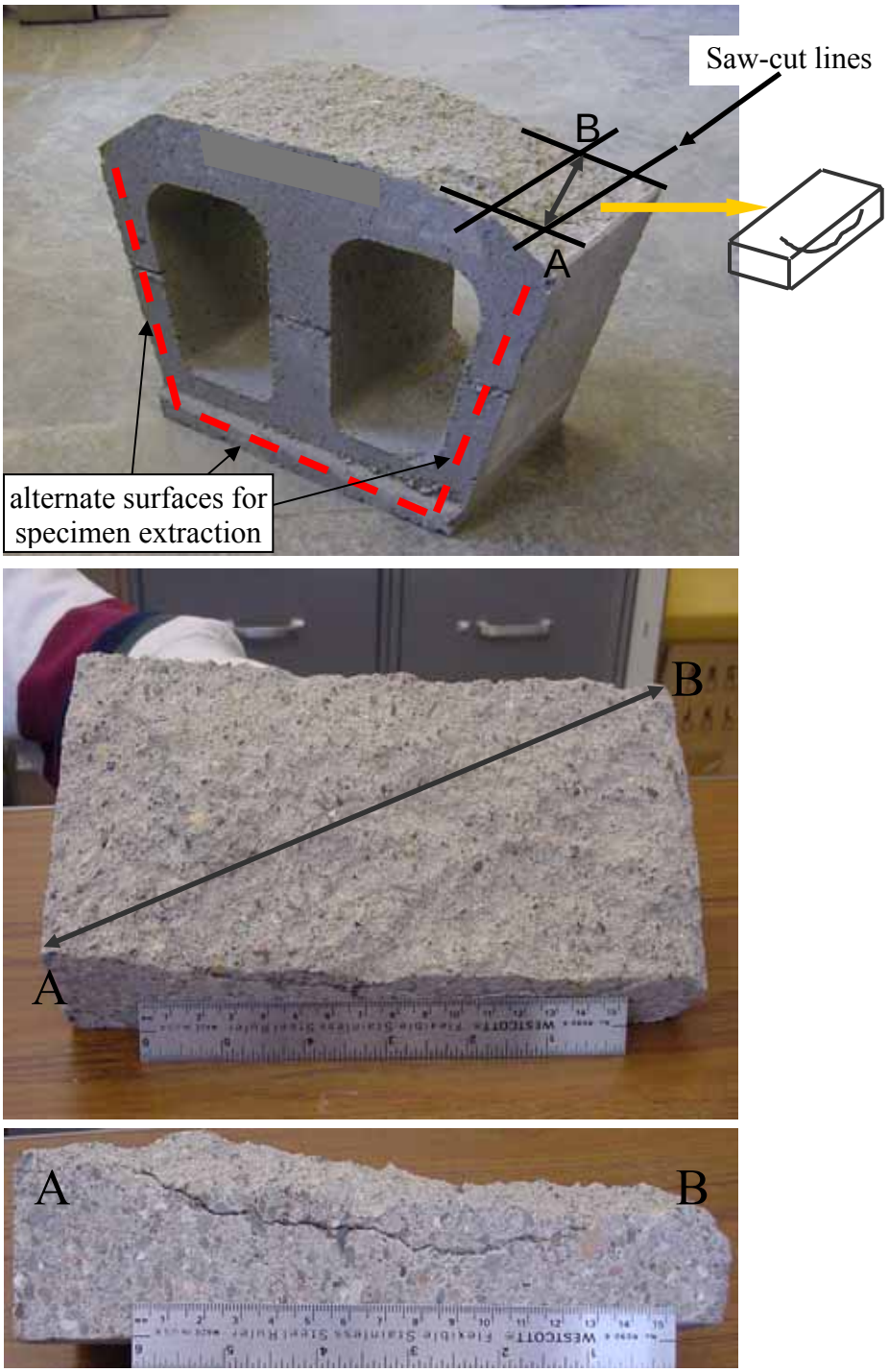

Figure 50. Photos. Section through region containing split face delamination.

4.2.4 Recommendations for Sampling

As mentioned in 4.2.1, two different approaches to sampling could be taken depending on the intended purpose of the tests (to evaluate production methods and/or mix designs or to qualify

units for projects). In either approach, the overall goal is to select units representative of the "lot" from which they are sampled and extract specimens representative of these units. Recommendations are offered in this section for specimen sampling. While these recommendations are intended for ASTM C 1262 (2003) freeze-thaw test specimens, they also apply to sampling for ASTM C 140 (2000) tests.

4.2.4.1 Sampling of SRW Units

- Units intended to evaluate the performance of as-manufactured products (for comparison of mixture designs, manufacturing methods, or quality of raw materials) shall be sampled at the manufacturing plant. These units shall be randomly sampled from a given production run for each scheduled production run. ASTM C 1262 (2003) requires that five units be sampled for freeze-thaw testing. For example, if SRW units are produced over 1 full day (8 hours), one unit could be sampled every 1 to 2 hours. These units shall be sampled near the end of the production line (i.e., after splitting and before stacking on pallets). Sampled units shall have been exposed to similar curing time and conditions (temperature and relative humidity) during manufacture and similar storage conditions after manufacture. These conditions shall be recorded.

- Units intended to evaluate the performance of products for use in projects shall be sampled either at the manufacturing plant or from pallets at jobsites. When sampling from pallets, the location on the pallet of the sampled units shall be recorded (interior of stack, exterior of stack, top units, middle units, bottom units, see figure 51). Pallet storage conditions (i.e., indoors at room condition until installation in project, outdoors and shrink-wrapped, or outdoors and unprotected) and ambient conditions (temperatures and precipitation) shall also be recorded.

  It is understood that many laboratories in the industry employ this sampling technique for freeze-thaw test specimens (personal communications, NCMA, May 2005).

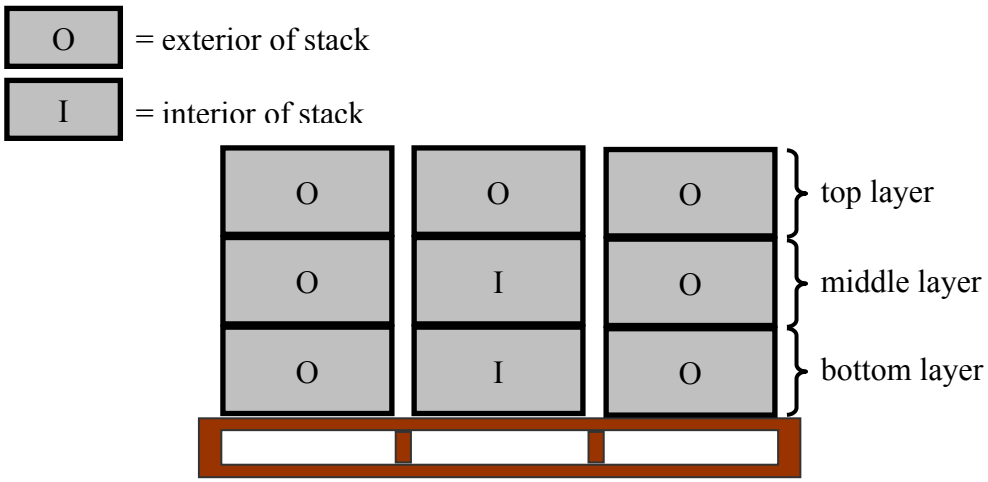

Figure 51. Drawing. Sampling of SRW units from pallet.

4.2.4.2 Extracting Specimens From SRW Units

- Specimens intended to evaluate the performance of as-manufactured products (for comparison of mixture designs, manufacturing methods, or quality of raw materials) shall be extracted from SRW units in such manner that the specimens cover the entire height of the unit, as shown in figure 52a. These specimens are more representative of the overall unit since each specimen covers all variations in properties along the casting direction. This method of specimen extraction is preferred over that shown in figure 52b, which covers only part of the variations along the casting direction. For specimens covering the full unit height, possible specimen sizes are therefore as follows:
    - For 200-mm (8-inch) tall unit: 200 mm (8inches) by 80 to 113 mm (3.1 to 4.4 inches) by 32 mm (1.25 inch).
    - For 150-mm (6-inch) tall unit: 150 mm (6 inches) by 107 to 150 mm (4.2 to 5.8 inches) by 32 mm (1.25 inches).

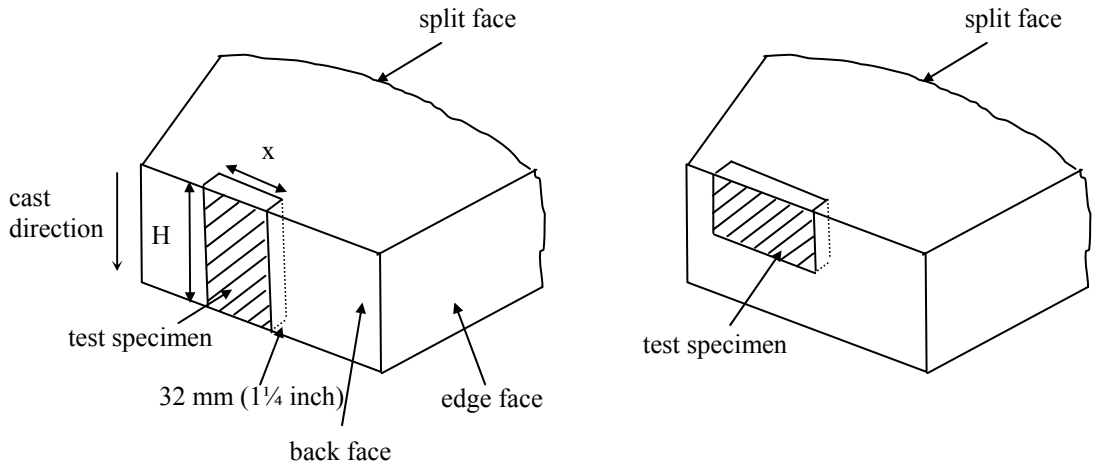

a. Preferred sampling method. b. Not recommended.

Figure 52. Drawings. Extraction of freeze-thaw specimens from SRW unit.

There are occasions when specimens shorter than the actual height of the SRW unit may be required. For instance, 150-mm-(6-inch-) long specimens need to be extracted from 200–mm- (8-inch-) tall units. Such situations could arise where available container sizes pose a constraint, or if the performance of 200 mm (8 inches) units were to be compared to that of 150-mm (6-inch) units using specimens of similar dimensions. Since the specimen is now shorter than the unit height, material along the full height of the unit will no longer be represented within each specimen. Representation thus needs to be done over several specimens. A recommended approach to attain full height representation of the unit is shown in figure 53 where three specimens of required length X are extracted from a unit of height H at different positions so that their combined result reflects all layers equally. It is noted that the rightmost specimen shown in this figure actually comprises two halves, which is permitted under ASTM C 1262 (the two halves are "tested as and considered as a single specimen," Clause 7.1.4). When tested as a single specimen, these two halves must be tested using the same container size as the other full specimens (i.e., those shown on the left and middle in figure 53). The goal is to maintain the same (mass of test solution) relative to (mass of specimen) in each test container.

It is noted that if shorter specimens are sampled in the manner shown in figure 53, it must be ensured that the total test area of all specimens in a set be within the range of total test area of all specimens as per ASTM C 1262 (2003). ASTM C 1262 (2003) requires five replicate test specimens with test area of 161 to 225 squared centimeters (cm^2) (25 to 35 squared inches ($inch^2$)) each. This adds up to 805 to 1125 cm^2 (125 to 175 $inch^2$) of test area per set. If specimens with an area of 150 by 75 mm (6 by 3 inches) are needed (test area of 113 cm^2 (18 $inch^2$)), nine specimens shall be sampled and tested (for a total area of 1013 cm^2 (162 $inch^2$). The reason for using nine specimens is because, as shown in figure 53, a set of three specimens is required to represent the face uniformly, and hence, only multiples of three-specimen sets can

preserve this uniform representation. In the same manner that ASTM C 1262 (2003) requires five specimens extracted from five separate units, smaller specimens (1, 2 or 3 shown in figure 54) should also be extracted from separate units.

Another important consideration regarding specimen extraction is that the actual size and shape of specimens cut from SRW units dictates the size and shape of container to be used (subject to the required clearance of surrounding test solution in ASTM C 1262 (2003)). The size and shape of container in turn influences the total number of containers that can be fit in a given shelf in freezer, which then influences the freezer air cooling pattern as discussed later in this chapter.

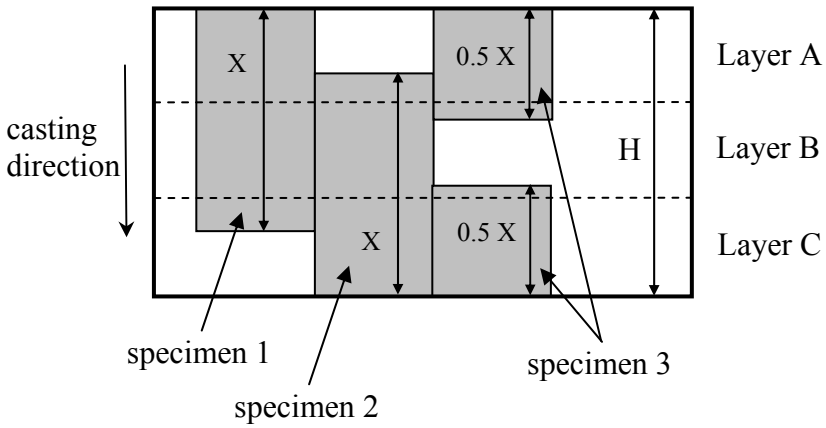

Figure 53. Drawing. Extraction of specimens shorter than the unit height (view into back face).

- Specimens intended to evaluate the performance of products for use in projects shall be sampled such that the specimens predominantly contain material from the middle layer (typically the lowest quality layer in a face) for the unit (figure 54). All specimens in a test set (e.g., five for ASTM C 1262 (2003)) shall be sampled in this same manner.

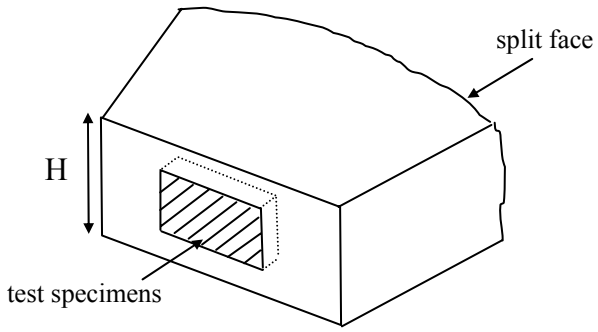

Figure 54. Drawing. Extraction of specimens from middle layer.

- Whenever it is necessary to sample specimens from near the split face of a unit, the laboratory technician shall thoroughly inspect test specimens for cracks or loose pieces prior to testing them. If present, cracked portions shall be trimmed off from the specimen by saw-cutting, or else the test specimen shall be discarded and another one extracted from the parent unit. Situations where sampling near the split face may occur include the following ones:

    - ASTM C 1262 (2003) Clause 7.1.1 states the following:

        > …cut the coupon from the exposed surface of the unit as the unit is used in service unless the exposed surface is a split, fluted (ribbed), or other nonplanar surface. In the case of a unit with an exposed nonplanar surface, cut the coupon from another flat molded surface.

      Compliance with this clause precludes the possibility of sampling material from the split face region. This would certainly be the case for a solid unit such as the one shown in figures 55 through 57. On the other hand, for a hollow unit (figures 58 through 60), the shaded section of the unit in figure 58 also fits the above requirement ("flat molded surface"), and as such, sampling from this region is allowed under ASTM C 1262 (2003). Figure 50, however, shows an example of a crack extending almost halfway into the portion of the unit circled in figure 58

    - Where it may be of interest to determine material properties in this region given that it is the outer exposed surface of the unit.

- Generally, it is recommended that sampling from the split face region be entirely avoided and that specimens be extracted from the back face as shown by the dashed lines in figures 55 and 58.

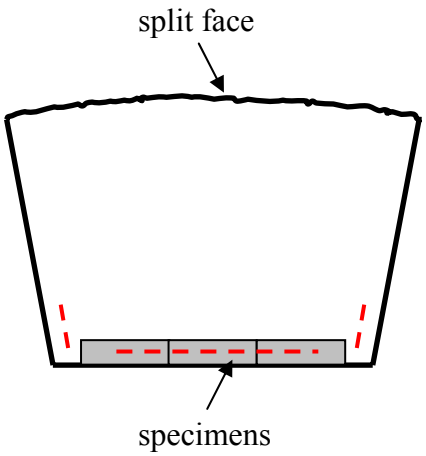

Figure 55. Drawing. Solid unit showing recommended sampling locations (red dashed lines).

Figure 56. Photo. Sample of solid unit.

Figure 57. Photo. Second sample of solid unit.

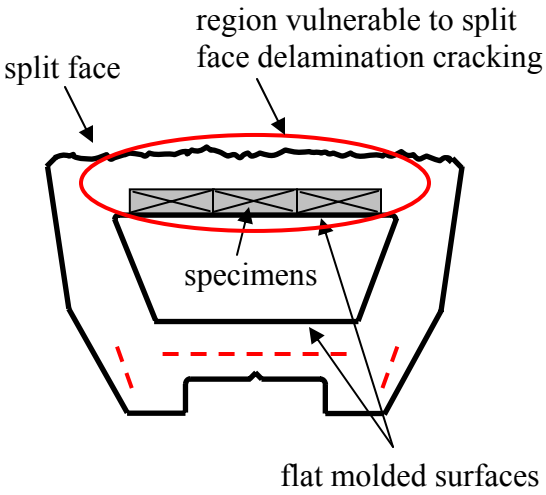

Figure 58. Drawing. Hollow unit showing recommended sampling locations (red dashed lines).

Figure 59. Photo. Sample of hollow unit.

Figure 60. Photo. Second sample of hollow unit.

4.2.4.3 General Laboratory Practice

- SRW units shall be carefully inspected for flaws such as cracks and chips (figure 61) particularly along the edges, and sampling from these regions shall be avoided. At times, the surface of the units may be scratched or damaged (figure 62), and these areas shall be avoided as well, particularly since this surface will be immersed in water or saline solution during testing. An example of a surface that is sound and free of defects is shown in figure 63.

Figure 61. Photo. Defects along edges of SRW units.

Figure 62. Photo. Scratched surface.

Figure 63. Photo. Example of sound surface.

- During saw-cutting, sufficient water shall be provided such that saw-cutting grime and loose particles are continuously flushed away and prevented from building up on the specimens. The specimens shall also be stable and not move during saw-cutting. Specimens shall also be cut at least 25 mm (1 inch) from the corners of the unit as shown in figure 64. This is to ensure that both specimen edges parallel to the height of the unit are saw-cut to match those of specimens taken near the middle of the unit.

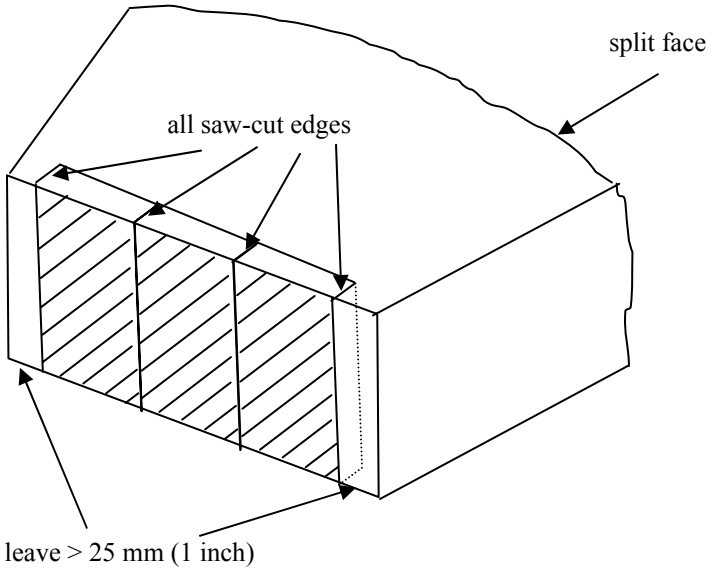

Figure 64. Drawing. Recommended clearance from edges.

- Clause 7.1.1 of ASTM C 1262 (2003) states that "immediately following saw-cutting, remove loose particles and residue from the coupon by rinsing in tap water and brushing with a soft bristle brush." The importance of this washing is illustrated in figures 65 and 66 showing a specimen before and after being washed immediately after saw-cutting. The wash water was collected, oven-dried and weighed to determine the mass of solid particles removed. This turned out to be approximately 0.2 percent of the dry mass of the specimen. While 0.2 percent of the specimen mass may not seem to be a large value, its significance is apparent when one considers that the commonly specified freeze-thaw mass loss limit is 1 percent of the specimen mass.

- **Detailed records shall be kept of the following items**:
    - Curing conditions (method, length, temperature and relative humidity).
    - Sampling method of units (from the production line in block plants or from pallets on jobsites, location of units in the pallet; and storage condition of units before arriving to test laboratory).
    - Specimen extraction locations in the units (face of unit, full height or not, together with a sketch).

Figure 65. Photo. Specimen before washing, following saw-cutting.

Figure 66. Photo. Specimen after washing, following saw-cutting.

4.2.4.4 Other Research

- This research primarily focused on 200-mm- (8-inch-) tall SRW units. There are 150-mm- (6-inch-) and 100-mm- (4-inch-) tall units also available in the market. Variations along the casting direction in these shorter units shall also be examined by evaluating properties at three layers along the casting direction, as shown in this chapter and in Chan et al. (2005a and b). If spatial distribution of properties such as the ones observed for 200-mm (8-inch) units are also observed in the shorter units, it implies that spatial variations may be related to manufacturing methods.

- A more detailed investigation on the relevance of manufacturing methods on distribution of properties in SRW units entail examining factors such as compaction (surcharge) load and energy, frequency and amplitude of vibration, duration of compaction, mix composition (stiff mix versus a wetter one), unit geometry, and curing conditions (method, chamber conditions, and duration).

4.3 VARIABILITY IN FREEZE-THAW EQUIPMENT USED IN ASTM C 1262 (2003)

The previous section (section 4.2) discussed sources of test variability that could arise from specimen sampling, and a set of recommendations was provided to reduce this risk. Now, given that a population of similar specimens (similar geometry, mass, and properties) has been procured for freeze-thaw testing, the next question that arises is: how certain can a laboratory be that each and every specimen in this population is exposed to the ASTM C 1262 (2003) temperature-time (T-t) requirements during freezing? This section briefly addresses this issue by first exploring the extent of spatial variability in temperature that can exist within freezers, the significance of this variability, and recommended solutions to manage this variability. More thorough coverage of this technical issue can be found in Chan (2006) and Hance (2005).

The clauses in ASTM C 1262 (2003) relevant to freezer equipment and to the freeze-thaw cycle follow:

- Clause 5.1.1:

  … the chamber or chambers shall be capable of maintaining the air temperature throughout the chamber within the specified test ranges when measured at any given time.

- Clause 8.2.1:

  During the freezing cycle, maintain the air temperature in the chamber at 0 ± 10°F (-18 ± 5°C) for a period of not less than 4.0 h and not more than 5.0 h. The cycle time does not include the time required for the air temperature in the chamber to reach the prescribed temperature.

- Clause 8.2.2:

  During the thawing cycle, maintain the air temperature around the containers at 75 ± 10°F (24 ± 5°C) for a period of not less than 2.5 h and not more than 96 h. The cycle time does not include the time required for the air temperature around the specimens to reach the prescribed temperatures.

These requirements are illustrated in the freezer-air cooling curve (T-t response) shown in figure 67 where various terms are defined. Cold soak is the time period during which the air temperature is between −18 °C ± 5 °C (0° ± 10 °F), and Clause 8.2.1 requires that cold soak be maintained for 4 to 5 hours. The cooling ramp is the portion of the cooling curve between the point at which the temperature starts falling until it reaches –18 °C ± 5 °C (0° ± 10 °F). ASTM C 1262 (2003) has no requirements for this cooling ramp. Together, the cooling ramp and cold soak comprise what is shown as the cooling branch of the curve. Similarly, on the warming side, the warm soak is the time period during which the air temperature is between 24 °C ± 5 °C (75 °F ± 10 °F); the warming ramp is the portion of the curve between the end of cold soak and the start of warm soak. While ASTM C 1262 (2003) requires the warm soak to be between 2.5 and 96 hours, it states no requirement on the warming ramp. Together, the warming ramp and warm soak comprise what is shown as the warming branch of the curve.

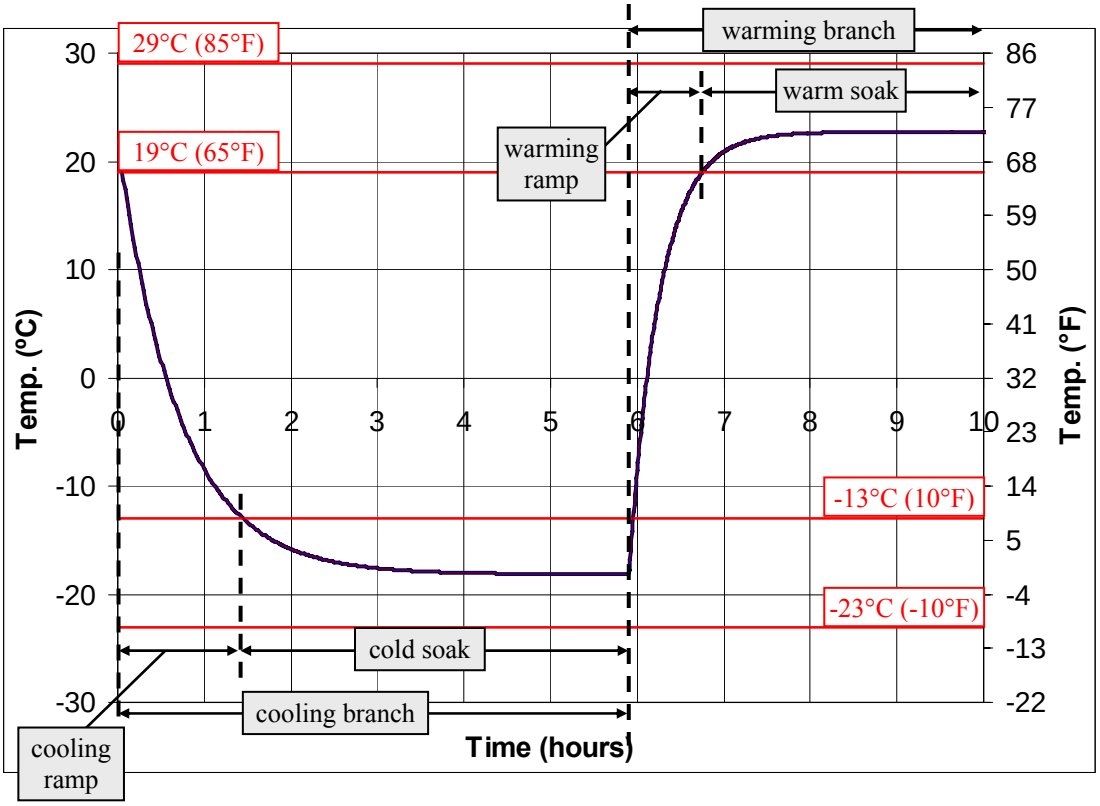

Figure 67. Graph. ASTM C 1262 (2003) freeze-thaw cycle—definitions.

Strict interpretation of the ASTM C 1262 (2003) clauses shown above suggests that the T-t conditions stated in Clause 8.2.1 must prevail throughout the chamber during freezing and the conditions in Clause 8.2.2 must exist around the specimens during thawing. This is reasonable if uniformity in exposure conditions is to be maintained among all specimens. However, as discussed in detail in Chan (2006) and Hance (2005) and briefly in the remainder of this section, freezer air cooling curves can vary from location to location inside a freezer, which affects specimen exposure. Such variation is influenced by, and can be partially controlled by the manner in which freezers are operated.

4.3.1 Comparison Between Different Freezers

Three different types of freezers were evaluated for internal temperature characteristics as briefly described in this section. The first was a chest freezer (figures 68 and 69) that can typically be purchased from appliance stores. This type of freezer cools the air within the freezer through its walls, and there is minimal air movement within the enclosed air space. Thus, high temperature gradients are likely inside this type of freezer. Since there are no automated temperature controls in these freezers, freeze-thaw cycling needs to be done manually (i.e., freezing by placing specimens into freezers and thawing by removing specimens from freezer and placing in laboratory air). Four such freezers were available for this study.

Figure 68. Photo. Closed chest freezer used in study.

Figure 69. Photo. Open chest freezer.

The second type of freezer was a walk-in environmental chamber (figures 70 through 72). Unlike the chest freezers, the walk-in freezer has ceiling mounted, fan-driven cooling and heating units that circulate conditioned air throughout the chamber, thereby promoting more uniform air temperature distribution. It operates at 2400 watts and has a cooling capacity of 0.13 watts per liter (watts/L) of freezer volume. This freezer has a programmable control device into which specified cooling and warming T-t profiles can be input and thus, continuous freeze-thaw cycles can be run without human intervention.

The third type of freezer was a cabinet freezer commonly used in testing laboratories. This freezer, shown in figure 73, is also equipped with cooling and heating units which are programmable to allow uninterrupted freeze-thaw cycling. Fans are also built into the unit to move air through the cabin for better air temperature distribution. This freezer operates at 5200 watts with a cooling capacity of 9.8 watts/L of freezer volume.

Figure 70. Photo. Walk-in freezer used in the study.

Figure 71. Photo. View of inside of walk-in freezer.

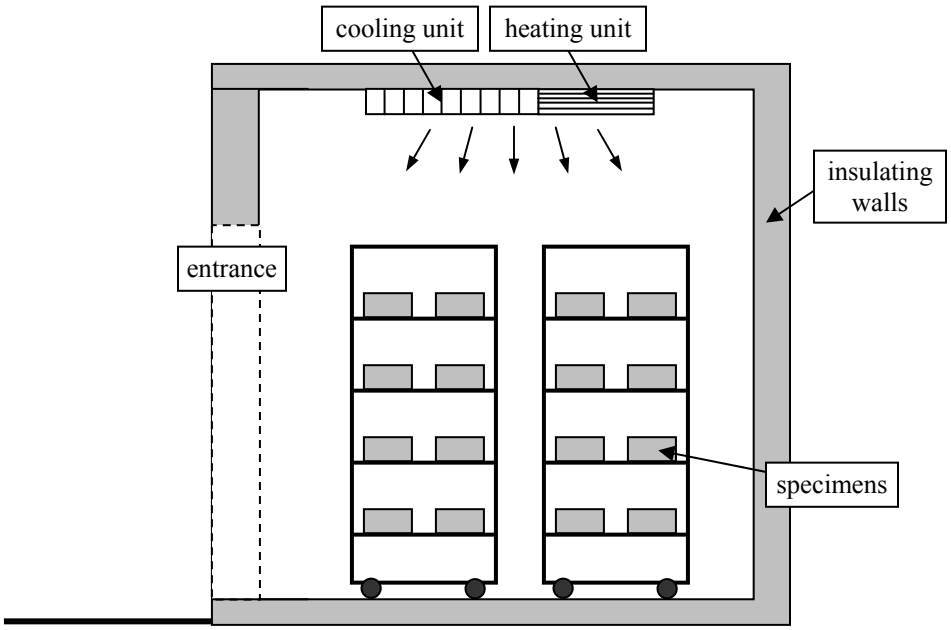

Figure 72. Drawing. Environmental chamber of walk-in freezer.

Figure 73. Photo. Cabinet freezer, closed.

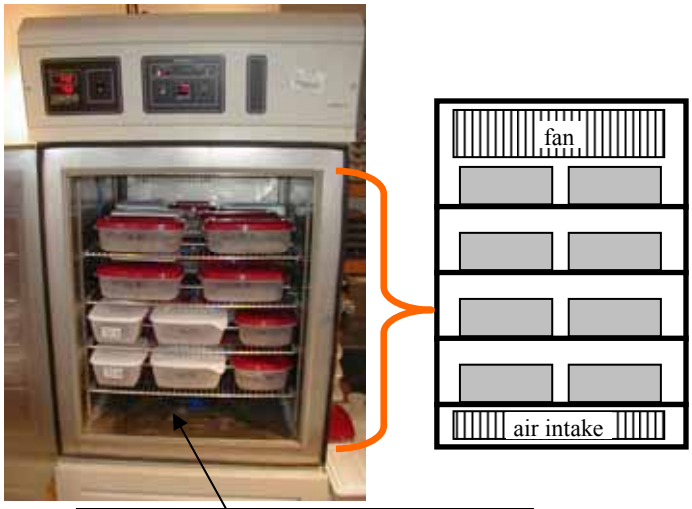

Figure 74. Photo and drawing. Inside of cabinet freezer.

For each freezer shown in figures 68–74, the temperature distributions throughout the chamber were accurately recorded while conducting test trials following ASTM C 1262 (2003). For each freezer, different tests were performed with varying numbers of test samples, up to the maximum sample number shown in table 2, which provides additional information on the freezers used in the study as documented by Hance (2005).

Table 2. Characteristics of the various freezers investigated (from Hance, 2005).

	Chest Freezer 1	Chest Freezer 2	Chest Freezer 3	Chest Freezer 4	Walk-in Chamber	Cabinet Chamber
Volume (liter (ft^3))	630 (22.2)	435 (15.4)	350 (12.4)	350 (12.4)	18000 (630)	530 (18.8)
Power (Watts)	130	170	120	120	2400	5200
Volume Cooling Capacity (Watts/L)	0.21	0.39	0.34	0.34	0.13	9.8
Maximum Number of Specimens	14	6	6	6	80	24
Specimen Cooling Capacity (Watts/Specimen)	9	28	20	20	30	220

4.3.1.1 Chest Freezer

In his thesis, Hance (2005) showed results of experiments carried out to determine the internal temperature variation in a chest freezer containing six ASTM C 1262 (2003) specimens. A wooden frame was built onto which 18 calibrated thermocouples were mounted to measure temperature inside the freezer at various locations (figure 75). These thermocouples were placed at a distance of about 25 to 50 mm (1 to 2 inches) from the interior wall surface.

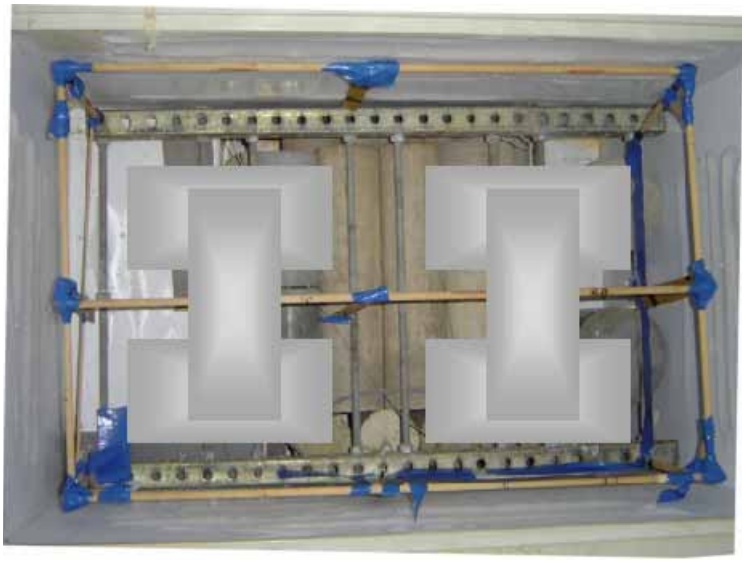

Figure 75. Photo. View of chest freezer with wooden frame and six specimens.

Figure 76 shows the T-t response in which the large spread in internal temperatures is shown. Hance's analysis of these temperatures was based on the ASTM C 1262-98 version which specifies a target cold soak temperature range of −17 °C ± 5 °C (−12 to −22 °C). A similar analysis is shown here but using the ASTM C 1262-98$^{\varepsilon 1}$ version which specifies a target cold soak temperature range of −18 °C ± 5 °C (−13 to −23°C) (this is also the version used throughout this FHWA project.)

Based on the average temperature T_{avg}, cold soak started at 0.9 hours when T_{avg} reached −13 °C (8.6 °F) and ended at 4.9 hours for a 4-hour cold soak period (the minimum recommended in ASTM C 1262, (2003)) at T_{avg} of −16.6 °C (12.2 °F). At the start of cold soak, the range between minimum and maximum measured temperatures was 6 °C (42.8 °F), and this range gradually decreased to 4.2 °C (39.6 °F) after 4 hours of cold soak. Figure 77 shows the standard deviation (σ) of the temperature measurements as a function of time, where it is seen that standard deviation gradually decreased with increasing soak time (hovering in the vicinity of 1.5 °C (34.7 °F)). The temperature variations for this chest freezer are summarized in table 3.

At the start of cold soak, approximately half of the temperature measurements are warmer than –13 °C (8.6 °F), while the other half are colder than –13 °C (8.6 °F). To increase the proportion of locations below –13 °C (8.6 °F), the temperature recorded at a single, random location (T_{random}) must therefore be colder than –13 °C (8.6 °F). Assuming that the temperature inside the freezer follows a normal distribution (with mean T_{avg} and standard deviation σ), the value of T_{random} must be such that:

$-13\ °C = T_{random} + 1.645\sigma$, to ensure that 95 percent of the temperature measurements are below –13 °C. Thus, $T_{random} = -15.5\ °C\ (4.2\ °F)$ Equation 2

$-13\ °C = T_{random} + 2.326\sigma$, to ensure that 99 percent of the temperature measurements are below –13 °C. Thus, $T_{random} = -16.5\ °C\ (2.3\ °F)$ Equation 3

[The above expressions are based on the standard normal distribution in which 95 percent of measurements is below a value of $T_{95\ percent} = T_{avg} + 1.645\sigma$ while 99 percent of measurements is below a value of $T_{99\ percent} = T_{avg} + 2.326\sigma$ (Miller and Freund, 1985). The aim here is to determine T_{avg} such that $T_{95\ percent}$ and $T_{99\ percent}$ are equal to −13 °C (8.6 °F). An average value of $\sigma = 1.5°C$ (4.2 °F) over the cold soak duration was used in these calculations].

The values of T_{random} calculated above indicate that due to variability in freezer internal temperature, the spot location must record an increasingly cooler temperature than –13 °C (8.6 °F) to ensure that most measured locations (95 and 99 percent considered) meet the –13 °C (8.6 °F) requirement.

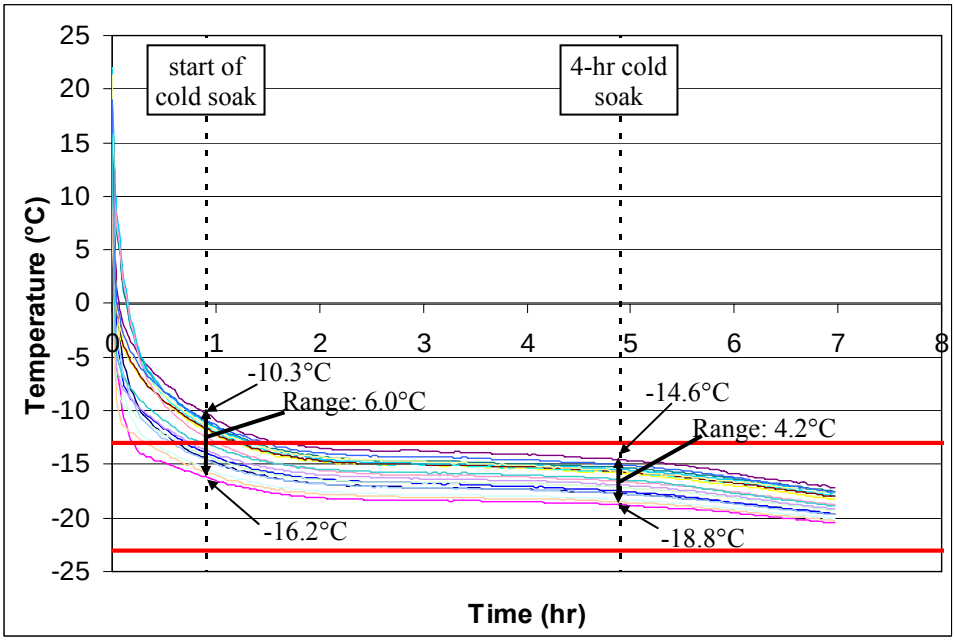

Tf = (9/5) * Tc + 32 {Tf = Fahrenheit, Tc = Celsius}

Figure 76. Graph. Internal temperature variations in chest freezer loaded with six specimens—T-t response.

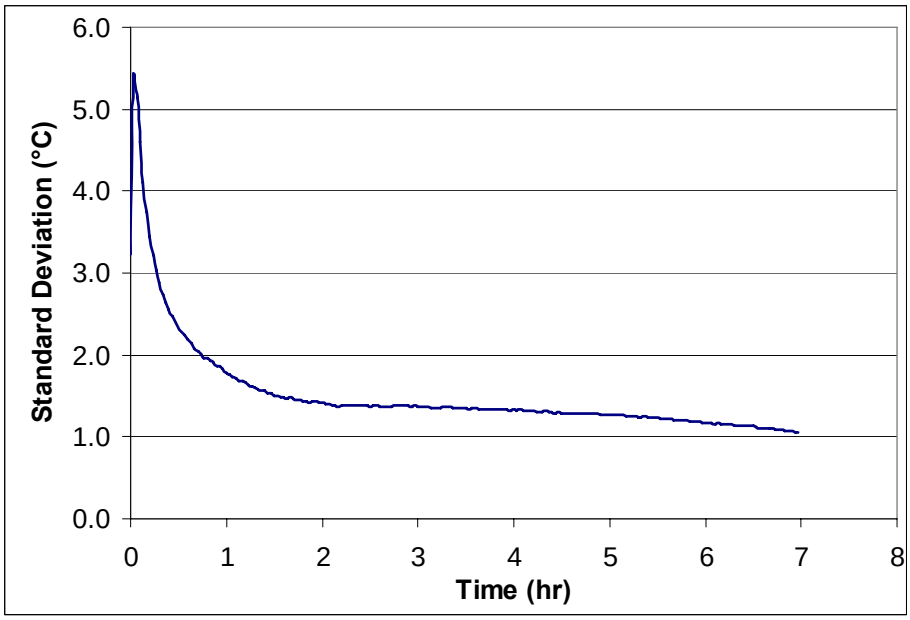

Tf = (9/5) * Tc + 32 {Tf = Fahrenheit, Tc = Celsius}

Figure 77. Graph. Internal temperature variations in chest freezer loaded with six specimens—standard deviation-time response.

Table 3. Temperature variations inside a chest freezer.

Part of Cycle	Avg T °C (°F)	Min T / Max T °C (°F)	Range °C (°F)	95 Percent C.I. About Avg*	95 Percent C.R.**
Start of cold soak	–13.0 (8.6)	–16.2 / –10.3 (2.8 / 13.5)	6.0 (10.8)	–16.0 / –10.0 (3.2 / 14.0)	6.0 (10.8)
End of 4-hour cold soak	–16.6 (2.1)	–18.8 / –14.6 (–1.8 / 5.7)	4.2 (7.6)	–19.6 / –13.6 (–3.3 / 7.5)	6.0 (10.8)

* Based on Avg. ± 2σ, where σ is about 1.5ºC over the duration of the cold soak period.
C.I. = confidence interval.
** C.R. = confidence range = estimated range within which 95 percent of the population exists.

4.3.1.2 Walk-in Environmental Chamber

Spatial temperature variability in the 18-m^3 (630-ft^3) walk-in chamber was evaluated by Hance (2005) using a similar approach. Eighteen calibrated thermocouples were located throughout the interior of this chamber as shown in figure 78. Evaluations were carried out at specimen quantities of 2, 20, 40, 60, 80, and 100 specimens. (Hance pointed out, however, that from a cooling capacity standpoint, 80 specimens appeared to be a reasonable upper limit for testing in this chamber). To illustrate the temperature variations in this chamber, results from the 60 specimen tests are shown in figures 79 and 80. Figure 79 shows the T-t response from the various thermocouples where it is observed that the band of curves was tighter than that obtained in the chest freezer. Again, based on average temperature, a 4-hour cold soak started at 4.3 hours with T_{avg} at –13 °C (8.6 °F) and ended at 8.3 hours with T_{avg} at –14.6 °C (5.7 °F). The range between minimum and maximum measured temperatures was 2.6 °C (4.7 °F) at start of cold soak and 1.6 °C (2.9 °F) at the end of the 4-hour cold soak. These parameters are summarized in table 4. The σ-t response is shown in figure 80. During cold soak, this parameter remained at about 0.4 ºC (compared to 1.5 °C for the chest freezer). During the warming ramp, values of the standard deviation were higher likely due to nonuniform temperature conditions resulting from the introduction of warm air (from the heaters) to an already cold environment.

Figure 78. Photo. View of walk-in chamber with thermocouples on shelving units and suspended from ceiling.

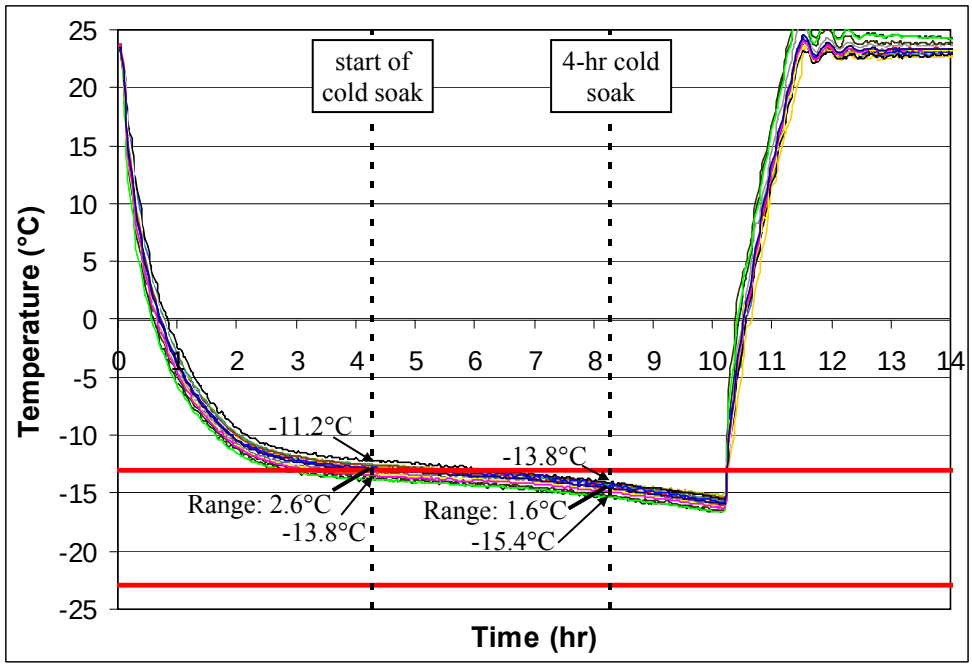

Tf = (9/5) * Tc + 32 {Tf = Fahrenheit, Tc = Celsius}

Figure 79. Graph. Internal temperature variations in walk-in chamber loaded with 60 specimens—T-t response.

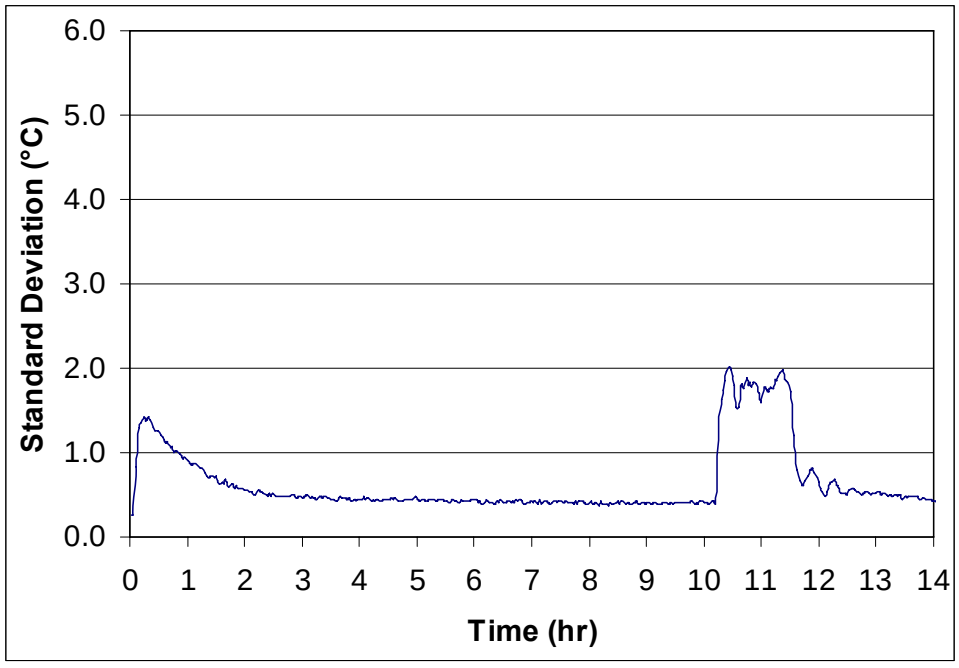

Tf = (9/5) * Tc + 32 {Tf = Fahrenheit, Tc = Celsius}

Figure 80. Graph. Internal temperature variations in walk-in chamber loaded with 60 specimens—standard deviation-time response

Table 4. Temperature variations inside the walk-in freezer loaded with 60 specimens.

Part of Cycle	Avg T °C (°F)	Min T / Max T °C (°F)	Range °C (°F)	95 Percent C.I. about Avg*	95 Percent C.R.**
Start of cold soak	–13.0 (8.6)	–13.8 / –11.2 (7.2 / 11.8)	2.6 (4.7)	–13.8 / –12.2 (7.2 / 10.0)	1.6 (2.9)
End of 4-hour cold soak	–14.6 (5.7)	–15.4 / –13.8 (4.3 / 7.2)	1.6 (2.9)	–15.4 / –13.8 (4.3 / 7.2)	1.6 (2.9)

* Based on Avg. ± 2σ, where σ is about 0.4ºC over the duration of the cold soak period.
C.I. = confidence interval.
** C.R. = confidence range

Compared to the chest freezer, the walk-in freezer exhibited more uniform temperature distribution, as indicated by the smaller standard deviation over the duration of the cold soak period (0.4 °C (32.7 °F) in walk-in freezer versus 1.5 °C (34.7 °F) in the chest freezer). This reduced temperature variation in the walk-in chamber was probably related to better air circulation imparted by the fans. As with the chest freezer however, due to variability in freezer internal temperature, the temperature recorded at a single, random location (T_{random}) must be colder than –13 °C (8.6 °F) to increase the proportion of measurements below –13 °C (8.6 °F). Assuming a normal distribution for the freezer internal temperature, the value of T_{random} must be such that:

$-13\ °C\ (8.6\ °F) = T_{random} + 1.645\sigma$, to ensure that 95 percent of the temperature measurements are below –13 °C (8.6 °F). Thus, $T_{random} = -13.7\ °C\ (7.4\ °F)$ Equation 4

$-13\ °C = T_{random} + 2.326\sigma$, to ensure that 99 percent of the temperature measurements are below –13 °C. Thus, $T_{random} = -16.5\ °C\ (2.3\ °F)$ Equation 5

[The rational behind these expressions is similar to the ones shown previously for the chest freezer. An average value of $\sigma = 0.4\ °C$ over the cold soak duration was used in these calculations].

As seen, due to the lower variability, the walk-in chamber required less "overshooting" (that is targeting of a spot temperature measurement lower than –13 °C (8.6 °F) to ensure that most locations are below –13 °C (8.6 °F)) than the chest freezer.

Figure 81 shows the average T-t plots for the freezer air with various numbers of specimens, where it is clearly seen that the performance of the freezer depends on the number of specimens. While the initial rate of temperature change was similar regardless of specimen quantity (at about 56 °C/hr or 100 °F/hr), the curves diverged by the end of the test. Further, with increasing quantities of specimens, the time to reach start of cold soak was substantially delayed. For instance, with 20 specimens, T_{avg} reached –13 °C (8.6 °F) at 2.0 hours, whereas with 40 specimens, T_{avg} reached –13 °C (8.6 °F) at 2.8 hours and with 80 specimens, T_{avg} reached –13 °C (8.6 °F) at 7.0 hours. This means that as the number of specimens is increased, total testing time is expected to increase, and the rates of freezing will decrease.

The temperature variations for each of these tests are summarized in table 5, in which the following trends were observed:

- As the specimen quantities increased, the average temperature at the end of cold soak (after 4 hours) was warmer. In comparing 2 and 60 specimens, the temperatures at the end of cold soak differed by about 2.0 °C (3.6 °F).
- As the specimen quantities increased, the range of measured temperatures at any given time also increased. This increase was particularly pronounced at the start of cold soak, where for two specimens, the range of temperatures was 1.5 °C (2.7 °F), while for 80 specimens the range was 2.5 °C (4.5 °F). Internal temperature variability in the freezer therefore increased with increasing number of specimens.

The overall significance of these results is that, as expected, freezer performance is dependent on specimen quantity in an interactive manner. As the number of specimens change, freezer performance is affected, which modifies the exposure condition of the specimens themselves. This freezer-specimen interaction must be taken into consideration in testing and will be discussed further.

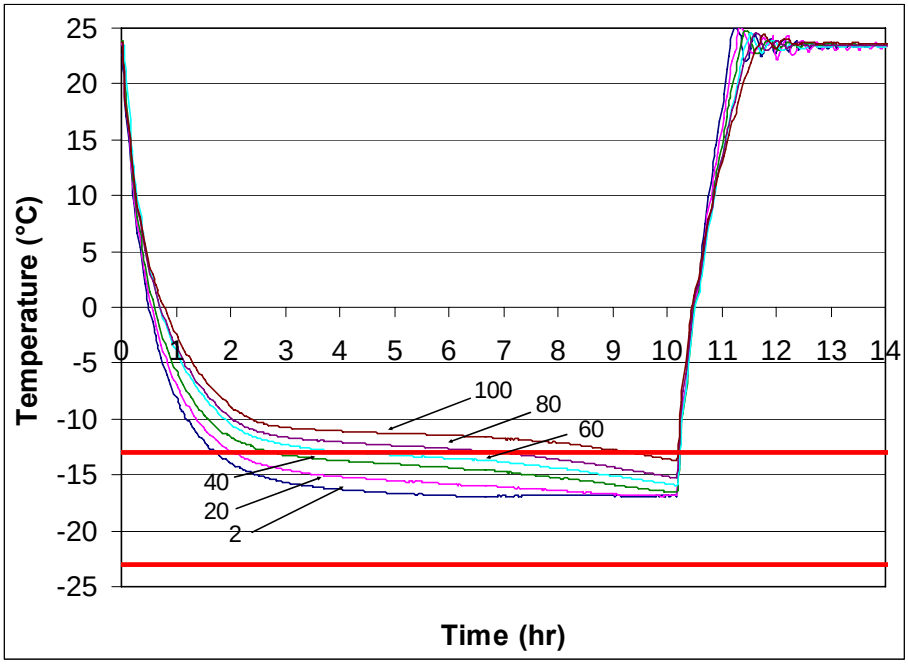

Tf = (9/5) * Tc + 32 {Tf = Fahrenheit, Tc = Celsius}

Figure 81. Graph. Average temperatures in walk-in chamber with varying quantities of specimens (values shown are number of specimens).

Table 5. Temperature variations inside the walk-in freezer loaded with varying specimen quantities.

Part of Cycle	Avg T °C (°F)	Min T / Max T °C (°F)	Range °C (°F)	95 Percent C.I. About Avg*	95 Percent C.R.**
Start of Cold Soak					
2 specimens	–13.0 (8.6)	–13.7 / –12.2 (7.3 / 10.0)	1.5 (2.7)	–13.6 / –12.4 (7.5 / 9.7)	1.2 (2.2)
20 specimens	–13.0 (8.6)	–13.7 / –12.4 (7.3 / 9.7)	1.3 (2.3)	–13.6 / –12.4 (7.5 / 9.7)	1.2 (2.2)
40 specimens	–13.0 (8.6)	–13.8 / –11.8 (7.2 / 10.8)	2.0 (3.6)	–13.6 / –12.4 (7.5 / 9.7)	1.2 (2.2)
60 specimens	–13.0 (8.6)	–13.8 / –11.2 (7.2 / 11.8)	2.6 (4.7)	–13.8 / –12.2 (7.2 / 10.0)	1.6 (2.9)
80 specimens	–13.0 (8.6)	–14.2 / –11.7 (6.4 / 10.9)	2.5 (4.5)	–14.0 / –12.0 (6.8 / 10.4)	2.0 (3.6)
100 specimens	–13.0 (8.6)	–14.2 / –11.6 (6.4 / 11.1)	2.6 (4.7)	–14.0 / –12.0 (6.8 / 10.4)	2.0 (3.6)
End of 4-Hour Cold Soak					
2 specimens	−16.8 (1.8)	−17.4 / −16.3 (0.7 / 2.7)	1.1 (2.0)	–17.4 / –16.2 (0.7 / 2.8)	1.2 (2.2)
20 specimens	−15.9 (3.4)	−16.4 / −15.5 (2.5 / 4.1)	0.9 (1.6)	–16.5 / –15.3 (2.3 / 4.5)	1.2 (2.2)
40 specimens	−14.6 (5.7)	−15.3 / −14.2 (4.5 / 6.4)	1.1 (2.0)	–15.2 / –14.0 (4.6 / 6.8)	1.2 (2.2)
60 specimens	–14.6 (5.7)	–15.4 / –13.8 (4.3 / 7.2)	1.6 (2.9)	–15.4 / –13.8 (4.3 / 7.2)	1.6 (2.9)
80 specimens	n.a.	n.a.	n.a.	n.a.	n.a.
100 specimens	n.a.	n.a.	n.a.	n.a.	n.a.

n.a. = data not available

4.3.1.3 Cabinet Freezer

Spatial temperature variability in the 0.53 m^3 (18.8 ft^3) cabinet freezer was assessed by placing 23 calibrated thermocouples throughout the freezer cabin. Evaluation of this freezer was carried out as part of the NCMA Foundation Study. At the time the freezer was received, four shelves were available, as shown in figure 74. Thermocouples were placed at each corner and the center of each shelf, as shown in figure 82. These thermocouples were typically located at about 25 mm (1 inch) above the shelf level. In addition, thermocouples were placed near the ceiling and the floor of the cabin, as well as adjacent to the freezer internal sensors. In total, 23 thermocouples were employed, and their locations are illustrated in figures 82 and 83.

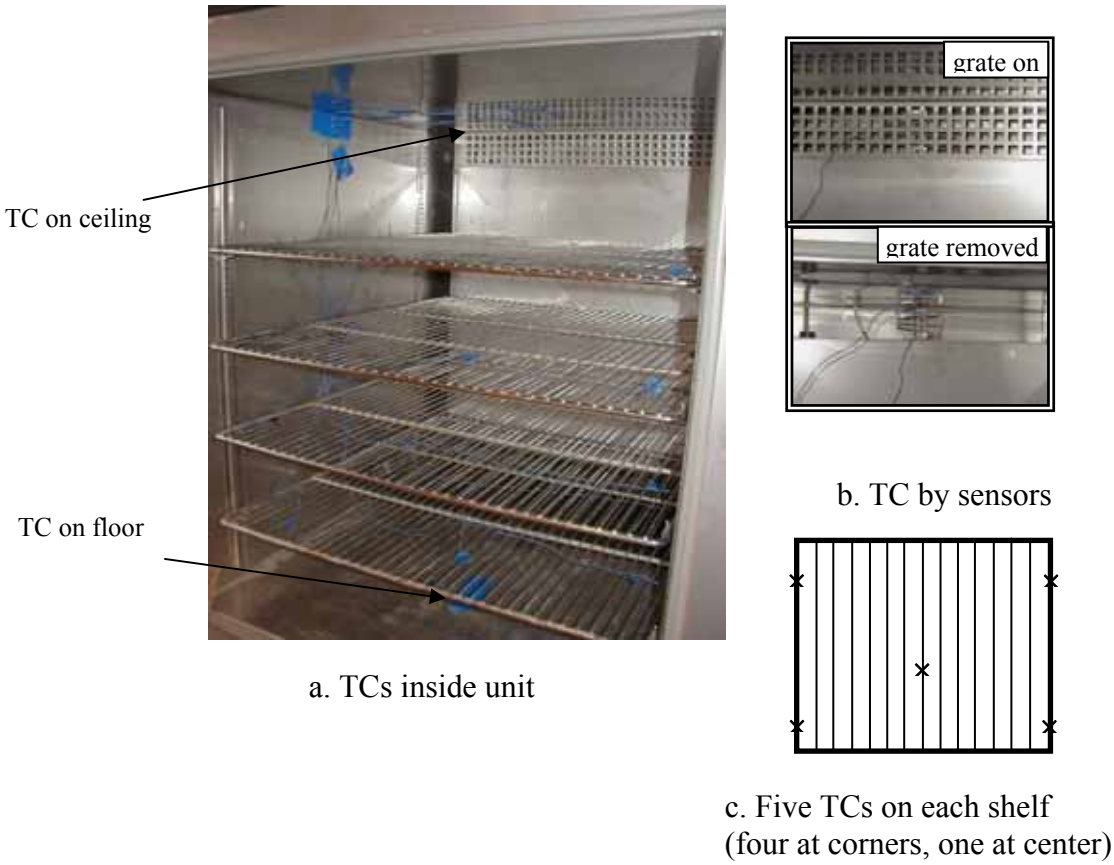

Figure 82. Photos and drawings. View of thermocouple (TC) placement in cabinet freezer instrument to tests.

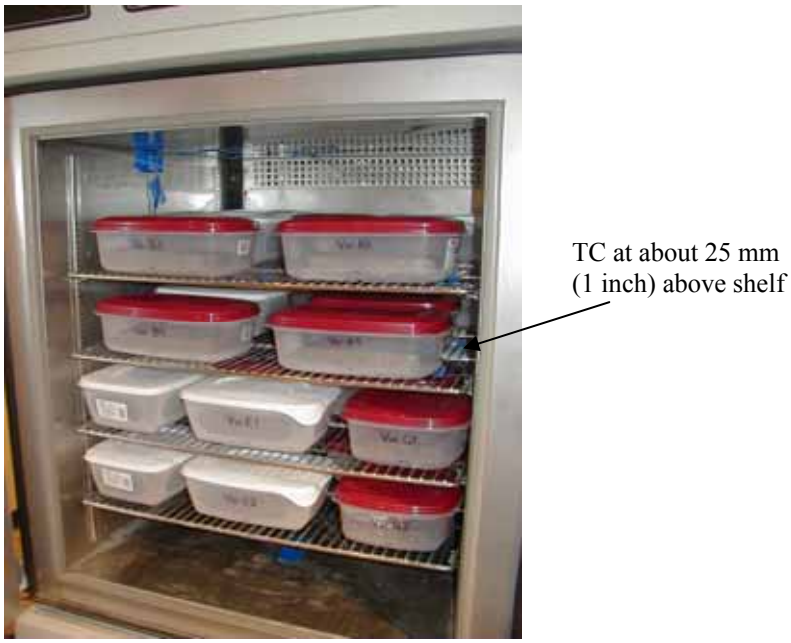

Figure 83. Photo. View of thermocouple (TC) placement with specimens in cabinet.

Evaluations were carried out using 0, 18 and 28 specimens. To illustrate the internal temperature variations, results from the 28 specimen tests are shown here. This was also the number of specimens tested in the NCMA study. Figure 84 shows the T-t response from the thermocouples where it is observed that the band of curves was tighter than that obtained in the chest freezer but not as tight as the one obtained with the walk-in chamber, especially at the onset of cold soak. Based on average temperature, a 4-hour cold soak started at 1.9 hours with T_{avg} at –13 °C (8.6 °F) and ended at 4.9 hours with T_{avg} at –18.3 °C (–0.9 °F). The range between minimum and maximum measured temperatures were 3.2 °C (5.8 °F) at start of cold soak and 1.4 °C (2.5 °F) at end of the 4-hour cold soak. These parameters are summarized in table 6. The standard deviation-t response is shown in figure 85 where the standard deviation is seen to gradually decrease from approximately 0.8 °C to 0.3 °C (33.4 °F to 32.5 °F) from start to end of cold soak (compared to almost constant values of about 0.4 °C (32.7 °F) in the walk-in freezer and 1.5 °C (34.7 °F) in the chest freezer). As with the walk-in freezer, values of standard deviation increased during warming ramp. As with the chest and walk-in freezers, due to variability in freezer internal temperature, the temperature recorded at a single, random location (T_{random}) must be colder than –13 °C (8.6 °F) to increase the proportion of measurements below –13 °C (8.6 °F).

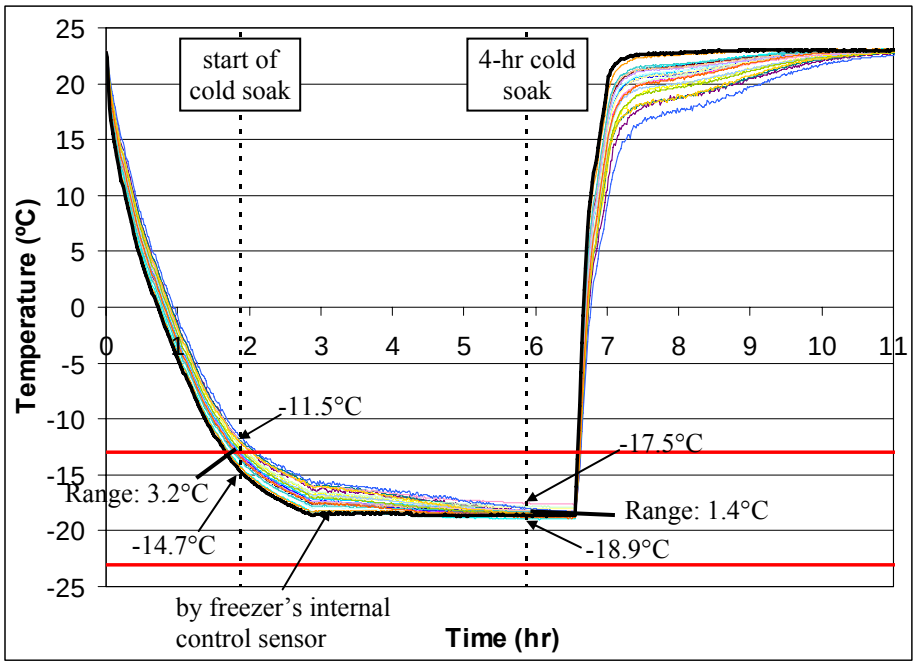

Tf = (9/5) * Tc + 32 {Tf = Fahrenheit, Tc = Celsius} for °F here.

Figure 84. Graph. Internal temperature variations in cabinet freezer loaded with 28 specimens—T-t response.

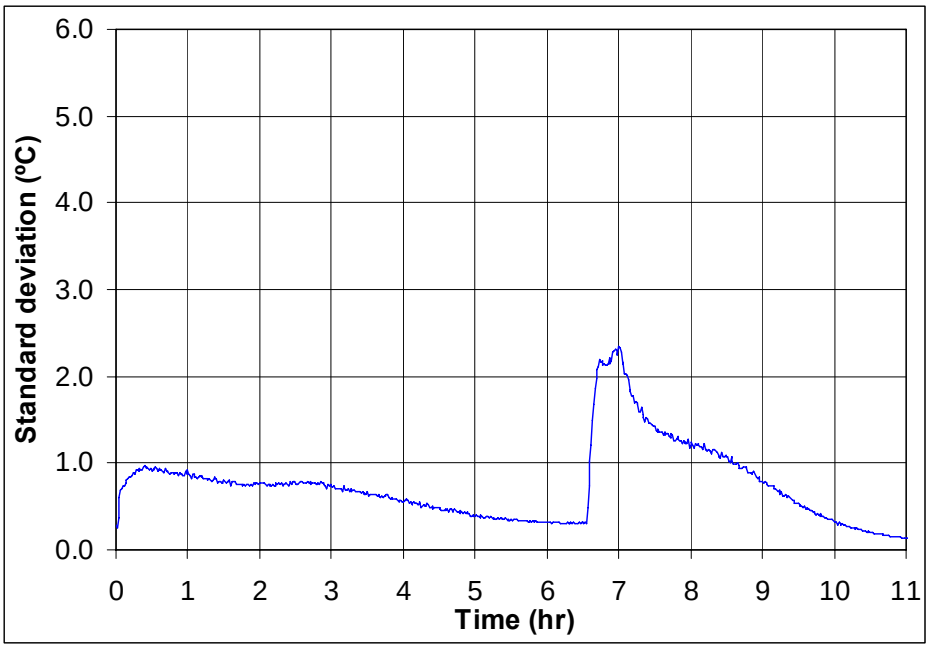

Tf = (9/5) * Tc + 32 {Tf = Fahrenheit, Tc = Celsius}

Figure 85. Graph. Internal temperature variations in cabinet freezer loaded with 28 specimens—standard deviation-time response.

Table 6. Temperature variations inside the cabinet freezer loaded with 28 specimens.

Part of Cycle	Avg T °C (°F)	Min T / Max T °C (°F)	Range °C (°F)	95 Percent C.I. About Avg*	95 Percent C.R.**
Start of cold soak	–13.0 (8.6)	–14.7 / –11.5 (5.5 / 11.3)	3.2 (5.8)	–14.2 / –11.8 (6.4 / 10.8)	2.4 (4.3)
End of 4-hour cold soak	–18.3 (–0.9)	–18.9 / –17.5 (–2.0 / 0.5)	1.4 (2.5)	–19.5 / –17.1 (–3.1 / 1.2)	2.4 (4.3)

* Based on Avg. ± 2σ, where σ averages about 0.6ºC over the duration of the cold soak period.
C.I. = confidence interval.
** C.R. = confidence range

Assuming a normal distribution for the freezer internal temperature, the value of T_{random} must be such that:

–13 °C (8.6 °F)= T_{random} + 1.645σ, to ensure that 95 percent of the temperature measurements are below –13 °C (8.6 °F). Thus, T_{random} = –14.0 °C (6.8 °F) Equation 6

–13 °C (8.6 °F) = T_{random} + 2.326σ, to ensure that 99 percent of the temperature measurements are below –13°C (8.6 °F). Thus, T_{random} = –14.4 °C (6.1 °F) Equation 7

As seen, the "overshooting" (that is the targeting of a spot temperature measurement lower than –13 °C (8.6 °F) to ensure that most locations are below –13 °C (8.6 °F)) is intermediate between that of the chest and walk-in freezers.

Knowing the locations of these thermocouples allowed mapping of the temperature inside the cabinet freezer to detect patterns within the freezer. This was done by selecting a time from the T-t record (3.5 hours arbitrarily selected), ranking the available temperatures at this time in order from coldest to warmest and splitting all the locations into six groups of three or four locations per group. These groups were then labeled from 1 at the coldest spots to 6 at the warmest spots. The result of this mapping is shown in figure 86 in which the overall coldest and warmest spots are also identified. The coldest locations generally were in the front part of the freezer (i.e., near the door) and on the higher shelves (including the ceiling), while the warmest locations were toward the back of the freezer in the lowest shelves (including the floor). The coldest overall location was right at the location of the freezer's built-in temperature sensor that is used to control the freezer cycles. This sensor is located near the fan. The warmest overall location was at the back of the bottommost shelf. This pattern of temperature distribution generally coincided with the flow of air within the chamber, illustrated in figure 87. As shown, the air coming out from the fan is the coldest air and reaches the top shelf and freezer front locations first. On the other hand, the back locations in the lower shelves are more or less sheltered, and as such, experience the warmest temperatures. The freezer's internal control sensors, positioned at the fan exit, were exposed to the coldest temperatures within the chamber. The T-t trace for this location is shown by the dark line in figure 84. This has important implications for test control as will be discussed later.

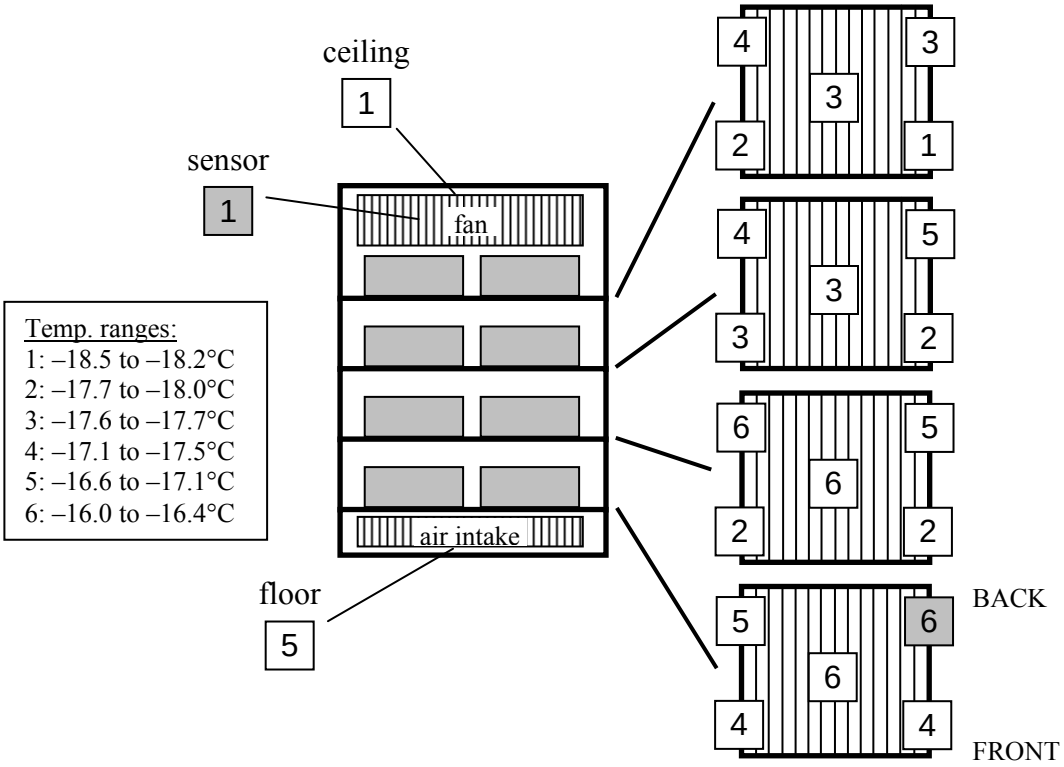

Figure 86. Drawing. Individual temperature locations (front view of freezer, plan view of each shelf).

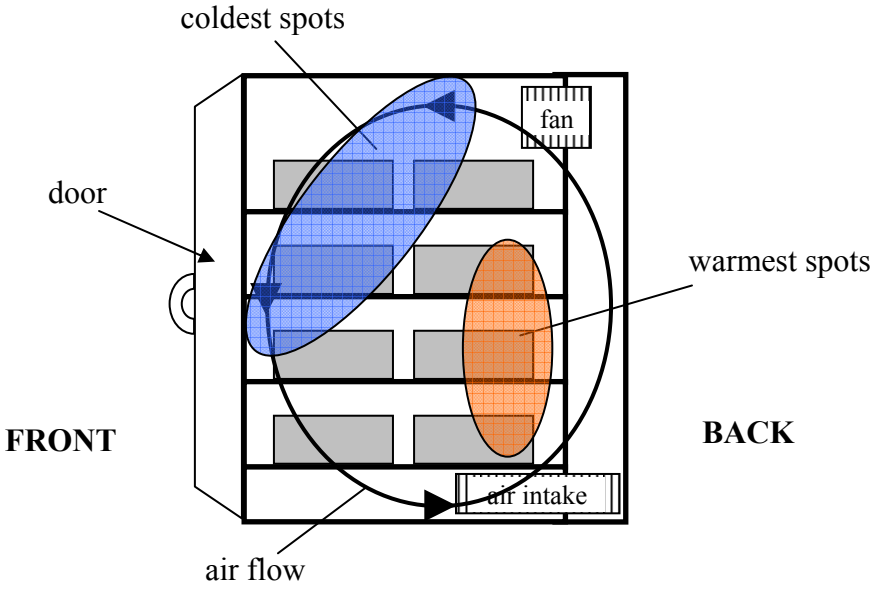

Figure 87. Drawing. Temperature mapping in cabinet freezer (side view of the freezer cabin).

The effect of the number of specimens is seen in figure 88 showing the average T-t plots for the freezer air for 0, 18 and 28 specimens. Unlike the walk-in chamber, the initial rate of temperature change depended on specimen quantity from 61 °C/hr (110 °F/hr) with no specimens, to 27 °C/hr (49 °F/hr) with 28 specimens. The times required for T_{avg} to reach –13 °C (8.6 °F) were 0.7, 1.5 and 1.9 hours for 0, 18 and 28 specimens, respectively. The temperature variations for each of these tests are summarized in table 7. It is interesting that temperature variability at the start of cold soak in the cabinet freezer, even without specimens in it, was larger than that observed in the walk-in chamber. The 95 percent confidence range was 3.4 °C (38.1 °F) for the cabinet freezer with 0 specimens and 1.6 °C for the walk-in freezer with 60 specimens. Although the reason for the larger variability observed in the cabinet freezer at start of cold soak is unclear, it is suspected that at this time (start of cold soak when T_{avg} reaches –13 °C (8.6 °F)), the cabinet freezer was still experiencing rapid temperature drops (see figure 89) and a stable, more uniform air distribution throughout the freezer had not yet been reached. Once in the cold soak zone at more stable temperatures, variability decreased. Overall, increasing the number of specimens increased variability.

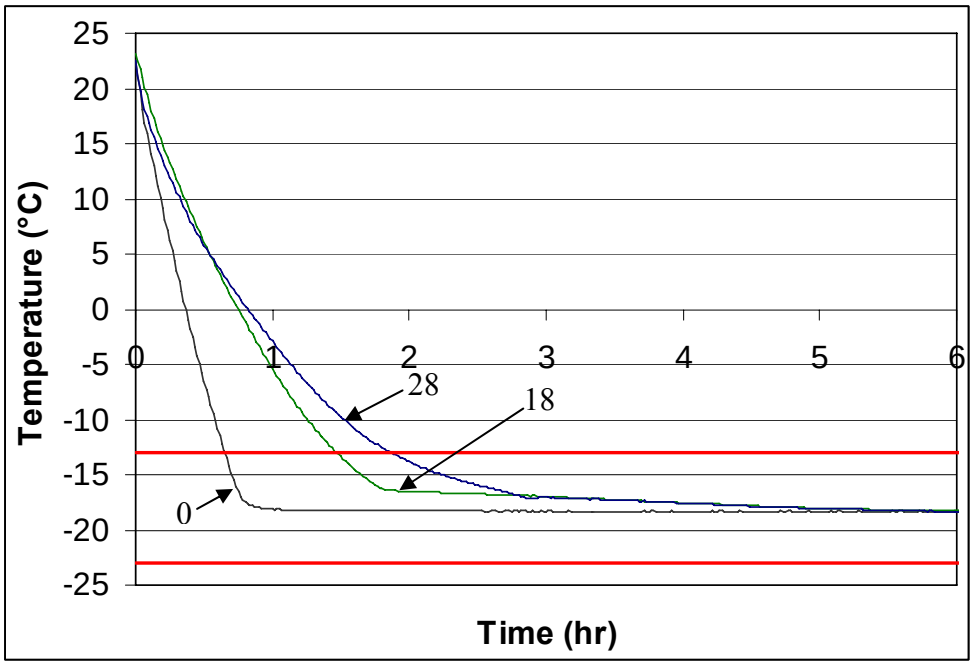

Tf = (9/5) * Tc + 32 {Tf = Fahrenheit, Tc = Celsius}

Figure 88. Graph. Average temperatures in cabinet freezer with varying quantities of specimens (values shown are number of specimens).

Table 7. Temperature variations inside the cabinet freezer loaded with varying specimen quantities.

Part of Cycle	Avg T °C (°F)	Min T / Max T °C (°F)	Range °C (°F)	95 Percent C.I. About Avg*	95 Percent C.R.**
Start of Cold Soak					
0 spec.	–13.0 (8.6)	–14.9 / –11.5 (5.2 / 11.3)	3.4 (6.1)	–14.6 / –11.4 (5.7 / 11.5)	3.4 (6.1)
18 spec.	–13.0 (8.6)	–15.4 / –11.3 (4.3 / 11.7)	4.1 (7.4)	–14.6 / –11.4 (5.7 / 11.4)	3.2 (5.8)
28 spec.	–13.0 (8.6)	–14.7 / –11.5 (5.5 / 11.3)	3.2 (5.8)	–14.2 / –11.8 (6.4 / 10.8)	2.4 (4.3)
End of 4-Hour Cold Soak					
0 spec.	–18.3 (–0.9)	–18.8 / –17.7 (–1.8 / 0.1)	1.1 (2.0)	–18.9 / –17.7 (–2.0 / 0.1)	1.2 (2.2)
18 spec.	–18.2 (–0.8)	–18.5 / –17.7 (1.3 / 0.1)	0.8 (1.4)	–18.8 / –17.6 (–1.8 / 0.3)	1.2 (2.2)
28 spec.	–18.3 (–0.9)	–18.9 / –17.5 (–2.0 / 0.5)	1.4 (2.5)	–19.5 / –17.1 (–3.1 / 1.2)	2.4 (4.3)

n.a. = data not available

4.3.1.4 Recommendations To Reduce Freezer Internal Variability

As seen from the previous sections, each of the freezers evaluated was capable of complying with ASTM C 1262 (2003) requirements, although the shapes of the T-t responses were quite distinct from freezer to freezer. Results of ASTM C 1262 (2003) tests conducted on specimens in different freezers (Haisler, 2004) showed that these kinds of shifts in T-t response (shown in figure 88) can have a very significant influence on specimen performance. The focus in this section is on how internal variability within a freezer can affect compliance with the test standard, and more importantly, how one can modify the freezer, specimen storage, or freezer controls to meet compliance with ASTM C 1262 (2003) and to provide consistent exposure conditions for all the samples contained in the freezer. Below are some recommendations for modifying ASTM C 1262 (2003) to meet these objectives.

It is evident that cold and warm spots exist within each freezer. Specimens that remain in these cold and warm spots can conceivably be subjected to different numbers (and types) of freeze-thaw cycles and exhibit different durabilities. One way to minimize discrepancies in exposure conditions is to move samples periodically during the course, which is currently specified in ASTM C 1262 (2003):

- Clause 8.2.4*:*
  At 25 ± 5 cycle intervals, remove containers from the test chamber.
  Open containers to visually inspect the condition of the specimens

and to adjust the water level to comply with 8.1.1 (13 mm or ½ inch depth).

- Clause 8.2.5:
  Every time a container is replaced into a multi-level freezing test chamber, the container shall be placed on the level immediately above the level on which it was previously located. If the container was previously located on the top level of a multi-level freezing chamber, replace it onto the bottom level.

Based on these clauses, specimens tested to 100 cycles would only be rotated four times through the entire duration of the test. Moreover, Clause 8.2.5 only mentions sample rotation in the vertical direction of the freezer. Hence, if a specimen is placed on the back side of the freezer, it is possible for it to remain on the back side through 100 cycles with the only difference being the shelf level. Similarly, there could also be specimens near the front of the freezer through the entire test. It is thus recommended that **s**pecimen rotation occur at intervals shorter than 25 cycles (say every 10 cycles), and that rotation be not only carried out in the vertical direction, but also within a shelf (e.g., front and back). This approach would allow for more uniform exposure of all specimens over 100 cycles.

As demonstrated earlier for the walk-in and cabinet freezers, the T-t characteristics in these freezers varied when loaded with different quantities of specimens. This variation is as expected due to the different thermal mass associated with different specimen quantities and due to the way that specimen loading may influence interval air flow and convective heat transfer to or from any given specimen. Variations in specimen quantities, however, could arise due to a number of possible reasons, which include (but are not limited to) laboratory testing demand and schedules, specimen or container size constraints, or the gradual removal of specimens that are considered failed.

On the issue of specimen and container size constraints, various possibilities exist which could ultimately result in different specimen quantities, with associated changes in T-t characteristics within the freezer. A simple but effective recommendation to address this issue is to standardize the container size to be used for ASTM C 1262 (2003) testing.

Removal of failed specimens (e.g., mass loss exceeded specification limit) during the course of a test also changes the total number of specimens in the freezer and thus changes the exposure for the balance of the specimens. While such situations are clearly dealt with in ASTM C 666 (2004) for rapid freeze-thaw of ordinary concretes, ASTM C 1262 (2003) has no provision for this. ASTM C 666 (2004) covers this situation as follows: “Whenever a specimen is removed because of failure, replace it for the remainder of the test by a dummy specimen,” (Clause 8.3, ASTM C 666, 2004). It is recommended that ASTM C 1262 (2003) adopt a similar provision and require that a failed specimen, upon removal from the chamber, be replaced by a “dummy” specimen to prevent fluctuations in the total mass inside the freezer during the course of a test.

Overall, it is seen that total specimen quantity in the freezer can vary for a number of reasons, which alters the temperature environment inside the freezer. This in turn changes the exposure

conditions of the specimen themselves. As such, it is important that laboratories conducting freeze-thaw tests survey their freezers before conducting tests, to identify these variations and the extent to which temperatures may be distributed in the freezer. Knowledge of this temperature variability should then be employed to plan tests cycles, the results of which can be used to optimize the testing regime for that given freezer. Complete details on this approach are provided in Chan (2006). This approach requires a test cycle to be run on a given freezer (with a given number of test specimens) with temperature monitored throughout the chamber, from which T-t and standard deviation-t curves can be generated. A reliability-based approach is then taken to optimize the control of the freezer to minimize locations within the freezer that are undercooled or overcooled, in other words to minimize the proportion of noncompliant locations within the freezer. This approach, which makes use of graphical reliability (R) curves, is described in appendix A, where it appears as an annex to a new proposed version of ASTM C 1262 (2003) based on the findings of this project. Additional information, including sample calculations, can be found in chapter 4 of Chan (2006).

It should be noted that this approach of performing trial tests and statistically optimizing actual tests based on these results has already been applied to the NCMA-funded study and other ongoing projects. It must also be emphasized that R-curves portray a specific interaction between the freezer and specimens. A given freezer loaded with a certain quantity of specimens of a particular size, mass and arrangement inside the freezer will possess a uniquely characteristic R-curve. Changing any of these variables will alter the form of the curve. Finally, R-curves cannot be determined a priori but must be determined individually for each freezer and specimen configuration.

4.4 CHARACTERISTICS OF THE FREEZE-THAW CYCLE

Section 4.3 focused on evaluating temperature variability inside a freezer during a typical freeze-thaw cycle. The objective of this evaluation was to enable maximizing the number of locations in the freezer that were compliant with ASTM C 1262 (2003) cold soak requirements, which consists of maintaining the freezer air temperature at –18 °C ± 5 °C (0° ± 10 °F) for 4 to 5 hours (note that this is irrespective of how fast the freezer cooled to this condition). However, as shown in figure 89, the T-t response of the SRW specimen itself (as measured from sensors embedded in the specimen, figure 90) follows a path that is distinct from that of the freezer air. This section discusses the ice formation process and damage mechanisms as the specimen undergoes the various stages in a freeze-thaw cycle.

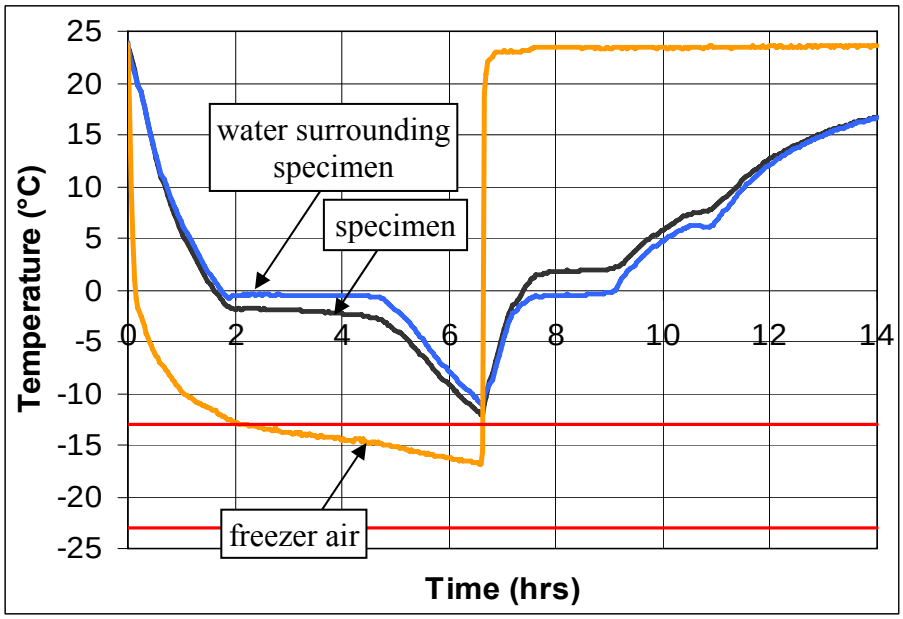

Tf = (9/5) * Tc + 32 {Tf = Fahrenheit, Tc = Celsius}

Figure 89. Graph. T-t curves for freezer air, water surrounding specimen and specimen.

Figure 90. Photo. Water surrounding specimen and specimen (as graphed in figure 89).

The work described in this section involved calorimetric methods to trace ice formation during freezing of plain water and 3 percent NaCl solution (salt as percentage of solution mass). The concept of freeze progress (or percent ice formed) was introduced to describe and quantify ice formation rates. Concentration changes in the salt solution during freezing were also examined. The work also includes the use of glass vials such as those shown in figures 91 through 94 to simulate freezing of solutions in saturated, confined spaces. Events taking place during freezing such as supercooling and expansion damage were traced along the T-t response of the solution. Other relevant aspects investigated included varying concentrations of salt solution, varying saturation levels, effect of cooling environment and estimation of ice pressures.

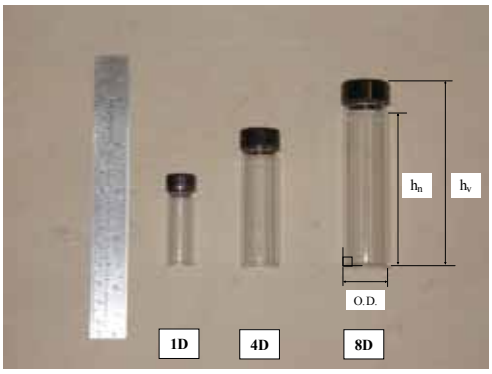

Figure 91. Photo. Temperature-monitored glass vials used to characterize freeze-thaw cycles and impact on water and saline solutions.

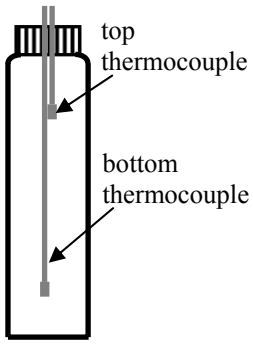

Figure 92. Drawing. Location of thermocouples.

Figure 93. Photo. Vials in freezer.

Figure 94. Photo. Broken vials.

4.4.1 Significance of Freeze-Thaw Cycle

Differences in the nature of the freeze-thaw environment can have an impact on specimen performance as evidenced from results obtained under this FHWA project and in the NCMA-funded project. In summary, for the NCMA study (described in detail in chapter 6 of Chan (2006)), specimens extracted from SRW units from a single production run were tested in two separate freezers: the walk-in chamber and the cabinet freezer, which were described earlier in this chapter. When tested according to ASTM C 140 (ASTM C 140, 2000), properties of the specimens evaluated in the two freezers differed by no more than 8 percent in their compressive strength (average 37 MPa (5,370 psi)) for specimens in walk-in chamber versus average 34 MPa (4,930 psi) for specimens in cabinet freezer), 2 percent in water absorption (127 versus 129 kg/m^3) and 2 percent in oven-dry density (2230 versus 2210 kg/m^3). Of the various test sets (labeled A to G) evaluated in the cabinet freezer, test set A specimens were similar to specimens tested in the walk-in freezer, which comprised nominal 200- by 100- by 32-mm-(8- by 4- by 1¼-inches-) size SRW coupons placed in 13 mm-(½ inch-) deep saline solution inside plastic containers of size 310 by 210 by 108 mm (12.3 by 8.3 by 4.3 inches), as shown in figures 95 and 96.

Figure 95. Photo. View of typical specimen in test set A in cabinet freezer and walk-in freezer (NCMA study).

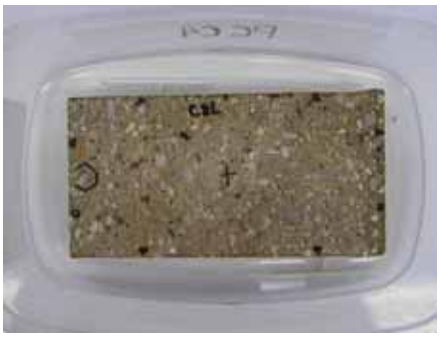

Figure 96. Photo. View of open container with specimen.

Figure 97 shows the percent mass loss (i.e., residues as percentage of initial specimen mass) through 200 cycles for 16 specimens in the walk-in freezer (lighter lines) and 4 specimens in test set A in the cabinet freezer (darker lines). The average mass loss of all specimens in the walk-in freezer, including the two specimens exhibiting sudden jumps in mass loss at about 80 and 100 cycles, was 0.2 percent after 100 cycles and 0.8 percent after 200 cycles. By contrast, the average mass loss of test set A specimens in the cabinet freezer was 0.4 percent after 100 cycles and 4.4 percent after 200 cycles. Thus, mass loss between specimens in the two freezers differed by up to a factor of 2 after 100 cycles and a factor of 5.5 times after 200 cycles. Structural integrity of specimens was monitored by changes in the relative dynamic modulus (RDM) of the specimens using resonant frequency methods (ASTM C 215, 1997). Figure 98 shows RDM through 200 cycles for these same specimens. The average RDM for specimens in the walk-in freezer was about 100 percent after 100 cycles and 79 percent after 200 cycles. By contrast, the average RDM of test set A specimens in the cabinet freezer was about 93 percent after 100 cycles and 4 percent after 200 cycles.

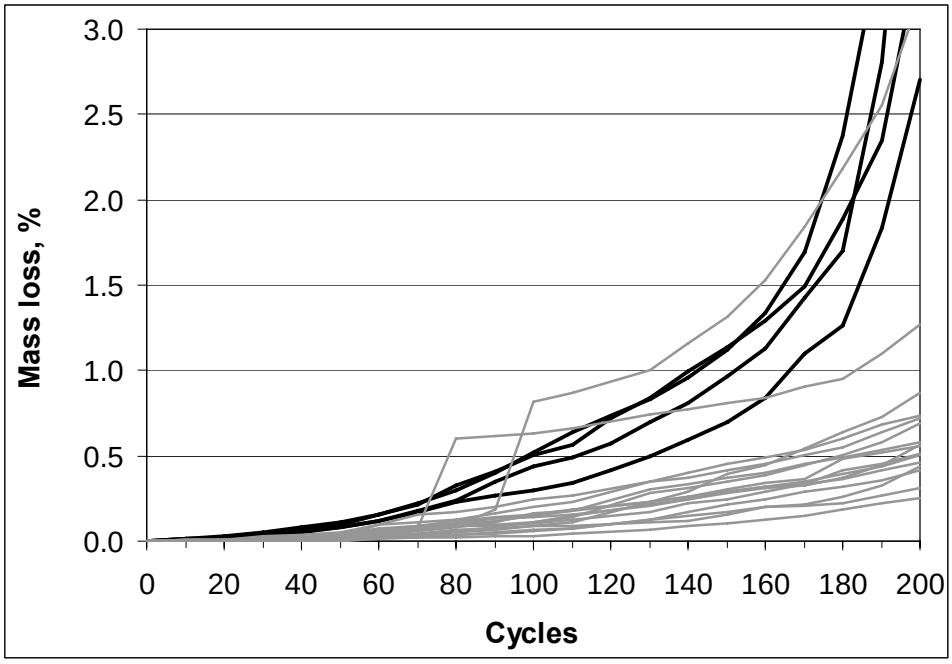

Figure 97 Graph. Comparative performance of specimens in test set A in cabinet freezer (darker lines) and specimens in walk-in freezer (lighter lines)—percent mass loss.

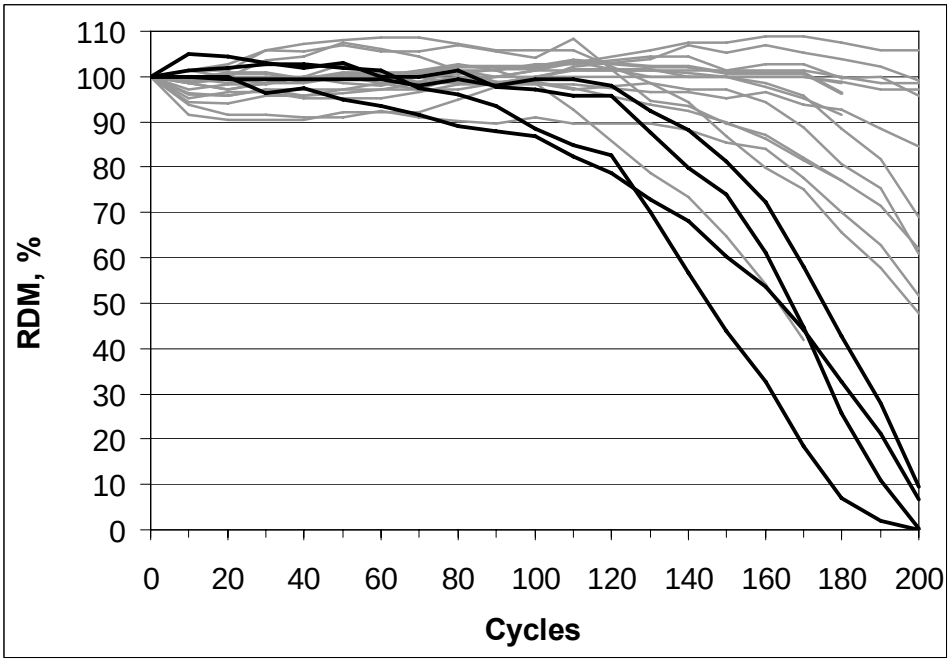

Figure 98. Graph. Comparative performance of specimens in test set A in cabinet freezer (darker lines) and specimens in walk-in freezer (lighter lines)—relative dynamic modulus.

As for the test environments in these two freezers, figure 99 shows freezer air T-t curves for typical cycles in the two freezers. Also shown are T-t curves for the solution surrounding instrumented specimens in the two freezers. Both freezer air cycles were fully compliant with

ASTM C 1262 (2003) test method requirements. Specimens in the walk-in freezer were subjected to a cold soak period of 4.8 hours, whereas specimens in the cabinet freezer were subjected to a cold soak period of 4.5 hours. Each freezer reached a different minimum air temperature at the end of cold soak (–16.9 °C (1.6 °F) in walk-in and –18.5 °C (–1.3 °F) in cabinet). The curves in figure 99 are reproduced again in figures 100 to 102 together with rates of change of freezer air temperature and solution temperature. Differences can be discerned in the following areas:

- Between 1.5 and 2 hours, the freezer air cooled at a rate of approximately –9 to –10 °C/hr (–16 to –18 °F/hr) in the cabinet freezer, compared to approximately –3 to –4 °C/hr (–5 to –7 °F/hr) in the walk-in freezer, which was almost a three-fold difference. This was also the time period during which the solution surrounding specimens in both freezers entered their freezing plateaus.

- Between 6 and 7 hours, the peak freezer air warming rate was 135 °C/hr (245 °F/hr) in the cabinet freezer, compared to about 88 °C/hr (160 °F/hr) in the walk-in freezer, which was a 50 percent difference. These peaks occurred immediately after the end of cold soak as the warming branch started.

- Before 2 hours, the cooling rate of the salt solution surrounding specimens was –18 °C/hr (–32 °F/hr) for the specimen in the walk-in freezer and –19 °C/hr (–34 °F/hr) for the specimen in the cabinet freezer. However, between 3 and 6 hours, after their respective freezing plateaus, the solutions cooled at –8 °C/hr (–14 °F/hr) in the cabinet freezer compared to about –4 °C/hr (–7 °F/hr) in the walk-in freezer, which was a two-fold difference.

- Between 6 and 7 hours, the peak solution warming rate was 33 °C/hr (59 °F/hr) in the cabinet freezer, compared to 14 °C/hr (25 °F/hr) in the walk-in freezer, which was almost a 2.5 times difference. These peaks also occurred immediately after the end of cold soak as the warming branch started.

- Moreover, the lengths of solution freezing plateaus were different in the two freezers. For the walk-in freezer, the freezing plateau was estimated to be approximately 1.9 hours long, while for the cabinet freezer, this was about 1.2 hours long. If it is assumed that the same volume of solution is frozen during this freezing plateau (which is a reasonable assumption, as will be shown in section 5.2.1), the solution froze 50 percent faster in the cabinet freezer compared to in the walk-in freezer.

A summary of the measured differences between the two freezers is provided in table 8. How these specific differences in freezer air and solution temperature translated to specimen performance is yet to be explored, although it is evident from the mass loss and RDM curves that disparities in the performance were obtained from specimens tested in these two environments. The following sections describe experimental work carried out with the objective of elucidating ice formation in specimens and how these link to their cooling curves and to the overall requirements of ASTM C 1262 (2003).

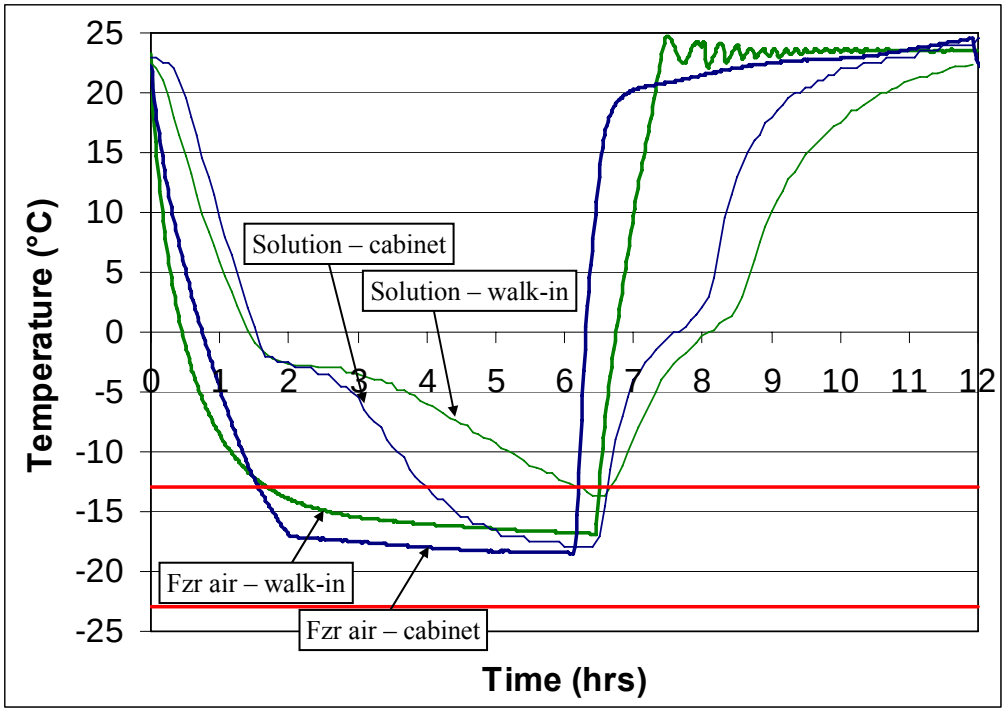

Tf = (9/5) * Tc + 32 {Tf = Fahrenheit, Tc = Celsius}

Figure 99. Graph. Cooling curves comparison for typical cycles in the two freezers.

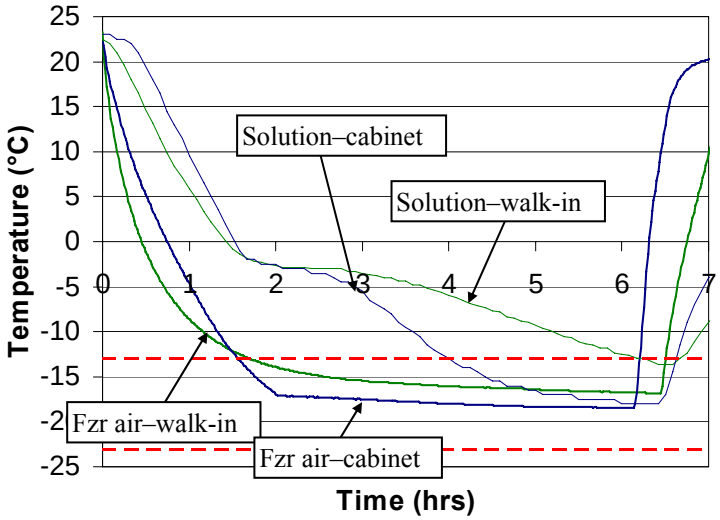

Tf = (9/5) * Tc + 32 {Tf = Fahrenheit, Tc = Celsius}

Figure 100. Graph. Rates of temperature change for curves in figure 99—temperature.

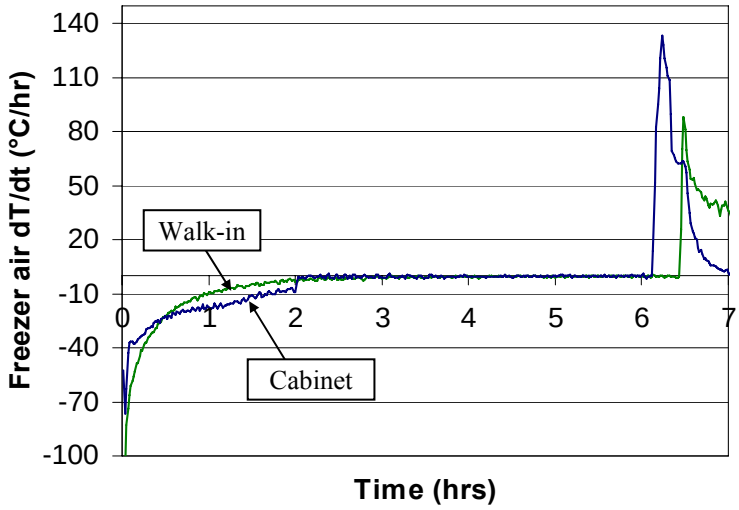

Tf = (9/5) * Tc + 32 {Tf = Fahrenheit, Tc = Celsius}

Figure 101. Graph. Rates of temperature change for curves in figure 99—freezer air.

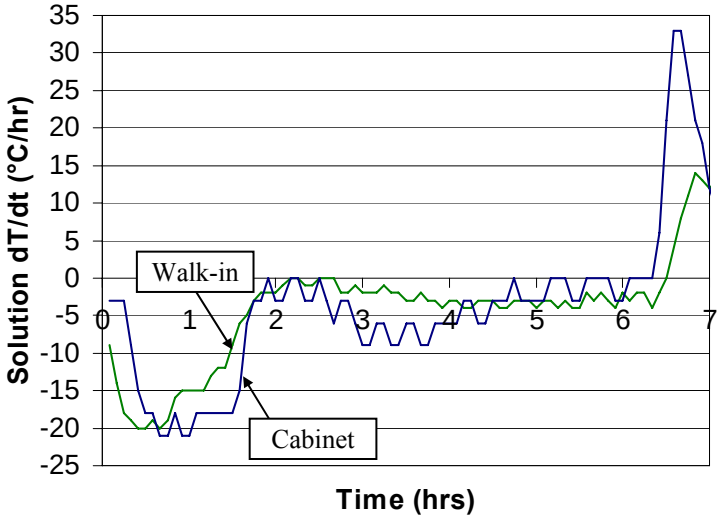

Tf = (9/5) * Tc + 32 {Tf = Fahrenheit, Tc = Celsius}

Figure 102. Graph. Rates of temperature change for curves in figure 99—solution.

Table 8. Comparison of cycle parameters between cabinet and walk-in freezers.

Parameter	Walk-in	Cabinet
Time To Reach:		
0°C (32°F)	0.5 hour	0.8 hour
Start of cold soak	1.7	1.6
Rate of air cooling at start of solution freezing plateau [a]	3 to 4 °C/hr (5 to 7 °F/hr)	11 °C/hr (20 °F/hr)
Minimum Attained Temperatures		
Freezer air	–16.9 °C (1.6 °F)	–18.5 °C (–1.3 °F)
Solution	–13.7 (7.3)	–18.0 (–0.4)
Rate of solution freeze [b]	160 g/hr (5.6 oz/hr)	250 g/hr (8.8 oz/hr)
Peak Warming Rates:		
Freezer air [c]	88 °C/hr (160 °F/hr)	135 °C/hr (245 °F/hr)
Solution [c]	14 (25)	33 (59)

[a] obtained from the tangent to the curves at T = –13 °C
[b] obtained by dividing (mass of solution) / (length of freeze plateau)
[c] immediately after end of cold soak

4.4.2 The Cooling Curve

Chan (2006) in chapter 2 of his dissertation, presented the cooling curve for water and salt solutions in general and discussed in a qualitative manner the various steps taking place during their freezing. This section describes attempts to establish a more quantitative and mechanistic perspective of the cooling curve used in ASTM C 1262 (2003). Findings from this investigation are first highlighted, followed by their application to the understanding of the response of freeze-thaw test specimens.

4.4.2.1 Ice Formation and Rates

Ice formation in plain water and in 3 percent NaCl solution was measured using a calorimetric approach. A so-called "coffee cup calorimeter" was used to determine ice formation in freezing liquids, namely plain water and 3 percent NaCl solution. In this simple test, ice formation is measured by measuring heat changes inside the calorimeter which can in turn be related to ice quantities. Here, ice formation was traced by the parameter freeze progress (FP) which was defined as FP = mass of ice/mass of initial liquid × 100 percent. FP was traced as a function of temperature and time, which enabled plotting this parameter along the cooling (T-t) curves of these liquids. These results are shown in figure 103 for plain water and figure 104 for 3 percent NaCl solution. Note that in the cooling curve for 3 percent NaCl solution, the freezing plateau was not as well-defined as it was for plain water. This is due to the freeze concentration process,

whereby the yet unfrozen portion in a saline solution becomes increasingly concentrated in salts as ice crystallizes out of solution during freezing (Sahagian and Goff, 1996). This process leads to the continuously decreasing freezing point of the solution which contrasts with the constant freezing point of water (at T of about 0 °C (32 °F)). As such, for the saline solution, a quasi-freezing plateau was defined as the region between supercooling and the region of maximum curvature (between t = 250 to 300 min). Figures 103 and 104 show FP-t curves; while figures 105 and 106 show the rates of ice formation (i.e., d(FP)/dt). The main conclusions drawn from this work follow:

- During the freezing plateau, about 90 percent of water crystallizes (i.e., FP is about 90 percent near the end of the plateau when maximum curvature is observed in the cooling curve).

- In 3 percent NaCl solution, FP was about 75 to 80 percent at the point of maximum curvature in the cooling curve. At a temperature of –18 °C (0.4 °F), the maximum FP is about 85–88 percent.

- At any given time during freezing, FP in the saline solution was less than in plain water.

- The rate of ice formation in saline was about $7/8^{th}$ that in water over the duration of the freezing plateau. Hence, ice formed from the saline solution almost as fast as it did from plain water. In both plain water and saline, this ice formation rate was maximum during the freezing plateau ("quasi freezing plateau" in saline) and decreased substantially near the end of the plateau. It is noted that actual observation of ice growth in glass vials (using the Direct Observation method described later in this chapter) shows that ice growth immediately following supercooling is up to 10 times slower in saline solution compared to plain water.

- Volumetric expansion, ε_V, could be related to FP as follows:

$$\varepsilon_V \text{ (percent)} = 0.09 \times \text{FP(percent)} \qquad \text{Equation 8}$$

Hence, most of the volume expansion is expected to occur and to occur fastest during the freezing plateau.

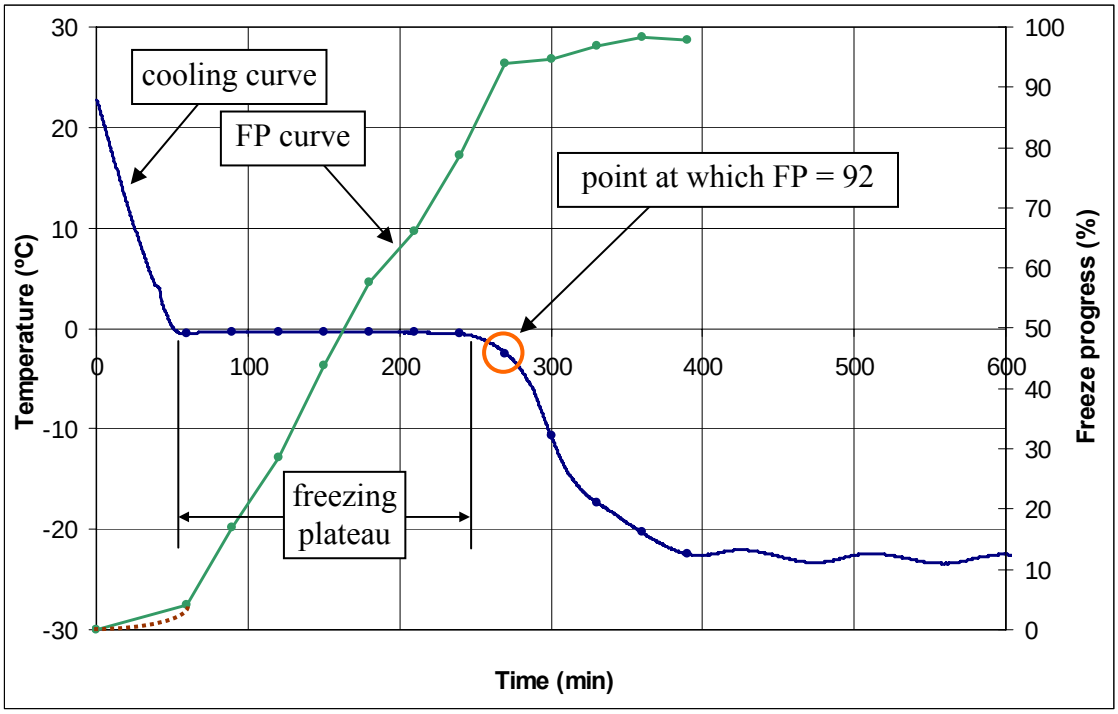

Figure 103. Graph. Cooling curves and FP-t curves for plain water.

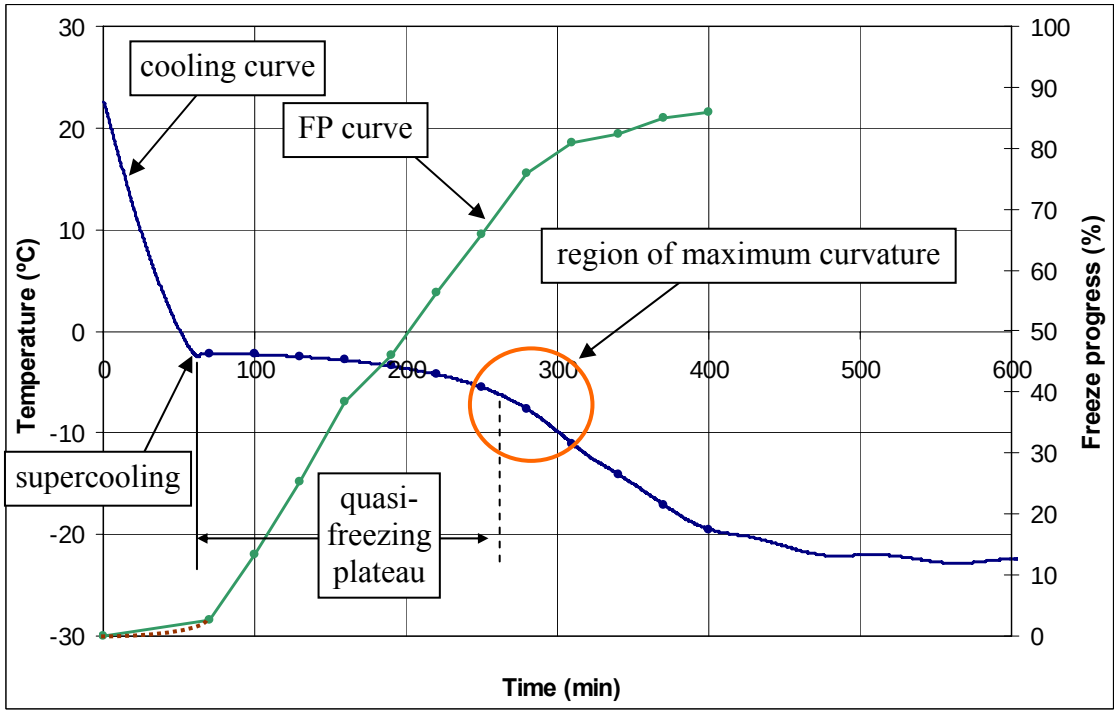

Figure 104. Graph. Cooling curves and FP-t curves for 3 percent NaCl solution.

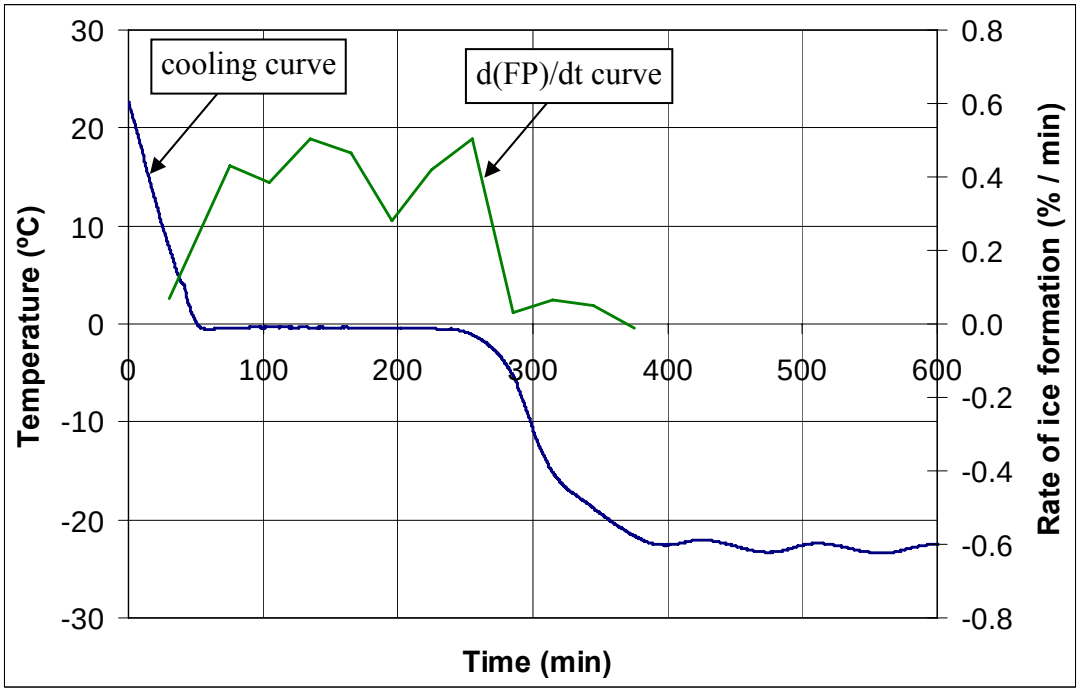

Figure 105. Graph. Cooling curves and rate of ice formation curves for water.

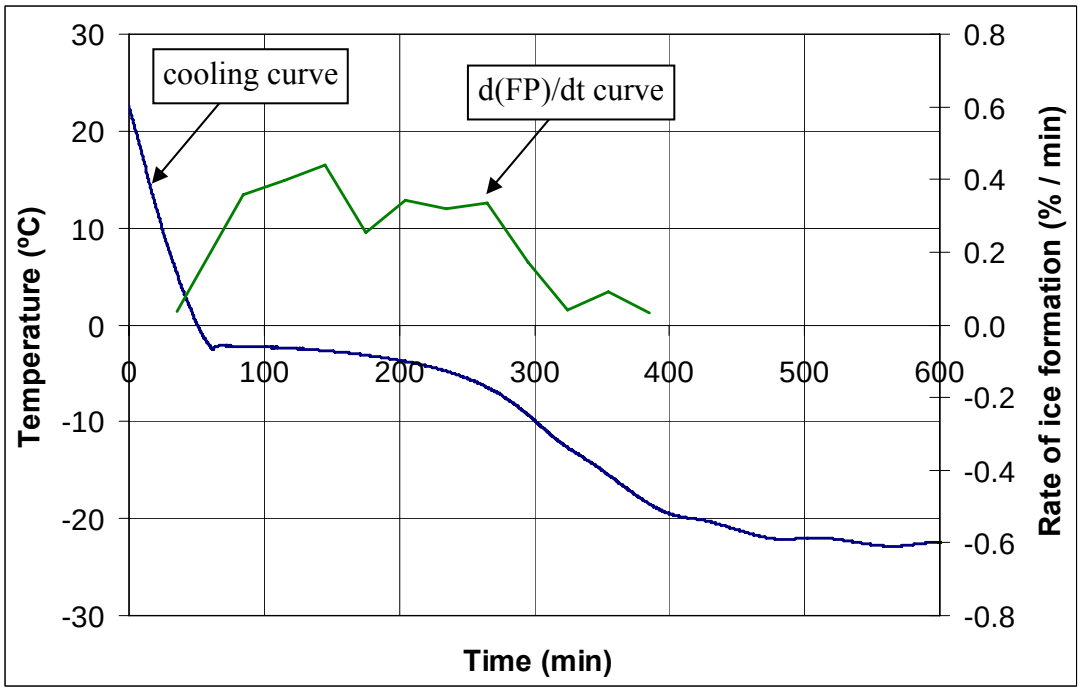

Figure 106. Graph. Cooling curves and rate of ice formation curves for 3 percent NaCl solution

Another result from this work was plots of FP versus T which are shown in figure 107 for water and 3 percent NaCl solution. Here, it is seen that for water most of the ice formed at about 0 °C (32 °F) while for the saline solution, ice formation was accompanied by reductions in temperature. At –18 °C (0.4 °F) which is the target cold soak temperature in ASTM C 1262 (2003), there was still about 15 percent unfrozen solution. The significance of this on ASTM C 1262 (2003) testing will be discussed later in this chapter.

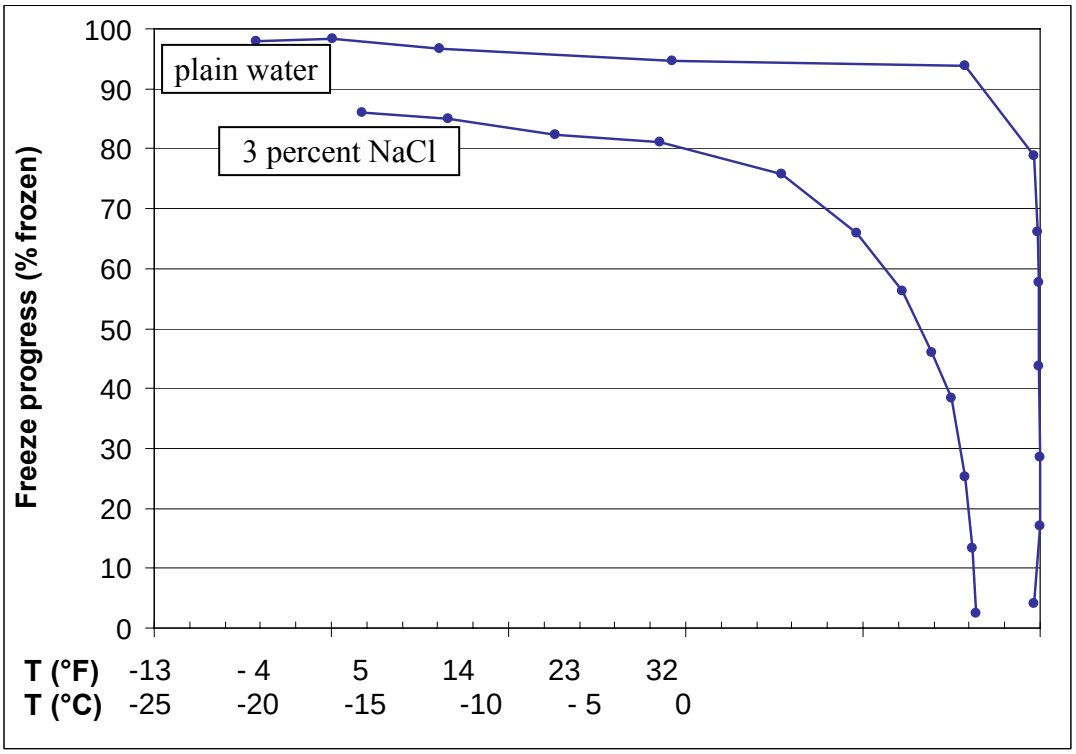

Figure 107. Graph. Plots of FP as function of temperature.

4.4.2.2 Changes in Concentration for Saline Solution

In addition to ice formation, changes in the concentration of the unfrozen solution were also measured and traced along the cooling curve for the 3 percent NaCl solution, as shown in figure 108. It is noted that beyond about 165 minutes cooling, measuring this concentration experimentally was difficult due to increased ice formation. Also plotted in figure 108 are concentration versus time values based on tabulated data in the *CRC Handbook of Chemistry and Physics* (CRC, 1988). It is seen here that at approximately halfway through the quasi-freezing plateau, the concentration of the unfrozen portion of the solution had risen up to about 5 percent from the initial 3 percent. Near the end of this quasi-plateau, this concentration was about four times the initial value. By the time the temperature of the solution was at the ASTM C 1262 (2003) cold soak target of –18°C (0°F), this concentration was at about six times the initial value. Figure 109 shows the rate of concentration change plotted together with the rate of ice formation (from figures 105 and 106). It is evident that ice formed most rapidly during the quasi-freezing plateau, whereas the concentration of the unfrozen solution increased most rapidly near the end of this plateau.

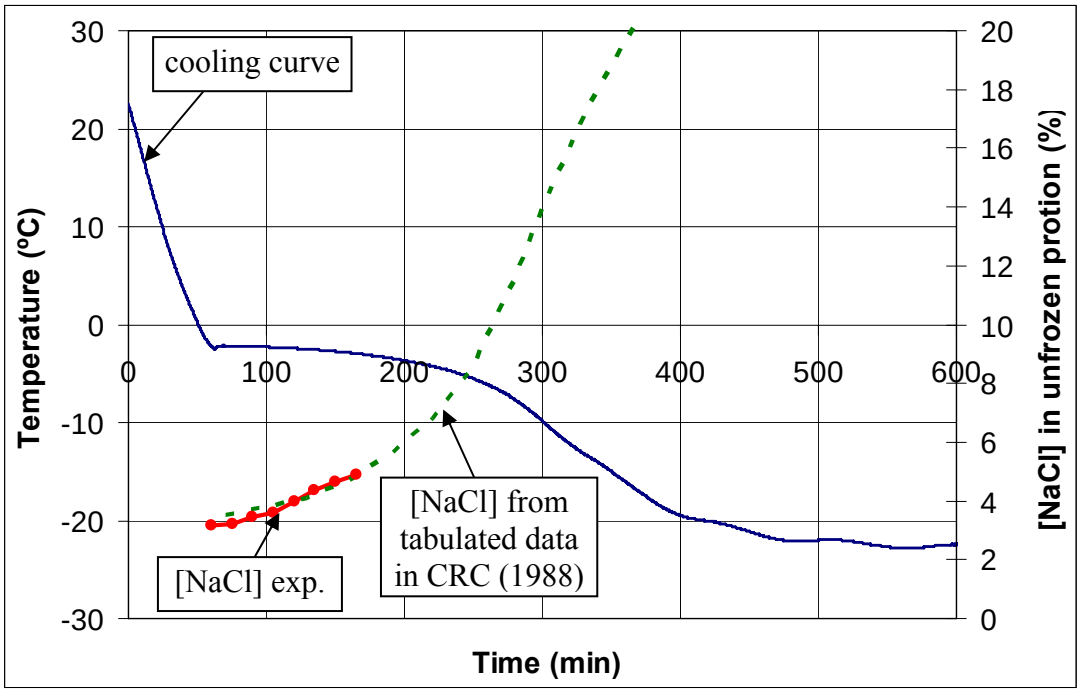

Figure 108. Graph. Changes in NaCl concentration in unfrozen solution.

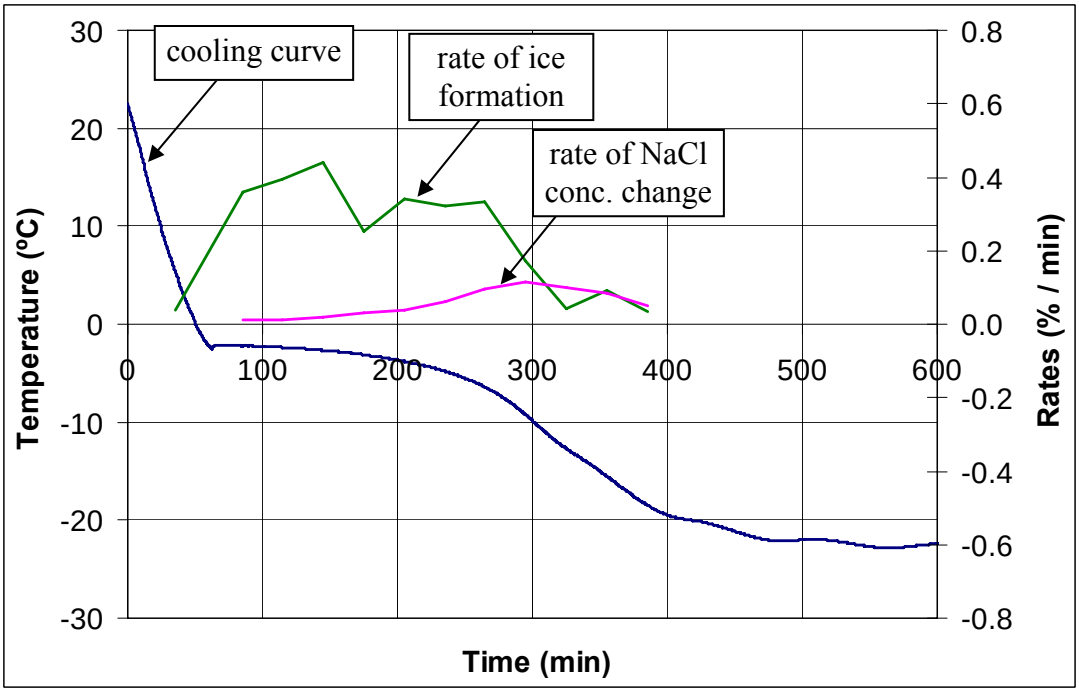

Figure 109. Graph. Rates of ice formation and concentration changes for initial 3 percent NaCl solution.

4.4.2.3 Damage Point

Various experiments were conducted in which water or saline solution-filled vials were utilized to model saturated, confined spaces. Expansion damage, as manifested by fracture of the vials, was detected using three different methods:

- *Circuit resistance method*, whereby an electric circuit was looped around the vial, and the resistance through this circuit was measured during freezing (figure 110). Rupture of the vial caused a break in the circuit and thus a spike in the measured resistance. The point at which this spike occurred was traced on the cooling curve of the freezing solution.

- *Strain gage method*, whereby strain gages were attached on the vial surface and monitored during freezing of the vials (figure 111).

- *Direct observation method*, whereby tests were carried out in a freezer with a see-through door opening which enabled direct visual observations of the events taking place during freezing (figure 112).

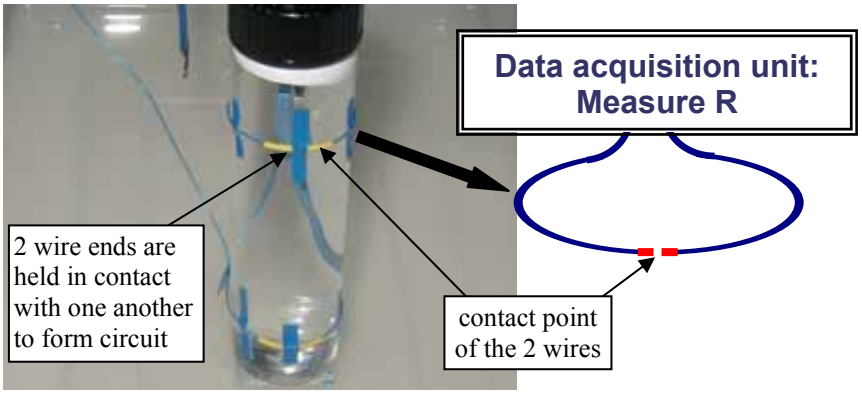

Figure 110. Photo and drawing. Circuit resistance for detecting expansion damage in freezing vials.

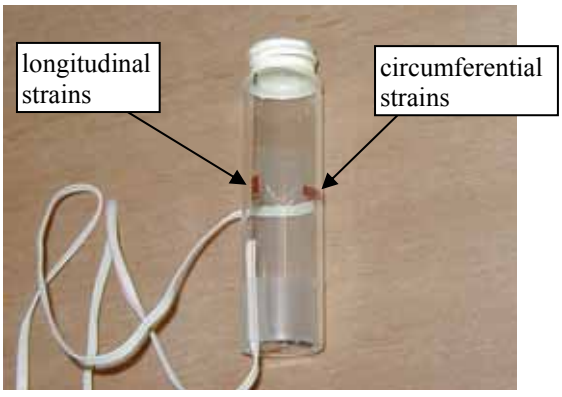

Figure 111. Photo. Strain gage for detecting expansion damage in freezing vials.

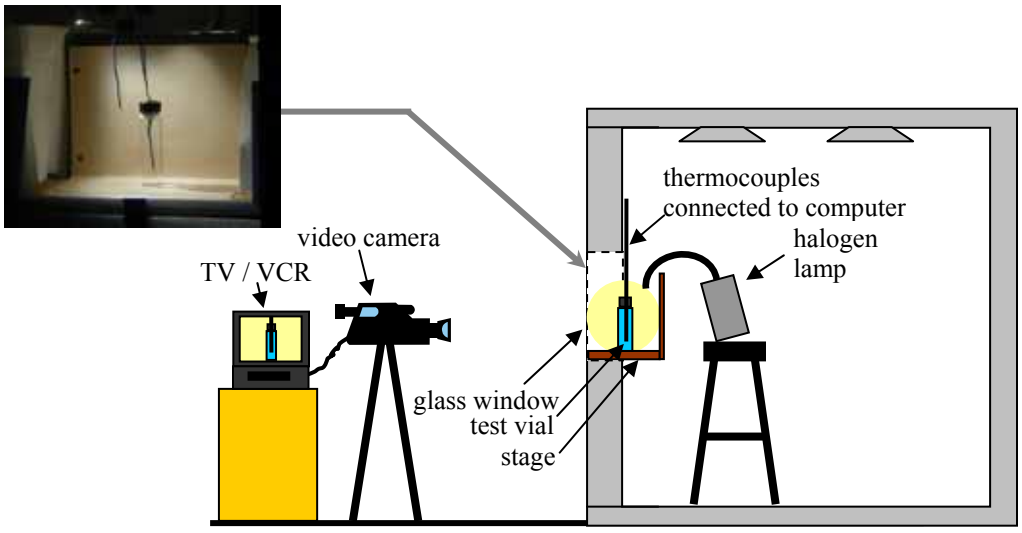

Figure 112. Drawing and photo. Direct observation for detecting expansion damage in freezing vials.

For circuit resistance tests, typical results are shown in figures 113 through 118 for different setups of the vials (water-filled unconfined vial, water half-filled unconfined vial, and water-filled mortar confined vial). In each case, thermocouples at two locations (top and bottom, see figure 92) were used to register the T-t response, and two wire loops were also setup at the approximate heights of the thermocouples. Figures 113 through118 show results for T-t response from the thermocouples as well as the resistance versus time response from the circuit. In all cases shown, at least one of the circuits broke near the end of the freezing plateau on the cooling curve. These points of rupture are also shown in the figures. These observations suggested that expansion damage in the vials occurred near the end of the freezing plateau, just before the temperature dropped further.

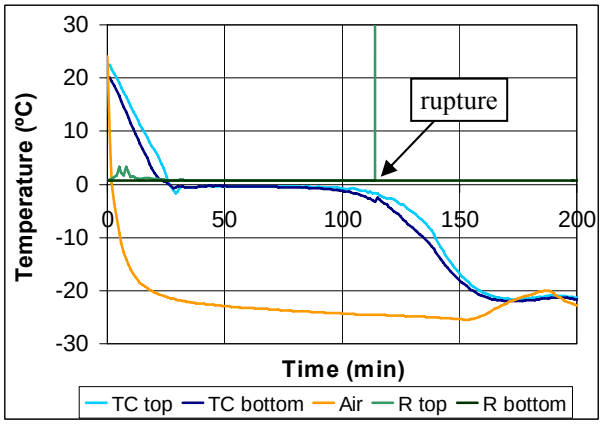

Figure 113. Graph. Results of water-filled unconfined vial in circular resistance test.

Figure 114. Photo. Water-filled unconfined vial.

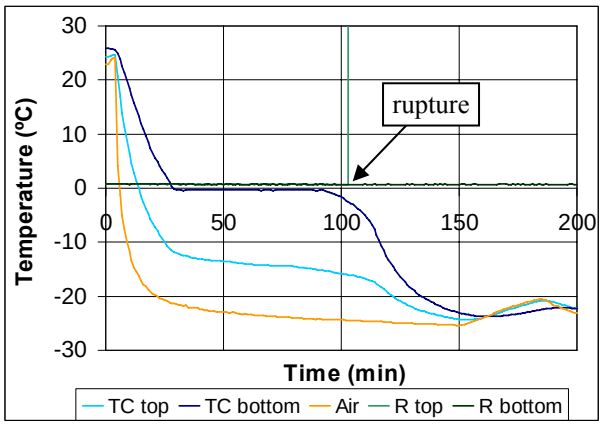

Figure 115. Graph. Results of water half-filled unconfined vial in circular resistance test.

Figure 116. Photo. Water half-filled unconfined vial.

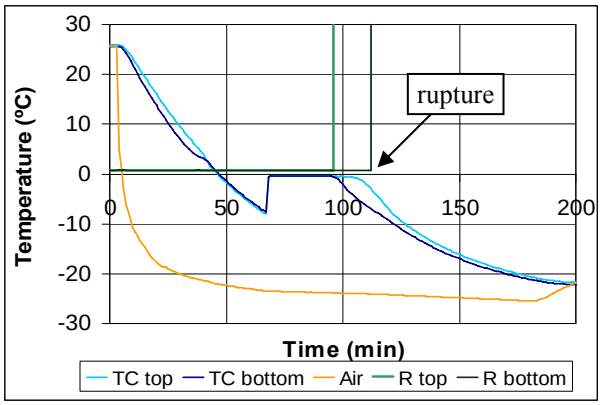

Figure 117. Graph. Results from water-filled, mortar-confined vial in circular resistance test.

Figure 118. Photo. Water-filled, mortar-confined vial.

For strain gage tests, results for vials filled with water and 3 percent NaCl solution are shown in figures 119 through 122. The T-t curves from thermocouples in the liquid are shown as well as the strain gage response along the circumferential direction at vial midheight. In both cases, there was substantial activity recorded along the freezing plateau. For water, the strain peaked sharply at the start of the plateau and reached another peak again just before the end of the plateau. This agrees with the result obtained using the circuit resistance method in which rupture was also detected near the end of the plateau. Figure 120 shows the multiple failure locations on the vial (cracking along the vial body and breakage of the cap). For 3 percent NaCl solution, the strain reached two consecutive peaks also at the start of the plateau and gradually subsided. Multiple fracturing along the vial was also observed (figure 122).

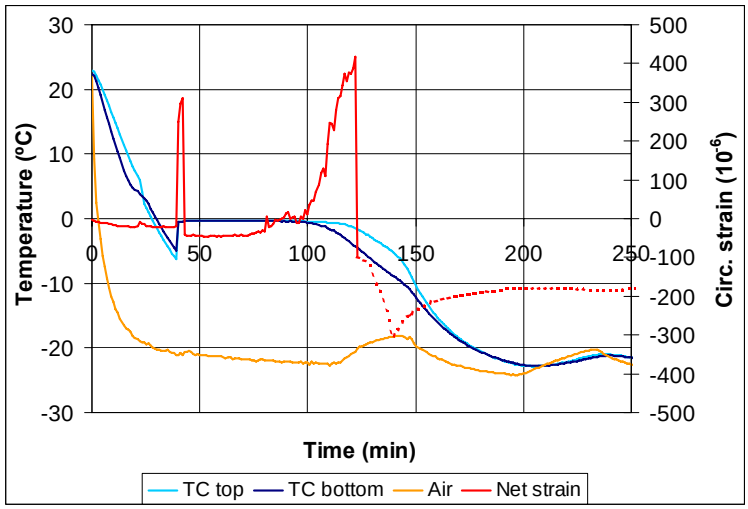

Tf = (9/5) * Tc + 32 {Tf = Fahrenheit, Tc = Celsius}

Figure 119. Graph. Results of strain gage method—plain water.

Figure 120. Photo. Vial after test.

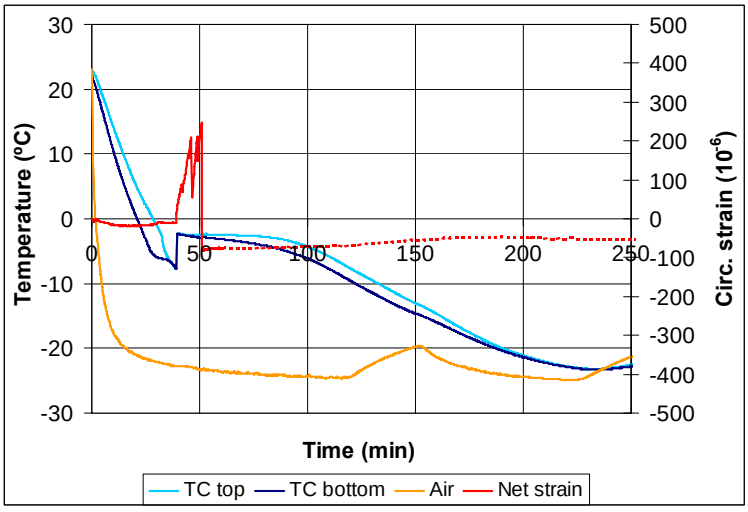

Tf = (9/5) * Tc + 32 {Tf = Fahrenheit, Tc = Celsius}

Figure 121. Graph. Results of strain gage method—3 percent NaCl solution.

Figure 122. Photo. Vial after test.

For the direct observation tests, results for vials filed with water and 3 percent NaCl solution are shown in figures 123 and 124, respectively, where the cooling curves are shown along with photos of the vial condition at various points on the curves. In these tests, it was observed that immediately after supercooling (at 50 mins in both figures 123 and 124), a cloudy phase propagated from the top to the bottom of the vial, filling the vial entirely with a crystalline network, as shown by figures 123b and 124b. This propagation event lasted anywhere from 5 to 10 seconds and marked the start of the freezing plateau. The plain water vial burst at around the 60-minute mark from start of cooling, and as shown in figure 123c, the bottom thermocouple was left exposed to freezer air, while the top thermocouple was still surrounded with ice. This is likely why the bottom thermocouple recorded a sudden drop in temperature, while the top thermocouple continued recording a full freezing plateau. As for timing, the "explosion" occurred at approximately one-quarter of the way into the freezing plateau as recorded by the top thermocouple. Similarly, the saline solution vial burst at around the 65-minute mark which corresponded to approximately one-third of the way into the quasi-freezing plateau as recorded by the bottom thermocouple (figure 124).

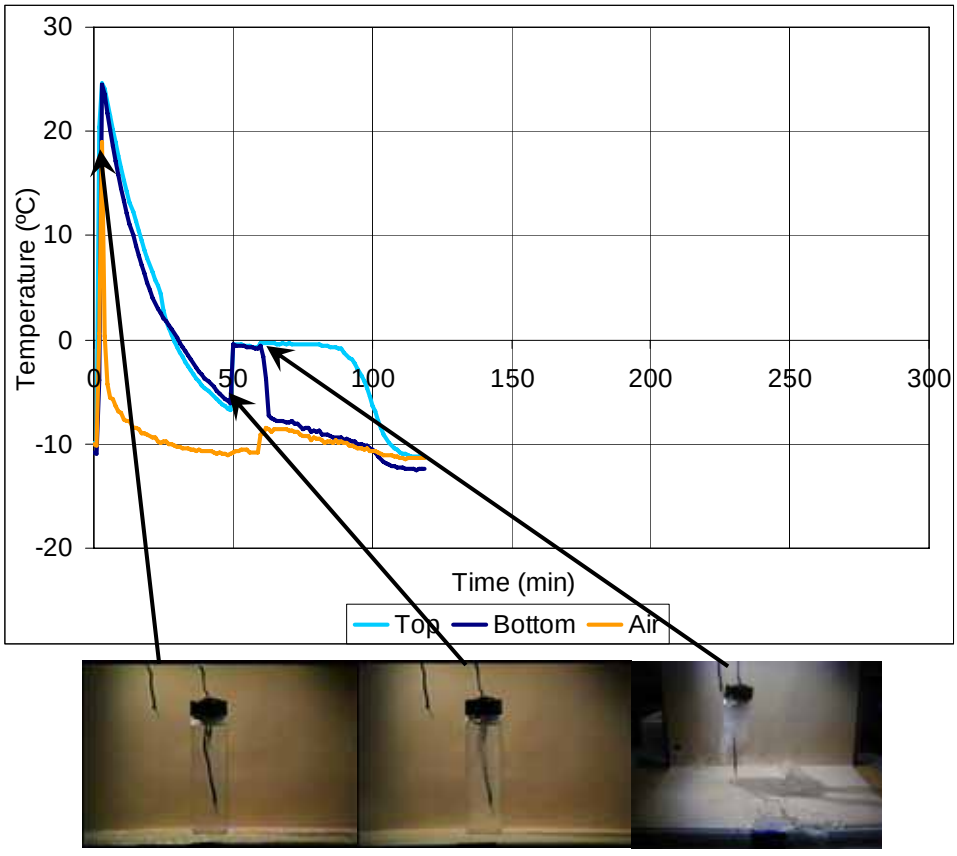

a. Test start b. Immediately after supercooling c. Vial breakage

$T_f = (9/5) * T_c + 32$ {T_f = Fahrenheit, T_c = Celsius}

Figure 123. Graph and photos. Results for direct observation method of damage detection (for water).

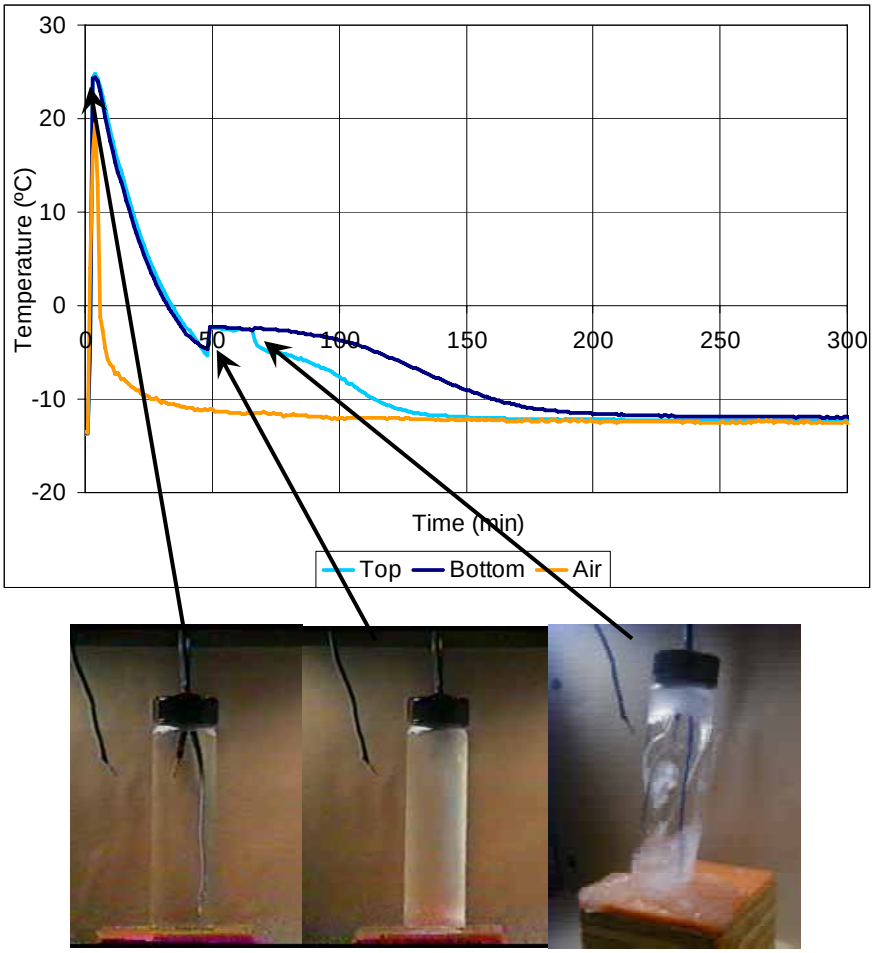

a. Test start b. Immediately after supercooling c. Vial breakage

$T_f = (9/5) * T_c + 32$ {T_f = Fahrenheit, T_c = Celsius}

Figure 124. Graph and photos. Results for direct observation method of damage detection (for 3 percent NaCl).

In summary, these vial tests, despite being performed via different approaches, all pointed toward the fact that expansion damage of the vials could occur at any point in the freezing plateau of the cooling curve. While the circuit resistance method indicated that rupture occurred at the end of the plateau, the other two methods suggested there were volume changes including the possibility of damage at any point during the plateau. Nevertheless, it appeared that in all cases, as long as a complete freezing plateau was observed in these tests, expansion damage would have occurred in the vials. Damage was not observed after the freezing plateau.

4.4.2.4 Connection to Freeze-Thaw Test Specimens

Cooling curves of ASTM C 1262 (2003) test specimens were monitored using thermocouples embedded in the specimens themselves. For each specimen of size 76 by 229 by 33 mm (3 by 9 by 1.3 inches), three thermocouples were grouted into predrilled holes in the specimens as shown in figures 125 and 126. The specimens were then placed in plastic containers that were 152 by 305 by 90 mm (6 by 12 by 3.5 inches), and the containers were subsequently filled with water to the 13-mm (½ inch-) level (figures 127 and 128). These instrumented specimens were subjected to ASTM C 1262 (2003) freeze-thaw cycles while their internal temperatures were monitored. An example of the response measured by one of these specimens was shown earlier in figure 89.

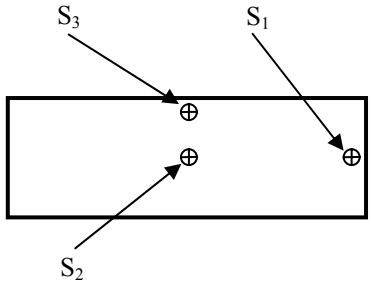

Figure 125. Drawing. Location of thermocouples (S_1, S_2, S_3) embedded in SRW specimen

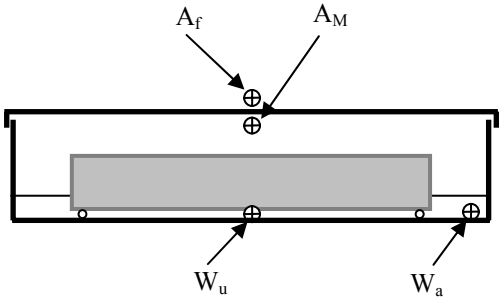

⊕ = thermocouple

Figure 126. Drawing. Location of thermocouples (A_f, A_m) and in water (W_u, W_a).

Figure 127. Photo. Container used to hold SRW blocks

Figure 128. Photo. Varying container sizes.

Figure 129 shows cooling curves for two instrumented SRW specimens that differed in their internal structure and material properties. SRW mix A was characterized by higher volume fraction of paste and lower volume fraction of total voids (air and compaction) compared to SRW mix B, as shown on the photos in figures 130 and 131.

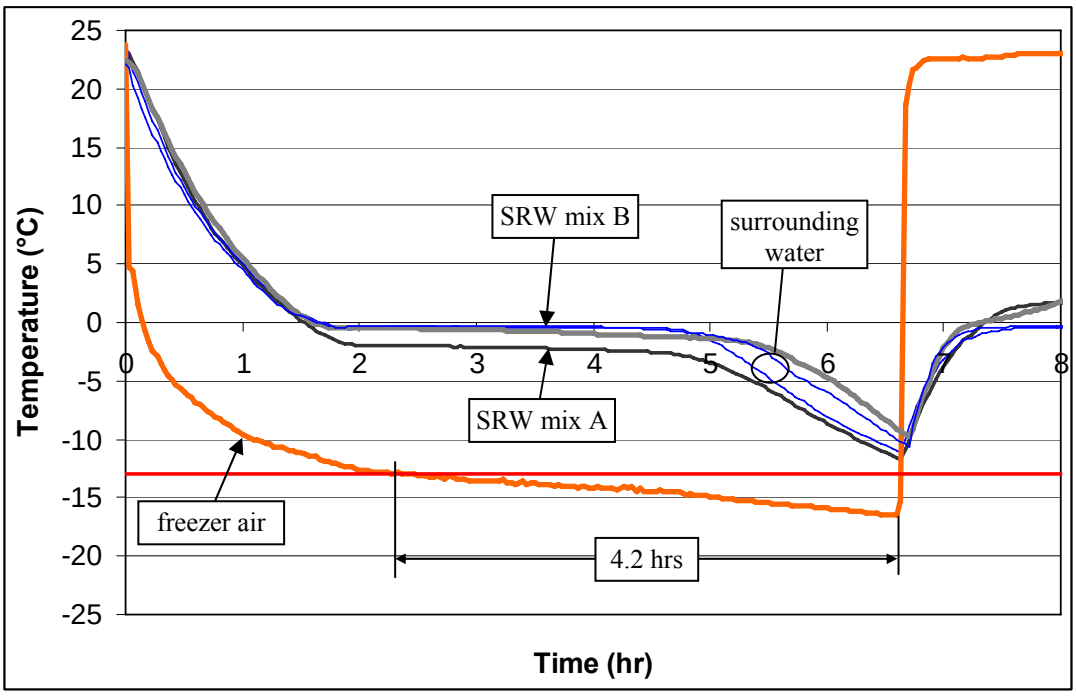

$T_f = (9/5) * T_c + 32$ {T_f = Fahrenheit, T_c = Celsius}

Figure 129. Graph. Cooling curves for SRW mix A and B.

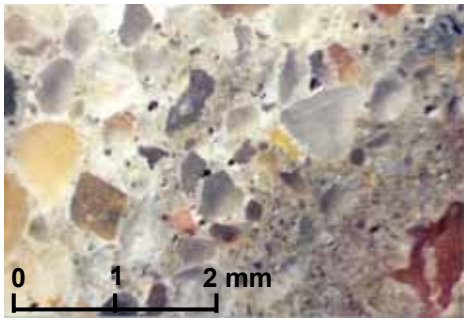

Figure 130. Photo. SRW mix A.

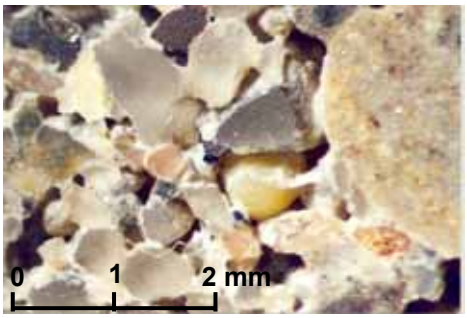

Figure 131. Photo. SRW mix B.

From the cooling curves of these specimens, it is seen that while pore water in mix B specimen froze at approximately the same temperature as the bulk water surrounding the specimen, pore water in mix A specimen had a slightly lower freezing point. In both cases, however, the cooling curve of the pore liquid in the specimens followed similar overall pattern as the cooling curve of the surrounding water as well as the liquids shown in preceding sections, which were characterized by a freezing plateau followed by a rapid descent in temperature. Based on our understanding of the processes occurring during freezing of liquids as presented earlier in this chapter, it is thus evident that various physical and chemical changes are taking place during freezing of solutions in the specimens. With this consideration, it also becomes apparent that specimens over a range of test conditions (e.g., specimens in different container sizes, in different locations in a freezer, in different freezers, and even from cycle to cycle) can exhibit

different cooling curves and possibly different extent of damage. The following parts show how specimen cooling curves may, however, vary under different conditions.

I. Varying volume of surrounding water

Specimen cooling curves were obtained by Hance (2005) in the walk-in freezer using the same instrumented specimens as those described above, but with varying volumes of surrounding water. These tests were conducted with the freezer loaded with a total of 40 specimens, and the results are reproduced in figure 132. The curve corresponding to a specimen immersed in water at the standard ASTM C 1262 (2003) depth of 13 mm (½ inch) is shown by the curve labeled "As spec." Variations to this condition involved changing the water volume by adding or removing 50 or 100 mL (1.7 to 3.4 fl oz) from the container, resulting in the other curves shown in the figure. It is interesting to note that while the initial cooling portions of the curves (prior to the freezing plateau) were similar in all cases, the lengths of freezing plateau and the shapes of the curve following the freezing plateau were dissimilar in each case. Increasing the volume of surrounding water had the primary effect of prolonging the freezing plateau. For the various curves in figure 132, the length of the freezing plateau was estimated using the method shown in figure 133, and these results together with other key parameters are summarized in table 9. It appears that in general, for every 50 mL (1.7 fl oz) increase in water, the freezing plateau was lengthened by about ½ hour. Another observation from these results is a difference in the final specimen temperature at the end of the cold soak periods. For every 50 mL (1.7 fl oz) increase in water, the specimen temperature increased by 0.7 to 2.2 °C (1.3 to 4.0 °F) after a 4-hour cold soak and by 0.1 to 0.7 °C (0.2 to 1.3 °F) after a 5-hour cold soak.

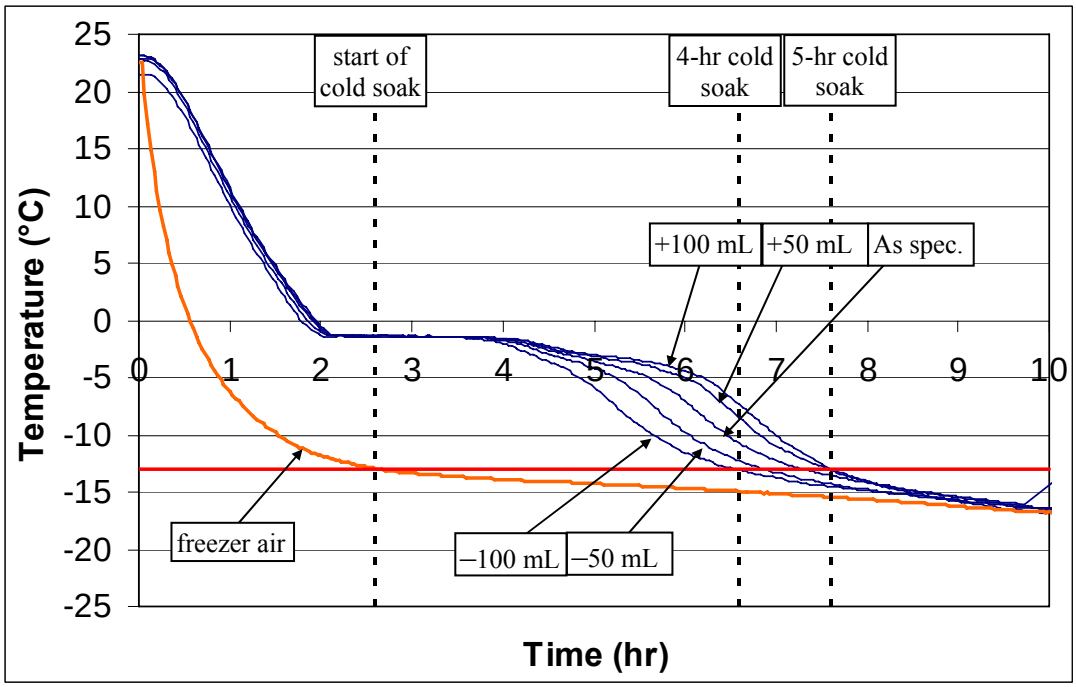

$T_f = (9/5) * T_c + 32$ {T_f = Fahrenheit, T_c = Celsius}

Figure 132. Graph. Specimen cooling curves for different volumes of surrounding water (reproduced from Hance, 2005).

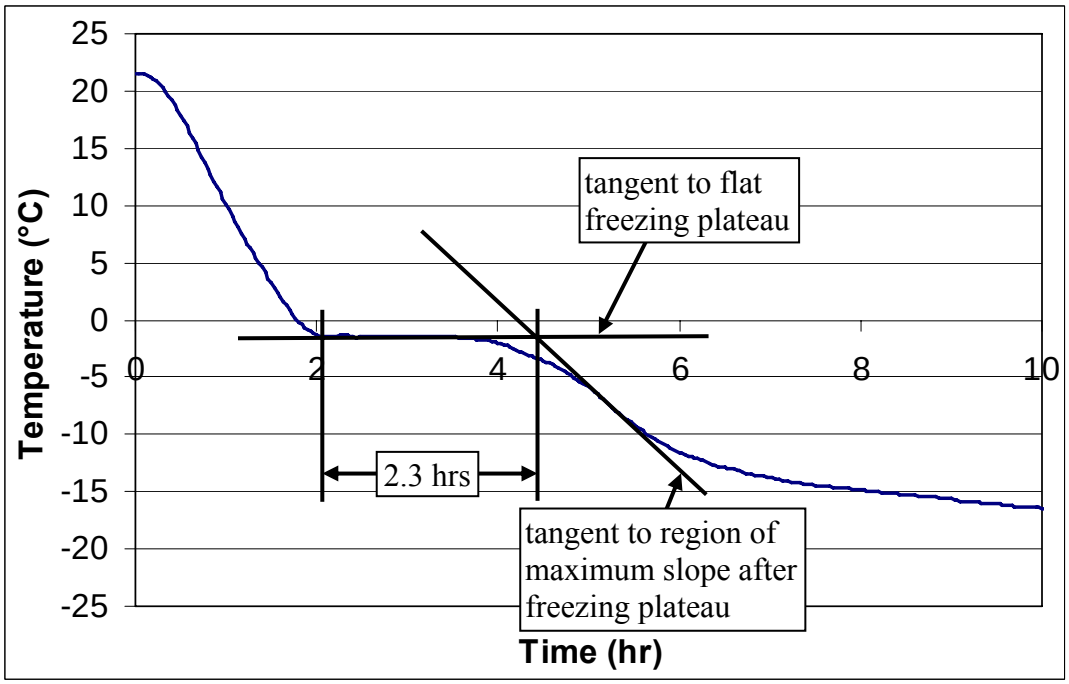

$T_f = (9/5) * T_c + 32$ {T_f = Fahrenheit, T_c = Celsius}

Figure 133. Graph. Simple approach to estimate length of freezing plateau.

Table 9. Measured differences for conditions of varying volumes of surrounding water.

Parameter	Surrounding Water Volume				
	–100 mL (3.4 fl oz)	–50 mL (1.7 fl oz)	As spec.	+50 mL (1.7 fl oz)	+100 mL (3.4 fl oz)
Specimen initial cooling rate, °C/hr (°F/hr)	14 (25)	14 (25)	14 (25)	14 (25)	13 (24)
Length of freezing plateau hours	2.3	2.7	3.0	3.4	3.6
Specimen temp. at 4-hour cold soak, °C (°F)	–13.1 (8.4)	–12.4 (9.6)	–10.9 (12.3)	–8.7 (16.3)	–7.6 (18.3)
Specimen temp. at 5-hour cold soak, °C (°F)	–14.5 (5.9)	–14.3 (6.2)	–13.6 (7.5)	–13.2 (8.2)	–13.1 (8.4)

This suggests that the specimen temperature is less sensitive to variations in surrounding water volume at a 5-hour cold soak (i.e., more time is required to remove the additional latent heat of fusion from the extra water.) However, at a given water volume, the difference in specimen temperature between 4 and 5 hours of cold soak ranged from 1.4 °C (2.5 °F) for the –100 mL (-3.4 fl oz) case to 5.5 °C (9.9 °F) for the +100 mL (3.4 fl oz) case. The slopes of the post freezing plateau part of the cooling curve were similar in all cases.

II. Varying container size

In a separate test, Hance varied the container size which correspondingly led to variations in water volume. Two container sizes were used: the same one as above (152 by 305 by 90 mm (6 by 12 by 3.5 inches)) and a smaller one (135 by 241 by 76 mm (5¼ by 9½ by 3 inches)). Both container sizes yielded clearances (specimen-to-edge of container distance) that were compliant with ASTM C 1262 (2003). The specimen cooling curves are shown in figure 134 where it is also seen that variations in this curve resulted from changes in container size. Key parameters for this comparison are shown in table 10.

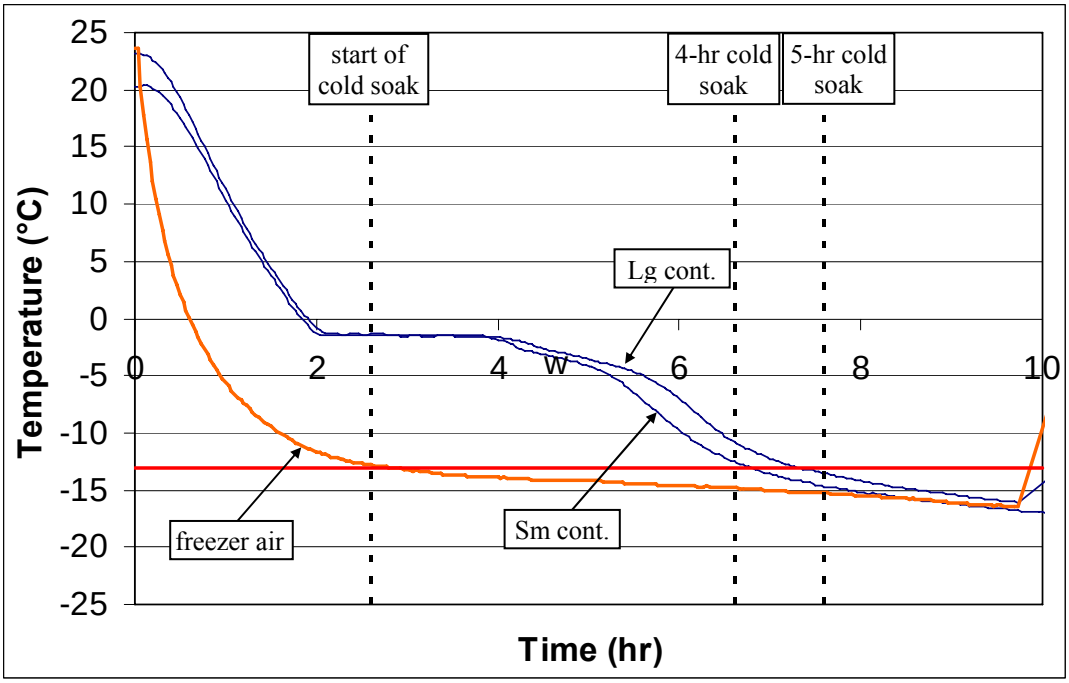

$T_f = (9/5) * T_c + 32$ {T_f = Fahrenheit, T_c = Celsius}

Figure 134. Graph Specimen cooling curves for different container sizes (reproduced from Hance, 2005).

Table 10. Measured differences for conditions of varying container sizes.

Parameter	Container Size	
	Small	Large
Specimen initial cooling rate, °C/hr (°F/hr)	13 (23)	13 (23)
Length of freezing plateau hours	2.8	3.2
Specimen temp. at 4-hour cold soak, °C (°F)	–13.0 (8.6)	–11.6 (11.1)
Specimen temp. at 5-hour cold soak, °C (°F)	–14.9 (5.2)	–13.9 (7.0)

III. Varying specimen quantities in a freezer

Section 4.3.1.2 demonstrated that the freezer air temperature in the walk-in chamber varied with increasing specimen quantities ranging from 2 to 100 specimens. In those tests, instrumented specimens were also placed in the freezer to obtain the specimen cooling curves under these conditions. The results are shown in figure 135 in which the freezer air temperature curves are reproduced. It is seen that substantial variations in actual specimen cooling response ensued by varying the number of specimens in the

chamber. Differences were seen in various parts of the cooling curve as summarized in table 11. Overall, specimen initial cooling rates were lower and final specimen temperatures were higher as the total specimen quantity increased. It is also noted that while freezer air temperatures did not drop significantly lower in going from a 4-hour cold soak to a 5-hour cold soak, specimen temperatures dropped an additional 1 °C (2 °F) during this extra hour.

Whether this additional 1 °C (2 °F) has any impact on the damage process in the specimens is not clear. The freezer air temperature curves shown in figure 136 for 2, 20, 40 and 60 specimens were compliant with ASTM C 1262 (2003) requirements. For 80 and 100 specimens, data collection was discontinued before the 4-hour cold soak was reached, but in these cases, the freezer air response could have been "made compliant" to ASTM C 1262 (2003) by simply extending the cooling time to the necessary time to achieve 4-hour cold soak (as long as it is below –13°C (8.6 °F).

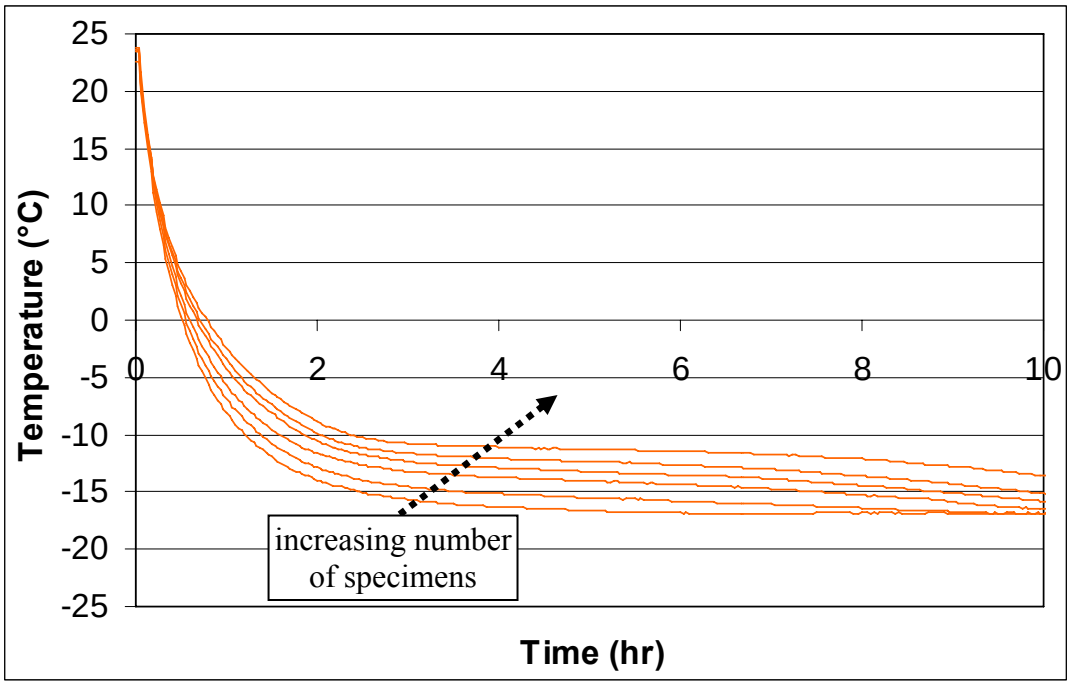

$T_f = (9/5) * T_c + 32$ {T_f = Fahrenheit, T_c = Celsius}

Figure 135. Graph. Cooling curves for varying specimen quantities in the walk-in chamber—freezer air.

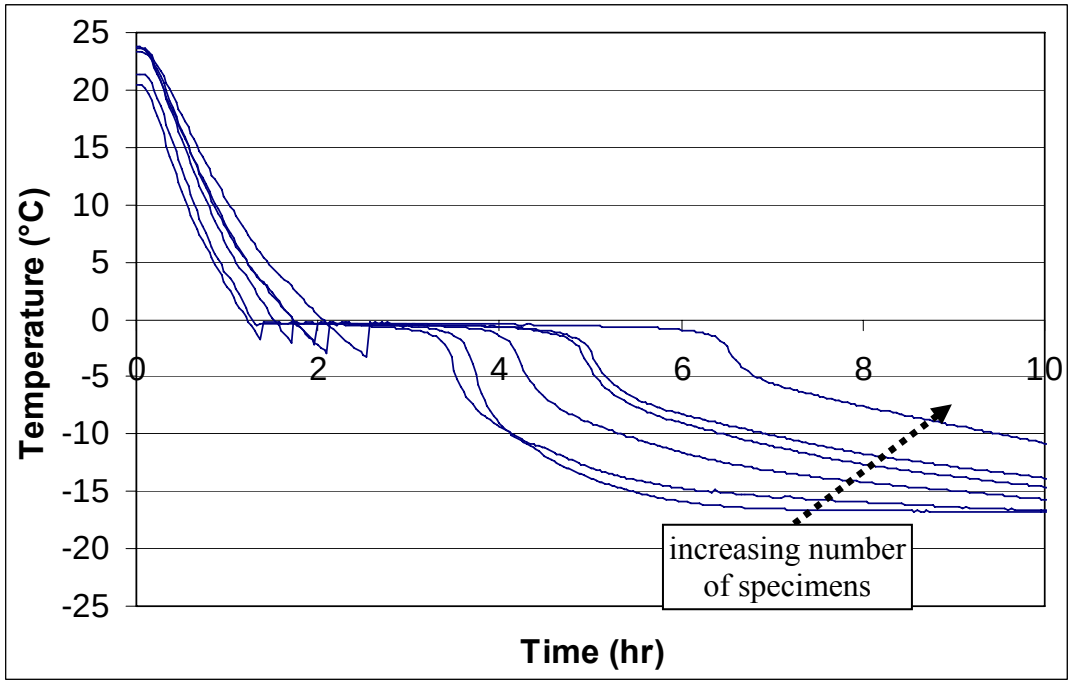

$T_f = (9/5) * T_c + 32$ {T_f = Fahrenheit, T_c = Celsius}

Figure 136. Graph. Cooling curves for varying specimen quantities in the walk-in chamber—specimen cooling curves.

Table 11. Measured differences for conditions of varying specimen quantities.

Parameter	Number of Specimens					
	2	20	40	60	80	100
Specimen initial cooling rate, °C/hr (°F/hr)	19 (34)	18 (33)	17 (30)	14 (26)	14 (25)	12 (21)
Length of freezing plateau hours	2.3	2.2	2.4	2.8	2.9	4.0
Freezer air temperature at 4-hour cold soak, °C (°F)	–16.8 (1.8)	–15.8 (3.5)	–14.6 (5.7)	–14.6 (5.8)	–	–
Specimen temperature at 4-hour cold soak, °C (°F)	–15.5 (4.1)	–14.8 (5.4)	–12.9 (8.8)	–12.9 (8.7)	–	–
Freezer air temperature at 5-hour cold soak, °C (°F)	–16.9 (1.6)	–16.1 (3.0)	–15.1 (4.8)	–15.3 (4.5)	–	–
Specimen temperature at 5-hour cold soak, °C (°F)	–16.4 (2.4)	–15.5 (4.1)	–14.0 (6.8)	–14.0 (6.9)	–	–

IV. Single location repeatability

The instrumented specimen was also used for tests inside the chest freezer presented in section 4.3.1.1. In one particular set of tests, the specimen was subjected to repeated freeze-thaw cycles in a single location of the freezer to determine the single-location repeatability of this particular freezer (note that for the chest freezer, cycling had to be performed manually). The specimen was placed in the lower back corner of the freezer as illustrated in Figure 138. The resulting freezer air and specimen cooling curves for seven cycles are shown in Figure 139. The overall range of freezer air temperatures among all seven cycles was about 1 °C (2 °F) during the time period of 2 to 4 hours. In general, the specimen cooling curves were more or less similar, particularly during initial cool down and over the freezing plateau. The main difference was in the cooling region beyond the freezing plateaus. Of all seven cycles, the shortest one had a freezer air cooling branch that was 6.4 hours long while the longest one had a cooling branch that was 6.9 hours long. The specimen temperature reached –9.2 °C (15.4 °F) in the shortest cycle and –10.2 °C (13.6 °F) in the longest cycle. As mentioned before, it is not certain whether this extra 1 °C (1.8 °F) drop in specimen temperature is significant as far as specimen damage is concerned.

Figure 137. Photo. View of chest freezer used for single-location repeatability tests.

Figure 138. Photo. View of chest freezer interior. The circled portion indicates the location of the instrumented specimen.

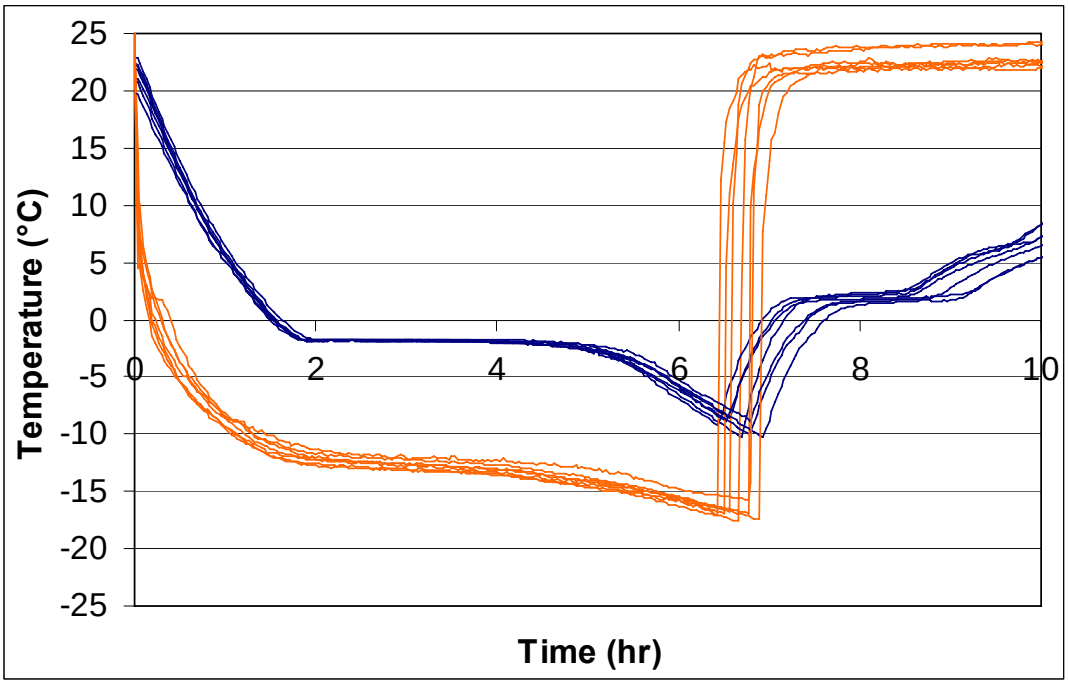

$T_f = (9/5) * T_c + 32$ {T_f = Fahrenheit, T_c = Celsius}

Figure 139. Graph. Freezer air and specimen cooling curves for seven cycles.

V. Different freezers

With data from instrumented specimen tests in the walk-in and chest freezers, it is also possible to compare responses in two different freezers. Figure 140 shows the specimen cooling curves under these two freezers. While both freezers were capable of complying with ASTM C 1262 (2003), some differences were observed in the overall shape of the air and specimen cooling curves. The specimen cooling curves, however, showed similar initial cool down rates (about 14 °C/hr (25 °F/hr)) and lengths of freezing plateaus (2.9 hours in chest freezer and 3.1 hours in walk-in freezer). The specimen temperatures at the end of a 4-hour cold soak were also similar (–11.4 °C (11.5 °F) in the chest freezer and –10.9 °C (12.4 °F) in the walk-in freezer).

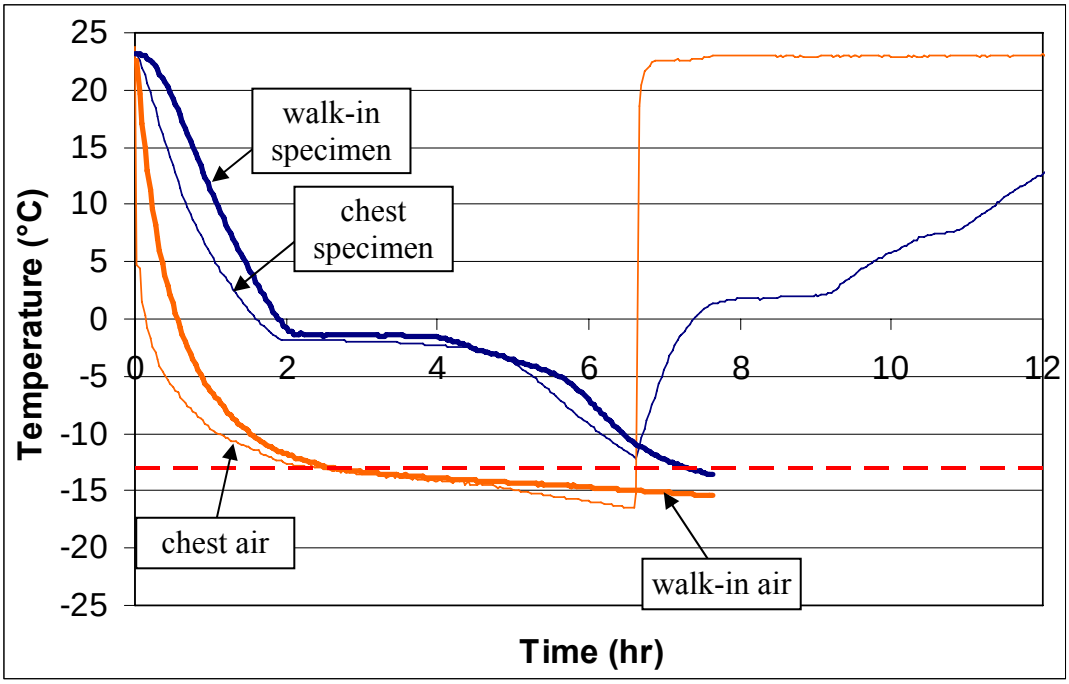

$T_f = (9/5) * T_c + 32$ {T_f = Fahrenheit, T_c = Celsius}

Figure 140. Graph. Comparison of specimen cooling curve in 2 different freezers (chest freezer with 6 specimens, walk-in freezer with 40 specimens).

In general, it is seen that variations in the exposure conditions of specimens can influence the actual cooling curve of the specimens themselves. One key finding from these studies is the fact that complying with ASTM C 1262 (2003) freezer air T-t requirements does not necessarily guarantee similar cooling responses in specimens. It appears that variations in the surrounding water volume and in the number of specimens inside the freezer caused the largest discrepancy among cooling curves. Variations in container size also caused differences in the cooling curve, but this is probably due to the variation in surrounding water volume. Specimens in the chest freezer loaded with 6 specimen's portrayed similar response to specimens in the walk-in freezer loaded with 40 specimens. This shows it is possible to attain similar specimen cooling responses even between separate freezers. Similarly, repeatability within a single location in the chest freezer was reasonable.

Note that in all specimen cooling curves considered above, the freezing plateau was completely traversed by the end of a 4-hour cold soak. Accordingly, from the standpoint of inducing expansion damage, it appears that the current 4-hour minimum cold soak in the ASTM C 1262 (2003) is adequate to fulfill this purpose. It is interesting to note that the cold soak requirement in an earlier version of this test method (ASTM C 1262-94) consisted of maintaining the chamber air temperature at –17.8 to –9.4 °C (0 to 15 °F) for 3.5 to 4.5 hours (for similar size specimens and containers). Using the curves in figure 129 as example, cold soak would start after 1 hour from start of test (based on the 1994 version of ASTM C 1262) and end after 4.5 hours cooling time at the earliest. However, after 4.5 hours, this specimen was still undergoing its freezing plateau and thus, full expansion damage potential is likely not realized. Hence, the cold soak requirement of 3.5 hours starting at –9.4 °C (15 °F) as required in the previous version of ASTM C 1262 (2003) is not adequate.

This discussion has applied observations from the vial tests to pore liquid in the specimens. While this approach may be valid for large pores where water exists in bulk state, it may not be valid in smaller pores where the surface effects become critical. One result of such effects is the depression of freezing point when water freezes in increasingly smaller pores. Figures 140 and 142 show various relationships from the literature between pore size and temperature at which ice formation is possible. Figure 141 shows that for pore radii above 50 nm (2×10^{-6} inches), freezing temperature of fresh water is close to 0 °C (32 °F). Figure 142 shows theoretical freezing points above –5 °C (23 °F) for pore sizes greater than 10 nm ($2.5 \text{ X } 10^{-7}$ in.) or 25 nm ($1 \text{ X } 10^{-6}$ inches), depending on the assumption regarding the controlling interface in the pores (solid-liquid or liquid-vapor) (Marchand et al., 1995). For SRW mixes, compaction voids can account for up to 25 percent of the volume fraction of the material and the sizes of these voids can range from fractions of a millimeter to several millimeters (see figures 130 and 131 for example). Freezing of water in these pores is therefore probably close to freezing in the bulk state. For smaller capillary and gel pores in the paste fraction of SRW mixes, the freezing point is likely to be depressed and to follow relationships similar to those shown in figures 141 and 142.

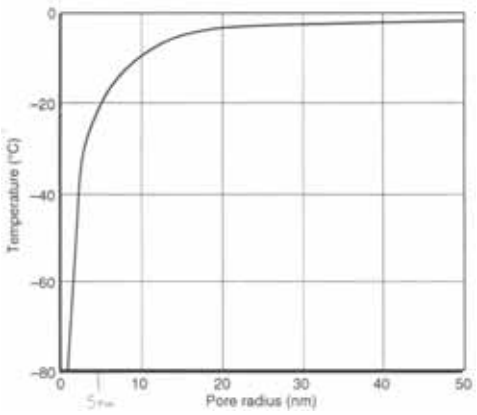

Figure 141. Graph. Relationship between size of pores and freezing point from Pigeon and Pleau (1995).

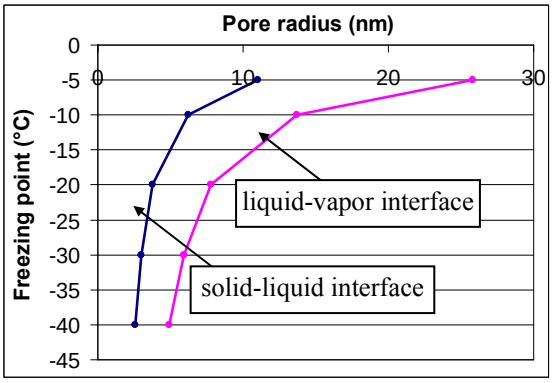

Figure 142. Graph. Relationship between size of pores and freezing point from Marchand et al. (1995).

$T_f = (9/5) * T_c + 32$ {T_f = Fahrenheit, T_c = Celsius}

In saline solution, aside from ice formation, a concentration change in the unfrozen portion of the solution was also measured that increased most rapidly near the end of the freezing plateau. Concentration gradients lead to osmotic pressures, which have been cited in the literature as a primary mechanism for deicing salt scaling (Harnik et al., 1980). Even without the presence of salts, Powers has pointed out that concentration differences due to freeze concentration of the pore solution can induce osmotic pressures large enough to damage the concrete (Powers, 1975). If osmotic effects due to concentration changes were significant, these effects are likely to become increasingly important after ice has started forming (once the freezing plateau has started) and throughout the duration of cold soak. For testing purposes, to minimize differences that may be incurred by different laboratories due to different cold soak durations, an upper limit on the cold soak period of the test is therefore required. The currently specified 5 hours in ASTM C 1262 (2003) may thus fulfill this purpose.

4.4.2.5 Rates of Temperature Change

In the same manner in which rates of temperature change were determined for freezer air and solution temperatures in section 4.4.1, rates of temperature change were also determined for an SRW specimen from its cooling curve. Temperature data from a specimen tested in the walk-in freezer loaded with 40 specimens (labeled "As spec." in figure 132) were used to calculate these rates. Figure 143 shows the T-t curve for freezer air, water surrounding specimen and specimen itself for one cycle (top graph). Directly below this graph are the rates of temperature change for the solution and specimen temperature, followed by a graph showing the difference in temperature between center of specimen and freezer air ($\Delta T = T_{freezer\ air} - T_{specimen}$).

From the dT/dt graphs, it is seen that the specimen and its surrounding water underwent similar patterns in terms in their temperature change rates, although the specimen dT/dt response appeared to lag that of the water. Despite the lag, peak dT/dt values for the specimen were not far from the peak dT/dt values for the water at the following times:

- During initial cooling (0 to 2 hours) in which dT/dt for water peaked at –21 °C/hr (–38 °F/hr), while dT/dt for the specimen peaked at –16 °C/hr (–29 °F/hr).

- Immediately following cold soak (at around 11 hours) in which dT/dt for the surrounding water peaked at 24 °C/hr (43 °F/hr), while for the specimen, this was 22 °C/hr (40 °F/hr).

Larger differences in peak rates of temperature change were observed at these times:

- After the respective freezing plateaus in which dT/dt for the surrounding water peaked also at –21 °C/hr (–38 °F/hr), while dT/dt for the specimen exhibited a peak at –7 °C/hr (–13 °F/hr).

- After the respective thawing plateaus in which dT/dt for water peaked at 31 °C/hr (56 °F/hr), while dT/dt for the specimen peaked at 11 °C/hr (20 °F/hr).

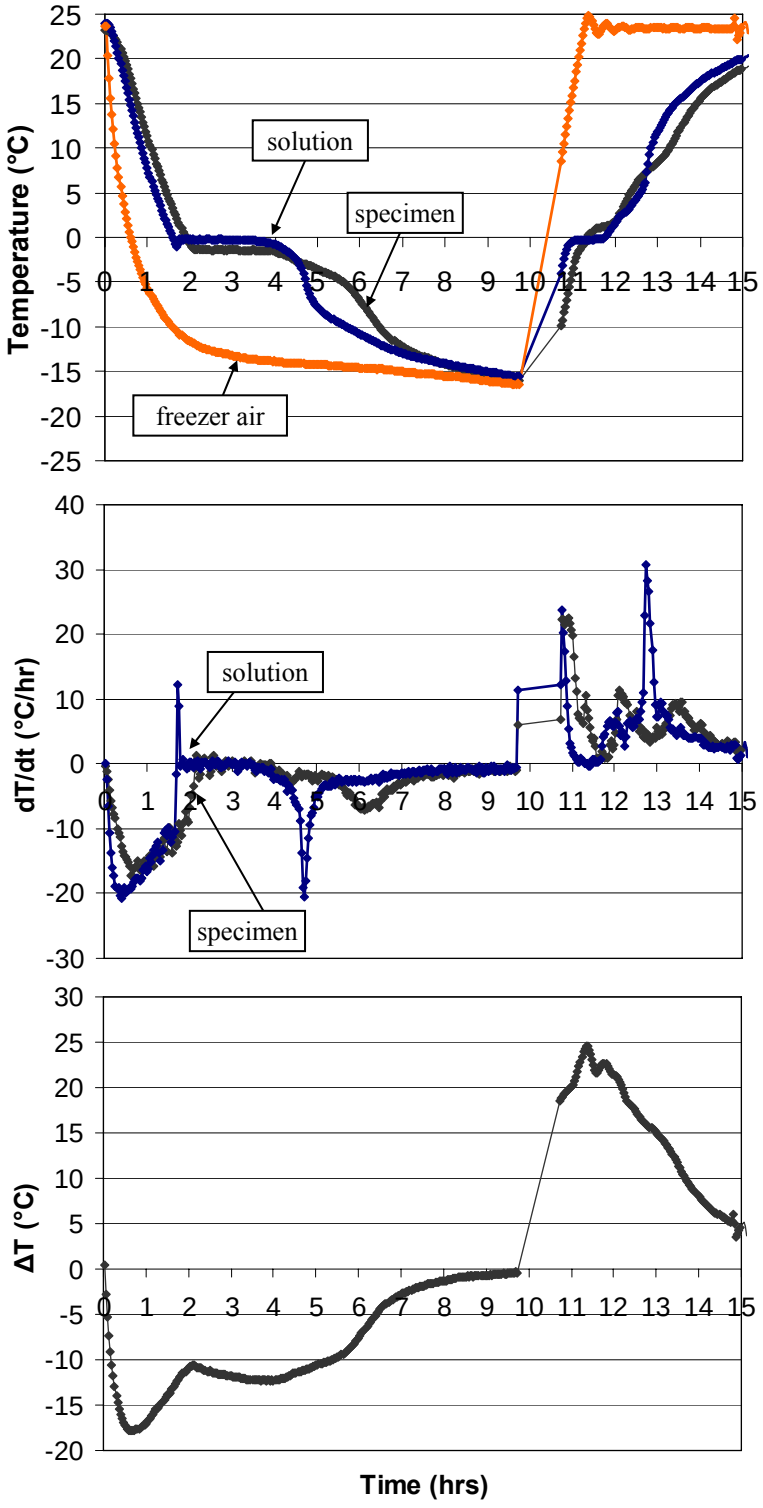

$T_f = (9/5) * T_c + 32$ {T_f = Fahrenheit, T_c = Celsius}

Figure 143. Graph. Rates of temperature change for specimen and surrounding water.

Thus, overall, it appears that peak rates in either cooling or warming of the specimen were similar to the corresponding rates in the surrounding water. This similarity in rates only happened when both specimen and surrounding water were at similar initial temperatures (24 °C (75 °F) during initial cooling and –16 °C (3 °F) during warming after cold soak). The peak rates of cooling in the specimen also occurred at approximately the same time as for water. However, when being cooled or warmed from different starting temperatures such as at the end of freezing plateaus or during thaw plateaus, the peak rates in temperature change differed for both specimen and surrounding water. Figure 143 shows the temperature difference between center of specimen and freezer air, ΔT. This graph shows that the largest temperature gradients occurred during initial cool down (from 0 to 1 hour) and for about 2–3 hours after end of cold soak.

4.4.3 Other Aspects Relevant to the ASTM C 1262 (2003) Test Method

While the 4 to 5 hour cold soak requirement in ASTM C 1262 (2003) may be adequate to induce damage in specimens as shown previously, there are other aspects of the freeze-thaw cycle that must also be considered. These are discussed here.

4.4.3.1 Concept of Frozen Solid

Despite setting a 5 hour maximum limit on cold soak, ASTM C 1262 (2003) permits extending the cold soak if the water (or solution) surrounding the specimens does not appear to be frozen solid. This is stated in Clause 8.2.1:

> Periodically, at the end of a freezing cycle, open the containers and visually inspect the specimens to determine if all the water surrounding the specimen is frozen solid. If not, extend the length of the freezing cycle to ensure that all water is frozen solid.

From this statement, it appears that the interpretation of what constitutes "frozen solid" is left up to the discretion of the test operator. Figures 144 and 145 show pictures of two specimens tested in 3 percent NaCl solution and removed from the freezer after a 4.5-hour cold soak. While the solution around figure 144 appeared to be completely frozen, the solution around the specimen figure 145 exhibited wet spots over it. Thus, while the specimen in figure 144 may be considered to have reached frozen solid conditions, the one in figure 145 may not be and consequently kept in the freezer for additional cold soak time. This decision thus affects the actual exposure condition of specimens.

This issue is better understood by examining the FP versus T curves shown earlier in figure 107. A solution with initial 3 percent NaCl concentration attains an FP of about 85 percent by the time its temperature reaches the target cold soak temperature of –18°C (0°F). This means there is still approximately 15 percent unfrozen solution that could either become entrapped within the ice or reside on the surface of the solution giving the impression that the solution is not yet frozen solid. Given that complete freezing of an NaCl solution is not possible until eutectic temperature is reached (–21°C (–6°F)), it is recommended that cold soak be limited to the current 5 hour maximum and that the condition of frozen solid be removed from the test standard.

Figure 144. Photo. Specimen after 4.5-hour cold soak in walk-in freezer appears frozen solid.

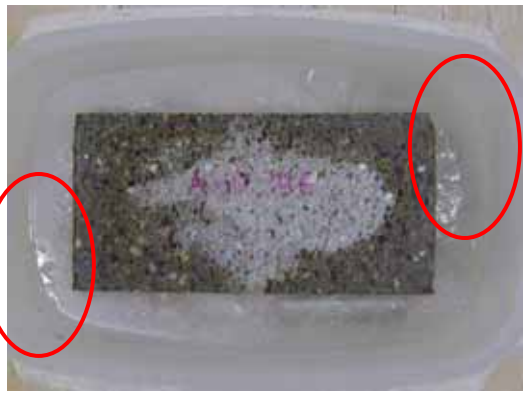

Figure 145. Photo. Second specimen, also after 4.5-hour cold soak in walk-in freezer, shows wet spots as indicated in the circled areas.

4.4.3.2 Temperature Tolerance

The current allowable cold soak temperature in ASTM C 1262 (2003) is –18 ± 5 °C (0° ± 10 °F). An inspection of the NaCl–H_2O phase diagram reveals that the eutectic point for this system exists at temperature of –21°C (–6 °F) which is the lowest temperature at which a solution will remain completely liquid. Below this point, solid ice and $NaCl{\cdot}2H_2O$ crystals are the thermodynamically stable phases which means that salts will crystallize from the remaining solution (Van Vlack, 1967). Although the extent to which NaCl crystallization may damage the concrete under these conditions was not investigated here, damaging pressures caused by salt crystallization from supersaturated conditions are well documented in the literature (Charola, 2000; Scherer, 2004; and Pigeon and Pleau, 1995). It is therefore recommended that unless otherwise demonstrated, the minimum allowable temperature during cold soak shall remain above –21 °C (–6 °F).

Recall that earlier in this chapter, it was mentioned that at cold soak temperatures above approximately –14 °C (7 °F), reliabilities of 100 percent were unattainable in the walk-in freezer. This issue in conjunction with the eutectic point issue mentioned above provide compelling reasons to tighten the allowable cold soak range from –18 ± 5 °C (0° ± 10 °F) to –18 ± 3 °C (0° ± 5 °F). This is in fact the allowable temperature range specified in ASTM C 672 (2004) for deicing salt scaling resistance of concrete.

4.4.3.3 Cooling Rates and Target Cold Soak Temperatures

While a target cold soak temperature range and duration are specified in ASTM C 1262 (2003), cooling rates are currently not specified (i.e., how fast the temperature drops from warm to cold soak). Cooling rates have been cited in the literature as being significant, especially for large pore systems (Petersson, 1999 and Scherer, 1993). Cooling rate is also a parameter in Powers' classical hydraulic pressure theory to estimate pressures in concretes (Powers, 1949).

One important outcome from the vial tests described earlier was the comparison of vial performance under two freezers with different cooling environments. Vials similar to those described in section 4.4.2.3 were prepared but instead of being filled to capacity, were only filled halfway. Figures 146 through 149 show the T-t response for these two vials, as well as pictures of them. While the vial tested in the chest freezer fractured (figure 147), the vial tested in the walk-in chamber did not exhibit signs of damage (figure 149). Table 12 shows a summary of relevant temperature parameters to compare the exposure conditions of these two vials. Generally, water in the chest freezer cooled about 1.2 to 1.6 times faster, and ice formed about 1.5 times faster than in the walk-in freezer.

Distinct modes of ice formation were also observed in these two vials. Figure 150 and 151 show views of a half-full vial after 30 and 40 minutes in the chest freezer. The growth of ice at the air-water interface is clearly seen. After 40 minutes (figure 151), the surface was hard enough to resist the weight of the screwdriver shown. In essence, an "ice plug" appears to have formed at the top of the liquid column and the yet unfrozen liquid below this plug was thus "enclosed." These vials were damaged as shown by the cracks in figure 147. On the other hand, as shown in figure 149, ice formed from within the liquid column in the walk-in freezer, and a rise in the column was observed. No damage was observed in this vial. Cooling rates may have played a role in determining whether or not damage occurred in these vials.

Given that cooling rates may play a role in inducing damage, actual specimen cooling rates are now presented and compared to cooling rates in other freeze-thaw test methods. For the specimen cooling curves presented in section 4.4.2.4, cooling rates were calculated by taking the difference between the specimen temperature after 4-hour cold soak and 20 °C (reference initial value) and dividing this difference by the time taken for the specimen to drop from 20 °C to the 4-hour cold soak point. This is expressed in equation 9:

$$\text{Cooling rate (°C/hr)} = \frac{(20°C - \text{Temp. of specimen after 4-hr cold soak})}{\text{time at 4-hr cold soak - time at T=20°C}} \qquad \text{Equation 9}$$

Note that this cooling rate is different from those shown in section 4.4.2.4 that corresponded to initial cooling rates from 20 °C to 0 °C. The reason for calculating cooling rates in the manner shown in equation 9 is to enable comparison of this parameter with other existing freeze-thaw test methods. Specimen cooling rates obtained using equation 9 is summarized in table 13.

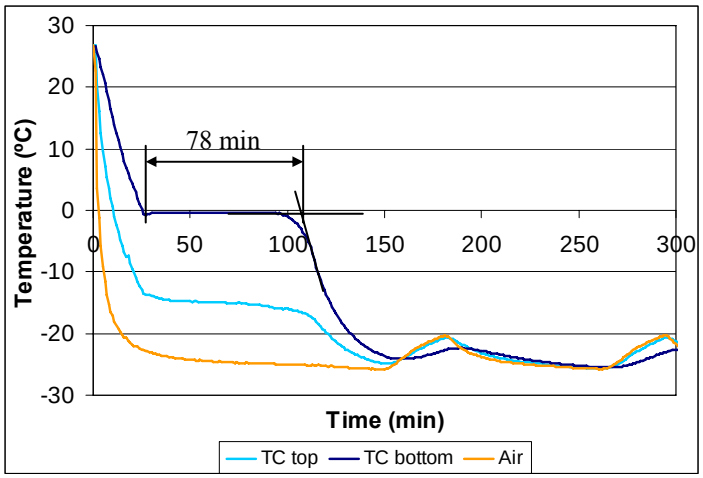

Figure 146. Graph. Results of cooling in chest freezer.

Figure 147. Photo. Half-filled vial after cooling in chest freezer.

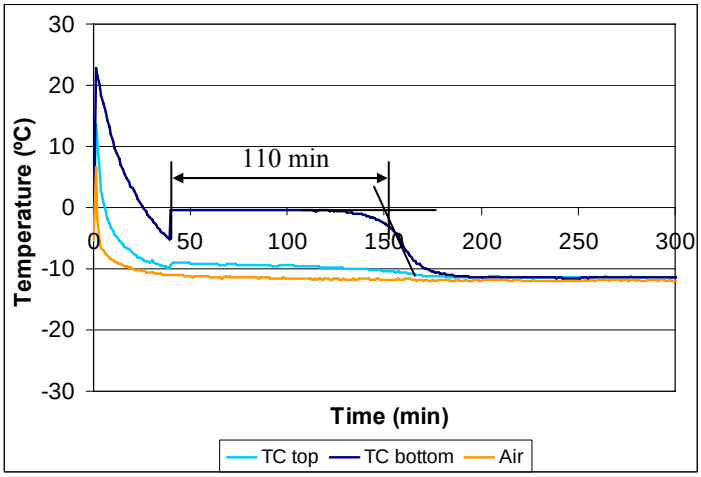

Figure 148. Graph. Results of cooling in walk-in freezer.

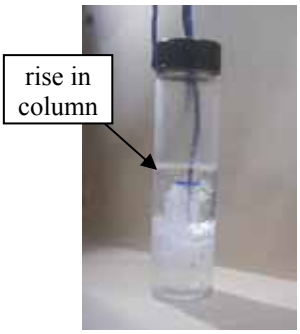

Figure 149. Photo. Half-filled vial after cooling in walk-in freezer.

Figure 150. Photo. Half-full vial after 30 minutes of exposure in the chest freezer.

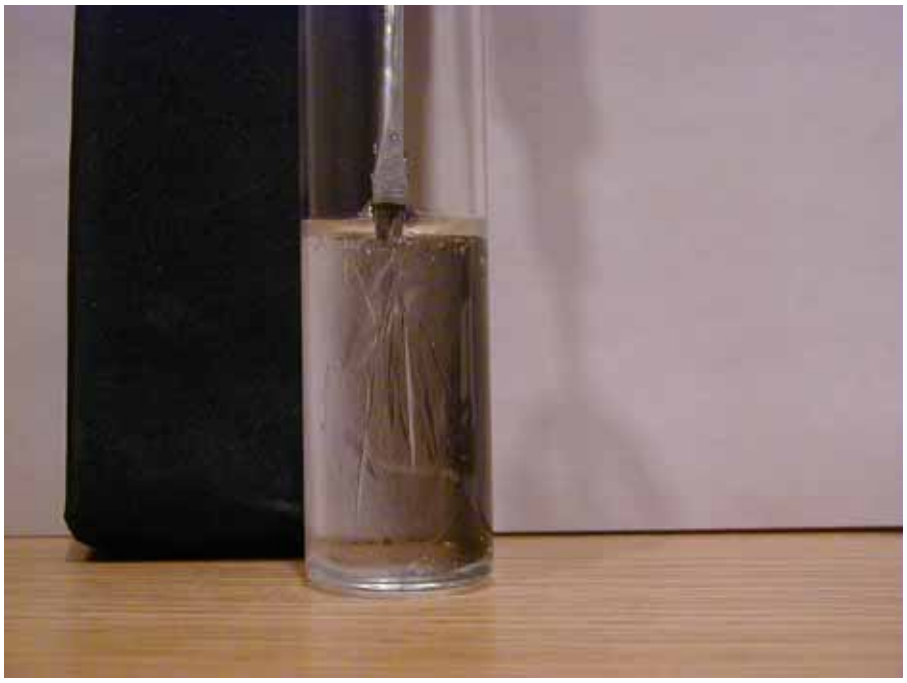

Figure 151. Photo. Half-full vial after 40 minutes of exposure in the chest freezer.

Table 12. Comparison of cooling curve characteristics for half-full vials in different freezers.

	Walk-in Freezer	Chest Freezer
Water cooling rate (°C/min) [a]	0.7 to 0.9	1.1
Length of freezing plateau (min) [b]	110	78
Approx. ice formation rate (g/min) [c]	0.14	0.20
Range of freezer air temperature during water freezing plateau (°C)	−10 to −12	−21 to −25

[a] Evaluated as the slope of water T-t curve between about 20 and 0°C for the bottom thermocouple.
[b] Evaluated in the manner shown in figures 146 through 149.
[c] Rate = volume of water / length of freezing plateau, assuming 90 percent of the total water freezes during the plateau.

Table 13. Comparison of specimen cooling rates for cooling curves of section 4.4.2.3

Variation of Condition (Figure)	Condition	Specimen Cooling Rate* °C/hr (°F/hr)
Different SRW mixes (figures 129–131)	SRW mix A	4.9 (8.8)
	SRW mix B	4.4 (8.0)
Varying volume of surrounding water (figure 132)	–100mL	5.2 (9.4)
	−50mL	5.2 (9.4)
	As spec.	5.0 (9.0)
	+ 50mL	4.6 (8.3)
	+100mL	4.4 (8.0)
Varying container size (figure 134)	Small	5.0 (9.0)
	Large	5.0 (8.9)
Varying specimen quantity (figures 135 and 136))	Two specimens	6.4 (11.5)
	20	5.8 (10.5)
	40	5.1 (9.1)
	60	4.1 (7.5)
Different freezers (figure 140)	Chest	5.0 (9.0)
	Walk-in	5.0 (9.0)

*From initial 20 °C (68 °F) to temperature at end of 4-hour cold soak.

As a point of reference, ASTM C 666 (2004) for rapid freeze-thaw testing of ordinary concretes specifies the specimen T-t regime shown in figure 152. The graph shown is for ASTM C 666 (2004), Procedure A which consists of freezing and thawing in water. For the target values shown in figure 152, average cooling rates of 5.9 to 14.8 °C/hr (11 to 27 °F/hr). It is seen that in general, the cooling rate of the ASTM C 1262 (2003) specimens presented in section 4.4.2.3 was near the lower end of the ASTM C 666 (2004) range.

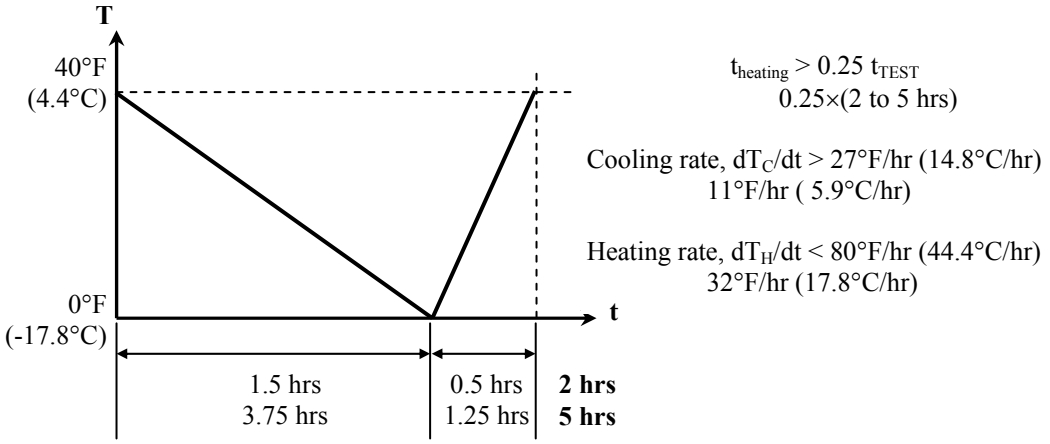

Figure 152. Diagram. ASTM C 666 (ASTM 2004), Procedure A specified T-t exposure of control specimen.

Another example of a specified specimen cooling curve is given by the European cube test for surface scaling and beam test for internal damage (Siebel, 1995). The specified cooling curve envelopes for these tests are shown in figure 153. Cooling curves for the specimens tested in the chest and walk-in freezers (specifically those shown in figure 140) are also plotted for comparison. It generally appears that the cooling curves obtained for the ASTM C 1262 (2003) test specimens followed more closely those of the cube test designed for surface scaling tests, except for the specimen temperature at end of cold soak.

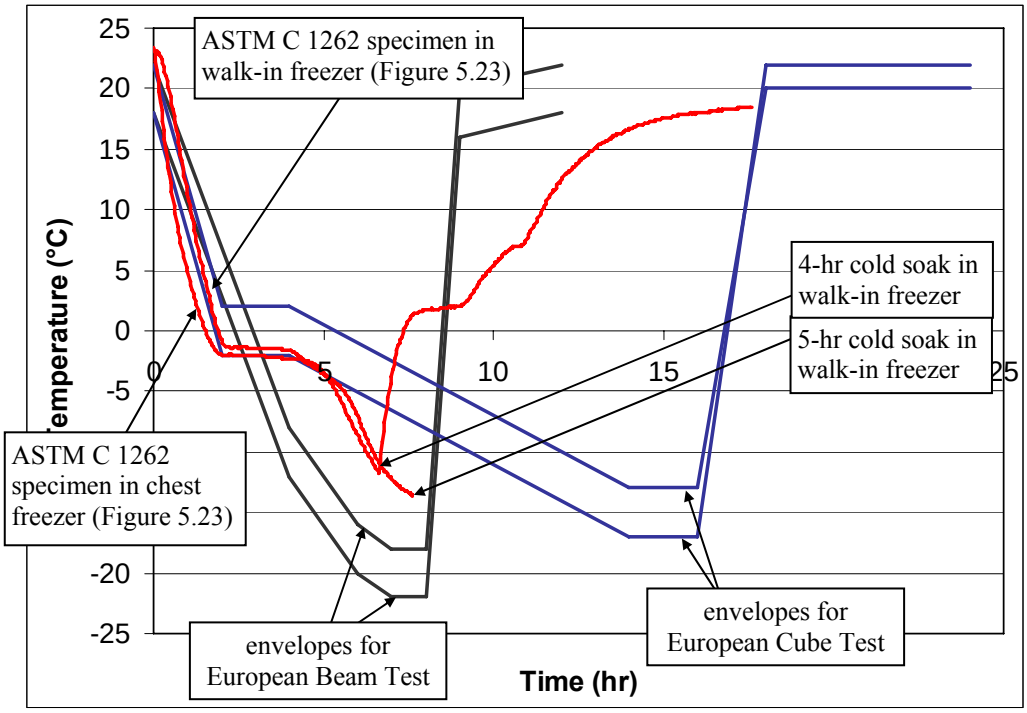

Figure 153. Graph. Comparison between cooling curves specified in European test methods and ASTM C 1262 (2003) specimens.

4.4.3.4 Degree of Saturation

The above observations on half-full vial tests also suggested that partially saturated systems may be damaged during freezing. For cementitious systems, it has been traditionally reported in the literature that damage can occur if the capillary pores are filled with water above a critical saturation of 91.7 percent (Cordon, 1966). The observations from these tests, however, suggest that damage can occur at saturation levels well below the critical value depending on the cooling environment. This has important implications for ASTM C 1262 (2003) that involves freezing and thawing of partially immersed specimens (figure 154). Local moisture content profiles could vary among specimens due to variations in capillary rise caused by sample microstructural differences, changes in ambient conditions, or even specimen geometry. It is recommended that further research be carried out to compare the performance between fully saturated and partially saturated specimens and to determine the extent that saturation effects may have on test variability.

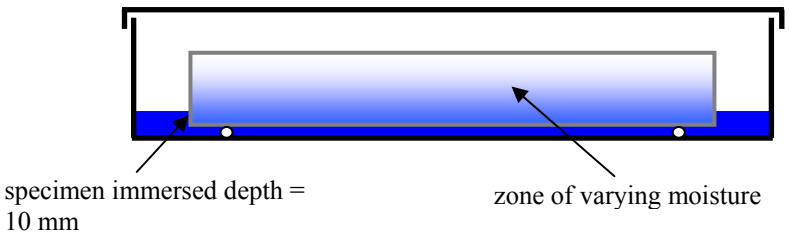

Figure 154. Drawing. ASTM C 1262 (2003) partially immersed specimen.

4.4.3.5 Warming Rate

Warming rates also are not currently specified in ASTM C 1262 (2003). Warming rates, especially while the ice is still solid (i.e., from the minimum test temperature to the point before ice melts), may contribute to damage in the cementitious material. This is because ice has a coefficient of thermal expansion of about 50×10^{-6} /°C (25×10^{-6} /°F) (Michel, 1978) which is approximately five times the value of about 10×10^{-6} /°C (5×10^{-6} /°F) for concrete (Neville, 1996). As such, during rapid temperature rise, the differential expansion between the ice and concrete can generate internal stresses. This potential damage mechanism has also been discussed in other references (Kaufmann, 2002; Kukko, 1992; Venečanin, 1984).

4.4.4 Summary—Implications for ASTM C 1262 (2003)

From the results and observations of the experimental work described in this chapter, it is apparent that a number of damage-inducing processes can take place during the freezing and thawing of specimens. It is key that specimens tested under different conditions such as different containers, container sizes, locations within a freezer or freezers undergo similar exposure if they are to experience similar forms and levels of damage. It has been demonstrated that variations in surrounding water volume and total quantity of specimens in the freezer can have an impact on the specimen cooling curves. The issue of surrounding water volume suggests that this parameter should be fixed to prevent variations arising from fluctuations in this parameter. The impact of specimen quantity was reflected by markedly different freezer air and specimen cooling curves for varying loads of specimens. For each load of specimens, however, ASTM C 1262 (2003) freezer air T-t requirements were still met which indicates that these requirements must be revised and tightened to avoid variations such as the ones presented here.

The current cold soak requirement of 4 to 5 hours at –18 ± 5 °C (0° ± 10 °F) appears adequate for inducing expansion damage due to ice formation in specimens. Extensions beyond the 5 hour maximum based on operator interpretations of frozen solid conditions (as is currently the case in Clause 8.2.1) are not recommended. As far as the cold soak length is concerned, as shown in tables 9, 10, and 11, one consequence of allowing a 1-hour window in cold soak times is that the minimum specimen temperature will reach different values. This discrepancy was particularly pronounced in the comparison of specimens with different volumes of surrounding water. Tightening the allowable cold soak time to 4.5 to 5 hours may thus be justified on this basis, although further investigation would be required to determine the effect of cold soak length on specimen performance and whether variations in cold soak length contribute to variability of test results. Moreover, modifying the length of cold soak may influence the manner in which freezers are operated. As far as temperature tolerance is concerned, it is also recommended that this be tightened for the reasons discussed in section 4.4.3.2.

Specifying target cold soak temperature ranges and durations still does not address the rate at which the freezer air temperature must cool down. For the freezers and thermal loads evaluated at Cornell, rates during initial cooling of freezer air have ranged as follows (based on the time taken for this temperature to drop from about 24 to –13 °C (75.2 to 8.6 °F):

- Chest freezer with 6 specimens: 15 °C/hr (28 °F/hr)
- Walk-in freezer with 2 specimens: 22 °C/hr (39 °F/hr)
  20 specimens: 19 °C/hr (33 °F/hr)
  40 specimens: 13 °C/hr (24 °F/hr)
  60 specimens: 9 °C/hr (15 °F/hr)
  80 specimens: 5 °C/hr (10 °F/hr)
- Cabinet freezer with 18 specimens: 25 °C/hr (44 °F/hr)
  28 specimens: 19 °C/hr (35 °F/hr)

Similarly, warming rates are not specified in ASTM C 1262 (2003). For tests at Cornell, freezer air warming rates have ranged as follows (based on the time taken for this temperature to rise from its value at end of cold soak to 19 °C (66 °F):

- Chest freezer with 6 specimens: 370 °C/hr (666 °F/hr)
  (specimens were physically removed from freezer and placed in laboratory air environment)
- Walk-in freezer with 2 specimens: 41 °C/hr (74 °F/hr)
  20 specimens: 37 °C/hr (67 °F/hr)
  40 specimens: 37 °C/hr (67 °F/hr)
  60 specimens: 34 °C/hr (61 °F/hr)
  80 specimens: 34 °C/hr (61 °F/hr)
- Cabinet freezer with 18 specimens: 53 °C/hr (95 °F/hr)
  28 specimens: 53 °C/hr (95 °F/hr)

As was shown in section 4.4.1 (describing selected results from the NCMA study), test specimens exhibited discrepancies in performance despite being tested in two freezer environments whose air temperatures complied with ASTM C 1262 (2003). Differences in the actual rates of cooling and warming were observed between the two freezers. Further research is vital to investigate the impact of cooling and warming rates on specimen performance. There are two parts to this issue. One is the cooling and warming rates of freezer air which is the control medium currently used in ASTM C 1262 (2003) and is easiest to measure in a testing laboratory. The other is cooling and warming rates of specimens themselves, which reflect actual mechanisms taking place in the material. Whether specifying a complete freezer air T-t curve—which would include cooling rate and duration, cold soak temperature and duration, warming rate and duration, and warm soak temperature and duration—necessarily yields consistent specimen cooling curves remains to be explored. It was noted from figure 140 that specimens placed in the chest and walk-in freezers exhibited similar cooling curves despite differences in the freezer air response, which shows promise in the attainment of similar specimen cooling curves. It is also noted that the specification of complete freezer air T-t characteristics may entail specification of particular types and performance of freezers, as well as the total number of specimens (actual test specimens and dummy specimens) in the freezer at any given time, as is currently done in ASTM C 666 (2004).

4.5 SYNOPSIS OF NCMA STUDY

As described in section 4.1, toward the end of this FHWA-funded project, the research team for this project performed additional, focused research funded by NCMA. Although this work was not formally linked to this FHWA project, it did build on the key findings of this project, and given the synergy between the two studies, it is logical and efficient to consider the findings from both projects when making recommendations and giving guidance to SHAs on freeze-thaw durability of SRW blocks. This section provides a brief summary of the main objectives and findings of the NCMA project that were performed at Cornell University. For more complete details of the NCMA-funded efforts, refer to chapter 6 of Chan's 2006 dissertation.

Overall, the NCMA funded project addressed the following general issues:

- ASTM C 1262 (2003) inherent test variability (significance of variations within the test method).
- Performance criteria assessment (i.e., what does a 1 percent mass loss represent.

The NCMA research project was divided into two main parts: variability test series and performance criteria (PC) test series. The scope of each of these parts is only briefly described in this section; the reader is directed to Chan (2006) for full details on the study. The specific findings from the NCMA study are not presented in this section (for conciseness), but the key findings were taken into account when compiling the main conclusions for this report (chapter 5) and for providing guidance to SHAs on how to ensure long-term durability of SRW blocks through prudent and scientifically-based testing (see appendix A for new version of ASTM C 1262 (2003) based on the findings of both the FHWA and NCMA studies).

4.5.1 Variability Test Series

Following up on potential sources of variability in ASTM C 1262 (2003) already discussed in this chapter, the NCMA study focused on the following issues:

- Varying solution levels.
- Different specimen sizes for the same container size.
- Different container sizes for the same specimen.
- Different specimen geometries (aspect ratios).

This series was intended to evaluate the effect of variations within the ASTM C 1262 (2003) by varying specimen and container sizes to the extremes of ASTM C 1262 (2003) tolerances. The tests in this series used 3 percent NaCl, and after every tenth cycle, the condition of the specimens was assessed by the following methods:

- Mass loss percentage (from the collected residues).
- Mass loss per unit test face area.
- Resonant frequency (ASTM C 215).
- Ultrasonic pulse velocity (ASTM C 597).
- Visual scaling rating (ASTM C 672).

The above tests assess different forms of specimen damage (note that ASTM C 1262 (2003) only relies on mass loss for damage assessment). While mass loss and scaling rating are sensitive to external forms of damage (i.e., loss of material from specimen surfaces), resonant frequency and pulse velocity are more sensitive to changes in specimen integrity (such as internal cracking). The evaluation of specimens using these various techniques allows observing how different forms of damage evolve with increasing freeze-thaw cycles and more importantly, enables comparing what certain forms of damage such as mass loss mean in terms of other forms of damage, such as specimen integrity, as measured from resonant frequency changes.

4.5.2 Performance Criteria (PC) Test Series

In addition to assessing specimen condition using mass loss, resonant frequency, ultrasonic pulse velocity and visual scaling rating, PC specimens were also tested for their modulus of rupture (MoR). The MoR is a useful mechanical property which characterizes the tensile capacity of the material. The primary objective of the PC Series was to correlate MoR to the other measured properties listed earlier. For these specimens, all measurements except for MoR were conducted after every 10^{th} freeze-thaw cycle. MoR tests were conducted on selected specimens at different mass loss levels so as to obtain a spread of MoR values over the mass loss range of 0 to 2 percent.

4.5.3 Significance of NCMA Project Findings

This NCMA study was quite comprehensive in the breadth of testing that was performed and the range of issues that were investigated. It is beyond the scope of this report to synthesize and present the conclusions and recommendations that emanated from this work. However, in chapter 4, some of the key findings of the NCMA study are presented, primarily those that are most relevant and have been integrated into guidance for SHAs currently testing, specifying, and using SRWs.

4.6 FROST DURABILITY INDICES FOR SRW UNITS

This section describes comprehensive testing of a range of SRW units obtained from commercial sources in North America. The main goal of this part of the project was to assess the durability of the units, using ASTM C 1262 (2003) (in water and 3 percent NaCl), and to identify which material characteristics, such as paste content, absorption, and microstructure, most relate to frost resistance. A main goal was to determine if one could measure select SRW block properties (other than frost resistance) and then predict frost resistance (as per ASTM C 1262 (2003)), based on these material properties. Briefly , the objective was to attempt to identify a frost durability index or frost durability indices that can be used as surrogate predictors for durability. It should be noted that this work was based on the standard ASTM C 1262 (2003) test method that existed at the time that this project was initiated, and as such, the testing described herein did not incorporate the various suggestions for improvements that were described throughout this chapter. The work presented herein was based entirely on research conducted under this FHWA project, and this summary draws from the following publications, especially the first one listed, developed under this project:

- Chan, C., Hover, K.C., Folliard, K.J. and Trejo, D., "Frost Durability Indices of Segmental Retaining Wall (SRW) Units," manuscript submitted to *ACI Materials Journal*, November 2005 (2005d).
- Haisler, J., *Freeze-Thaw Durability of Segmental Retaining Wall Blocks,* Master of Science thesis, The University of Texas at Austin, 2004.
- Chan, C., Hover, K.C., and Folliard, K.J., "Performance of Segmental Retaining Wall (SRW) Units: from Laboratory to Field," *Construction Materials, Proceedings of CONMAT 05 and Mindess Symposium* (eds. N. Banthia, T. Uomoto, A. Bentur and S.P. Shah), Vancouver, Canada, Aug. 21–24, 2005 (2005c).

4.6.1 Background

The frost durability of SRW blocks is most commonly assessed by using ASTM C 1262 (2003), which involves freeze-thaw cycling of specimens in either water or 3 percent NaCl solution up to a prescribed number of cycles (typically 100). At this point, the condition of the specimens is evaluated, and their mass loss is determined and compared to specifications such as ASTM C 1372 (2003). The overall test may require up to 2 to 3 months before completion due to the time required for carrying out each full cycle, periodic specimen inspection, and logistical factors. As a result, quicker assessments of freeze-thaw durability, such as the use of frost durability indices, may gain wider popularity in this industry.

In ordinary concretes, the spacing factor as determined by the methods of ASTM C 457 (2004) has been commonly used as an indicator of frost resistance, with a transition between durable and nondurable concretes existing somewhere between a spacing factor of 200 to 250 μm (0.008 to 0.010 inch) (Hover, 1994). Although ASTM C 457 (2004) tests can be performed on SRW concretes, the applicability of the spacing factor to SRW concretes has been questioned. This is in part due to the different nature of voids comprising SRW concretes compared to those in ordinary concretes (Marchand et al., 1998). The NCMA has suggested an index to assess frost resistance of SRW concretes based on simple parameters such as compressive strength, 24-hour absorption and unit weight of SRW units (Thomas, 2003). These parameters, obtained from ASTM C 140 (2000) testing, are combined in the following manner:

$$I = \frac{(\text{unit weight, kg/m}^3 \text{ or pcf}) \times (\text{compressive strength, MPa or psi})^{1/2}}{(\text{water absorption, kg/m}^3 \text{ or pcf})} \qquad \text{Equation 10}$$

Units possessing larger values of I were generally shown to have better likelihood of meeting test specifications (typically, maximum 1 percent mass loss after 100 cycles). For instance, for freeze-thaw tests in water, only about 10 percent of specimens with I < 58 $MPa^{1/2}$ (700 $psi^{1/2}$) met specifications. However, 43 percent of specimens with I of about 133 $MPa^{1/2}$ (1,600 $psi^{1/2}$) and 71 percent of specimens with I > 208 $MPa^{1/2}$ (2,500 $psi^{1/2}$) met specifications (Thomas, 2003). In a review of previous research work, Hance determined that frost durability of dry concrete products correlated well with cement content (Hance, 2005). Minimum cement contents of 252 to 395 kg/m^3 (425 to 665 lbs/yd^3) were generally required for frost resistance in water and 320 to 380 kg/m^3 (540 to 640 lbs/yd^3) for frost resistance in the presence of deicing salts.

This section describes analyses of common SRW material characteristics as frost durability indices. Properties considered included those obtained from common tests such as ASTM C 140 (compressive strength, absorption and unit weight) and ASTM C 642 (2002) (boiled absorption and volume of permeable voids). In addition, characteristics obtained from microscopy analyses (ASTM C 457 (2004)) were also evaluated. The utility of the NCMA index as a frost durability index was also assessed.

4.6.2 Databases of SRW Block Freeze-Thaw Performance and Material Properties

As part of this project, databases of ASTM C 1262 (2003) freeze-thaw mass loss and material characteristics properties from ASTM C 140, C 642 and C 457 tests were obtained for SRW units from 5 different manufacturers (labeled A to E). For manufacturers A to D, two different types of SRW units were evaluated: units that satisfied DOT specifications in the State of the project (henceforth called DOT units), and units that did not necessarily satisfy DOT specifications (called nDOT units). DOT units tended to be denser with lower amounts of compaction voids compared to nDOT unit. For manufacturer E, nDOT SRW wall and cap units were evaluated. Hence, a total of 10 different types of SRW units were evaluated.

Table 14 shows the scope of ASTM C 1262 (2003) freeze-thaw tests conducted on these SRW units. For DOT and nDOT units from manufacturers A to D, tests were conducted in water and 3 percent NaCl solution inside two different types of temperature-controlled freezers: large walk-in freezer and Tenney freezer (a cabinet style freezer). For the units from manufacturer E, the tests were carried out inside a commercial chest freezer. These various types of freezers were all capable of meeting T-t requirements of ASTM C 1262 (2003). For manufacturers A to D units, five replicate specimens were tested per set, while for manufacturer E units, three replicate specimens were tested per set. The data available from these tests consisted of the percent mass loss after 100 cycles.

Table 14. Scope of ASTM C 1262 (2003) test program.

Large Walk-in Freezer		Tenney Freezer		Chest Freezer	
Plain Water	**3 Percent NaCl**	**Plain Water**	**3 Percent NaCl**	**Plain Water**	**3 Percent NaCl**
A-DOT	A-DOT	A-DOT	A-DOT	E-wall	E-wall
A-nDOT	A-nDOT	A-nDOT	A-nDOT	E-cap	E-cap
B-DOT	B-DOT	B-DOT	B-DOT		
B-nDOT	B-nDOT	B-nDOT	B-nDOT		
C-DOT	C-DOT	C-DOT	C-DOT		
C-nDOT	C-nDOT	C-nDOT	C-nDOT		
D-DOT	D-DOT	D-DOT	D-DOT		
D-nDOT	D-nDOT	D-nDOT	D-nDOT		

Table 15 shows a summary of the standard material property tests performed on the SRW units. The number of replicate specimens tested varied for each type of SRW unit and generally ranged from 3 to 12 specimens. With respect to the ASTM C 457 (ASTM, 2004) compositional parameters, the total (air and compaction) void and paste contents refer to the volumetric fraction of these phases as determined from microscopy examinations. Air and compaction voids were distinguished during the microscopy tests using the following decision rule: a compaction void

was defined as a void in which less than three-fourths of its boundary was a paste-void interface, while an air void was defined as a void in which more than three-fourths of its boundary was a paste-void interface irrespective of shape of void as shown in figure 155. With respect to the ASTM C 457 (2004) air void parameters, the specific surface is defined as the boundary surface area of air voids divided by the volume of the voids; the spacing factor is the average half-distance between two voids. It is noted that these air void parameters were developed for ordinary concretes in which spherical bubbles are assumed to exist. One of the aims of this study was to assess the applicability of these parameters (determined in the usual way for concretes) for SRW concretes.

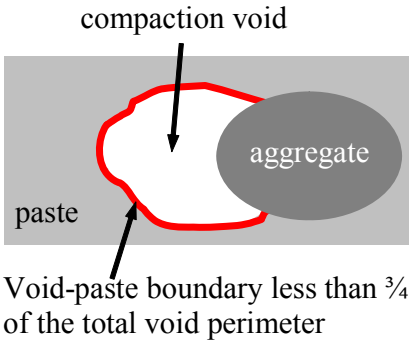

Figure 155. Drawing. Definition of compaction void in ASTM C 457 (2004) testing.

Table 15. Standard test methods and material properties evaluated for SRW units.

ASTM C 140	ASTM C 642	ASTM C 457
• 24-hour absorption	• Boiled absorption	Compositional Parameters:
• Oven-dry density	• Volume of permeable voids	• Total void content [a]
• Compressive strength	• Specific gravity after immersion and boiling	• Paste content
		Air void parameters: [b]
		• Specific surface
		• Spacing factor

[a] Total air and compaction void content.
[b] Calculated using total air and compaction void content.

In addition to the above characteristics, other parameters were also determined using the characteristics shown in table 15. These are as follows:

$$\text{Average surface area per void} = \frac{\text{specific surface}}{\text{total air and compaction void content}} \qquad \text{Equation 11}$$

$$\text{Paste-Total voids ratio} = \frac{\text{paste content}}{\text{total air and compaction void content}} \qquad \text{Equation 12}$$

$$\text{Saturation coefficient} = \frac{\text{24 - hour absorption}}{\text{boiled absorption}} \qquad \text{Equation 13}$$

Also, NCMA index (I) as in equation 10

Several other relationships were also explored without much success. This section only focuses on results obtained with the parameters shown above.

4.6.3 Synthesis of Data

The overall experimental program involved shared testing responsibilities between two laboratories. While the majority of freeze-thaw tests were conducted in one laboratory, the majority of material property testing was conducted in another laboratory. It was therefore deemed inadequate to directly correspond mass-loss values to material characteristics as single (x, y) data points for each of the various SRW mixes evaluated, given the fact that specimens for each of these tests were extracted from separate parent SRW units. Consequently, an alternate method of reducing the data was employed as shown in figure 156. Here, it is shown that for each type of SRW unit (e.g., manufacturer X DOT), there was a range of freeze-thaw mass-loss values from the three or five specimens tested in the set. Similarly, there was a range of values for a given material property from the various replicate specimens tested in the set (3 to 12 specimens). Hence, for this particular SRW unit, the mass loss versus property relationship could be represented by any point in the shaded box bound by the minimum and maximum mass-loss values in the ordinate and the minimum and maximum values of the material property in the abscissa. This set of data points bound by the shaded box was then reduced in one of two ways explained below.

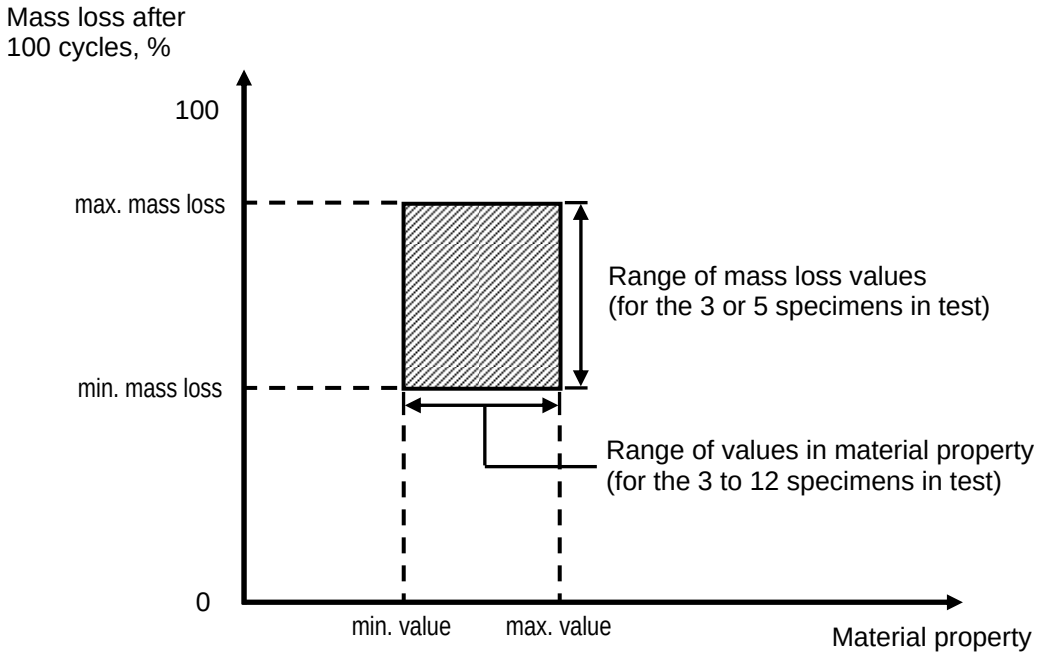

Figure 156. Graph. Relating mass loss to material property for a given SRW unit type.

As a first approach, the shaded box in figure 156 could be reduced to a single data point representing the geometrical centroid of the box for a particular manufacturer (figure 157). The use of centroids for this purpose was deemed reasonable for several reasons. First, various data sets consisted of only three to four data points which was not sufficient to fully describe a

statistical distribution. For these particular sets, the centroid was used as an approximate representation of the region bound by the maximum and minimum values in each axes. For larger data sets (five or more data points), the data points appeared to be normally distributed as confirmed using the statistical test of normality, and the centroid was thus taken as a representation of the shaded box. This process could then be repeated for all other SRW unit types to produce a data series as shown in figure 157. Each data point in this series represented results for one type of SRW unit. The disadvantage of this method is that by using single data points, the significant scatter in the data is ignored.

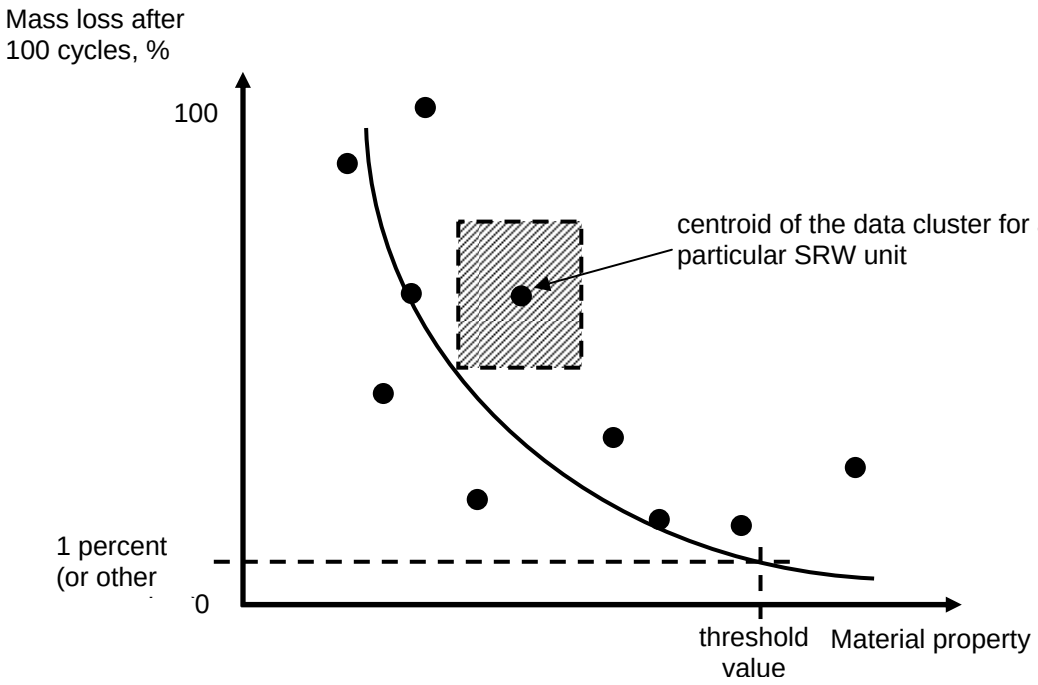

Figure 157. Graph. Mass loss versus material property for each of the SRW units evaluated using centroids.

A different approach to represent the shaded box of figure 156 was to focus on its boundary points. This method would take into account the range in test results and perhaps be more representative of the actual nature of the data. Hence, for a given SRW type, its mass loss versus property relationship would be represented by four points (figure 158). When repeated for all other SRW unit types, a series of data points representing the corners of all boxes would be produced as shown in figure 158.

A data series constructed by either one of the methods shown in figure 157 or 158 provided a qualitative representation of the behavior of the variables considered. In addition, a relationship was fitted through the data points to obtain a quantitative interpretation of the dependence between variables. Curve fitting was performed using the software Table Curve 2D®, Version 4, from AISN Software Inc (copyright 1989–1996). In this program, the user has the option of choosing the types of equations to be fitted through the data points. The option *Curve-Fit Simple Equations* was selected for this study. The result of the analysis consisted of a listing of

expressions ranked in order from highest to lowest correlation coefficient (R^2). Typically, the equation with the highest R^2 value was selected as being representative of the relationship between variables. These R^2 values were also used to compare the correlation strength between the various material characteristics considered and mass loss from freeze-thaw testing. In addition to R^2 values, standard errors were also obtained for each curve fit. Furthermore, from the above plots, it was possible to determine approximate threshold values of the material property above or below which the mass loss would exceed a mass-loss limit (e.g., 1 percent in ASTM C 1372(2003)). This concept is illustrated in figures 157 and 158.

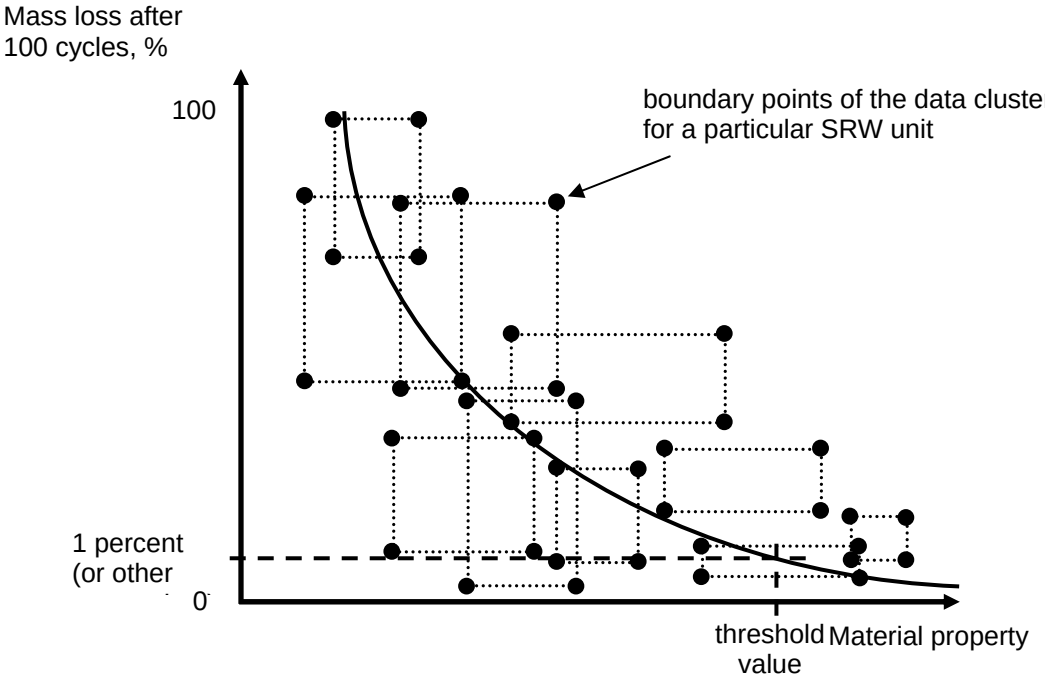

Figure 158. Graph. Mass loss versus material property for each of the SRW units evaluated using boundary points.

4.6.4 Discussion of ASTM C 1262 (2003) (in Water) Results

Results of the above analyses are shown in figures 159 to 184 for ASTM C 1262 (2003) freeze-thaw mass loss in water and the following material characteristics: figures 159 and 160, compressive strength; figures 161 and 162, 24-hour absorption; figures 163 and 164, unit weight; figures 165 and 166, NCMA index; figures 167 and 168, boiled absorption; figures 169 and 170, volume of permeable voids; figures 171 and 172, saturation coefficient; figures 173 and 174, total air and compaction voids content; figures 175 and 176, paste content; figures 177 and 178, paste-to-total-voids ratio; figures 179 and 180, specific surface; figures 181 and 182, spacing factor; and figures 183 and 184 spec surf/total voids content. In each pair of figures, one corresponds to data representation by boundary points while the other corresponds to data representation by centroids. With respect to the number of data points in each graph, it is noted that for units from manufacturers A to D, tests were carried out in two types of freezers, and as

such, two sets of data per SRW unit type from these manufacturers were available. Hence, the total number of "boxes" in the upper graphs or "centroid" points in the lower graphs was equal to 18 (4 manufacturers (A to D) × 2 unit types (DOT and nDOT) × 2 freezers + manufacturer E × 2 unit types (wall and cap) × 1 freezer).

From figures 159 to 184, the scatter in test results was evident by the size of the constructed boxes. This scatter was particularly evident for freeze-thaw mass-loss as reflected by the height of the boxes. Despite this scatter, trends in the data were generally discernable and as expected. For example, mass loss increased with increasing total voids content and absorption (24-hour and boiled) and with decreasing paste content and unit weight. Lower mass loss also corresponded to higher values of the NCMA index, which was in agreement with the trends reported by Thomas (2003). The decreasing mass loss with increasing specific surface was comparable to the trend expected for conventional concretes. As for spacing factor, the observed trend was actually opposite to that expected for ordinary concretes, where lower spacing factors are characteristic of systems with more closely spaced air voids and hence better frost durability. It is possible that this parameter cannot be applied to SRW concretes in the same manner as applied to ordinary concretes perhaps due to differences in the air void structure. Mass loss also decreased with increasing value in the parameter (spec. surf.) / (total voids volume). This parameter could be envisioned as the amount of surface area afforded per unit volume of voids.

To supplement observations of trends in the data in these plots, curves were fit into the data series to provide a quantitative sense of these trends. The inset boxes in figures 159 to 184 show the expressions for the best-fit curves, along with their corresponding R^2 and standard error values for each material property considered. (That these equations are only valid within the range of values of SRW unit characteristics covered by the test data sets.) It is apparent that these equations were generally of power or exponential form which suggested that the mass loss was fairly sensitive to the characteristics considered. This sensitivity can also be visually detected from the shape of the curves where the mass loss exhibited steep changes relative to most of the material characteristics.

With respect to the R^2 values, it is noted that these were generally fairly low (up to 0.33 for analysis with boundary points and up to 0.69 for analysis with centroids), which was likely due to the scatter in test data. These R^2 values were nevertheless used as a comparative basis of the correlation strength among the various material characteristics evaluated. In addition to the above analysis that was conducted for all available mass-loss results, an additional set of analyses was carried out on subsets of the previous databases that had a maximum mass loss of 5 percent. This separate analysis was carried out because, in practice, for SRW mixture qualification, freeze-thaw tests may be discontinued as soon as test specimens exhibit a substantial amount of mass loss (several times greater than the maximum allowed by project specifications). This concept is illustrated in figure 185. Table 16 shows a summary of various characteristics evaluated ranked in order from highest to lowest R^2 value for both analysis covering mass loss up to 100 percent and maximum 5 percent (ranking of these characteristics based on standard error yielded similar results). Here, it is seen that the paste-to-total-voids ratio consistently ranked among the top three in each form of analyses. Its components, paste content ranked in the top three in two of the four analysis, and total voids content ranked at the top in one of the analysis. These results demonstrate the significance of material compositional

parameters on the durability of the SRW unit. The NCMA index ranked reasonably high (top three in two analysis cases and top five in another case), which was likely due to the correlation strength of the 24-hour absorption and to some extent, the unit weight. ASTM C 642 (2002) parameters were modest in their ranking, while ASTM C 457 (2004) air void parameters ranked in the lower third of all parameters considered. The observation that mass loss correlated better with paste content rather than strength was in agreement with the results from Ghafoori and Mathis (1998), where cement content showed highest correlation to mass loss and with the literature review findings of Hance (2005). The saturation coefficient, which is commonly used as frost criterion for clay or shale bricks (ASTM C 672), was not suitable for the SRW units evaluated in this study. Hence, it is evident that typical frost performance criteria for other types of porous materials (spacing factor for ordinary concretes and saturation coefficient for bricks) may not be equally applicable to SRW concretes.

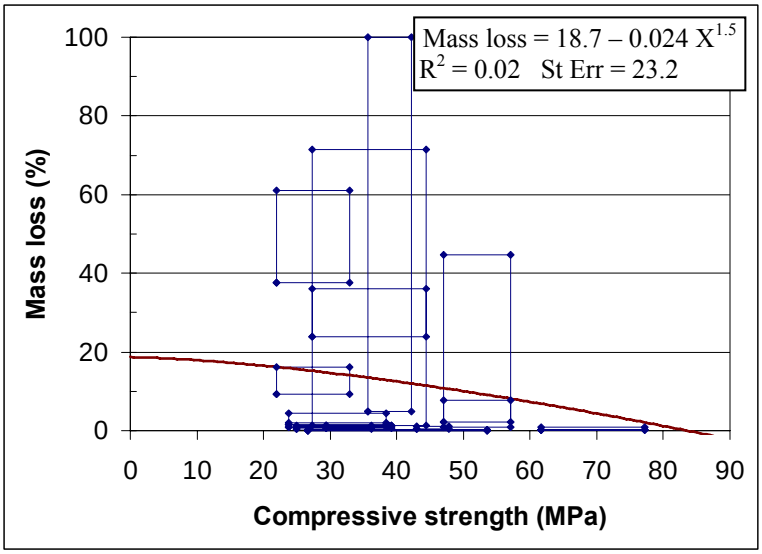

Figure 159. Graph. ASTM C 140 compressive strength. Data representation by boundary points.

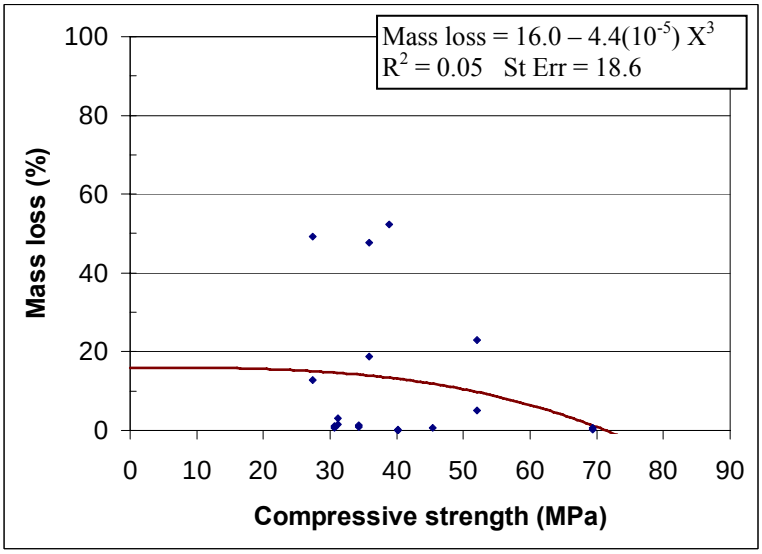

Figure 160. Graph. ASTM C 140 compressive strength. Data representation by centroids.

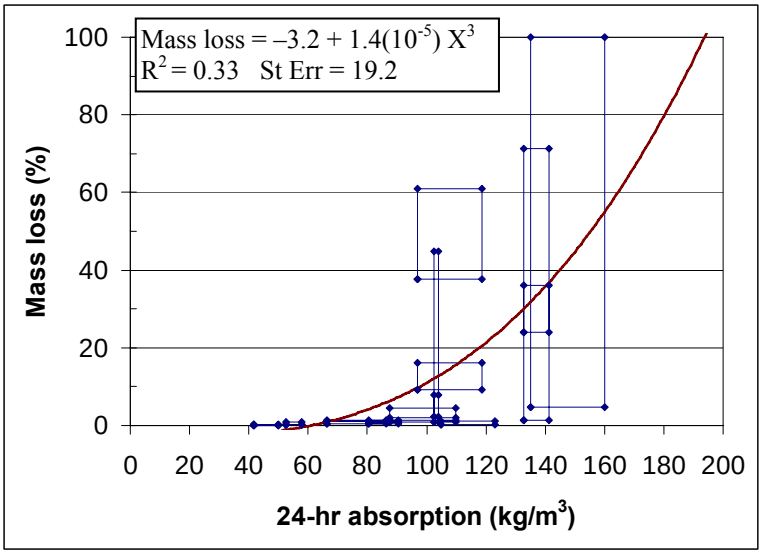

Figure 161. Graph. ASTM C 140 24-hour water absorption. Data representation by boundary points.

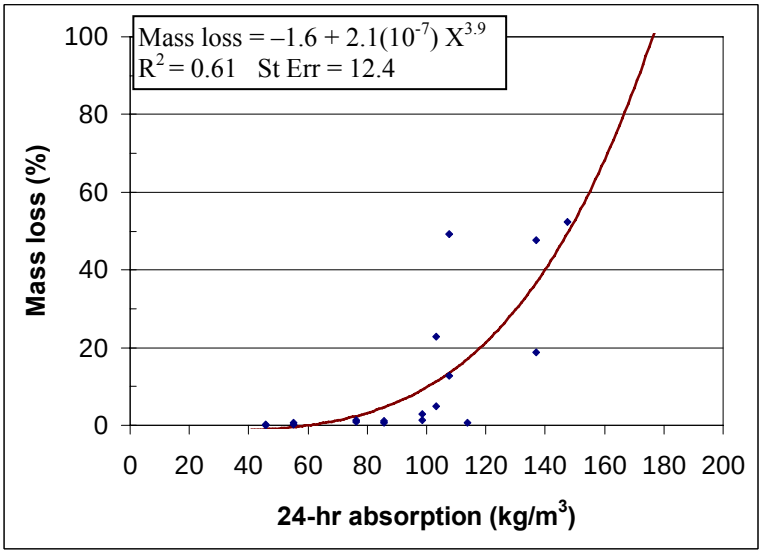

Figure 162. Graph. ASTM C 140 24-hour water absorption. Data representation by centroids.

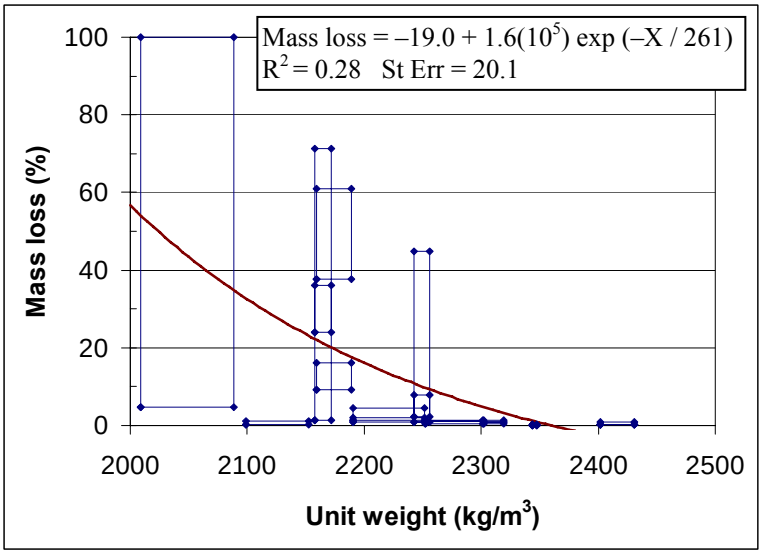

Figure 163.Graph. ASTM C 140 Unit weight. Data representation by boundary points.

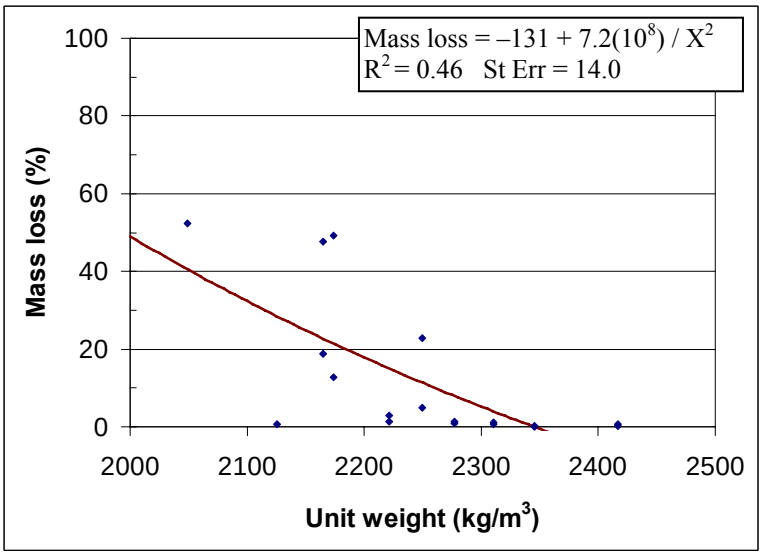

Figure 164. Graph. ASTM C 140 Unit weight. Data representation by centroids.

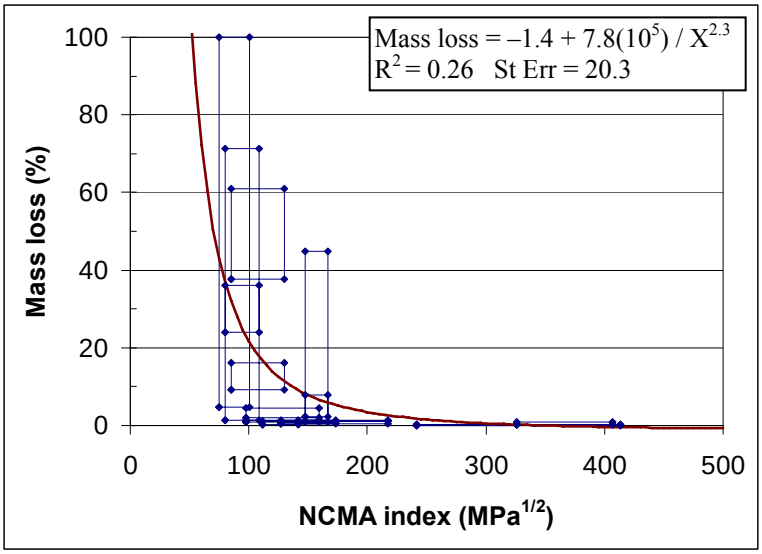

Figure 165. Graph. NCMA index. Data representation by boundary points.

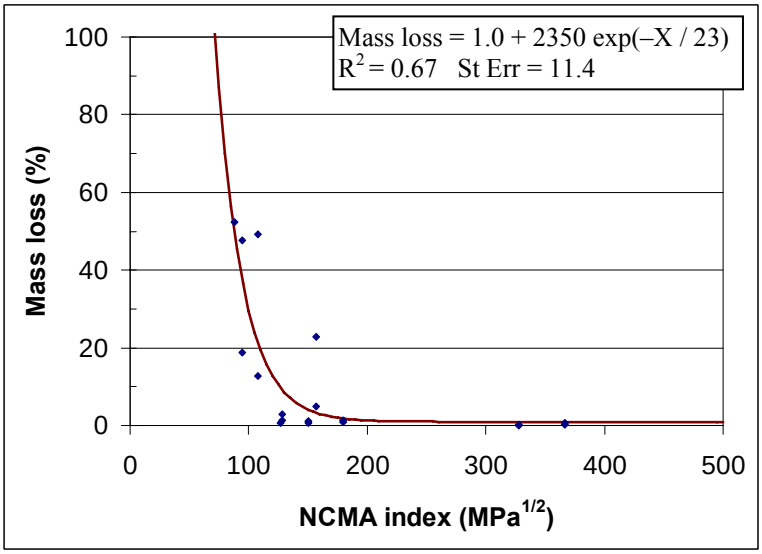

Figure 166. Graph. NCMA index. Data representation by centroids.

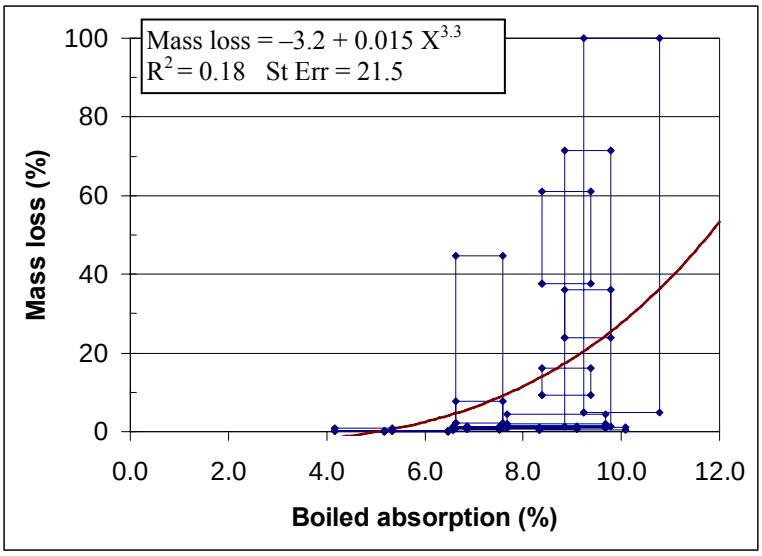

Figure 167. Graph. ASTM C 642 Boiled absorption. Data representation by boundary points.

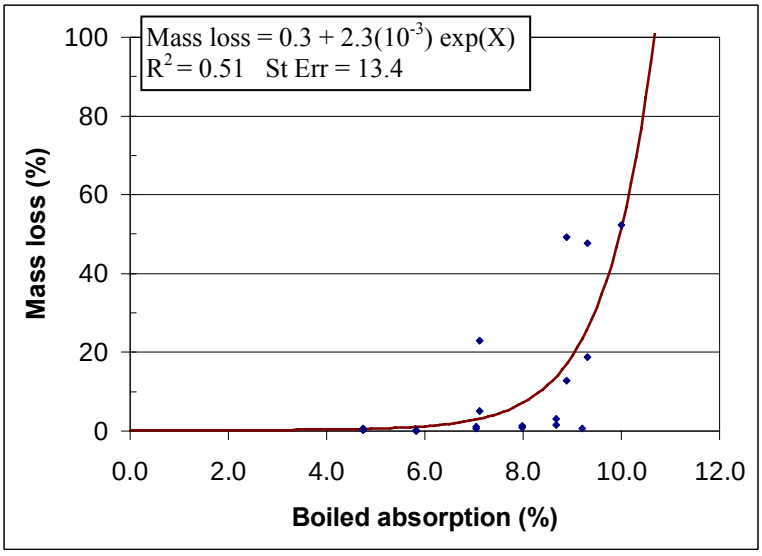

Figure 168. Graph. ASTM C 642. Bottom graph. Data representation by centroids.

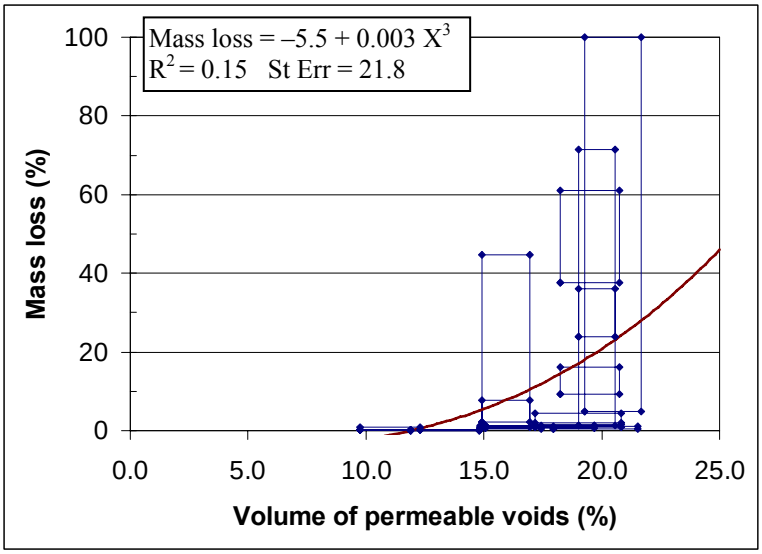

Figure 169. Graph. ASTM C 642. Volume of permeable voids. Data representation by boundary points.

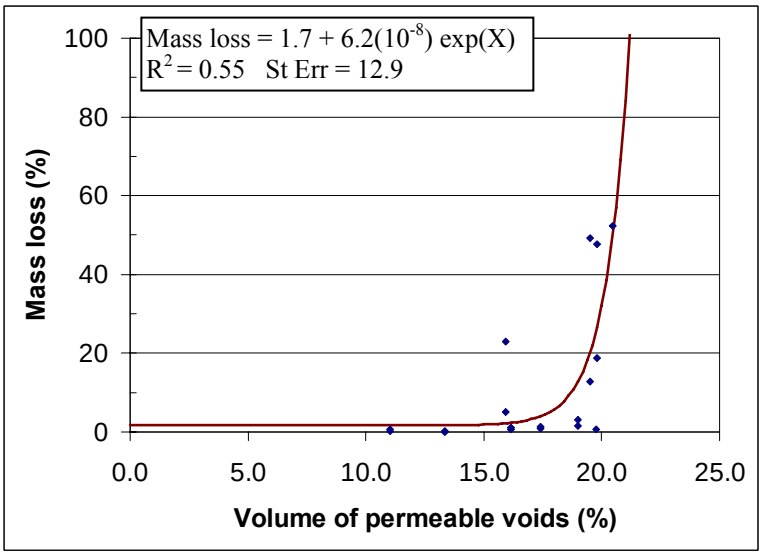

Figure 170. Graph. ASTM C 642 Volume of permeable voids. Data representation by centroids.

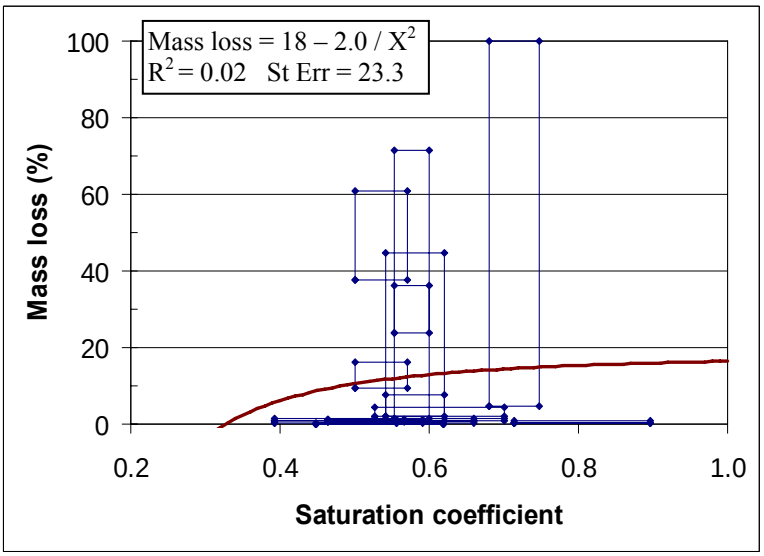

Figure 171. Graph. Saturation coefficient. Data representation by boundary points.

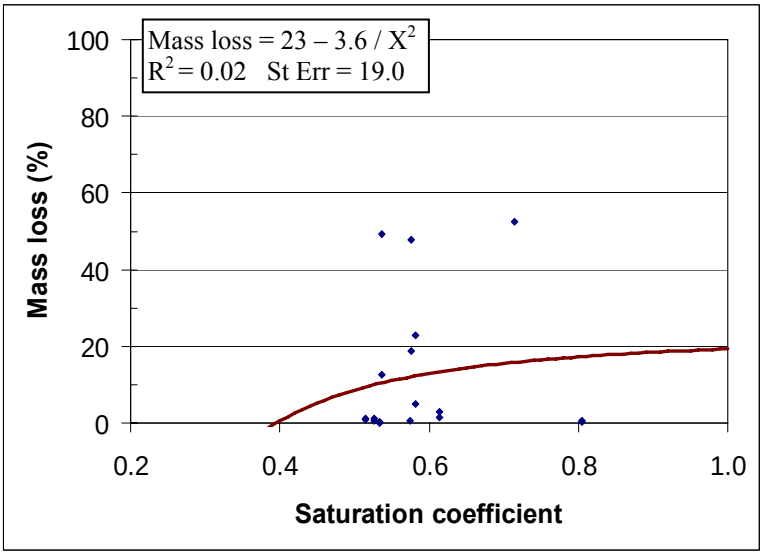

Figure 172. Graph. Saturation coefficient. Data representation by centroids.

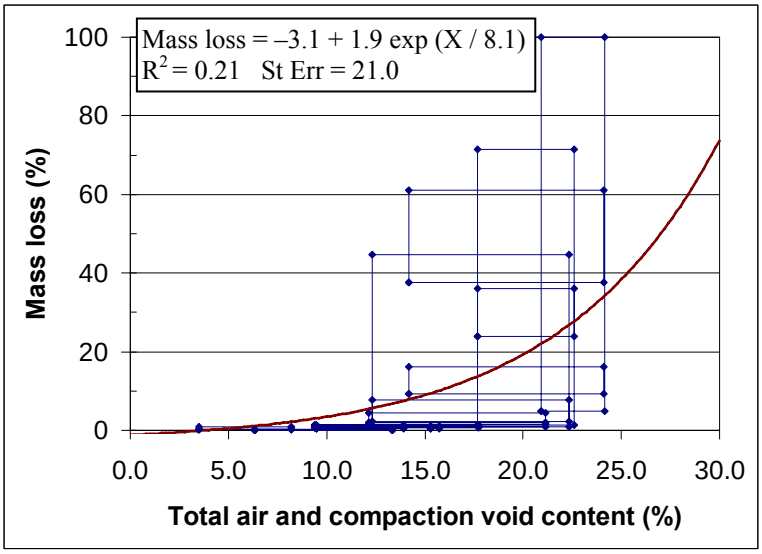

Figure 173. Graph. Total air and compaction voids content. Data representation by boundary points.

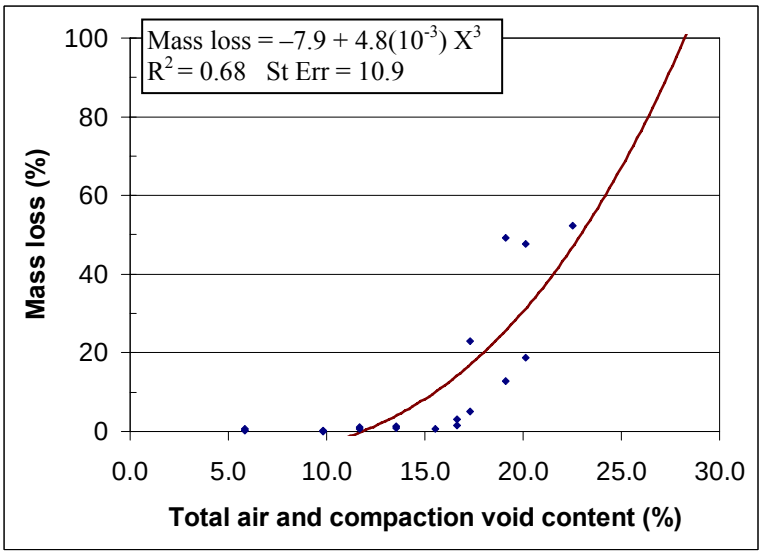

Figure 174. Graph. Total air and compaction voids content. Data representation by centroids.

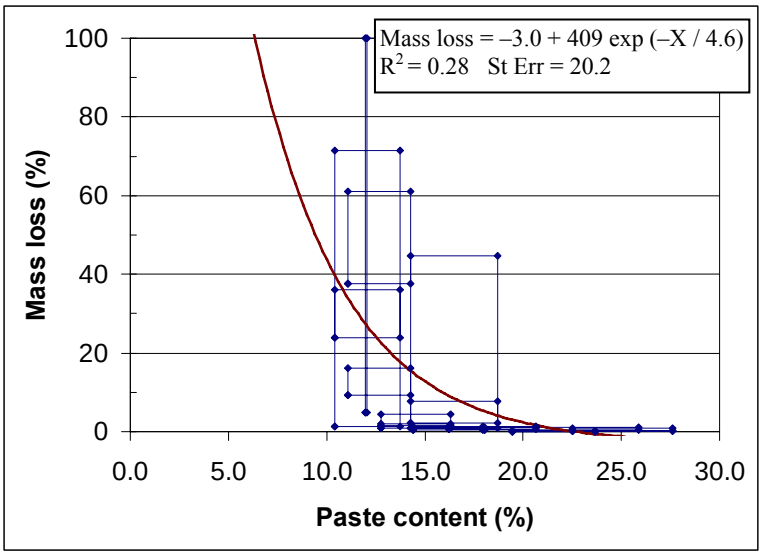

Figure 175. Graph. Paste content. Data representation by boundary points.

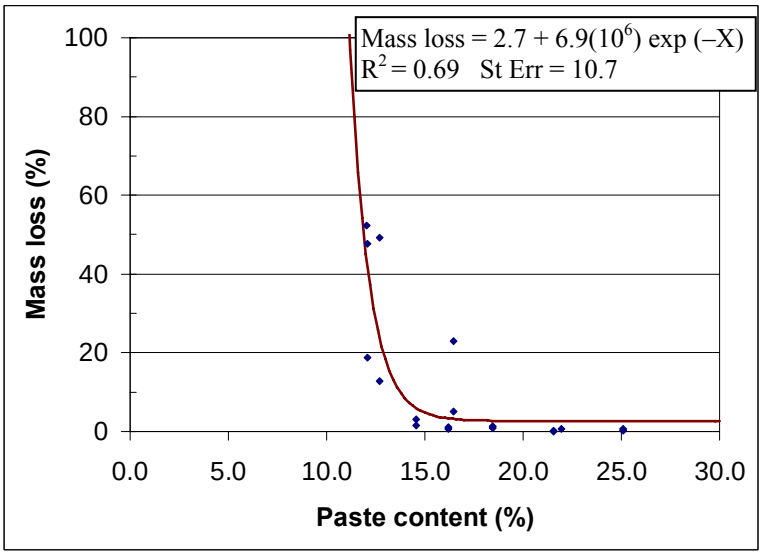

Figure 176. Graph. Paste content. Data representation by centroids.

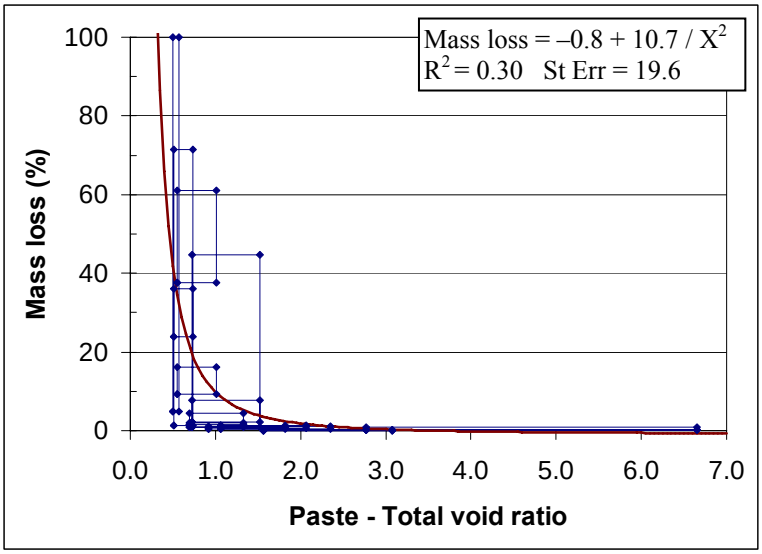

Figure 177. Graph. Paste-to-total-void ratio. Data representation by boundary points.

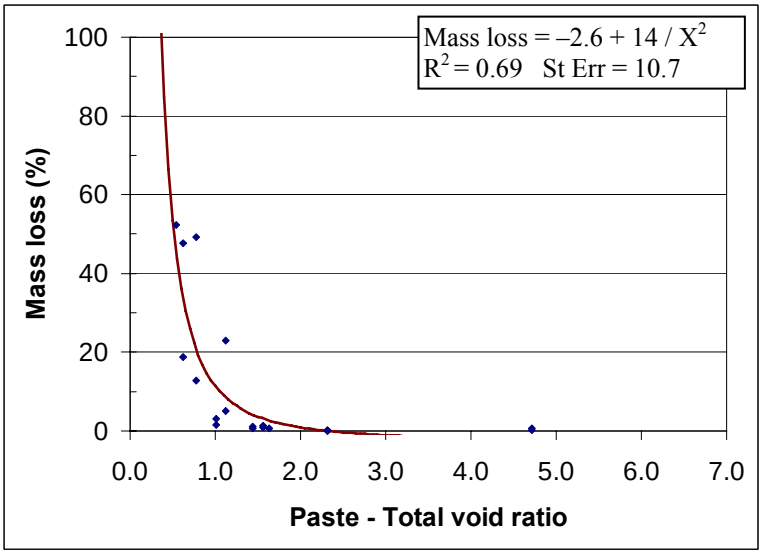

Figure 178. Graph. Paste-to-total-voids ratio. Data representation by centroids.

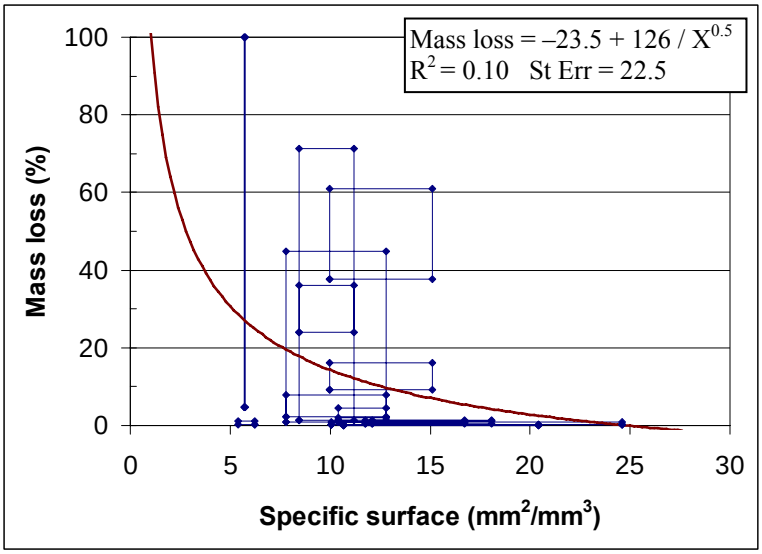

Figure 179. Graph. ASTM C 457 Specific surface. Data representation by boundary points.

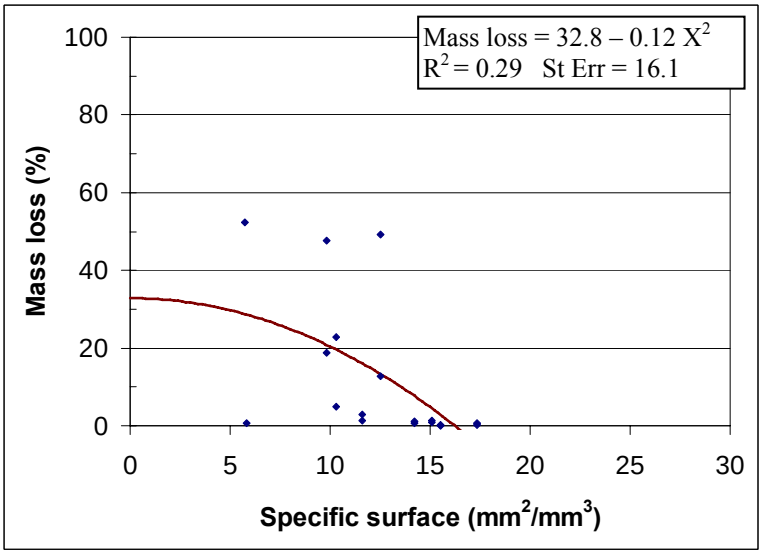

Figure 180. Graph. ASTM C 457 Specific surface. Data representation by centroids.

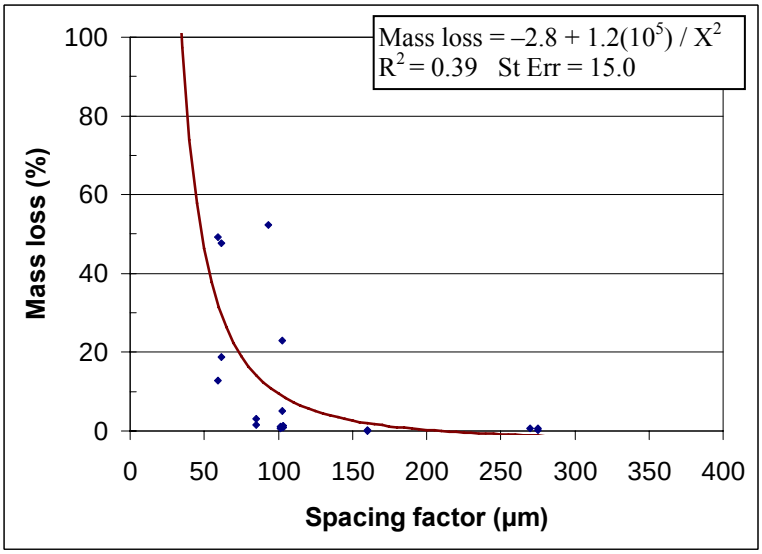

Figure 181. Graph. ASTM C 457 spacing factor. Data representation by boundary points.

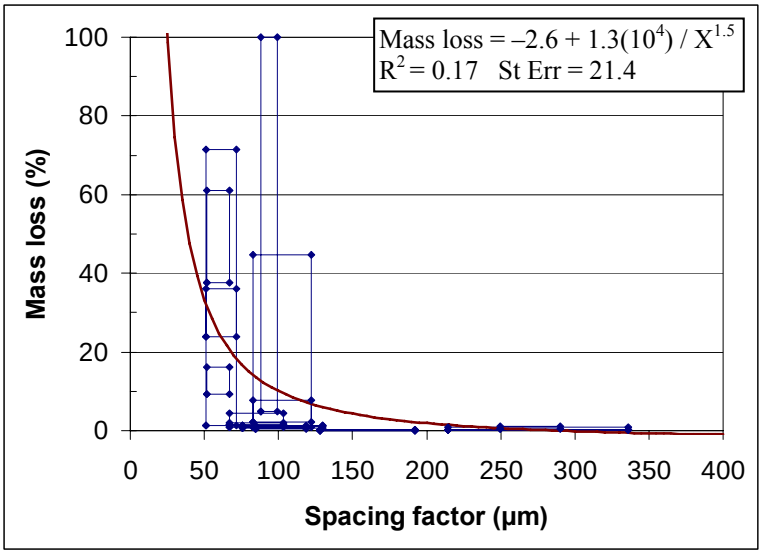

Figure 182. Graph. ASTM C 457 Spacing factor. Data representation by centroids.

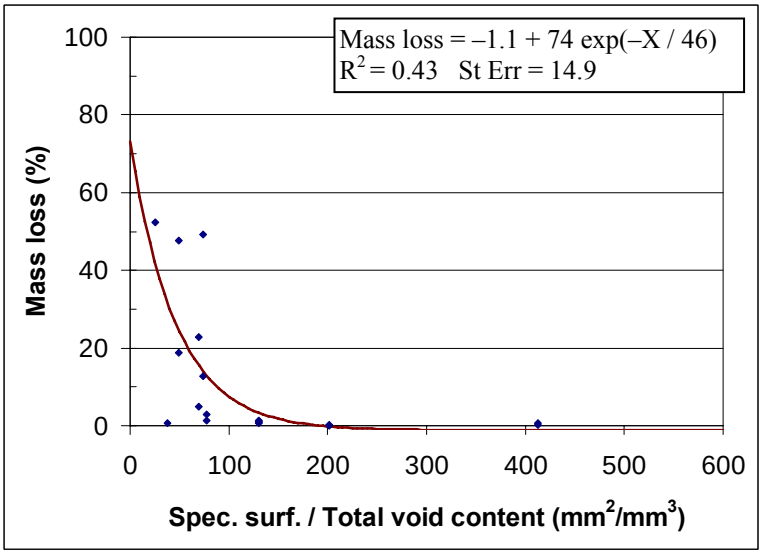

Figure 183. Graph. Specific surface/total void content. Data representation by boundary points.

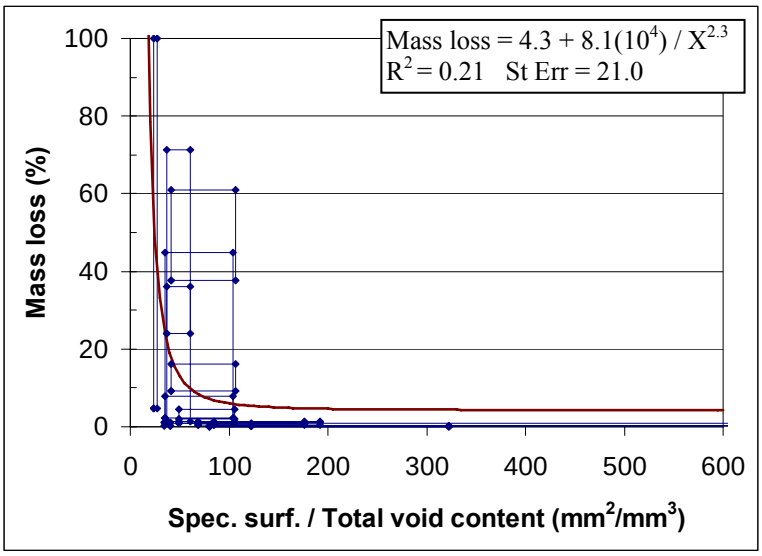

Figure 184. Graph. Specific surface/total void content. Data representation by centroids.

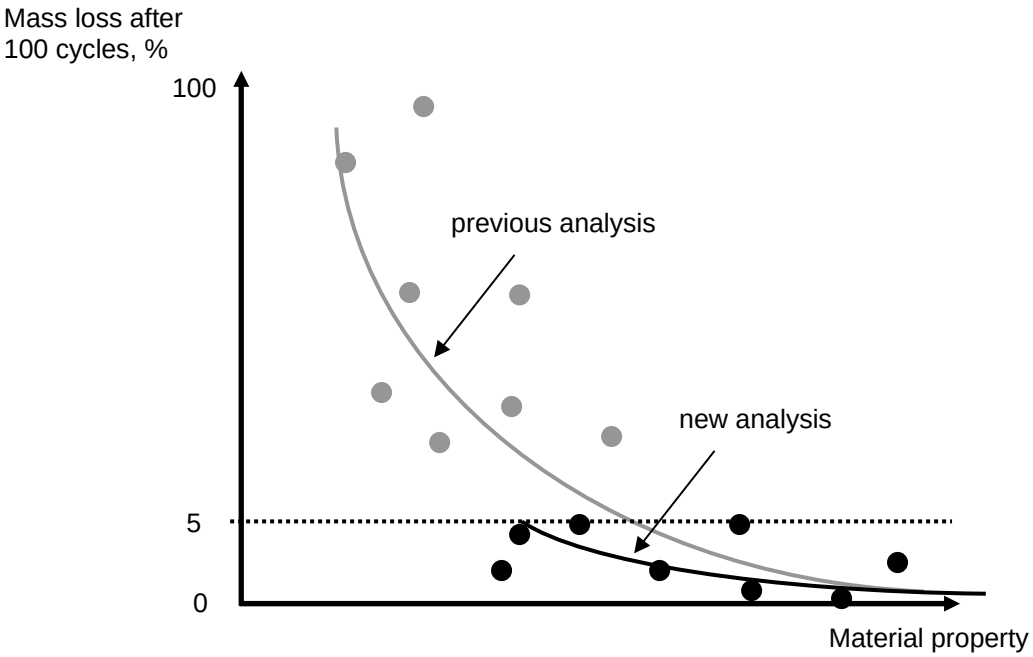

Figure 185. Graph. Evaluation of data points for mass loss less than 5 percent only.

Table 16. Ranking of material properties using different types of analyses.

Rank	Mass Loss Up to 100 percent				Mass Loss Up to 5 percent			
	Boundary Points		Centroids		Boundary Points		Centroids	
	R^2	StErr	R^2	StErr	R^2	StErr	R^2	StErr
1	24A*	0.33 19.2	P/V	0.69 10.7	24A	0.40 0.93	TV	0.86 0.55
2	P/V	0.30 19.6	P	0.69 10.7	P/V	0.38 0.95	α/TV	0.60 0.95
3	P	0.28 20.2	NCMA	0.68 11.4	NCMA	0.37 0.95	P/V	0.54 1.06
4	OD	0.28 20.1	TV	0.68 10.9	OD	0.36 0.95	α	0.41 1.14
5	NCMA	0.26 20.3	24A	0.61 12.4	P	0.36 0.95	24A	0.36 1.19
6	TV	0.21 21.0	VPV	0.55 12.9	α/TV	0.35 0.97	P	0.32 1.29
7	α/TV	0.21 21.0	BA	0.51 13.4	TV	0.34 0.98	L	0.30 1.31
8	BA	0.18 21.5	OD	0.46 14.0	BA	0.29 1.01	NCMA	0.25 1.36
9	L	0.17 21.4	α/TV	0.43 14.9	VPV	0.26 1.03	OD	0.18 1.34
10	VPV	0.15 21.8	L	0.39 15.0	L	0.20 1.07	BA	0.15 1.37
11	α	0.10 22.5	α	0.29 16.1	α	0.12 1.12	VPV	0.15 1.37
12	f_m	0.03 23.2	f_m	0.05 18.6	f_m	0.07 1.15	f_m	0.01 1.47
13	SC	0.02 23.3	SC	0.02 19.0	SC	0.02 1.18	SC	0.01 1.46

* Notation: f_m = compressive strength; 24A = 24-hour absorption; OD = oven-dry density; NCMA = NCMA index; BA = boiled absorption; VPV = volume of permeable voids; TV = total air and compaction void content; P = paste content; P/V = paste to total voids ratio; α = specific surface; L = spacing factor; α/TV= specific surface / total voids; SC = saturation coefficient

It is noted that, despite the helpfulness of curve fits in providing a quantitative interpretation of these data series, the actual behavior of mass loss relative to material characteristics is probably best discerned from the nature of the data itself. For instance, from figures 159 to 184, it is evident that the constructed boxes resembled some form of step function, whereby mass loss could range from being negligible to almost 100 percent in the region to one side of a certain critical value of the material property, but be low (less than about 1.5 percent) on the other side of this critical value. As such, it is possible that threshold values in most of the material characteristics exist beyond which there is a greater likelihood of larger mass loss. For the particular SRW units evaluated, the threshold values are summarized in table 17. With respect to ASTM C 140 (2000) parameters, these threshold values would have satisfied the specification values of ASTM C 1372 (2003) (Comp. strength: 57 MPa (8,270 psi) threshold versus minimum 21 MPa (3,050 psi) spec., 24-hour absorption: 85 kg/m^3 (5.3 pounds per cubic foot (pcf)) threshold versus maximum 208 kg/m^3 (13 pcf) spec. for normal weight SRW units). With respect to ASTM C 457 air void parameters, the threshold value for specific surface (15 mm^2/mm^3 or 375 inch^2/inch^3) was found to be similar to those found for concretes of satisfactory frost resistance (16 mm^2/mm^3 or 400 inch^2/inch^3 in Neville (1996)). The threshold value for spacing factor (120 μm or 0.005 inch) differed from the maximum 200 to 250 μm (0.008 to 0.010 inch) values of frost durable concretes. In fact, these threshold values would not be comparable since the trend in mass loss relative to spacing factor appeared to be different for SRW concretes than for normal concretes.

Table 17. Threshold values of material properties determined from figures 159 to 184.

Property	Threshold Value
ASTM C 140	
Comp. strength	57 MPa (8,270 psi)
24-hour absorption	85 kg/m^3 (5.3 pcf)
Oven-dry density	2260 kg/m^3 (141 pcf)
NCMA index	170 MPa$^{1/2}$ (2,050 psi$^{1/2}$)
ASTM C 642	
Boiled absorption	6.5 percent
Volume of perm. voids	15 percent
ASTM C 457 Compositional Parameters	
Total air and comp. voids	12 percent
Paste content	19 percent
Paste / Total voids ratio	1.5
ASTM C 457 Air Void Parameters	
Specific surface	15 mm^2/mm^3 (375 inch^2/inch^3)
Spacing factor	120 μm (0.005 inch)
Spec. surf. / Total voids	106 mm^2/mm^3 (2,650 inch^2/inch^3)

4.6.5 Discussion of ASTM C 1262 (2003) (in 3 percent NaCl solution) Results

Figures 186 and 187 show the mass loss versus paste-to-total-voids ratio plots for tests in 3 percent NaCl solution. Greater data scatter was observed in these tests, as evidenced by the longer boxes in the vertical direction. This implied it was possible for some specimens to significantly outperform other specimens obtained from the same SRW unit (same composition and manufacturer). Although the mass loss generally decreased with increasing paste-to-total-voids ratio similar to the trend observed in water, there were instances of units with relatively high paste-to-total-voids ratio that also showed significant mass loss. This observation occurred similarly for other material characteristics and indicates that units considered of high quality when in tested water may still display a substantial mass loss when tested in saline.

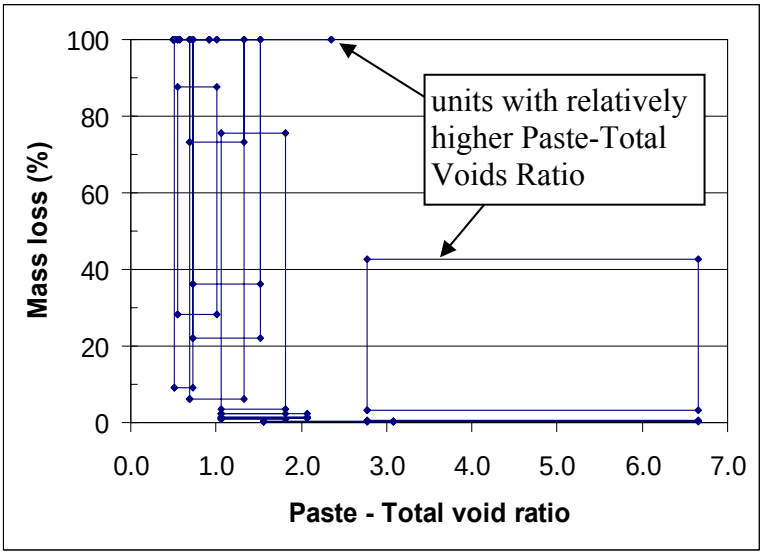

Figure 186. Graph. Mass loss in 3 percent NaCl solution versus paste-to-total-voids ratio. Data representation by boundary points.

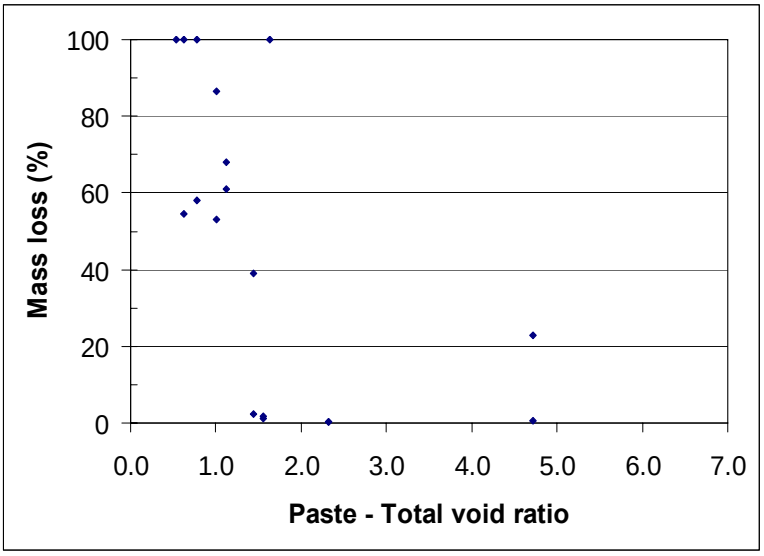

Figure 187. Graph. Mass loss in 3 percent NaCl solution versus paste-to-total-voids ratio. Data representation by centroids.

4.6.6 Summary

Various common SRW concrete material characteristics were assessed for their potential as frost durability indices by evaluating their correlation to ASTM C 1262 (2003) freeze-thaw mass loss. Of all parameters considered, the paste-to-total-voids ratio exhibited the strongest correlation to freeze-thaw mass-loss in water. Its components, paste content and total voids content, also exhibited strong correlations demonstrating the importance of unit composition on frost durability. The NCMA index showed fair correlation to mass loss, which was likely attributed to the correlation strength of the 24-hour water absorption. The spacing factor and saturation coefficient displayed low correlation to mass loss implying that these parameters may not be applicable to SRW concretes in the same way that they apply to ordinary concretes and clay bricks respectively. The threshold compressive strength value was determined to be well above the minimum specification value, while the 24-hour water absorption was well below the maximum specification value. This implied that SRW units that barely meet standard specification for these material characteristics may not necessarily be guaranteed frost durability. Finally, it was demonstrated that trends and observations drawn from water tests may not be entirely applicable to saline solution tests due to the higher data scatter in saline tests. Units considered of high quality when tested in water may display substantial mass loss when tested in saline.

4.7 SYNOPSIS OF STUDY ON EFFECTS OF ALTERNATIVE DEICING SALTS ON SRW BLOCK DURABILITY

As described in chapter 3, significant damage has only been observed for SRW blocks in the field when the blocks are exposed to high levels of both moisture and deicing salts (or fertilizer). The key role that deicing salts play in field damage seems to justify the need to include salts in freeze-thaw testing in the laboratory. A significant amount of laboratory work has already been described in this report that included the use of salt solution, and in each case, the salt used was

3 percent NaCl solution. However, in highway applications, it is becoming more common for alternative deicing salts to be used, especially $MgCl_2$. To address this point, a comprehensive study was initiated under this FHWA project in which the durability of SRW blocks was assessed while exposed to four different deicing salts and one commercially available fertilizer. For conciseness, only a brief synopsis of this study is presented herein. Full details can be found in:

- Chan, C, Hover, K., and Folliard, K., "Durability of Segmental Retaining Wall (SRW) Concretes to Different Deicing Salt Types," manuscript submitted to Transportation Research Board, August 2006 (2006b).

In this study, two different SRW concretes were subjected to freeze-thaw cycles (following ASTM C 1262 (2003)) and continuous warm immersion tests to determine possible chemical effects from the salts. The salts used in these tests included:

- Sodium chloride (NaCl), i.e., rock salt.
- Calcium chloride ($CaCl_2$) (often marketed as a "nonsalt deicer").
- Magnesium chloride ($MgCl_2$) (magnesium chloride heptahydrate flakes).
- Calcium magnesium acetate, ($[CaMg_2\ (CH_3COO)_2]_6$), CMA.
- Fertilizer consisting of 32 percent nitrogen, 3 percent phosphorus, 5 percent potassium.

The results of the freeze-thaw testing are summarized in figure 188. At 3 percent concentration (by mass of solution), NaCl solution was the most detrimental of all salts evaluated under freeze-thaw conditions. Freeze-thaw mass loss of specimens tested in NaCl solution (about 85 percent after 100 cycles) was approximately twice that of specimens tested in all other salt solutions (30 to 50 percent) (compared to about 1 to 2 percent in plain water). It generally appeared that as the solution freeze-point depression (ΔT_{fr}) increased, the number of cycles taken before reaching 1 percent mass loss decreased. It is worth noting the fertilizer solution used in the tests was capable of causing as much freeze-thaw damage as most other deicing salt solutions, which has important implications for SRWs in areas frequently exposed to fertilizing compounds. It is recommended that freeze-thaw tests also be performed with similar salts but at varying concentrations to achieve similar ΔT_{fr} for all test solutions.

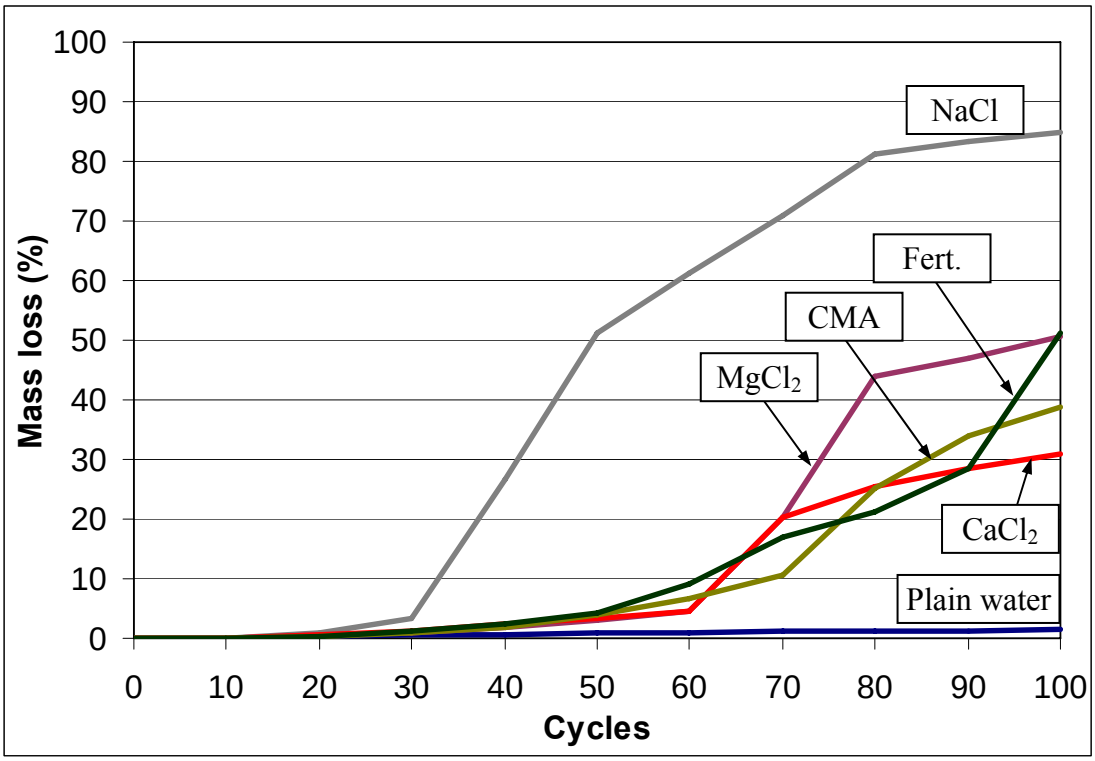

Figure 188. Graph. Average ASTM C 1262 (2003) mass loss for all salt solutions evaluated.

In tests involving continuous immersion in warm solutions, particles of mix A and B were damaged by solutions of both CMA and $MgCl_2$, while no damage was detected in other salt solutions even after 15 months of immersion.

4.8 RESEARCH ON DEVELOPMENT OF MORE REALISTIC FREEZE-THAW TEST FOR SRW BLOCKS

This section describes research aimed at developing a new, more realistic approach to testing SRW blocks. It is intended to address some of the shortcomings of ASTM C 1262 (2003), such as issues with sampling (and inherent variability for specimens extracted from a given block), repeatability (or lack thereof), and applicability to real-world exposure conditions (due to overly severe conditions induced in ASTM C 1262 (2003)). With this in mind, research was initiated under this FHWA project to develop and assess a testing regime that would allow for the testing of full SRW units or multiple SRW units stacked in a given formation (including cap units on top) under simulated field conditions. By grouping the SRW blocks in a simulated wall setup, deterioration that replicates field conditions is more likely to occur because stresses or restraint caused by adjacent blocks and drainage typical of that found in the field can be simulated. Thus, a new test method that represents field conditions would be useful so that SHAs and manufacturers can better assess the freeze-thaw durability performance of SRW blocks. The research herein consisted of two testing phases: the first phase consisted of performing trial tests on smaller-scale SRW blocks and the second phase used the information from the first phase testing to develop a standard test to evaluate the freeze-thaw performance of larger-scale SRW blocks typically used in transportation infrastructure systems.

4.8.1 Phase I Investigation

A preliminary freeze-thaw test procedure was developed and testing performed to assess the freeze-thaw performance of smaller, commercially available SRW blocks. It was anticipated that these results would provide preliminary information for the Phase II test procedure. The Phase I tests were performed to identify and resolve issues with the initial setup design, identify key parameters of the experiment, and set standards for the Phase II procedure. The focus of developing this new test method was to replicate field environmental conditions as closely as practical by implementing slower temperature changing rates, longer temperature hold times, and spray exposure conditions instead of ponding.

Equipment necessary for constructing the test setup included a programmable temperature-controlled environment, a spray system with cyclic capabilities, and a test chamber large enough to hold six to nine SRW blocks. The programmable, temperature-controlled chamber was able to control the temperature from −20 °C to 24 °C (−4 °F to 75 °F) and was able to ramp at least 0.55 °C (1 °F) per minute on the freezing cycle. The environmental chamber also incorporated a spray system for applying salt or fresh water solutions. A drawing of the exposure chamber used in this study is shown in figure 189.

The overall dimensions of the chamber were 0.9 m wide by 1.8 m long by 1.5 m tall (3 ft by 6 ft by 5ft). The chamber support structure was built with a 51 mm (2 inch) angle iron frame to support the weight of the SRW blocks. The top and sides of the chamber were fixed with sheets of Plexiglas® to retain the spray solution during testing. The chamber was equipped with a drain system that recycled the solution.

The spray system consisted of eight 6 mm (0.25 inch) stainless steel spray nozzles with 2 mm (0.081 inch) maximum free passage orifices and a 19 L (5 gal) per minute maximum flow rate to ensure complete coverage of the SRW block samples. The spray nozzles were attached to 9.5 mm (0.375 inch) stainless steel tubing that was fixed in the chamber. Four nozzles were positioned in front of the wall and four above the wall to ensure complete exposure to the test solution. A ball valve was placed before each set of nozzles to regulate the flow. A ¾ HP 316 stainless steel centrifugal pump was used to pump the solutions. This pump was controlled by electrical timers (mechanical timers can also be used) that enabled the pumps to turn on for 15-minute intervals during the thaw cycle. A 49 L (13 gal) polypropylene reservoir was used to store the spray solution. A return line from the pump discharge was installed to prevent damage to the pump if the spray nozzles became blocked.

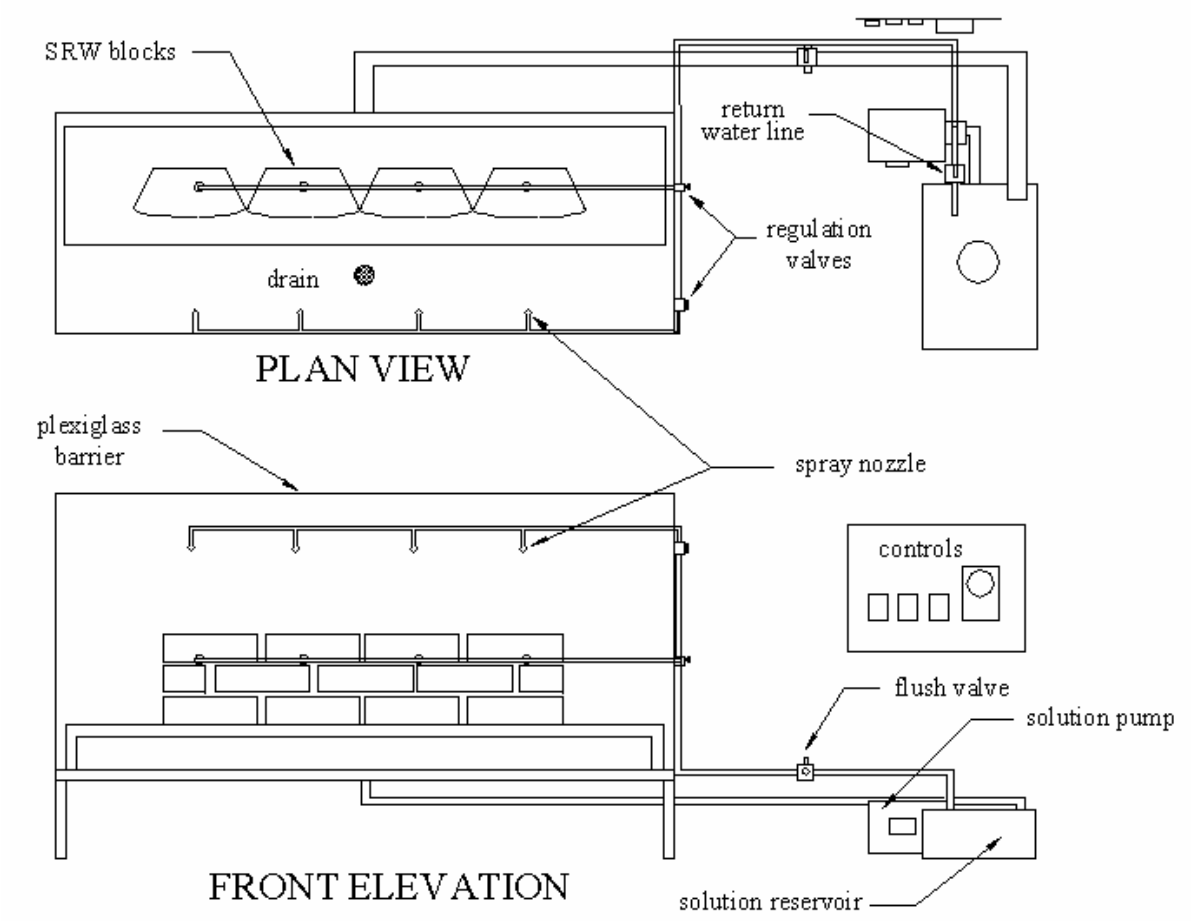

Figure 189. Drawing. Exposure chamber.

Four experiments were completed during the Phase I testing. The Phase I plan consisted of evaluating sets of 13 SRW blocks in each test. The temperature ramp rate, the temperature hold times, and the solution type were investigated in this phase. Table 18 provides an overview of the parameters investigated for each of the tests conducted.

Table 18. Phase I experimental program.

Smaller SRW Blocks		Temperature Hold Time (Hours)	Percent NaCl	
			0	3
Temperature Ramp Rate °C/min (°F/min)	0.18 (0.3)	1	*NT*	*Test 2*
	0.33 (0.6)	1	*Test 1*	*Test 3*
	0.55 (1.0)	2	*NT*	*Test 4*

NT = not tested

To prepare the blocks for testing, the blocks were oven dried at 113 °C (235 °F) for 24 hours, labeled, and then weighed. These values were recorded as oven dry weights. After the weights were recorded the blocks were submerged in water until they reached saturation (typically after 48 hours). The blocks were then removed from the solution, surface dried, and these weights were recoded as original saturated weight. After these data were obtained, the blocks were stacked in the freeze-thaw chamber. The first three rows of blocks as shown in figure 190 (labeled A through L) were used for mass loss measurements. The top block, identified as Block M, was used for temperature measurements.

The chamber temperature varied from −18 °C to 16 °C (0 °F to 60 °F). The temperature ramp rates were adjusted to achieve specified temperature changes in the blocks. The cycles consisted of the hold times shown in table 18.

Figure 190. Photo. Freeze-thaw test setup showing SRW blocks.

To evaluate the internal temperature of the SRW blocks a 6.35-mm (0.25-inch) hole was drilled in the back of Block M to the center of the block. A Type J thermocouple was inserted into this hole and the hole was backfilled with approximately 25.4 mm (1 inch) of mortar made from a mixture of water, cement, and the block drill dust. The remaining hole was then filled with an insulating foam spray. The block temperature ramp rates and hold times were monitored to define the appropriate parameters for the actual test.

The blocks were sprayed with solution (either NaCl solution or water) for 15 minutes prior to the start of the freeze cycle. The samples were exposed to 10 freeze-thaw cycles and then evaluated for freeze-thaw damage by visual inspection. These blocks were then saturated for at least 12 hours to restore any evaporated moisture during the testing. As already noted, the surface of the blocks was dried and the blocks were weighed after every 10 cycles. After weighing, the blocks were restacked in the chamber in the same order as the original stacking. Photographs of the blocks were obtained for a visual record, and the test cycle was repeated.

Small commercial landscaping SRW blocks were procured for the Phase I testing. The typical dry weight of these blocks was 12 kg (26.5 lbs), and the dimensions of these blocks are shown in figure 191. All of the surfaces were relatively smooth except the front surface. The front surface consisted of a split face.

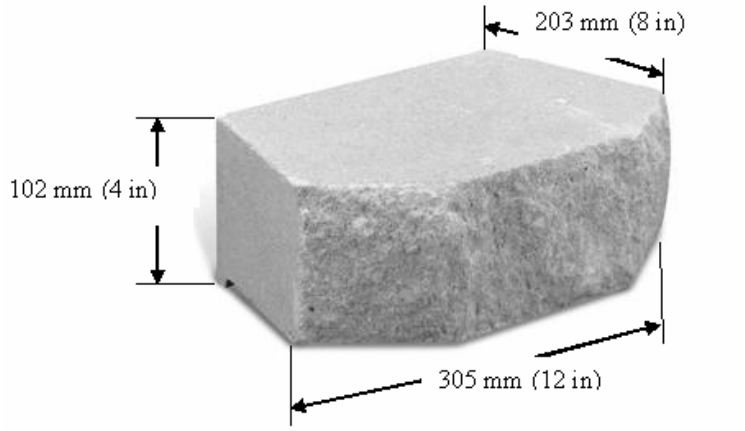

Figure 191. Photo. Smaller SRW block testing in Phase I.

The freeze-thaw performance of the smaller SRW blocks was assessed by measuring the mass loss of the blocks (based on saturated weights) after the blocks were subjected to 10 freeze-thaw cycles. Figure 192 shows the weight loss for block samples from test 1 (ramp rate of 0.33 ^{o}C/min (0.6 ^{o}F/min) with 1 hour hold time sprayed with water). Figures 193 through 195 show the weight loss values for samples from test 2 (ramp rate of 0.18 ^{o}C/min (0.3 ^{o}F/min) with 1-hour hold time sprayed with 3 percent NaCl solution), test 3 (ramp rate of 0.33 ^{o}C/min (0.6 ^{o}F/min) with 1-hour hold time sprayed with 3 percent NaCl solution), and test 4 (ramp rate of 0.55 ^{o}C/min (1.0 ^{o}F/min) with 2-hour hold time sprayed with 3 percent NaCl solution), respectively.

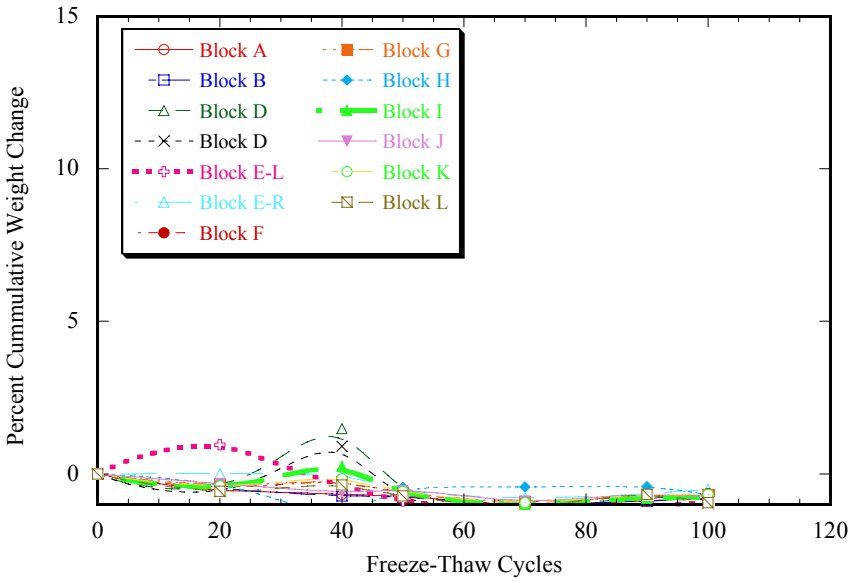

Figure 192. Graph. Percent weight change for samples from test 1 (ramp rate of 0.33 °C/min (0.6 °F/min) with 1-hour hold time, sprayed with water).

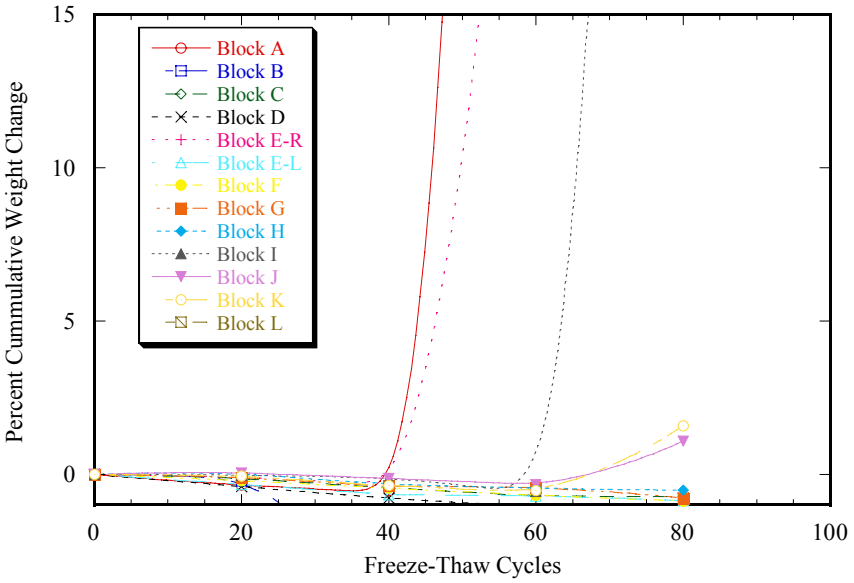

Figure 193. Graph. Percent weight change for samples from test 2 (ramp rate of 0.18 °C/min (0.3 °F/min) with 1-hour hold time, sprayed with 3 percent NaCl).

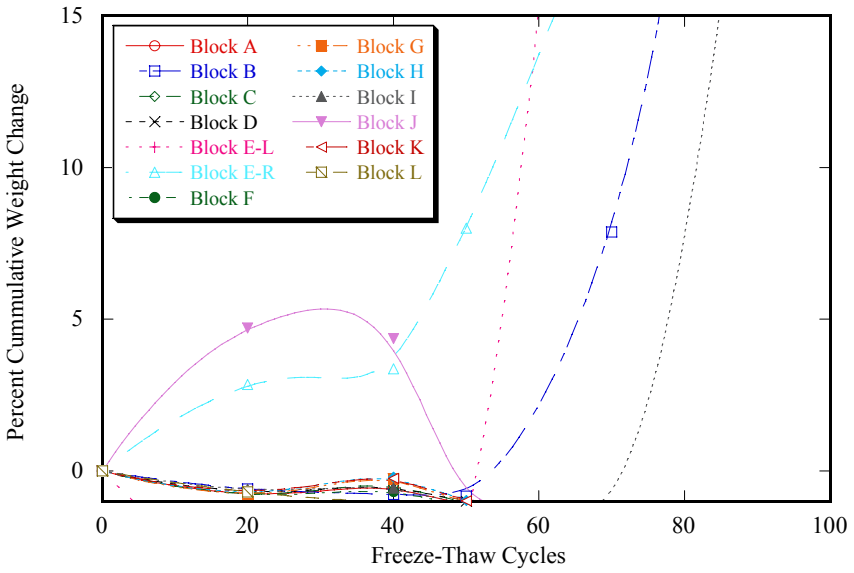

Figure 194. Graph. Percent weight change for samples from test 3 (ramp rate of 0.33 °C/min (0.6 °F/min) with 1-hour hold time, sprayed with 3 percent NaCl).

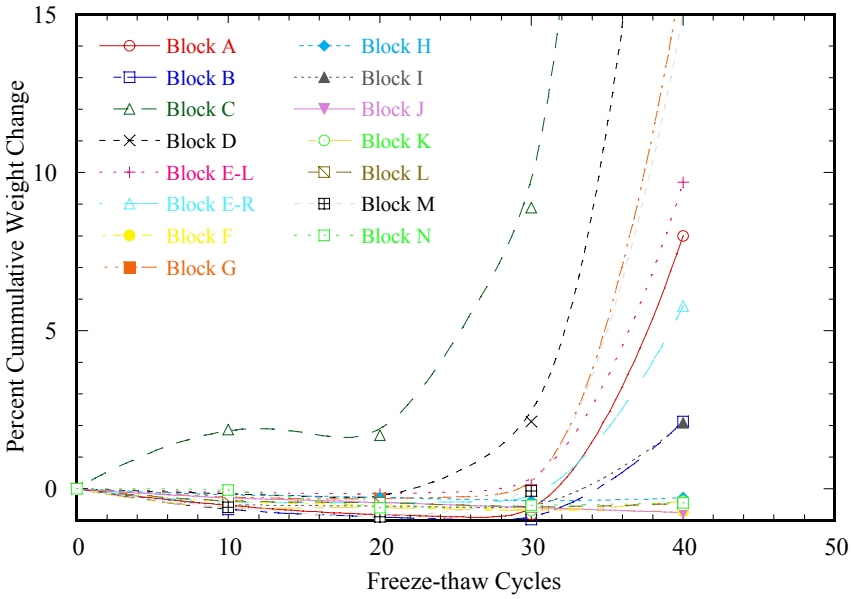

Figure 195. Graph. Percent weight change for samples from test 4 (ramp rate of 0.55 °C/min (1.0 °F/min) with 2 hour hold time, sprayed 3 percent NaCl).

It can be seen from figure 192 that samples exposed to water-spray exhibited limited weight loss after 100 freeze-thaw cycles, whereas several blocks exposed to the same ramp rates and hold times, but exposed to the 3 percent NaCl solution (figure 193) exhibited significant mass loss after 80 cycles. Three of the blocks in test 2 suffered severe deterioration and were considered to fail the test based on an arbitrary 5 percent mass loss criteria, and two other blocks showed significant distress as shown in figure 193. This clearly shows that the presence of salt increases the potential for damage, just as in the field and in ASTM C 1262 (2003), but it should be noted that not all the blocks showed significant damage in this test.

Figures 193 through 195 show the influence of temperature ramp rates and temperature hold time on the freeze-thaw performance of small SRW blocks. Three samples exposed to Test 2 conditions (ramp rate of 0.18 °C/min (0.3 °F/min) failed before 100 freeze-thaw cycles. Four of the samples exposed to the Test 3 conditions (ramp rate of 0.33 °C/min (0.6 °F/min) failed before 100 freeze-thaw cycles. Although this tends to indicate that faster rates lead to more failures, because of the limited number of tests performed, only limited conclusions can be made. However, when evaluating the samples that were exposed to the Test 4 conditions (ramp rate of 0.55 °C/min (1.0 °F/min) with 2 hour hold time sprayed with 3 percent NaCl solution, seven small SRW blocks failed, indicating that the faster ramp rates and/or the longer hold time accelerated the freeze-thaw deterioration. The time for the cycling of the environment is approximately 1 hour. This time and the hold time are approximately 3 hours. As noted earlier, 2 to 3 hours are typically required to reach freezing conditions in the field. Although the test likely does freeze the sample in less time than that typical of field conditions, it is slower than the standard test procedure and likely better represents field conditions. Figures 196 and 197 show typical damage triggered by this test, with the manifestation of damage mimicking typical freeze-thaw distress observed in field situations.

Figure 196. Photo. Typical cracking and spalling from freeze-thaw damage from test 1.

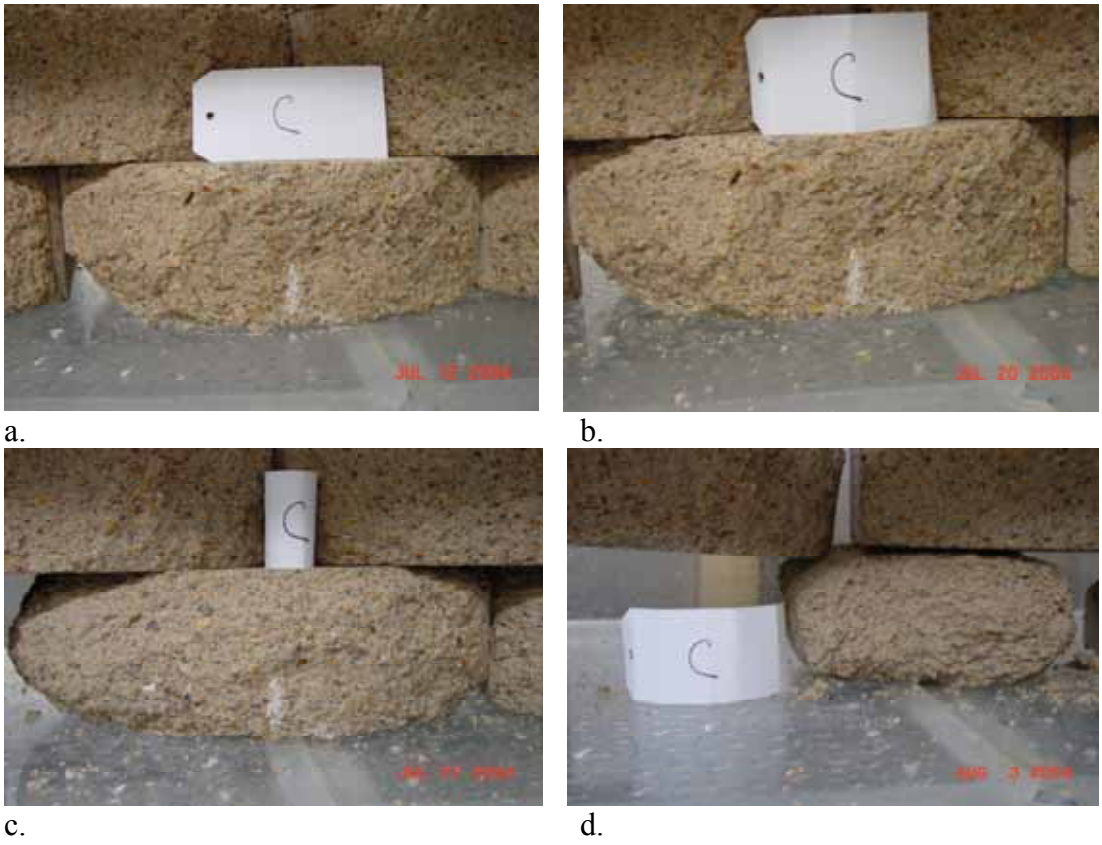

a. b. c. d.

Figure 197. Photos. Freeze-thaw deterioration over 40 cycles from Test 4: a. after 10 cycles, b. after 20 cycles, c. after 30 cycles, and d. after 40 cycles.

Test 4, which included a ramp rate of 0.55 °C/min (1 °F/min), a 2-hour temperature hold time, and exposure to 3 percent NaCl yielded the most deterioration and also provided representative deterioration failures found in the field. The other test conditions produced some freeze-thaw deterioration of the SRW blocks, but these deterioration rates were slower and would likely add a significant time to the tests. Based on the findings from Phase I, these test conditions (Phase I, Test 4) were selected for Phase II testing described next.

4.8.2 Phase II Investigation

After the Phase I testing was complete and the parameters for testing SRW blocks were identified, several larger SRW blocks were procured for testing. These larger SRW blocks consisted of blocks from three manufacturers and included SHA-approved (based on ASTM C 1262 (2003) testing in water and/or saline) and non-SHA-approved SRW blocks. The test parameters included the parameters identified in the Phase I work.

The samples tested in the Phase II program were procured from three different manufacturers identified herein as manufacturers A, B, and C. The number of blocks received from the manufacturers limited the amount of testing. However, it was anticipated that a good indication of the applicability of this test method could be determined from testing the blocks provided. Unlike the smaller SRW blocks tested in Phase I, this testing included the evaluation of SRW caps. Manufacturers provided only a limited number of these caps and as such, testing was

limited. The experiment plan for the Phase II testing is shown in table 19. These blocks are shown in figures 198 through 200.

Table 19. Experimental plan showing number of blocks tested in Phase II.

SRW Block Manufacturer	SRW Block Certification	Solution Type	
		Water	3 Percent NaCl
Block A	SHA-approved	6 Blocks	6 Blocks
	Non-SHA-approved	0 Blocks	6 Blocks
Block B	SHA-Approved	0 Blocks	3 Blocks
	Non-SHA-approved	0 Blocks	3 Blocks
Block C	SHA-approved	3 Blocks	3 Blocks
	Non-SHA-approved	3 Blocks	3 Blocks

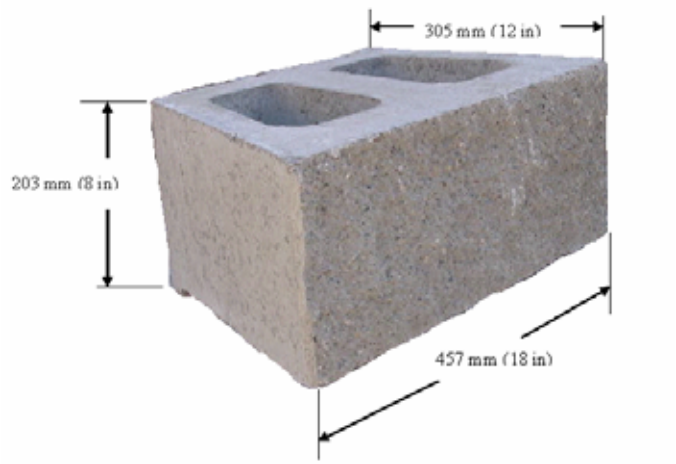

Figure 198. Photo. SRW block from manufacturer A.

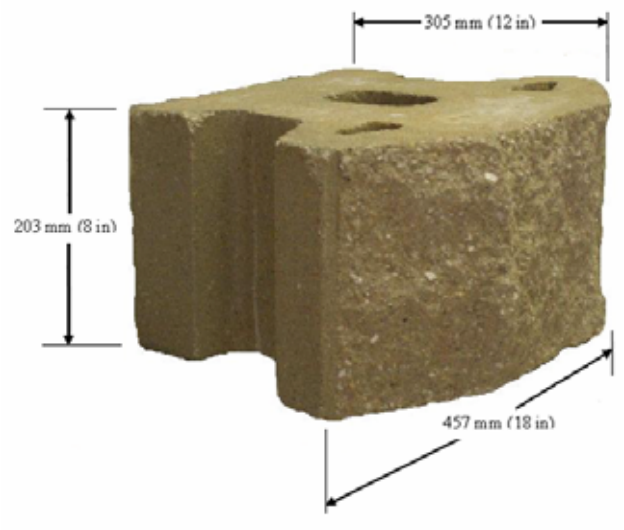

Figure 199. Photo. SRW block from manufacturer B.

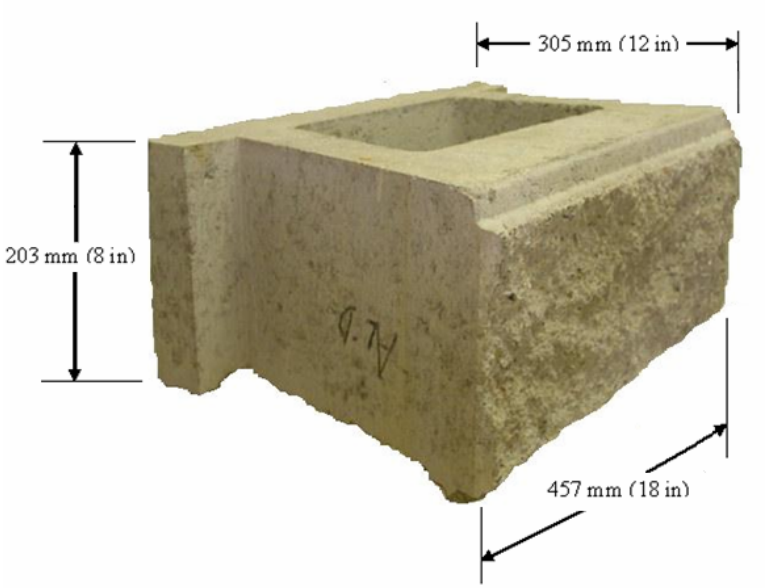

Figure 200. Photo. SRW block from manufacturer C.

Because the presence of deicing salts in field-damaged SRW blocks appears to be the most critical parameter when considering field exposure conditions and because block characteristics affect the ingress of salt, chloride profiles were determine for several blocks in this Phase II study. Samples for determining diffusion coefficients were cored from three sides of the blocks, exposed to a chloride solution, and then evaluated following the method developed by the Strategic Highway Research Program (1992).

Unlike Phase I, where a large number of samples could be placed in the test chamber, the larger SRW blocks used in Phase II limited the amount of blocks that could be tested at one time. Figure 201 shows a typical block stacking for the Phase II testing.

Figure 201. Photo. Typical stacking for larger SRW blocks tested in Phase II.

As with the smaller blocks, the larger blocks were saturated, surface dried, and weighed prior to and during testing. Blocks were re-placed in their designated test locations after each weight loss measurement. Blocks on the bottom row were identified as 1 through 3 (left to right) and 4 through 6 on the upper row (left to right). Only, 2 non-SHA-approved cap blocks were available from manufacturer A for testing. To protect the block interiors from direct solution spray when caps were not available, an acrylic sheet was placed on the top of the blocks.

The larger SRW blocks were also equipped with thermocouples to monitor the temperature at the center of the block. One thermocouple was placed at the center of the SRW block, and another was used to monitor the environmental room temperature. The thermocouple was placed in the block by first drilling a 6.35-mm-(0.25-inch-) diameter hole approximately 102 mm (4.0 inches) to the center of the block at the specified location. The thermocouple was placed in the hole and backfilled with a mortar mixture paste made from the SRW bock drill dust, cement, and water. Temperatures were recorded at 10-minute intervals during the test. As the freeze-thaw experiments were conducted, the temperature was monitored in order to make necessary changes such that freezing and thawing conditions could occur at the center of the SRW blocks. A typical graph of temperature readings from 20, 12-hour-long, freeze-thaw cycles are shown in figure 202.

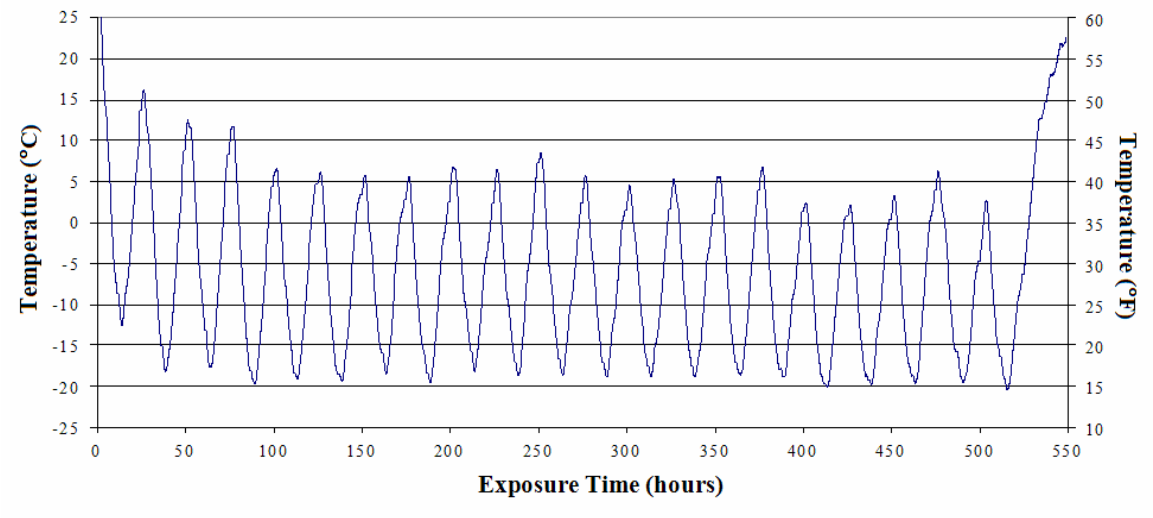

Figure 202. Graph. Typical block temperature data from Phase II investigation.

The larger SRW blocks exposed to the freeze-thaw testing regime were assessed visually and used weight loss. Because of the longer times between assessing the weight loss, an additional visual inspection was performed. After every 10th freeze-thaw cycle the larger SRW blocks were visually inspected for damage resulting from the freeze-thaw cycles. When damage was observed, photographs were obtained. The damaged areas were then monitored for progression of the degradation. The results of the chronological degradation of the SRW blocks was then compiled and compared with the distress identification rating (DIR) developed by Embacher et al. (2001). The basic qualitative damage ranking established by Embacher et al. is as follows:

Severity Levels

Low: Deterioration is localized and minor, exhibiting some local discoloration but no significant loss of material.

Medium: Deterioration is present in most areas that might be saturated during freezing and thawing. Discoloration is easily observed and affected areas are exhibiting tight cracks.

High: Deterioration is extreme and affected areas are exhibiting open cracks.

Each of the larger SRW block sets was assigned a ranking based on this criteria. The SHA-approved larger blocks from manufacturer A that were blocks exposed to water exhibited a DIR rating of low for most of the blocks. However, a few blocks were near the medium deterioration ranking. A typical block from this set is shown in figure 203. SHA-approved SRW blocks from manufacturer A that were exposed to the 3 percent NaCl solution exhibited very little visible freeze-thaw degradation. These blocks had some localized discoloration and minor deterioration that accumulated at the bottom of the test chamber. As such, the DIR rating assigned to this group of larger blocks was low. Figure 204 shows the typical condition of this group of blocks after the freeze-thaw testing. The non-SHA-approved blocks exposed to water (figure 205) or NaCl solution (figure 206) were also visually assessed, but damage was generally quite minimal with the exception of the non-SHA-approved cap block shown in figure 205, which was given a DIR rating of high.

Figure 203. Photo. SHA-approved block from manufacturer A (water exposure).

Figure 204. Photo. SHA-approved block from manufacturer A (3 percent NaCl solution exposure).

Figure 205. Photo. Non-SHA-approved cap from manufacturer A (water exposure).

Figure 206. Photo. Surface of non-SHA-approved block from manufacturer A (3 percent NaCl solution).

In general, the larger SRW blocks from manufacturer A exhibited low DIR ratings. For these blocks, the performance difference between the SHA-approved and non-SHA-approved blocks could not be distinguished. The test did indicate that some caps did exhibit damage when subjected to the test procedure. Differences in performance between the water and NaCl exposure conditions were insignificant.

Figures 207 and 208 shows the weight changes for the SHA-approved blocks from manufacturer A exposed to the NaCl and water solutions. Figure 209 shows the results from the non-SHA-approved blocks exposed to the NaCl solution. All sets exhibited weight gains and losses throughout the testing period. It is believed that the weight gains were a result of increased microcracking of the blocks and/or a continuous increase in the degree of saturation of the blocks. When the blocks were saturated after 20 cycles it is believed that the microcracks (or cracks) were filled with water, increasing the weight of the surface dried, saturated block. However, it is interesting to note that only one block from the SHA-approved SRW blocks from manufacturer A exceeded 5 percent weight loss, indicating that the weight change testing provides similar results as the DIR rating system presented earlier. From figures 207 and 208 it can be seen that the weight loss of several blocks either exceeded or were very close to 5 percent. However, a clear distinction between the SHA-approved and non-SHA-approved blocks cannot be determined from this testing.

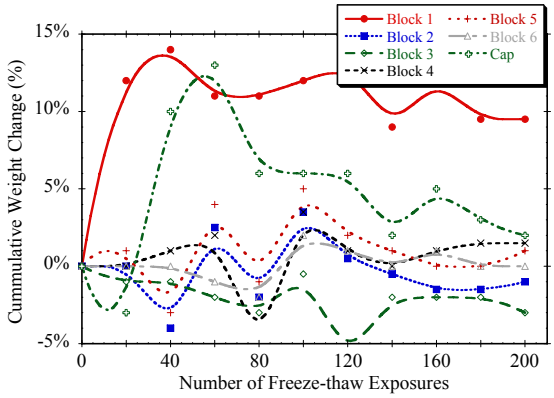

Positive values indicate weight loss

Figure 207. Graph. Percent weight change as a function of freeze-thaw exposure cycles for SHA-approved SRW blocks exposed to NaCl solution—from manufacturer A.

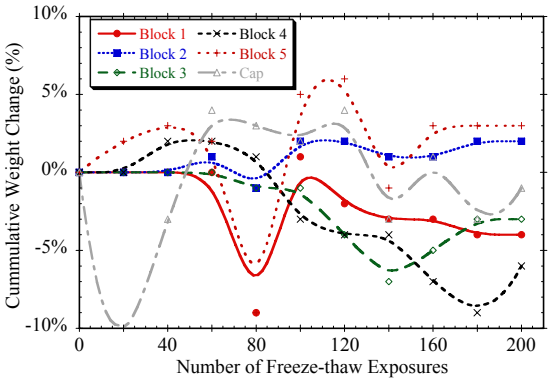

Figure 208. Graph. Percent weight change as a function of freeze-thaw exposure cycles for SHA-approved SRW blocks exposed to water—from manufacturer A.

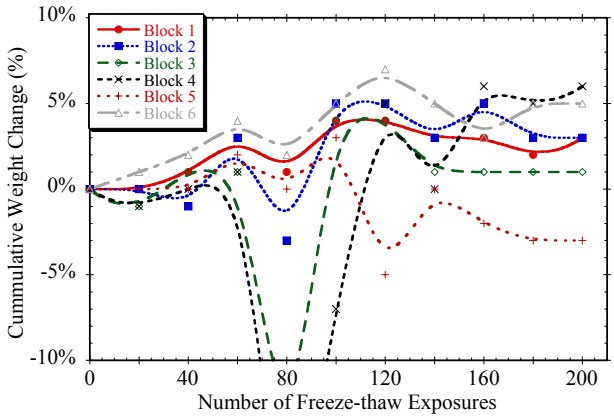

Figure 209. Graph. Percent weight change versus freeze-thaw exposures for non-SHA-approved SRW blocks from manufacturer A exposed to NaCl solution (positive values indicate weight loss).

Three SHA-approved and three non-SHA-approved blocks from manufacturer B were also visually assessed for freeze-thaw performance. Because only a limited number of blocks were available for testing, these blocks were subjected to salt solution only. Figure 210 shows the typical SHA-approved block after exposure to 200 freeze-thaw cycles. The blocks from manufacturer B exposed to the NaCl solution exhibited a DIR rating of low to medium. The medium ranking was assessed because some blocks exhibited tight cracks after the freeze-thaw exposure. The non-SHA-approved blocks from manufacturer B exhibited very similar performance as the SHA-approved blocks.

Figure 210. Photo. SHA-approved block from manufacturer B (NaCl Solution).

Figures 211 and 212 show the weight change of the SHA-approved and non-SHA-approved SRW blocks from manufacturer B. Only one block, a non-SHA-approved block, exhibited weight losses of greater than 5 percent. The difference in performance between the SHA-approved versus non-SHA-approved blocks was minimal, and if a difference does exist, this testing could not distinguish this difference.

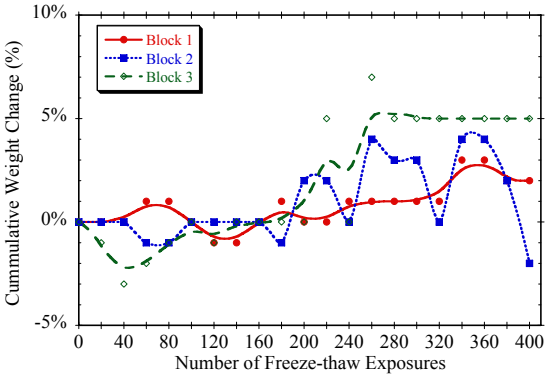

Positive values indicate weight loss.

Figure 211. Graph. Percent weight change for manufacturer B SRW blocks exposed to NaCl solution resulting from freeze-thaw cycling for SHA-approved blocks.

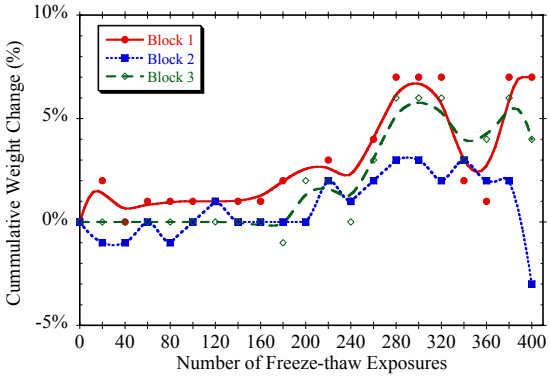

Figure 212. Graph. Percent weight change for manufacturer B SRW blocks exposed to NaCl solution resulting from freeze-thaw cycling for non-SHA-approved blocks.

The SRW blocks from manufacturer C also fared quite well, in both water and NaCl solution. Figures 213 and 214 show typical SHA-approved blocks from this set, exposed to water and NaCl solution. Some blocks exhibited corner cracking, but these cracks were generally present before the freeze-thaw testing began (the damage likely occurred during transportation). Only minor discoloration was observed on this set of blocks. The non-SHA-approved blocks exhibited similar results from the visual assessment and all larger SRW blocks from manufacturer C exhibited a DIR ranking of low.

Figure 213. Photo. SHA-approved C block exposed to fresh water.

Figure 214. Photo. SHA-approved C block exposed to 3 percent NaCl solution.

Figures 215 and 216 show the weight change of the blocks as a function of the number of freeze-thaw cycles for the larger SRW blocks from manufacturer C exposed to the NaCl spray. With the exception of one block from each of the SHA and non-SHA-approved blocks, the blocks exhibited some early weight loss. This was likely due to material loss from the surface. However, after about 200 cycles most of the blocks exhibited significant weight gains. This could indicate that the blocks began cracking and absorbing more solution; however, the cracking was not significant to result in spalling of the block material.

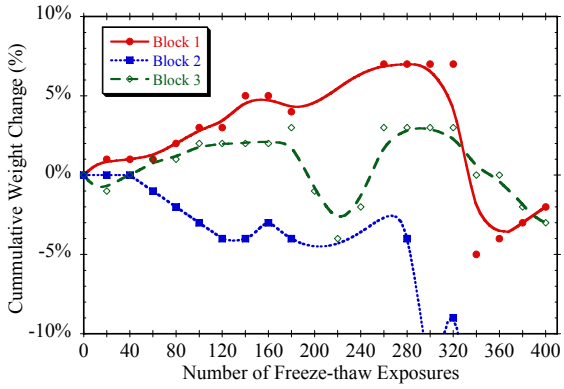

Positive values indicate weight loss

Figure 215. Graph. Percent weight change resulting from freeze-thaw cycling of SRW blocks exposed to NaCl solution for SHA-approved blocks—from manufacturer C.

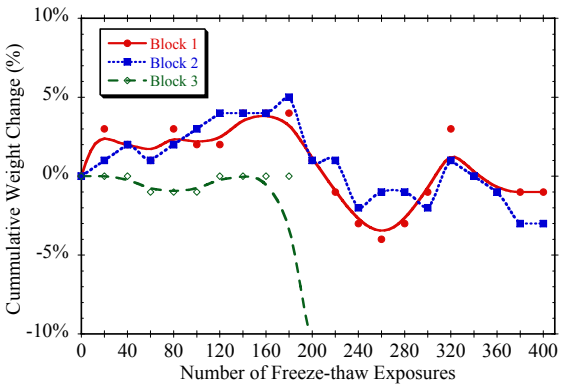

Figure 216. Graph. Percent weight change resulting from freeze-thaw cycling of SRW blocks exposed to NaCl solution for non-SHA-approved blocks—from manufacturer C.

Figures 217 and 218 show the freeze-thaw performance versus exposure cycles for SRW blocks from manufacturer C exposed to water spray. Prior to approximately 160 cycles, the majority of the blocks exhibited a relatively steady increase in weight loss. After approximately 160 cycles several of the blocks exhibited weight gain. This is similar to what was observed for the samples exposed to the NaCl solution. Comparisons between the performance of blocks exposed to NaCl solution and water is inconclusive as the scatter of the results are significant.

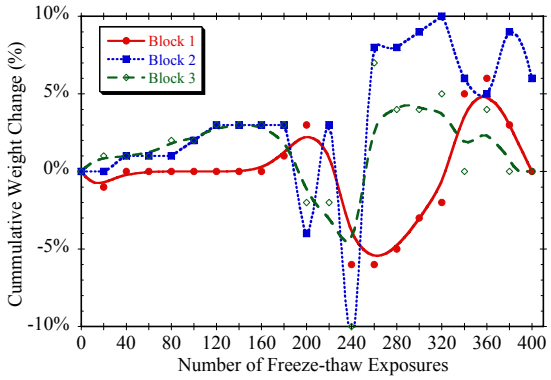

Positive values indicate weight loss

Figure 217.Graph. Percent weight change resulting from freeze-thaw cycling of SRW blocks from manufacturer C. Blocks exposed to water for SHA-approved blocks.

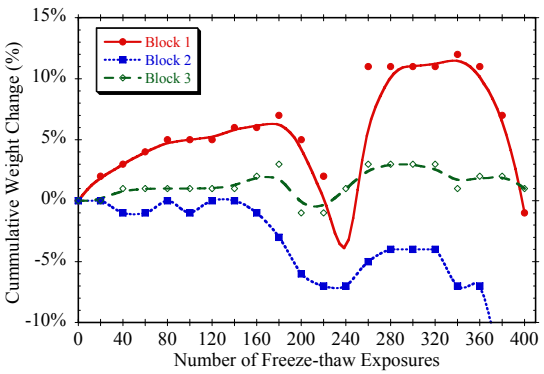

Figure 218. Graph. Percent weight change resulting from freeze-thaw cycling of SRW blocks from manufacturer C. Blocks exposed to water for non-SHA-approved blocks.

The chloride diffusion coefficients for the larger SRW block samples tested in Phase II are shown in table 20. The chloride diffusion coefficients of the non-SHA-approved blocks were higher than those of the SHA-approved SRW blocks. The mean chloride diffusion coefficients determined for the larger SRW blocks exhibit diffusion coefficients similar to that of concrete with high water-cement ratios (typically greater than 0.7).

Table 20. Chloride diffusion coefficients for larger SRW block samples.

SRW Block Designation	Sample	Exposure Time	
		3-Week Exposure	6-Week Exposure
		Diffusion Coefficients (m^2/s)	
Non-SHA-approved	1	3.05E-11	*NT*
	2	*NT*	6.88E-11
	3	9.50E-11	*NT*
	4	*NT*	2.06E-11
Mean		*6.28E-11*	*4.47E-11*
Std. Dev.		*4.56E-11*	*3.41E-11*
SHA-approved	1	*NT*	2.15E-11
	2	3.48E-11	*NT*
	3	*NT*	2.47E-11
	4	2.56E-11	*NT*
Mean		*3.02E-11*	*2.31E-11*
Std. Dev.		*6.51E-12*	*2.26E-12*

4.8.3 Summary

The intent of this work presented in this section was to attempt to develop a test procedure that could better mimic the freeze-thaw performance of SRW blocks under field conditions while at the same time maintaining reasonable test duration. A test procedure was developed, modified, and evaluated using several different block types and exposure conditions. A summary of the findings of this research is presented below.

In general, this test provided a useful assessment of the freeze-thaw performance of small SRW blocks (Phase I) exposed to both water and NaCl solutions. The deterioration of smaller SRW blocks tested in the laboratory under the conditions defined is similar to deterioration of SRW blocks exposed to freeze-thaw conditions in the field. It should be noted, however, that the blocks used in Phase I were not of the same quality as those typically used in highway applications, and the blocks were not necessarily produced with frost resistance as a priority.

Whereas the SRW blocks tested in Phase I showed significant damage in a reasonable number of freeze-thaw cycles, the blocks tested in Phase II (using the most severe conditions from Phase I) performed much better, showing relatively little distress. It is certainly possible that these units eventually would have shown significant distress, but increasing the duration of the test was not feasible within the constraints of this project, nor would it have been feasible if this test were considered as a standard test. The higher quality of all the blocks used in Phase II, compared to Phase I, was evident in the improved durability, even when exposed to NaCl solution. Some of the cap units did show some distress in Phase II, but damage was not severe.

The assessment of saturated block weight as a damage index may not be a good measure for assessing the freeze-thaw performance of larger SRW blocks. As the blocks undergo freeze-thaw cycles, microcracking and cracking of the material likely occurs. When the SRW blocks are saturated after being subjected to freeze-thaw cycles, the blocks absorb water in these microcracks and cracks, offsetting the reduction in weight from the material loss resulting from the freeze-thaw test. Thus, two mechanisms that are changing the weight of the sample are likely taking place: scaling is likely reducing the weight of the blocks and higher solution absorption is likely increasing the weight of the blocks. The overall weight change represents the sum of these weight changes.

The diffusion coefficient of the larger SRW blocks (SHA- and non-SHA-approved) was found to be similar to that of high water-cement ratio concrete. This indicates that chloride ions can be transported at a relatively high rate into the blocks. This is also consistent with chloride profiling from actual SRW blocks from the field as previously described in chapter 3.

Although this newly developed testing method was not able to significantly damage typical SRW blocks used in highway applications, it does show promise as a conceptual approach. It allows for the testing of full SRW units (or several units stacked as a wall) under more realistic field conditions. However, the test did not appear to be severe enough to trigger damage in a reasonable period of time. It is recommended that future research be conducted using a similar method, with modifications to the exposure cycles to increase the potential for damage. This could involve the use of more rapid freezing rates or longer hold times. This approach, if successfully modified, could also be used as an ideal method for assessing mitigation techniques

for in-service SRWs. For example, the benefits of applying silanes or other surface coatings could be assessed under more realistic field conditions. This is especially important given the possibility that nondurable SRW blocks already in service could benefit from any treatment that would extend their service lives.

4.9 OTHER RESEARCH

There was a significant amount of research conducted under this FHWA project that, for conciseness, was not included in this final project report. In particular, the research described in Hance (2005) on the effects of compaction voids on frost resistance for laboratory-prepared SRW mixtures was quite extensive, and readers are directed towards this Master of Science thesis for complete details. Some of the key findings of this compaction void study are highlighted in chapter 5 and tied to other findings from this project.

4.10 SUMMARY

This chapter summarized the key findings from a comprehensive laboratory program focused on SRW block durability. Significant progress was made in several key areas, including gaining a better understanding of the variability of SRW units and spatial variations of key properties, the mechanisms of frost damage and salt distress, the underlying reasons for high variability in ASTM C 1262 (2003) test results, the impact of SRW material properties and microstructure on durability. A more detailed summary of the key findings from this laboratory program is presented in chapter 5, and recommendations and guidelines based on these findings are presented.

CHAPTER 5: CONCLUSIONS AND RECOMMENDATIONS FOR FUTURE WORK

5.1 INTRODUCTION

This chapter presents overall conclusions from this FHWA-funded research project. It also draws, in a much more limited fashion, from some of the key findings from parallel research conducted on a NCMA-funded project. The key findings are presented and grouped in the following categories:

- Field Performance and Durability of SRW Blocks.
- SRW Material Characterization and Sampling.
- Frost Durability of SRW Units.
- General Freeze-Thaw Testing and Processes.
- ASTM C 1262 (2003) Test Method.

After presenting the main conclusions under each of the above categories, recommendations are presented for future research on the topic of frost resistance of SRW blocks. Lastly, to assist in the implementation of the key project findings into practice, a newly annotated version of the ASTM C 1262 (2003) test method is included (as appendix A), which captures the findings from this research work into recommended amendments to the standard.

5.2 CONCLUSIONS—FIELD PERFORMANCE AND DURABILITY OF SRW BLOCKS

The following conclusions can be drawn from the field evaluations of SRW blocks with regard to resistance to freeze-thaw cycles and deicing salts:

- Based on general evaluations of SRWs in various cold-weather regions in the United States and based on detailed evaluations of SRWs in Minnesota and Wisconsin, most SRWs have performed well, with little signs of frost damage or salt distress.

- However, there are some cases where durability-related problems with SRWs are quite severe. These field evaluations clearly show that exposure to both moisture (e.g., rain or snow) and salts is a prerequisite to damage, strongly suggesting that any attempt to assess durability in the laboratory should include saline solutions as part of the testing regime.

5.3 CONCLUSIONS—SRW MATERIAL CHARACTERIZATION AND SAMPLING

The following conclusions can be offered with respect to material properties of SRW mixes evaluated:

- Material properties follow systematic spatial variations over an SRW unit. The existence of these spatial variations was evident for different grades of SRW units manufactured at different block plants. While standard properties such as compressive strength, absorption and density measured for these units complied with ASTM C 1372 (2003) standard specifications for SRW units, the choice of sampling location within a unit can lead to

misinterpretations on material uniformity (or variability). This type of spatial variability of properties in an SRW unit comprises within-unit variability, and chapter 3 discussed in detail the implications of this form of variability, and recommendations were provided on how to sample specimens from a unit. Between-unit variation should be a topic for future research, and this will be discussed in more detail in the Recommendations section.

- A stratified random sampling approach for extracting specimens from SRW units yields lower variability than simple random sampling approach. In stratified random sampling, specimen sampling is carried out in a more systematic manner reflecting the expected distribution of properties over an SRW unit. For the units investigated in this study, variations in properties were observed along the casting direction of the units. The simplest form of stratified random sampling for a three-specimen test set thus consists of sampling a specimen from each of the three layers along the height of the unit and averaging the test results. Other size test sets consisting of two or five specimens can also be selected under stratified random sampling, but the computation of average value of the measured property for the test set needs to be adjusted accordingly (Chan et al., 2005b).

- Split face delaminations are not likely related to durability of SRW units but can affect assessment of SRW units.

- SRW unit paste content (volume fraction) and compaction void content (volume fraction) are inversely related to one another. For all SRW mixes investigated in this research, their paste and compaction void contents as determined based on ASTM C 457 (2004) microscopy methods exhibited an inverse relationship. Mixes with higher paste content displayed lower compaction void contents and vice versa, as shown in figure 219. In almost all these mixes, total aggregate content was less than 70 percent. It is interesting to tie this observation with reported literature on dry-mixed concrete performance and durability (chapter 2). While on the one hand, there are conflicting reports on the role of compaction voids on freeze-thaw durability of dry concretes, there is consistency and agreement on the necessity of minimum paste contents to achieve frost durable mixes. As will be shown below, above minimum paste content, frost-durable mixes can be achieved despite the presence of compaction voids.

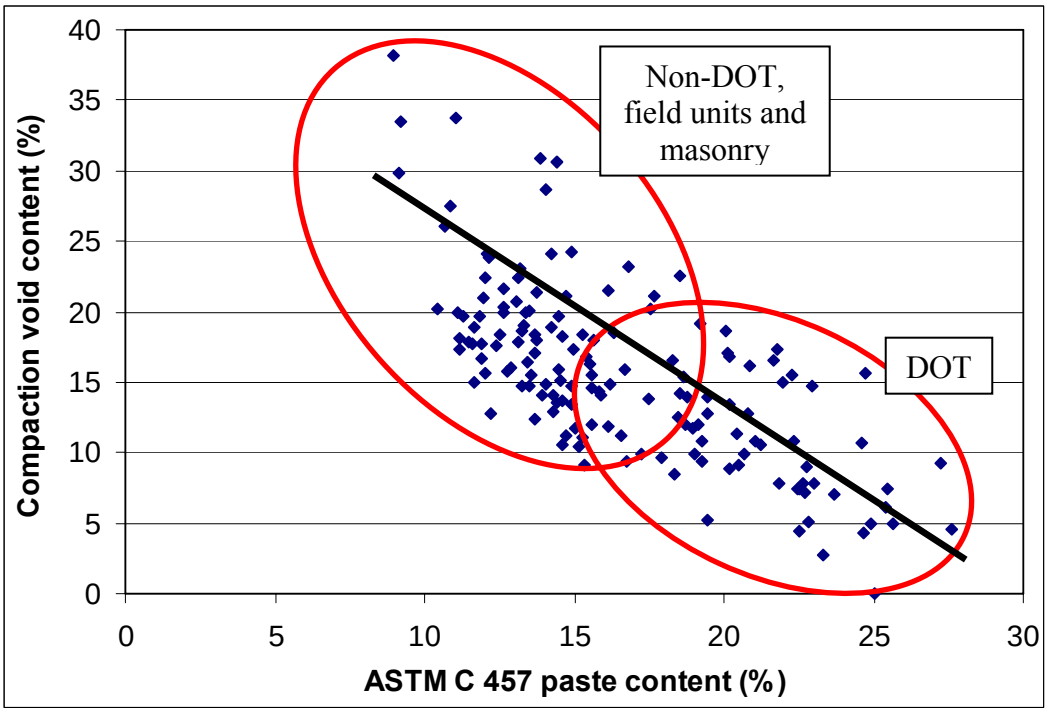

Figure 219. Graph. Compaction void content versus paste content for all SRW mixes evaluated.

5.4 CONCLUSIONS—FROST DURABILITY OF SRW UNITS

The conclusions in this section pertain specifically to the durability of SRW units, as determined from test results and observations gathered in the course of the FHWA project.

- **Saline conditions exacerbate freeze-thaw damage.** ASTM C 1262 (2003) tests conducted on SRW units in both water and 3 percent NaCl solution conclusively prove the increased damage induced by the presence of salts in solution. The only exception to this trend was a particular SRW mix whose performance was best among all mixes evaluated (mass loss less < 0.2 percent after 100 cycles in water and < 0.3 percent after 100 cycles in saline). Aside from this particular mix, saline accelerated damage by reducing the number of cycles to reach a certain mass loss (e.g., 1 percent) by up to eight times compared to water. This is shown by an example in figures 220, 221, and 222 where it is seen that wall units in water required about 90 cycles to reach 0.5 percent mass loss compared to about 13 cycles in saline solution, while cap units in water required about 20 to 40 cycles to reach 1 percent mass loss compared to less than 10 cycles in saline solution. Moreover, while damage in water consisted primarily of surface scaling, damage in saline solution comprises internal cracking and complete degradation of the specimens (figures 221 and 222). In a separate study evaluating the relative frost damage caused by different types of deicing salts (Chan et al., 2006b), it was concluded that the number of cycles required to reach 1 percent mass loss decreased with increasing freeze point depression of the solution. As expected then, specimens tested in plain water

(zero freeze-point depression) exhibited the least damage and those tested in 3 percent NaCl solution which had the highest freeze point depression (1.8 °C (3.2 °F)) of all salts investigated exhibited fastest damage. This research did not have the opportunity to explore in detail mechanisms causative of accelerated damage under saline conditions. Chapters 2 and 4 discuss possible mechanisms including osmotic pressures due to concentration changes as well as "brine entrapment." These suspected mechanisms are based on studies performed at Cornell on ice formation quantities and rates and changes in concentration of salt in solution together with data from the literature.

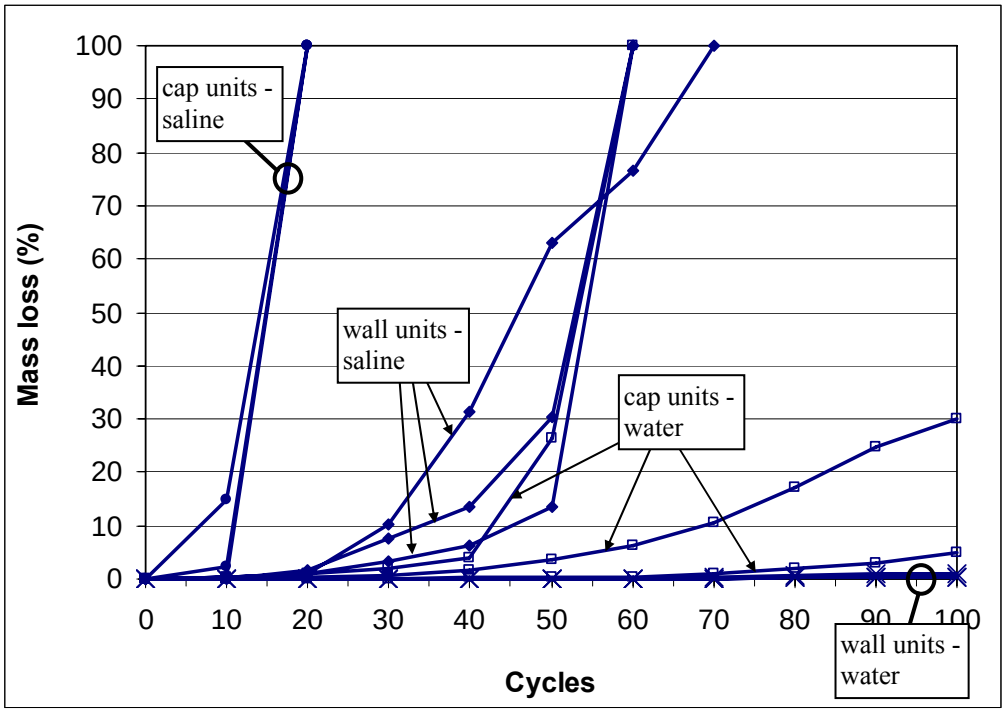

Figure 220. Graph. Mass loss versus cycles.

Figure 221. Photo. Comparison of water versus saline tests on wall unit after 100 cycles in water. Specimens were from a single manufacturer.

Figure 222. Photo. Comparison of water versus saline test on wall unit after 60 cycles in saline. Specimens were from a single manufacturer.

- **Paste volume fraction (paste content) in the mix is critical for frost durability.** While this conclusion has been reached by several other researchers (see chapter 2), independent studies carried out under the FHWA project also point toward this same result. Using laboratory-made mixes, Hance (2005) deduced that critical paste content existed in the range of 16 to 18 percent. As pointed out in chapter 4, ASTM C 1262 (2003) freeze-thaw mass loss follows a 2nd order behavior of the following form:

$$\text{Mass loss, percent} = a \times \text{cycles}^2 \qquad \text{Equation 14}$$

where a = mass loss prediction constant which depends on material and test conditions (specimen size, container size, and freezer)

For the mixes tested by Hance (2005), the dependence of "a" on paste content is shown in figure 223. The increased sensitivity of "a" to paste content at paste contents below about 16 percent is evident from this figure.

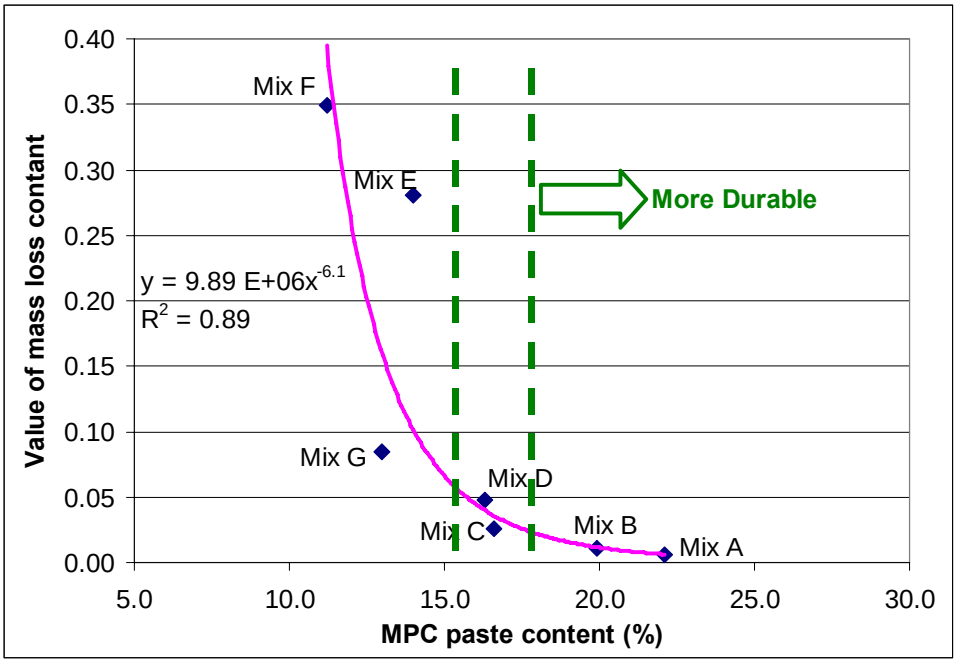

(MPC = modified point count)

Figure 223. Graph. Dependence of mass loss prediction constant "a" on paste content (Hance, 2005).

Using data from freeze-thaw tests and material property measurements on SRW units from various manufacturers, Chan et al. (2005d) determined that paste content (of all material characteristics evaluated) correlated best to freeze-thaw durability. Paste content of at least 19 percent characterized mixtures whose mass loss did not exceed about 1.5 percent after 100 cycles in water. The concept of critical paste content can be further discerned from figure 219 which shows the region of DOT units (i.e., units compliant with DOT freeze-thaw specifications) as well as the region of non-DOT units (i.e., units that do not necessarily meet DOT specifications). An overlap between these two zones at paste contents of about 16 to 18 percent is shown. Thus, mixes with excellent freeze-thaw durability (DOT mixes in this case) required at least this amount of paste (16 to 18 percent). The graph in figure 219 also indicates that the presence of 10 to 15 percent compaction voids is not entirely detrimental to the frost durability of SRW mixes.

- One aim of the FHWA study was to evaluate a number of material characteristics for their potential as frost durability indices. This was accomplished by assessing the correlation between various material characteristics and freeze-thaw mass loss. Of all parameters considered, paste content, total air and compaction void content and paste-to-total air and compaction void ratio were found to correlate best to frost resistance. Threshold values were identified as values of the material characteristics above or below which the probability of mass loss exceeding about 1.3 percent after 100 cycles in water increased. An example is shown in figure 224 for paste-to-total air and compaction void ratio. For the parameters listed above, threshold values for the mixes investigated in this study were as follows: paste content (19 percent minimum), total air and compaction void content (12 percent maximum) and paste-to-total air and compaction void ratio (1.5

minimum). One other significant outcome of this study was the fact that ASTM C 457 (2004) spacing factor, used to assess frost durability of ordinary concretes, is not equally applicable to SRW mixes. This is because spacing factors were developed assuming a uniform spatial distribution of spherical air bubbles in concrete. This type of internal structure and air void distribution are not applicable to SRW mixes. Similarly, it was determined that saturation coefficient, as used to assess frost durability of clay bricks, also is not applicable to SRW mixes.

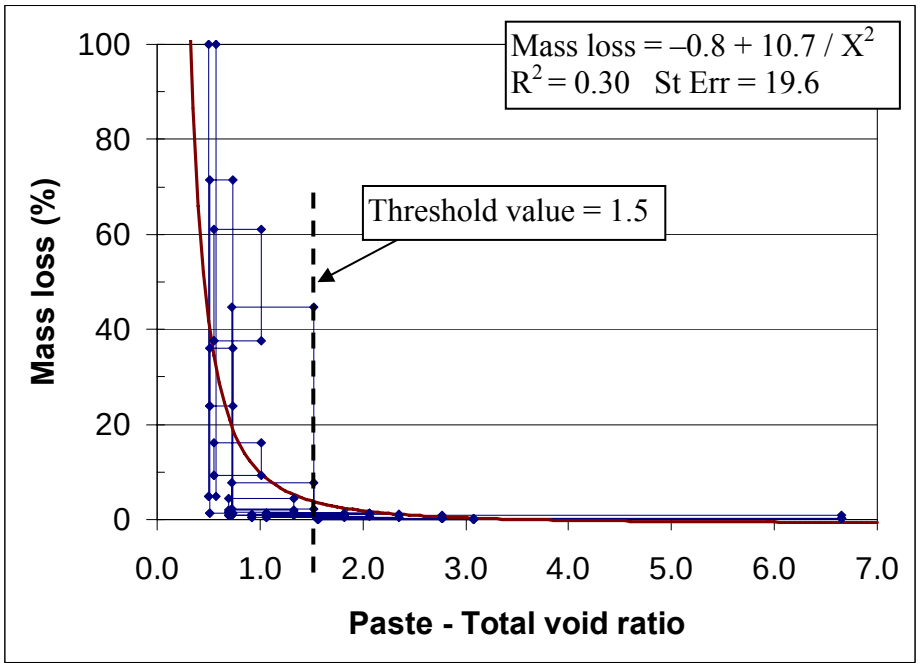

Figure 224. Graph. Relationship between mass loss after 100 cycles in water and paste-to-total air and compaction void ratio.

In a separate study by SEM (2004), a neural network based analysis was conducted to determine parameters most influential to freeze-thaw durability. For tests in water, it was determined that density, water absorption, percent non-connected voids, and whether air-entraining or freeze-thaw enhancing admixtures were added to the mix were most influential to freeze-thaw durability. For tests in saline, compressive strength, percent nonconnected voids, use of high water content, and whether air-entraining or freeze-thaw enhancing admixtures were added to the mix were found to be most influential. The importance of high water content (which accordingly yields greater paste volume) agreed with the findings from this project. Both the SEM study and this FHWA-funded project also concluded that relationships between freeze-thaw durability and material properties are difficult to determine due to variability in test results.

- On the issue of ASTM C 457 (2004) air void parameters, as already mentioned above, studies at Cornell University determined that spacing factor cannot be applied to SRW mixes in the same way that they apply to ordinary concretes. Scanning electron microscope tests conducted on the two best performing DOT mixes revealed the presence

of small spherical air voids (about 10 μm (0.0004 inch) in size) in both mixes. In ordinary concretes, finer air voids are related to greater air void specific surface areas and lower spacing factors which improve the frost durability of the concrete (Pigeon and Pleau, 1995). The role of the observed small air voids in SRW units on frost durability of these units is not certain at this time and needs to be further researched.

- At 3 percent salt concentration, NaCl is the most detrimental of all deicing salts evaluated, while the specific fertilizer evaluated was capable of inducing a similar level of frost damage to SRW specimens as other types of deicers. This conclusion relates to ASTM C 1262 (2003) tests involving 3 percent salt solutions made using different types of deicing chemicals, including a high-nitrogen fertilizer. At this 3 percent concentration, specimens tested in NaCl solution suffered the most damage out of all salts evaluated. Another significant conclusion from this study was the fact that specimens tested in a fertilizer solution displayed as much damage as those tested in solutions of $MaCl_2$, calcium chloride ($CaCl_2$) and CMA. This result has important implications for SRWs near fertilized areas. Moreover, it was concluded that the number of cycles required to reach 1 percent mass loss appeared to decrease with increasing freeze point depression of the solution. This result also has practical implications since deicing applications are typically keyed to freeze point depression of the salts used, with salts and concentrations selected for ambient temperatures. While $MaCl_2$ and CMA solutions were found to cause damage to SRW units under freeze-thaw conditions, samples continuously immersed in these solutions at 60 °C (140 °F) also exhibited damage after about 6 months immersion. Mass loss (mass of residues expressed as percentage of original sample mass) of specimens in these solutions was estimated to be about 5 to 7 percent after 20 months immersion in $MaCl_2$ solution and 10 to 15 percent after 20 months immersion in CMA solution. Samples immersed in other warm salt solutions did not exhibit damage after this same period of time.

5.5 CONCLUSIONS—GENERAL FREEZE-THAW TESTING AND PROCESSES

These conclusions pertain to general freeze-thaw testing of cementitious materials and are not limited to the ASTM C 1262 (2003) testing of SRW mixes only.

- Each freezer has a unique internal T-t characteristic (shape of T-t response) and level of variability, both of which vary with heat extraction capacity and operating efficiency of the freezer, and the number and mass of specimens inside the freezer.

- Variations in T-t characteristics and temperature variability inside each freezer mean that:
    - Specimens located in different parts of the freezer will receive different exposures.
    - A single point measure of temperature in the freezer not only is not representative of the overall conditions inside the freezer, but its use as the controlling temperature for cycle length can lead to a large proportion of internal freezer locations falling out of compliance with test method requirements.

  Chapter 4 demonstrated that in the case of the Tenney freezer, the location of the freezer internal sensor also coincided with the coldest measured location in the freezer. Taking the ASTM C 1262 (2003) test method for example, the minimum required length of cold soak is 4 hours. It was shown that if the freezer were programmed for a cold soak of 4 hours based on this internal sensor temperature, the result would be that all other locations in the freezer would fall short of the required cold soak time (undercooling). A review of other freeze-thaw test methods reveals similar provisions for cold soak requirement (i.e., cold soak duration based on specified freezer air or specimen temperatures) as shown in table 21.

  While ASTM C 666 (2004) attempts to maintain temperature uniformity throughout the freezing chamber by specifying that the temperature "at any point on the surface of any specimen container shall be within 3 °C (6 °F) at any given time," the other methods do not appear to address the issue of temperature variability inside the freezers. Thus, in the same manner as described in section 4.3.1 for ASTM C 1262 (2003), in these other freeze-thaw test methods, the actual location of the control temperature (whether specimen or freezer air) may experience differing frost exposures due to the spatial variability of freezer air temperature. How temperature variability in the other freezers affects compliance of specimens to their respective test method is an issue to be further explored and a topic for future research. This research, however, demonstrated the importance of surveying a freezing environment to gather information of the range of temperature distribution which can in turn be used to optimize the freezing cycle.

Table 21. Comparison of cold soak requirement in freeze-thaw test methods

Test Method	Specified Temperature °C (°F) (Record Location)	Required Cooling Condition
ASTM C 666 [a] Rapid freeze-thaw testing of concretes	–18 ± 2 (0 ± 3) (specimen temp.)	Specimen temperature to be lowered to specified range within 1½ to 3¾ hours
ASTM C 672 [b] Deicing salt surface scaling test	–18 ± 3 (0 ± 5) (specimen temp.)	Specimen temperature to be lowered to specified range within 16 to 18 hours
ASTM C 67 [c] Freeze-thaw testing of clay tiles	< –9 (< 16) (freezer air temp.)	Specimens to be placed in freezing chamber for 19 to 21 hours. Air temperature in chamber must stay below the specified value after 1st hour.
CSA A231.1 [d] Surface scaling of precast concrete paving slabs	–15 ± 3 (5 ± 5) for last 2 hours of freezing (specimen temp.)	Specimens to be placed in freezing chamber for 15 to 17 hours. Specimen temperature must be within specified range in last 2 hours of freezing
ASTM C 1262 (2003) Freeze-thaw testing of SRW units	–18 ± 5 (0 ± 10) (freezer air temp.)	Freezer air temperature to be maintained within specified range for 4 to 5 hours.

[a] ASTM C 666 (2004), [b] ASTM C 672 (2004), [c] ASTM C 67 (2003), [d] CSA A231.1 (1999)

- Freezer reliability curves (R-curves) are a convenient representation of the conditions prevalent in a freezer under a particular set of factors, including type of freezer, cooling capacity, and number of specimens, and are a useful tool for the planning of test cycles. Detailed discussions on R-curves and an example of its application in the NCMA study can be found in chapter 6 of Chan's dissertation (2006). This R-curve approach is described as an annex to the modified version of ASTM C 1262 (2003) (appendix A).

- Water and 3 percent NaCl solution undergo a series of physical and chemical changes during freezing as the freezing plateau is traversed (FHWA report and section 5.1). Experimental work confirmed that it is also during the freezing plateau that expansion takes place in either liquid. By the end of this freezing plateau, 90 percent of plain water has crystallized, and 75–80 percent of a 3 percent NaCl solution has crystallized.

- Using calorimetric methods, the rate of ice formation in 3 percent NaCl solution was measured to be 7/8th as fast as in plain water during the freezing plateau. The main difference from an ice-formation standpoint between saline and water is in the total amount of ice formed at the final test temperature, e.g., at –18 °C (0 °F). At this temperature, more than 95 percent of plain water has crystallized and about 85 percent of a 3 percent NaCl solution has crystallized.

- From vial freezing tests, it was confirmed that 3 percent NaCl solution, like plain water, causes expansion damage in vials completely filled with the liquid. This damage can occur violently as observed in direct observation of freezing vials filled with 3 percent NaCl solution, which exhibited an explosive rupture similar to that observed with plain water.

- Experiments measured and confirmed changes in salt concentration in the unfrozen solution during freezing of a 3 percent NaCl solution (process known in the literature as freeze concentration, (chapter 2). The rate of change of this concentration occurs most rapidly near the end of the freezing plateau (FHWA). At this point, the concentration of salt in the unfrozen portion is about 4 times the initial 3 percent concentration.

5.6 CONCLUSIONS—ASTM C 1262 (2003) TESTING AND SPECIMEN PERFORMANCE

The conclusions in this section relate directly to the ASTM C 1262 (2003) test method, based on results and observations obtained throughout this FHWA project, as well as the NCMA study. For conciseness, the NCMA study was only briefly highlighted in this report, but the key findings are included herein as the synergistic efforts of the FHWA and NCMA projects have combined to address issues that neither study could have done on its own. For conclusions based solely on the NCMA study, readers are directed to chapter 6 of Chan (2006) for background information and testing details.

- The ASTM C 1262 (2003) is a flexible freeze-thaw test method that can be readily employed by different testing laboratories.

- A result of this flexibility is variability in test results. This variability manifests itself in various forms whether within-replicate specimens in a test set, between-specimens tested in different freezers in the same laboratory or between-specimens tested in different laboratories. The practical significance of this variability rests in the following areas:
  - SRW mixes cannot be optimized if test results are not repeatable, demonstrated by the low correlation between freeze-thaw mass loss and various material characteristics.
  - Variability in test results may lead to conflicts during mix qualification for projects if disparities exist in test results obtained by a manufacturing plant and a project owner.

  At a given number of cycles (e.g., 100 cycles), variability is more pronounced in mixes of intermediate quality, as exemplified by the results in figure 220. Mixes of either excellent quality (mass loss of less 1 percent after 100 cycles) or poor quality (with rapid deterioration such as the cap units in saline in figure 220) display more repeatable mass loss results among replicate specimens.

- Different freezers containing varying quantities of specimens need to be programmed differently to obtain maximize compliance with ASTM C 1262 (2003) T-t requirements. The decision on cycle length is aided by R-curves, which can only be obtained through prior survey of the freezer (chapter 4).

- Analyses of hypothetical freezer T-t curves (section 4.4.2) demonstrated that a walk-in freezer could no longer achieve 100 percent compliance with ASTM C 1262 (2003) requirements if its average air temperature were warmer than about –14 °C (7 °F) or if the temperature standard deviation were greater than 3 percent of the average temperature.

- Variations in surrounding water volume and total quantity of specimens in the freezer have pronounced impact on specimen cooling curves.

- Despite variations in specimen quantity, volume of surrounding water, size of container or freezer type, the current 4- to 5-hour cold soak appears sufficient to ensure that the freezing plateaus of specimens are fully traversed.

- Similarities in specimen cooling curves between chest and walk-in freezer and single-location repeatability in chest freezer show promise that consistent specimen cooling curves are attainable.

- Interpretation of the term "frozen solid" as per ASTM C 1262 (2003), Clause 8.2.1 can cause confusion and unintended variations in the cycle length. It is recommended that this statement be removed from the test standard and that cold soak length is restricted to the current 4- to 5-hour period.

- Specimen and container size and shape dictate the maximum number of specimens that can be accommodated within a given freezer. The number of specimens in the freezer in turn influences the overall freezer-specimen system as follows:
  - As the quantity of specimens increases, the maximum attainable reliability (R) in the freezer decreases.
  - As the quantity of specimens increases, the cooling response (cooling curve) of specimens themselves is affected as displayed by slower initial cooling rates and longer freezing plateaus. The shape of the R-curves accordingly changed with varying specimen quantities. This effect was particularly pronounced in the walk-in freezer where increases in the number of specimens resulted in shrinking R-curves with correspondingly lower proportion of locations meeting the cold soak requirements. Thus, in any given freezer, increasing the number of specimens makes it more difficult to comply with ASTM C 1262 (2003). In addition to this, the cooling curve of instrumented specimens varied with varying specimen quantities in the walk-in freezer. The decreased compliance with ASTM C 1262 (2003) and the altered specimen cooling curves are thus related to total specimen quantity.
  - Compliance with ASTM C 1262 (2003) freezer air T-t requirements does not guarantee similar specimen cooling responses. As shown in chapter 4, the average freezer air temperature in the walk-in freezer loaded with 20, 40, 60, and 80 specimens complied with ASTM C 1262 (2003) requirements (although at a much longer cycle time for larger specimen quantities). However, different specimen cooling responses ensued from each of these thermal loads.

- Compliance with ASTM C 1262 (2003) freezer air T-t requirements does not guarantee similar specimen performance. For example, for the NCMA study, significant differences in performance were measured for specimens tested in two different freezers. Average mass loss in similar size and geometry specimens tested in similar containers were as follows:
    - After 100 cycles: 0.4 percent (Tenney) and 0.2 percent (walk-in).
    - After 200 cycles: 4.4 percent (Tenney) and 0.8 percent (walk-in).

- From the NCMA study, it appears that mass loss increases with an increase in the following parameters:
    - Ratio of mass of solution to mass of specimens.
    - Specimen surface area (total or wetted) to volume ratio.
    - Increased ratio of immersed specimen volume to total specimen volume.

- With respect to mass loss, variations in test parameters lead to the following results:
    - For similar specimens and containers, under filling of solution in the containers appears to increase mass loss.
    - For the same container size, smaller specimens exhibit larger mass loss.
    - For the same specimen size, specimens in smaller containers display greater mass loss.
    - There appears to be little effect from specimen geometry, although increasingly square specimens exhibited lower mass loss compared to rectangular specimens (after 150 cycles, average mass loss was 0.9 percent for square specimens and 1.0 percent for rectangular specimens)

- The performance ranking among test sets in the short-term (after 50 cycles) is not representative of their rankings in the longer term (after 100 cycles).

- Mass loss appears to follow a 2^{nd} order polynomial form from start of the freeze-thaw tests until a certain number of cycles (mass loss threshold point) which varies from specimen to specimen but was generally between 130 and 160 cycles (except for test set B whose threshold point was at 80 cycles). For reference, a 1 percent mass loss was reached between 110 and 160 cycles.

- Resonant frequency testing (based on ASTM C 215 (1997)) can be conveniently performed on SRW specimens, and the sensitivity of resonant frequencies to changes in specimen structural integrity makes this test a valuable one for the evaluation of freeze-thaw deterioration of SRW specimens. Close attention must be paid to procedural details to ensure consistency in measured frequencies.

- The performance ranking among of SRW specimens as measured using resonant frequency testing differs from the performance ranking based on mass loss measurements.

- The relative dynamic modulus (RDM)* linear threshold point (number of cycles at which rate of resonant frequency ceases to be linear) occurs prior to the mass loss linear

threshold point (number of cycles at which rate of mass loss ceases to be linear) in all specimens evaluated indicating that loss of integrity of specimens may accelerate prior to being detected by mass loss alone.

$$* \text{RDM} = \left(\frac{f_c}{f_o} \right)^2 \times 100 \qquad \text{Equation 15}$$

where f_c = resonant frequency after c freeze-thaw cycles
f_o = initial resonant frequency (at 0 freeze-thaw cycles)

- Below mass loss of about 0.5 percent, mass loss (of all test methods) appeared to be most sensitive to changing specimen condition (primarily due to loss of material from the sides of specimens). Beyond about 0.5 percent mass loss, however, once cracks started forming in specimens, resonant frequency methods were more appropriate for detecting changes in specimen integrity.

- Risky specimens are defined as those with mass loss in the vicinity of 1 percent (0.8 to 1.2 percent) but with RDM less than 60 percent. Approximately one-third of all variability series specimens fell in this category. For these specimens, a 1 percent mass loss was not indicative of actual internal conditions or pending damage in them. At 1 percent mass loss, these specimens exhibited RDM of 3 to 76 percent.

- For the specimens in this study, below mass loss of about 0.5 percent, mass loss (of all test methods) appeared to be most sensitive to changing specimen condition (primarily due to loss of material from the sides of specimens). Attention must be paid to isolated events such as popouts whose significance to overall specimen condition can be better discerned by observing rates of mass loss. At larger mass loss, resonant frequency methods appear to be most sensitive to changes in specimen integrity and thus a more suitable test.

- Specimens in this study exhibited a critical moisture content of about 5.6 to 5.8 percent and a critical moisture gain of about 0.8 to 1.1 percent below which RDM values changed little and above which RDM values dropped considerably, in most cases, to RDM of 0 percent. This observed behavior concurred with the theory of critical degree of saturation (S_{CR}) proposed by Fagerlund (1975). Degree of saturation is defined as the ratio of actual moisture content to the total moisture content required to fill the open porosity in the material. This theory states that each particular material (with a certain combination of material properties such as strength and pore properties) possesses a unique value of S_{CR}, and significant frost damage does not occur until the actual degree of saturation (S_{ACT}) in the material exceeds S_{CR}. For ordinary concretes, S_{CR} is in the range of 0.75 to 0.90 (Fagerlund, 1977). For the SRW specimens tested in this study, S_{CR} (calculated as the ratio of moisture content to ASTM C 642 (2002) boiled absorption) was in the range of 0.76 to 0.83.

- The values of critical moisture gain are similar (0.8 to 1.1 percent) for specimens in the two freezer environments which had previously exhibited markedly different performance in mass loss, resonant frequency, pulse velocity, and visual scaling rating. Above a moisture gain of about 1.0 to 1.2 percent, mass loss also increases dramatically in these specimens.

- Moisture gain values for specimens in a given set of replicate specimens exhibits lower coefficient of variation compared to mass loss values. This makes the measurement of moisture gain an attractive supplement to the ASTM C 1262 (2003) method.

- As far as specification values for mass loss are concerned, the current ASTM C 1372 (2003) limits of 1 percent maximum mass loss after 100 cycles (for all five specimens in a set) and 1.5 percent maximum mass loss after 150 cycles (for four out of five specimens in a set) pertain to tests in water. For reference, the Mn/DOT has criteria based on tests conducted in saline as follows (Mn/DOT, 2001):

  > The freeze/thaw durability of wall units tested in accordance with ASTM C 1262 (2003) in a 3 percent saline solution shall be the minimum of the following:
  > 1) The weight loss of each of five test specimens at the conclusion of 90 cycles shall not exceed 1 percent of its initial weight; or
  > 2) The weight loss of 4 out of 5 specimens at the conclusion of 100 cycles shall not exceed 1.5 percent of its initial weight, with the maximum allowable weight loss for the 5th specimen to not exceed 10 percent.

  In this respect, all specimens tested in this study complied with such specifications. However, it was just pointed out that there exists risky specimens which comprised approximately one-third of the specimen population in the variability series (of the NCMA study). For these specimens, a 1 percent mass loss was not indicative of actual integrity or pending internal damage in specimens. For these specimens, a mass loss of 0.7 percent is more sensible as a limit before substantial loss of specimen integrity. In most cases, it was evident that specimens had reached their critical moisture gains and past their RDM threshold points (beyond which RDM decreases at an accelerated rate) beyond mass loss of 0.7 percent.

5.7 RECOMMENDATIONS—ASTM C 1262 (2003) TESTING FOR SRW UNITS

Based on the findings from this study, recommendations for the freeze-thaw testing of SRW units have been developed and can be found in appendix A as a set of suggested revisions in a newly annotated version of the ASTM C 1262 (2003) test method. Based primarily on the FHWA project findings, but also on the NCMA results, revisions are made to SRW unit sampling and specimen extraction, freezer evaluation and survey, details of the freeze-thaw cycle, and other procedural items. Changes to the test standard are carried out in the following form:

- Current text to be removed is crossed out.
- New text is in bold face and underlined.
- New figures are identified by their bold face and underlined caption.

Commentaries are also provided to explain the nature of changes. In addition, a version of ASTM C 1372 (2003) is included in which comments on specifications for SRW units have been provided. These two documents are included in appendixes A and B as a stand-alone product to assist SHAs in rapidly implementing the main findings from this study.

5.8 RECOMMENDATIONS—FUTURE RESEARCH

5.8.1 SRW Material Characterization—Between-Unit Variability

Although within-unit variability was examined in detail in this study, limited data on unit-to-unit variability was obtained. In the NCMA study, variations in test results among specimens in the same test set suggest variable quality within a production run. This notion had also been alluded to in this report in the discussion of sampling SRW units from a block plant. A study to evaluate this would involve sampling units at various stages in a production run (e.g., five units at every 10 or 20 percent of the total run) and conducting ASTM C 140 (2000) standard properties, ASTM C 457 (2004) air void analysis, and ASTM C 1262 (2003) freeze-thaw tests on specimens from these units to determine if systematic variations in material properties exist over the course of a production (within a run, within a pallet, within a day, or within a week).

5.8.2 Frost Durability of SRW Units—Frost Index

As mentioned in chapter 4, the spacing factor as currently defined in ASTM C 457 (2004) for ordinary concretes cannot be applied to SRW mixes in the same way it is applied to ordinary concretes. Future studies could target developing a parameter, similar in concept to the spacing factor, but for dry concrete mixes which possess a network of interconnected compaction voids. Such studies should employ a more mechanistic approach in the development of this parameter which takes into consideration the degree of saturation of these compaction voids, their interconnectivity, and their shapes, among other factors.

5.8.3 Dilation Tests for SRW Specimens

Accelerated freeze-thaw damage in the presence of salts was the topic of much research in this project. It was found in chapter 4 that 3 percent NaCl solutions were capable of inducing expansion damage similar to plain water. In addition to expansion potential, the larger proportion of unfrozen brine in saline solutions leads to greater probability of damage due to crusting (i.e., entrapment of unfrozen brine within a frozen shell, see chapter 2) (Personal communication, Scherer). Both these effects suggest that substantial expansion should accompany damage in specimens tested in saline solution. Future investigations could evaluate length change of SRW specimens tested in saline solution and compare these to specimens tested in water. Length change measurements also provide insight as to whether compaction voids are beneficial or not for frost durability (in the same way as air-entrained concretes are evaluated through the critical dilation test, ASTM C 671(2002)).

5.8.4 Acoustic Emission Testing

The methods of damage detection described in chapter 4 were focused on damage of a liquid filled vial which simulated a water-filled SRW pore. Actual damage in an SRW specimen may be detected using acoustic methods. Further research is needed to assess the applicability of this method and to relate findings on where damage takes place during a freeze-thaw cycle to the current ASTM C 1262 (2003) cycle.

5.8.5 Effect of Freeze-Thaw Cycle on Specimen Performance

One significant outcome from the NCMA study was the confirmation that compliance with ASTM C 1262 (2003) T-t requirements did not necessarily guarantee similar specimen performance. As described earlier, even with 100 specimens in the walk-in chamber, the freezer air could still meet ASTM C 1262 (2003) requirements provided that sufficient cooling time was allowed for the freezer air to reach the required ranges. The resulting specimen cooling curves were, however, quite distinct from those obtained in a freezer with less specimens. The effect of freeze-thaw cycle on specimen performance thus deserves further attention and investigation. Future research should consider the effects of varying each parameter of the freezer air cooling curve—cooling rate, cold soak length (4 hours versus 5 hours), cold soak temperature, warming rate, and warm soak length (2.5 hours versus say 6 hours)—on ensuing specimen performance. This information will be valuable for future revisions of the ASTM C 1262 (2003) test standard.

On the length of cold soak, it was pointed out in chapter 4 that despite variations in test parameters (container size, surrounding water volume, and number of specimens in freezer), a 4-hour cold soak appeared enough to traverse the freezing plateau of specimens. As such, expansion damage from water freezing in SRW pores is likely to have occurred by this 4-hour cold soak. Future research is therefore needed to confirm whether the most damage in the specimen is realized within a 4-hour cold soak or whether additional damage is induced by extending to 5-hour cold soak. Results from this investigation carry practical implications on total cycle length and total test time.

5.8.6 Effect of Specimen Preconditioning

There are two recommended future research topics on the effect of specimen preconditioning on SRW performance. Both recommendations are based on the confirmation from this research that a critical saturation exists in SRW specimens.

5.8.6.1 Effect of Pretest Exposure

ASTM C 1262 (2003) currently allows specimens to "dry for not less than 48 hours in laboratory air at a temperature of 24 ± 8 °C (75 ± 15 °F) and a relative humidity of less than 80 percent" immediately after saw-cutting. Thereafter, the specimens are partially immersed in 13 mm (½ inch) of test solution before start of freezing and thawing. The effect of the drying period should be examined further by evaluating the effect of different drying conditions such as varying drying times (e.g., 48, 72, or 96 hours) or tighter temperature and relative humidity ranges on specimen performance. As a starting point, the mass of specimens should be measured as function of drying time to determine the extent of changes in moisture content. Recall from the NCMA study that at "moisture gains" of about 0.8–1.1 percent, specimens suffered rapid reduction in RDM.

5.8.6.2 Effect of Saturating Specimens Prior to Freeze-Thaw Testing

SRW specimens evaluated in this research exhibited critical saturation in the range of 0.76–0.83, which was obtained by dividing critical moisture content by boiled absorption. According to Fagerlund (1975), concretes whose degree of saturation is above critical are rapidly deteriorated within several freeze-thaw cycles. This suggests that specimens that have been saturated by boiling ought to deteriorate more rapidly compared to ones which have been preconditioned as required in ASTM C 1262 (2003) (e.g., absorption by capillarity). The use of boiled absorption to precondition specimens should be investigated as an alternative method to accelerate freeze-thaw testing.

5.8.7 Significance of Mass Loss and 1 Percent Limit on Different Grades of SRW Mixes

One of the main objectives of the NCMA study was to determine the significance of mass loss with respect to other material parameters (such as resonant frequency, pulse velocity, scaling rating, and modulus of rupture) and to determine the adequacy of the 1 percent mass loss limit. The findings from this study are covered in chapter 6 of Chan (2006). For the particular SRW mix evaluated, it was generally found that at 1 percent mass loss, one-third of specimens tested exhibited RDM less than 60 percent. Above 1 percent mass loss, MoR values were less than half of the initial undamaged value. It is not certain whether other grades of SRW mixes would display similar trends. It is thus highly recommended that similar studies be conducted on a range of SRW mixes, specifically those that are intended for use in projects where acceptance criteria such as 1 percent maximum mass loss apply. Building this database of actual specimen structural integrity as function of mass loss will provide further insight as to whether the current 1 percent limit is indeed reasonable or whether it needs to be modified.

5.8.8 Partial Versus Full Immersion of Specimens

The issue of whether ASTM C 1262 (2003) test specimens should be partially or fully immersed in water or 3 percent NaCl solution remains open. Further experiments should be conducted to evaluate modes of damage and variability in fully immersed specimens compared to partially immersed ones.

5.8.9 Database of Mass Loss Prediction Constants

Independent studies (Hance, 2005 and NCMA Study, chapter 6 of Chan (2006)) have confirmed the existence of a second order trend in mass loss relative to cycles for very different SRW mixes. One study could involve compiling ASTM C 1262 (2003) data for SRW mixes of different grades, from different manufacturers, tested in different laboratories, tested in different freezers and tested in water and in saline solution to confirm the existence of this second order behavior and evaluate the *mass loss prediction constant* for each of these sets of results. From this collection of *mass loss prediction constants*, conditions which influence this parameter the most may be identified which may in turn be utilized to develop prediction tools for freeze-thaw durability for SRW mixes.

5.8.10 Efficacy of Silane or Other Coatings/Sealants in Mitigating Damage for Inservice SRW Blocks.

Early attempts to evaluate silanes under conditions similar to ASTM C 1262 (2003) were inconclusive. It is possible that evaluating silanes in tests that involve full or partial immersion in water or solution is not appropriate or does not accurately assess the actual mode of action that silanes would impart in SRW blocks in the field. It is recommended that this topic be investigated in further detail in the laboratory, especially in tests that allow for testing of full blocks or walls in simulated field conditions (see section 4.8). It is also strongly recommended that the performance of SRW blocks already treated with silanes or other coatings/sealants be monitored to determine the long-term field performance of SRW blocks treated with such compounds. It would be especially useful to treat blocks with varying degrees of distress (at the time of treatment) to determine if there is an optimal time to treat existing walls to realize the best long-term improvement in SRW block durability.

5.8.11 Freeze-Thaw Performance—Field and Laboratory Correlation Based on Critical Moisture.

The NCMA studies demonstrated that for the particular specimens tested, there appeared to be a *critical moisture content (or moisture gain)* above which specimens deteriorated at an increasingly faster rate. This observation concurred with Fagerlund's critical degree of saturation (S_{CR}) theory, which states that every material has a unique level of saturation above which the material degrades rapidly within a few freeze-thaw cycles. In this theory, a material is considered safe provided that its degree of saturation (S_{ACT}) is less than the critical value, and the period of *frost immunity* in field concretes is the time required for S_{ACT} to reach S_{CR} (Pigeon and Pleau, 1995). In a similar manner, it is worth investigating these concepts for SRW mixes, where moisture contents of in-service SRWs may be determined directly from the field or from SRWs tested in the laboratory under simulated field conditions. This information, coupled with *critical*

moisture contents for a particular SRW mix may provide information on *frost immunity* of field units. This type of investigation may help bridge the currently existing gap between field and laboratory results.

APPENDIX A:
NEWLY PROPOSED VERSIONS OFASTM C 1262 (2003)—FREEZE-THAW TEST FOR SRW BLOCKS)

Standard Test Method for
Evaluating the Freeze-Thaw Durability of ~~Manufactured Concrete Masonry Units and Related Concrete Units~~[4]
Segmental Retaining Wall (SRW) Units
(modeled after ASTM C 1262 – 05a)

ASTM C 1262 CLAUSES	COMMENTARY
1. Scope*	
1.1 This test method covers the resistance to freezing and thawing ~~manufactured concrete masonry and related concrete units~~ **of Segmental Retaining Wall (SRW) units**. Units are tested in a test solution that is either water or 3 percent saline solution **(3 percent salt by weight of solution)** depending on the intended use of the units in actual service.	
~~NOTE 1—Concrete masonry and related concrete units include units such as hollow and solid concrete masonry units, concrete brick, segmental retaining wall units, concrete pavers, and concrete roof pavers.~~	
1.2 *This standard does not purport to address all of the safety concerns, if any, associated with its use. It is the responsibility of the user of this standard to establish appropriate safety and health practices and determine the applicability of regulatory limitations prior to use.*	
2. Referenced Documents	
2.1 *ASTM Standards:*	*C 2.1—This revised version of ASTM C 1262 provides the option of conducting resonant frequency testing on SRW coupons to determine their relative dynamic modulus (RDM).*
C 140 Test Methods of Sampling and Testing Concrete Masonry Units and Related Units	
C 215 Test Method for Fundamental Transverse, Longitudinal, and Torsional Resonant Frequencies of	

Concrete Specimens

C 1093 Practice for the Accreditation of Testing Agencies for Unit Masonry

C 1209 Terminology of Concrete Masonry Units and Related Units

3. Terminology

3.1 Terminology defined in Terminology C 1209 shall apply for this test method.

4. Significance and Use

4.1 The procedure described in this test method is intended to determine the effects of freezing and thawing on ~~concrete~~ **SRW** units in the presence of water or saline solution

4.2 The procedure is not intended to provide a quantitative measure to determine an expected length of service for a specific type of concrete unit.

NOTE 2—The testing laboratory performing this test method should be evaluated in accordance with Practice C 1093.

NOTE 3—Compressive strength and absorption tests should be performed on different but representative specimens. While compressive strength and absorption values by themselves have been shown by research to not be reliable indicators of durability, they have been shown to be good reference values for units manufactured from a given set of materials.

5. Apparatus

5.1 *Freezing-and-Thawing Apparatus*:

5.1.1 In the event that a chamber or chambers are used to subject the specimens to the specified freezing or thawing cycles, or both, the chamber or chambers shall be capable of maintaining the air temperature ~~throughout the chamber~~ **at all specimen locations** within the specified test ranges when measured at any given ~~time~~ **cycle**. If the apparatus operates automatically, it must be able to provide reproducible cycles within the specified temperature requirements.

(See commentary C 8.3.1 below)

5.1.2 The apparatus includes a non-

(See commentary C 7.1.4 below)

rigid plastic container for each test specimen and test specimen supports as illustrated in Fig. 1. The containers shall be of sufficient size to provide ~~a minimum of 1/8 in. (3 mm) and a maximum of 1-1/2 in. (38 mm)~~ **1-3/16 ± 1/24 in. (30 ± 1 mm)** test solution surrounding the specimen. Test specimen supports to hold the specimen above the container bottom shall be two 1/8 ± 1/24 in. (3 ± 1 mm) rods of a solid noncorrosive, nonabsorptive material (brass, plastic, etc.). **Supports in the specimen longitudinal and transverse directions shall be provided (see Note 5).** The container shall be flat enough that when the specimen coupon is set on the support rods the specimen shall not deviate from level by more than 1/16 in. (2 mm) from one end of the specimen to the opposite end.

NOTE 4—An example of a container that fulfills this requirement for a 4 in. × 8 in. (100 mm × 200 mm) coupon cut from 8 in. (200 mm) tall units is the Rubbermaid® "Servin' Saver Plus" 1.1 Gal / 4.0 L container.

NOTE 5—A recommended setup for longitudinal and transverse support of the specimen consists of an I-shaped support formed by attaching pieces of 1/8 ± 1/24 in. (3 ± 1 mm) rod to form the I.

5.2 *Temperature-Measuring Equipment*—Thermometers, resistance thermometers, or thermocouples, capable of measuring the temperature at various points within the test chamber to within 2°F (1°C) **of the temperature measured by a sensor that has been calibrated to a standard reference temperature**.

5.3 *Scales*—Scales for weighing full-size specimens shall have a capacity of at least 50 percent greater than the weight of the largest specimen tested and shall be accurate to at least 1 g (0.002 lb). Scales for weighing the filter paper and specimen residue (spall), as required in 8.2.3, shall be accurate to at least 0.2 g (0.0005 lb).

5.4 Dynamic Testing Apparatus

shall conform to the requirements of Test Method C 215.

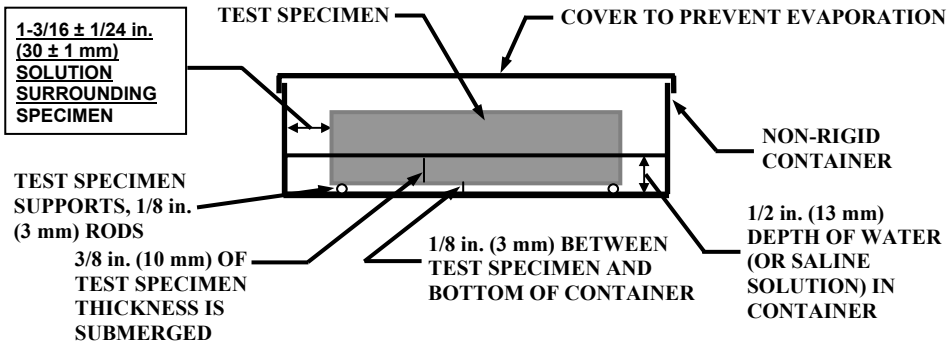

FIG. 1 Test Specimen in Freezing–and–Thawing Container

6. Sampling

6.1 *Selection of Test Specimens*—Select whole units representative of the lot from which they are selected. The units shall be free from visible cracks or structural defects **and shall not have been previously exposed to below-freezing temperatures**.

6.2 *Number of Specimens*—**From the whole units selected in 6.1, randomly** Select five units for freezing and thawing tests. If compression and absorption tests are to be performed on the same set of units in accordance with Test Methods C 140, select additional units as required. Specimens (coupons) used for Test Methods C 140 tests shall not be used as specimens for freezing–and–thawing tests.

C 6.2—Variability in properties and freeze-thaw performance among SRW units within a "lot," as defined in 6.1, needs to be further investigated. If the lot consists of 1 day's production, then units shall be sampled at various different times in the day and tested. If the lot consists of several days' production, then units shall be sampled on a daily basis for testing. Knowledge of between-unit variability will enable developing more specific requirements in 6.1 and 6.2. For example, a sampling frequency of "1 unit per X units" or "1 unit per Y hours production" can be specified depending on the observed level of variability.

6.3 *Identification*—Mark each freezing–and–thawing specimen so that it is identifiable at any time.

7. Preparation of Test Specimens

7.1 *Freezing–and–Thawing Test Specimens*—Test specimens shall consist

of solid coupons saw-cut from full sized units. Do not saw-cut test specimens from units that have been previously oven-dried. Do not subject test specimens to oven-drying prior to completion of freezing–and–thawing testing.

7.1.1 One coupon shall be cut from each of the five sampled units. Using a water-cooled saw, cut the coupon from ~~the exposed surface of the unit as the unit is used in service unless the exposed surface is a split, fluted (ribbed), or other nonplanar surface. In the case of a unit with an exposed nonplanar surface, cut the coupon from another~~ **a** flat molded surface**, on the surface of the unit that is opposite to the split surface as illustrated in Fig. 2. Cut the coupons at least 1 in. (25 mm) away from the corners of the unit and in such manner that the coupon is centered at mid-height of the unit (Fig. 2).** Immediately following saw-cutting, **thoroughly** remove loose particles and residue from the coupon by rinsing in tap water and brushing with a soft bristle brush **until the coupon surfaces are clean (saw-cut aggregates clearly visible)**. Do not fully immerse coupons in water.

C 7.1.1—Sampling from the back face has two advantages: it avoids sampling near the split face where cracks and delaminations have been frequently observed, and it ensures consistency in properties (there is evidence that properties over an SRW unit vary from split to back face). Sampling from the back face has the disadvantage that it is not the exposed surface of the unit, the one of interest. Moreover, there is data to prove that properties of specimens sampled from the back face have lower water absorption and higher flexural strength than those sampled from the split face. One approach that can be taken is to tighten freeze-thaw specifications for specimens sampled from the back face, recognizing that these specimens are of likely higher quality than those sampled from the split face.

7.1.2 Place the coupons on edge on a 3/8 in. (10 mm) or coarser mesh such that there is an air space of not less than 1 in. (25 mm) between coupons. Allow the coupons to dry for not less than 48 h in laboratory air at a temperature of 75 ± 15°F (24 ± 8°C) and a relative humidity of ~~less than 80 percent~~ **45 to 55 percent**.

C 7.1.2—The 45 to 55 percent relative humidity is adapted from ASTM C 672 which also requires a drying period for specimens prior to start of freeze-thaw testing.

7.1.3 The thickness of each coupon shall be 1-1/4 in. (32 mm) ± 1/16 in. (2 mm), unless the unit does not permit this minimum thickness, in which case the thickness shall be the maximum thickness that can be obtained from the unit. The thickness of the coupon shall not be less than 3/4 in. (19 mm).

C 7.1.3—It is not clear at this time whether variations in coupon thickness affect test results. Thickness variations do, however, affect total mass of specimen (for specimens with the same face test area), and as concluded in the NCMA study, variations in specimen mass relative to solution mass affect mass loss measurements. The issue of

specimen thickness must be evaluated and consideration should be made as to whether or not a constant thickness should be specified.

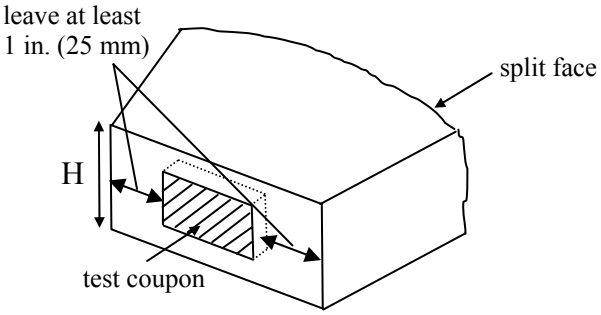

FIG. 2 Extraction of Test Coupon from SRW Unit (figure not to scale)

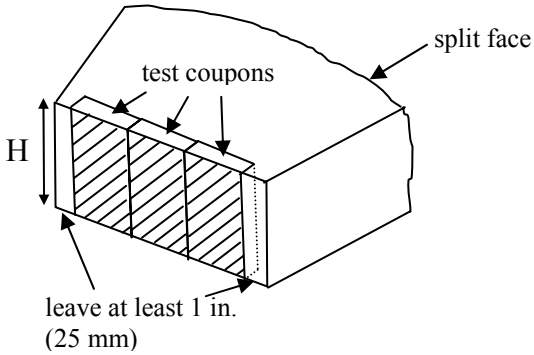

FIG. 2 for C 7.1.1 Alternate Extraction Method of Test Coupons from SRW Unit (figure not to scale)

7.1.4 The area of the submerged **bottom** surface of the test specimen shall be ~~at least 25 in.^{2} (161 cm^2) and shall not exceed 35 in.^{2} (225 cm^2)~~, **between 31 in^2 (200 cm^2) and 33 in^2 (210 cm^2)** unless the unit does not permit a coupon meeting the minimum area, in which case the test specimen shall consist of two coupons. The combined area of the two coupons shall be ~~at least 25 in.^{2} (161 cm^2) and shall not exceed 35 in.^{2} (225 cm^2)~~ **between 31 in^2 (200 cm^2) and 33 in^2 (210 cm^2)**. These two coupons shall be tested as and considered to be a single specimen.

NOTE 6—For combinations of specified container (5.1.2) and coupon sizes (7.1.4), approximately 300 g of test solution is required to obtain a depth of 1/2 ± 1/16 in. (13 ± 2 mm) (8.3.1).

C 7.1.4—It is understood that the current allowable range of container and coupon sizes is intended to provide flexibility to different laboratories testing a variety of different manufactured products including concrete masonry units, segmental retaining wall units, concrete pavers, and roof pavers. It can be demonstrated that for the current tolerances, specifically in the amount of surrounding solution, the energy required to cool a coupon surrounded by 1 1/2 inches (3.8 cm) of water is up to 5 times larger than the energy required to cool a similar size coupon surrounded by 1/8 inch (0.32 cm) of water. In addition, the combination of permissible container and coupon sizes can result in ratios of

mass of surrounding water (or solution) to mass of specimen (i.e,. $m_{water}/m_{specimen}$) as high as 0.40 for a 35 inch^2 (226 cm^2) coupon surrounded by 1-1/2 inches (3.8 cm) of water to as low as 0.06 for a 25 inch^2 (161 cm^2) coupon surrounded by 1/8 inch (0.32 cm) of water. In the studies conducted at Cornell for NCMA, mass loss approximately doubled in going from $m_{solution}/m_{specimen}$ of 0.15 to 0.30.

Based on these data, the range $m_{solution}/m_{specimen}$ has been narrowed by specifying coupon size as well as the clearance between specimen and container. Thus, 4 inch by 8 inch (10 cm by 20 cm) (coupons are tested in containers of about 6.4 inches by 10.4 inches in size (16 cm by 26 cm) (Rubbermaid® "Servin' Saver Plus" 1.1 Gal / 4.0 L). Coupons cut from 6-inch (15 cm-)tall units are then required to be 5-1/3 inches by 6 inches (14 cm by 15 cm) and be tested in containers of about 7.7 inches by 8.4 inches (20 cm by 21 cm) in size. Coupons cut from 4-inch-(10-cm-)tall units are then 4 inches by 8 inches (10 cm by 20 cm) provided there is sufficient space in the SRW unit or two 4 inch by 4 inch (10 cm by 10 cm) coupons tested as one coupon. These coupons (4 inch(10 cm)) are tested in the same containers as those used for coupons cut from 8-inch (20-cm-)tall units.

One likely problem is the long-term availability of said containers in the market. For test results to be repeatable and comparable, test containers (material and dimensions) must be standardized. Another option is to specify custom-made containers with exacting dimensions meeting the above specifications.

8. Procedure

8.1 *Survey of Freezing-and-Thawing Test Chamber*:

8.1.1 The chamber shall be surveyed for its internal temperature distribution prior to actual freeze-thaw testing of specimens. This survey shall be performed according to the procedures outlined in the Annex. The survey shall be performed on a chamber loaded with the same number and type of containers, coupons, and solution in the same arrangement as will be used in actual freeze-thaw testing of specimens.

8.1.2 Determine *Freezer Reliability Curves* from the survey (see Annex). If *Reliabilities* less than 95 percent are measured, remove 10 percent of the containers from the chamber and repeat the survey. Continue this process until *Reliabilities* greater than 95 percent are consistently attained. The remaining amount of containers in the chamber shall then be the maximum amount of containers that may be used in actual freeze-thaw tests.

NOTE 7—Dummy coupons of the same mass as actual test coupons are acceptable for the survey. The test solution used during the survey shall be similar to that used for actual freeze-thaw testing.

C 8.1.2—The current ASTM C 1262 requires that the freezer air T-t conditions be maintained "throughout the chamber." Although the meaning of "throughout" is not clear (i.e., "at all points in the freezer" or "at all specimen locations"), it may imply "everywhere" in the chamber (note: the word "throughout" is defined in Merriam-Webster's dictionary as "in or to every part; EVERYWHERE"). As such, complying with ASTM C 1262 (2003) may entail attaining R = 100 percent at all cycles. For the Tenney freezer with 28 specimens and the walk-in freezer with 20 specimens, R = 100 percent was consistently attained. However, as noted in section 4.4.5, somewhere between 20 and 40 specimens, R is no longer 100 percent for the walk-in freezer. Similarly, the chest freezer with six specimens exhibited R less than 100 percent. The issue of whether R needs to consistently be 100 percent at all cycles, or whether lower R values such as R = 95 percent are acceptable remains open. Note that when R = 0.95, the probability that any given specimen will experience 100 consecutive fully compliant cycles is about 60 percent. For other R values, this probability is:

$$R = 0.96 - 66 \text{ percent}$$

R = 0.97 – 74 percent
R = 0.98 – 85 percent
R = 0.99 – 90 percent

8.1.3 During actual freeze-thaw testing, the length of *Cooling Branch* (see Annex) shall be such that *Reliabilities* greater than 95 percent are attained. The internal temperature distribution of the chamber shall be monitored during actual freeze-thaw testing to monitor the chamber performance and the reproducibility of cycles. If fluctuations in the performance of the chamber are detected, the length of *Cooling Branch* shall be adjusted accordingly to maintain *Reliabilities* greater than 95 percent.

NOTE 8—It is recommended that at least 5 cycles in every 25 freeze-thaw cycles be monitored.

~~8.1~~ **8.2** *Specimen Conditioning*:

~~8.1.1~~ **8.2.1** After preparation of the freezing–and–thawing test specimens in accordance with Section 7, place the specimen in the container ~~face down on the specimen supports~~ such that the non-saw-cut surface of the specimen is in contact with the specimen supports. Add a sufficient amount of test solution at a temperature of 60 to 80°F (16 to 27°C) to the container to achieve a test solution depth of 1/2 ± 1/16 in. (13 ± 2 mm). Do not pour test solution directly onto the specimen. The test solution shall be either potable tap water or a 3 ± 0.1 percent (by weight) sodium chloride saline solution **(0.03 lbs of salt to 0.97 lbs of water)**. ~~Seal the container and store~~ **Close container lids tightly and store containers** on a level surface in laboratory air as defined in 7.1.2.

NOTE 4 **9**—The submerged portion of the specimen is 3/8 in. (10 mm) of its thickness. There is 1/8 in. (3 mm) of test solution between the bottom of the container and the face of the specimen.

C 8.2.1—The effect of partial immersion should be re-evaluated. Scherer and Valenza (2005) have conducted experiments in which concrete slabs are ponded with saline solution on one face. Swelling of the slabs is observed and this swelling increased with increasing salt concentration. Under freezing conditions, swelling is further enhanced. This may be related to the observation of transverse cracks in specimens.

~~8.1.2~~ **8.2.2** After 1 h ± 15 min, open the container and add test solution as necessary to maintain the water level required in 8.1.1. Reseal the container. After another 23 h ± 1 h, remove the specimen from the test solution and allow to drain for 1 min **± 15 sec.** by placing it on a 3/8-in. (10-mm) or coarser sieve, removing visible surface test solution with a damp cloth. Immediately weigh the specimen to the nearest 1 g (0.002 lb) and record as W_p. **Immediately test for fundamental frequency (optional). If fundamental frequency is measured, the total time period from removal of specimen from container to resonant frequency measurement shall not exceed 15 mins. nor should specimen surfaces become visibly dry before frequencies are measured.**

NOTE ~~5~~ **10**—The weight W_p as determined in ~~8.1.2~~ **8.2.2** is not required to be reported at the conclusion of the test, nor is it used to calculate the reported weight loss of the specimen throughout the test. However, because the initial dry-weight of the specimen is not determined until the completion of freezing–and–thawing testing by adding the dry-weight of the collected residue to the dry-weight of the remains of the specimen (see ~~8.3.5~~ **8.4.5**), this W_p weight is needed as a reference weight to be used during the testing to estimate percentage weight loss and to predict relative performance between test specimens.

NOTE 11—Testing of fundamental frequency of SRW coupons requires close attention to test technique to avoid confusing frequencies for different modes of vibrations. Carefully aligning the location of impact and accelerometer (in the impact resonance method) as shown in Fig. 3a usually results in the transverse vibration mode being the dominant form of vibration for a specimen with 2:1 aspect ratio. To verify that the observed frequency peaks correspond to the transverse vibration mode, the location of impact and accelerometer may be offset as shown in Fig. 3b, in which case the torsional vibration mode becomes dominant. The frequency corresponding to this torsional may thus be distinguished from the transverse mode.

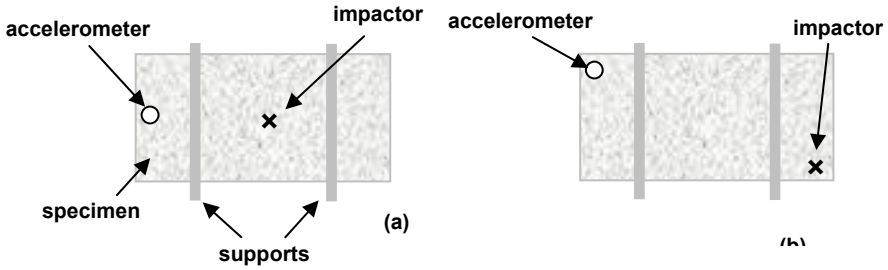

FIG. 3 Possible vibration modes for SRW specimen

~~8.1.3~~ **8.2.3** Return the specimens to the container and adjust test solution level as required in ~~8.1.1~~ **8.2.1**.

~~8.1.4~~ **8.2.4** Test solution added to the containers shall be at a temperature of 60 to 80°F (16 to 27°C).

~~8.2~~ **8.3** *Cyclical Testing*:

~~8.2.1~~ **8.3.1** Begin the test with a freezing cycle. Place the containers into the freezing test chamber such that each container is surrounded by a minimum air space of 1/2 in. (13 mm) on all sides. During testing the container shall be level within 1/16 in. (2 mm). **The air temperature in the chamber shall be maintained within the limits shown in Fig. 4.** During the freezing cycle, maintain the air temperature in the chamber at ~~0 ± 10°F (-18 ± 5°C)~~ **0 ± 5°F (-18 ± 3°C)** for a period of not less than 4.0 h and not more than 5.0 h **(cold soak)**. **Hence, the time at which the warming ramp (shown by the dashed lines) starts may vary depending on the length of cold soak, as determined from the Chamber Survey (8.1). The rates of freezer air warming shall conform with the limits shown in Fig. 4.** ~~The cycle time does not include the time required for the air temperature in the chamber to reach the prescribed temperature. Periodically, at the end of a freezing cycle, open the containers and visually inspect the specimens to determine if all the test solution surrounding the specimen is frozen solid.~~

C 8.3.1a—Spacing between specimens may influence the flow of air between specimens and affect cooling rates. It has been observed that cooling rates in the Tenney freezer increased slightly when the spacing between containers was increased and this is suspected to be caused by enhanced air flow between containers. Spacing between test containers may be more significant for a freezer such as the Tenney freezer in which air flow is essentially from top to bottom of freezer, and the passage of air from one shelf level to the next occurs in the space between containers and between containers and freezer wall.

C 8.3.1b—A complete freezer air T-t requirement (Fig. 4) is specified in this annotated version of C 1262 (2003). This is because findings from the FHWA and NCMA studies confirmed two important results:

- *Meeting the current ASTM C 1262-05 freezer air T-t requirements does not lead to similar specimen cooling curves.*
- *Meeting the current ASTM C 1262-05*

~~If not, extend the length of the freezing cycle to ensure that all test solution is frozen solid.~~

NOTE 12—An example of a chamber that meets the temperature-time requirement in Fig. 4 is the Tenney Environmental (A Lunaire Company) chamber, Model No. T20S-2.0 shown in Fig. 5.

NOTE ~~6~~ **13**—Temperature probes should be used to monitor the air temperature throughout the chamber. If warm units are placed into a freezing chamber, the air temperature within the chamber rises. The start of the freezing cycle time period begins only after the temperature of the air within the chamber is within the permissible range. Typically, constant temperature monitoring is not necessary, but it should be preformed through the first several cycles to ensure that the specimens remain in the freezing chamber for the appropriate length of time to comply with the cycle requirements. The same procedures should also be used to verify compliance with thawing cycle requirements in 8.2.6.

freezer air T-t requirements does not lead to similar specimen performance.

Thus, in addition to specifying cold and soak lengths and durations as is done in the current C 1262, the cooling and warming rates must also be specified.

The freezer air T-t envelopes shown in Fig. 4 are based on the data obtained at Cornell University for a freezer loaded with 28 specimens (also refer to section 8.3.3). It is recognized that variations in specimen load may produce freezer air curves outside the bounds from those shown in Fig. 4. The curves shown in Fig. 4 are intended for a testing laboratory wishing to reproduce the test conditions of the NCMA freezer at Cornell.

Furthermore, an open question is the issue of how the T-t envelopes in Fig. 4 reflect actual field exposure of SRWs. This is a topic that must be investigated further by comparing actual cooling rates and performance of SRW units in field and laboratory conditions and revising the freezer-air requirements in the test method accordingly.

Another issue is the total number of specimens in the freezer. Chapter 4 showed that different coupon and container sizes can lead to variations in the total specimen quantity in the freezer and how variations in total specimen quantity lead to fluctuations in freezer performance. If a standardized container is used, it is then possible for the test method to specify total specimen quantity in the freezer and maintain this total quantity fixed (see section 8.3.3). This means that anytime during the course of a test that a specimen is considered "failed" and removed from the

population in the freezer, it should be replaced by a similar dummy specimen. This practice is in use in ASTM C 666 for ordinary concrete testing.

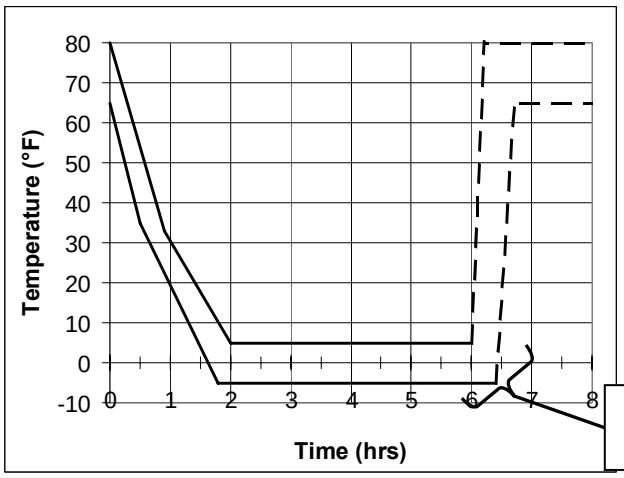

Points from which the envelope curves in the adjacent graph were produced			
Lower Limit		Upper Limit	
t (hrs)	T (°F)	t (hrs)	T (°F)
0.0	65	0.0	80
0.5	35	0.9	33
1.8	- 5	2.0	5
6.4	- 5	6.0	5
6.7	65	6.2	80
8.0	65	8.0	80

actual time of warming ramp may vary depending on results of Freezer Survey

FIG. 4 Chamber Air Temperature Limits

Internal dimensions: 1 m (39½ in.) deep × 0.76 m (30 in.) wide × 0.91 m (36 in.) high

Operating capacity: 5200 watts

FIG. 5 Example of Freezing-and-Thawing Apparatus

~~8.2.2~~ **8.3.2** ~~After the freezing cycle, immediately begin the thawing cycle. During the thawing cycle, maintain the air temperature around the containers at 75 ±~~

~~10°F (24 ± 5°C) for a period of not less than 2.5 h and not more than 96 h. The cycle time does not include the time required for the air temperature around the specimens to reach the prescribed temperatures. Each container shall be surrounded by a minimum air space of 1/2 in. on all sides. If the air surrounding the containers is not continuously circulated during the thawing cycle, the containers shall be laid out in a single layer without stacking in the vertical direction.~~ Periodically, at the end of a thawing cycle, open the containers and visually inspect the specimens to determine if no ice remains. If ice is still present, extend the length of the thawing cycle to ensure that all ice has thawed.

NOTE 14—There is evidence that the length of thawing cycle may affect overall freezer performance. Freezers programmed for thawing cycles shorter than 6 h have been observed to lose cooling efficiency in subsequent cycles. It is therefore recommended that freezer performance be monitored during tests, as indicated in 8.1.3 and Note 8, and the lengths of *Cooling* and *Warming Branches* be adjusted accordingly if fluctuations in freezer performance are detected.

8.3.3 The total number of specimens in the freezer shall be maintained at 28. Whenever a specimen is removed because of failure, replace it for the remainder of the test by a dummy specimen (see Note 7 for definition of dummy specimen).

C 8.3.3—Note again that the 28 specimens specified in section 8.3.3 are intended to reflect the test conditions at Cornell in the NCMA study for which the freezer air envelopes in Fig. 4 were produced. Other specimen quantities are expected to alert the freezer air response and thus different specification envelopes are required.

~~8.2.3~~ **8.3.4** One freezing–and–thawing cycle is defined as a completed freezing cycle followed by a completed thawing cycle.

~~8.2.4~~ **8.3.5** At 20-cycle intervals for those specimens tested in water and at 10-cycle intervals for those specimens tested in saline solution, remove containers from the test chamber and collect residue in accordance with ~~8.3~~ **8.4**. Open containers

to visually inspect the condition of the specimens and to adjust the test solution level to comply with ~~8.1.1~~ **8.2.1**.

NOTE ~~7~~ **15**—There is some evidence that frequency of sampling influences results. Therefore, variations from cycle intervals for residue sampling are only appropriate when this method is used for research purposes rather than compliance purposes. Collecting and reporting residue at regular intervals provides information about the performance of the specimens throughout the duration of the test and also permits plotting results of weight loss relative to number of cycles of exposure.

~~8.2.5~~ **8.3.6** Every time a container is replaced into a multi-level freezing test chamber, the container shall be placed on the level immediately above the level on which it was previously located. If the container was previously located on the top level of a multi-level freezing chamber, replace it onto the bottom level. **Containers in the front and back locations of the freezer shall be switched around, and containers in the left and right locations in the freezer shall also be switched around.**

~~8.2.6~~ **8.3.7** If the test method is being used to document compliance of a set of specimens with specific freezing–and–thawing durability criteria, repeat the freezing–and–thawing cycle to reach the specified number of cycles. After the specified number of cycles have been completed, collect residue in accordance with ~~8.3~~ **8.4**.

~~8.3~~ **8.4** *Collection of Residue*:

~~8.3.1~~ **8.4.1** Weigh to the nearest 0.2 g (0.0005 lb) and record as W_f a filter paper of high wet strength and smooth surface that has come to equilibrium temperature with the lab environment. Remove a single specimen from its container. Immediately rinse the specimen with water (if the specimen is tested in saline solution, use saline solution to rinse the specimen) using a squeeze bottle, being careful to collect in the specimen

C 8.4.1—While the current ASTM C 1262 requires that the top surface of coupons not be immersed in water at any time, it has been consistently observed that moisture condenses and freezes on the underside of container lids. Upon thawing, this water drips back on the coupon surface where it either sits or gets absorbed into the coupon. The amount of such moisture falling back on the coupon appears to vary randomly

container the rinse water (or saline solution) and all loose particles from the specimen. Consider any pieces that separated from the specimen as part of the residue. Pour the test solution from the specimen container through the filter paper to collect the residue (spall) from the test specimen. Replace the specimen in the container. Using fingertips and a squeeze bottle, remove loose particles from all surfaces of the specimen, again being careful to collect all rinse water (or saline solution) and loose particles in the specimen container. The top surface of the specimen shall not be immersed in test solution at anytime and the collected rinse water (or saline solution) shall not exceed a depth of 1/2 in. (13 mm) in the container. Remove the specimen from the container, pour the rinse water (or saline solution) through the filter paper, and rinse the specimen container until all residue (spall) in the specimen container is collected on the filter paper. Rinse the residue from specimens tested in saline solution three times with water to remove any soluble salt.

NOTE ~~8~~ **16**—The filtering may be expedited by using filter paper rated at a faster speed or vacuum filtration, or both. This is acceptable as long as the test solution that passes through the filter paper (filtrate) is clear to the naked eye. If it is cloudy, then filter papers of increasingly slower speeds should be used until the filtrate is clear.

from coupon to coupon. While the effects of variable moisture content on specimen performance is not certain at this time, the effect discussed under this commentary may be overcome as follows:

- *If fully immersed specimens are specified in future ASTM C 1262 (2003) versions, this condensed moisture will no longer be an issue.*
- *By providing lids with an incline so the condensed moisture can run down to the side of the container rather than dripping on the coupon.*

8.4.2 Use a damp cloth to remove moisture films from all specimen surfaces, immediately weigh the specimen to the nearest 1g (0.002 lb) and record as W_s (optional) and right away test for fundamental frequency (optional). If W_s and fundamental frequency are measured, the total time period from removal of specimen from container to resonant frequency measurement shall not exceed 15 mins and specimen surfaces shall not become

C 8.4.2—Experiments conducted in the NCMA study demonstrated the influence of varying specimen moisture conditions (in this case due to drying) on resonant frequency. Resonant frequencies of specimens were found to not vary by more than 1 percent in the first 15 minutes from removal of specimen from container.

visibly dry before frequencies are measured.

~~8.3.2~~ **8.4.3** If testing is to be continued, return the specimen to the container positioned on its supports. Check that the specimen container still meets the flatness requirement of 5.1.2. If it fails to meet the flatness requirement, use a different container. Add fresh test solution to the container in accordance with ~~8.3.1~~ **8.2.1**, and seal the container.

~~8.3.3~~ **8.4.4** Repeat the procedures described in ~~8.3.1 and 8.3.2~~ **8.4.1, 8.4.2 and 8.4.3** with each remaining specimen.

~~8.3.4~~ **8.4.5** Dry all the filter paper and residue (spall) collected from each specimen at 212 to 239°F (100 to 115°C) for not less than 4 h and until two successive weighings at intervals of 2 h ± 15 min show an increment of loss not greater than 0.2 percent of the last previously determined weight. Place the filter paper and residue in a draft-free location within the laboratory for a period of 2 h ± 15 min to allow the filter paper and residue to come to equilibrium temperature with the laboratory environment. Weigh the filter paper and residue to the nearest 0.2 g (0.0005 lb) and record as W_{f+r}. Calculate the residue weight, W_r, as follows:

$$W_r = W_{f+r} + W_f \quad (1)$$

where:

W_r = weight of residue (spall), g (lb),

W_{f+r} = weight of the dried residue and filter paper, g (lb), and

W_f = initial weight of the filter paper, g (lb).

8.4.6 At each residue collection interval (after *n* cycles), calculate the following parameters (optional):

W_{rn} = total accumulated residue weight from start of test to current cycle (2)

$$W_{sn} = W_s + W_{rn} \quad \textbf{(3)}$$

where:

W_{sn} = total surface dried weight of specimen at current cycle, g (lb),

W_s = surface dried weight of specimens at current cycle (8.4.2), g (lb), and

W_{rn} = accumulated residue weight from start of test to current cycle (Eq. 2), g (lb)

~~8.3.5~~ **8.4.7** At the completion of the freezing–and–thawing testing, dry each specimen at 212 to 239°F (100 to 115°C) for 24 ± 1 h. Weigh to the nearest 1 g (0.002 lb) the final oven-dried specimen and record as W_{final}. Calculate the initial weight of the specimen, $W_{initial}$, as follows:

$$W_{initial} = W_{final} + W_{residue} \quad \text{~~(2)~~}\textbf{(4)}$$

where:

$W_{initial}$ = calculated initial weight of the specimen, g (lb),

W_{final} = final weight of the specimen, g (lb),

and

$W_{residue}$ = total accumulated residue weight (equal to the sum of the residue weight, W_r, from each evaluation period, g (lb).

9. Calculation and Report

9.1 **Percent Weight Loss –** Determine ~~and report~~ the cumulative weight loss of each residue collection interval expressed in terms of g (lb) and as a percent of the

calculated initial weight of the specimen, $W_{initial}$, determined in accordance with ~~8.3.5~~ **8.4.7**. Where the coupon thickness is less than 1.25 in. (32 mm), the percentage and cumulative weight loss shall be multiplied by a value equal to the actual thickness in inches (mm) divided by 1.25 in. (32 mm). Report these values for each specimen as well as the average of the specimens tested.

9.2 Moisture Parameters (optional) – Determine the moisture content of the specimens at each residue collection interval as follows:

$$MC_n = \frac{(W_{sn} - W_{initial})}{W_{initial}} \times 100 \text{ percent} \quad (5)$$

where:

MC_n = **moisture content at each residue collection interval, percent,**

W_{sn} = **total surface dried weight of specimen at each residue collection interval (Eq. 3), g (lb), and**

$W_{initial}$ = **calculated initial weight of the specimen, g (lb).**

Determine the moisture gain of the specimens at each residue collection interval as follows:

$$MG_n = \frac{(W_{sn} - W_p)}{W_{initial}} \times 100 \text{ percent} \quad (6)$$

where:

MG_n = **moisture gain at each residue collection interval, percent,**

W_{sn} = **total surface dried weight of specimen at each residue collection interval (Eq. 3), g (lb),**

W_p = **initial pre-freeze surface dried weight of specimen (8.2.2), g (lb), and**

$W_{initial}$ = **calculated initial weight of**

C 9.2—The equations used to calculate moisture parameters are based on the following reasoning. At each residue collection interval (after n cycles), the surface-dried mass (W_s) of each specimen is measured (this is equivalent to measuring W_p in section 8.2.2, i.e., $W_p = W_s$ at 0 cycles). However, because of continued mass loss with increasing cycles, W_s represents the surface-dried mass of only the remaining portion of the specimen. Hence, to estimate the total surface-dried mass of the specimen, the cumulative residue mass up to n cycles needs to be added to W_s (equation 3). This calculation is similar to equation 4 to determine the initial oven-dried mass of the specimen. The only difference here is that the surface-dried mass is obtained rather than the oven-dried mass. Once the total surface-dried mass W_{sn} of the specimen is obtained at n cycles, the moisture content is determined from equation 5 and the moisture gain from equation 6.

Findings from the NCMA study confirmed the existence of a critical moisture content above much specimen resonant frequencies dropped at an increasingly rapid rate. This observed behavior concurred with the theory of critical degree of saturation (S_{CR}) proposed by Fagerlund (1975). Degree of saturation is defined as the ratio of actual moisture content to the total

the specimen, g (lb).

moisture content required to fill the open porosity in the material. This theory states that each particular material (with a certain combination of material properties such as strength and pore properties) possesses a unique value of S_{CR}, and significant frost damage does not occur until the actual degree of saturation (S_{ACT}) in the material exceeds S_{CR}. For ordinary concretes, S_{CR} is in the range of 0.75 to 0.90 (Fagerlund, 1977). For the SRW specimens tested in the NCMA study, S_{CR} (calculated as the ratio of moisture content to ASTM C 642 (2002) boiled absorption) was in the range of 0.76 to 0.83.

9.3 Relative Dynamic Modulus (RDM) of Elasticity (optional) – Calculate the value of RDM as follows:

$$RDM_n = (f_c/f_o)^2 \times 100 \text{ percent} \quad (7)$$

where:

RDM_n = relative dynamic modulus of elasticity after n cycles of freezing and thawing, percent

f_n = fundamental frequency after n cycles of freezing and thawing

f_o = fundamental frequency after 0 cycles of freezing and thawing

9.4 The report shall also include the following information:

a) **Date and location of SRW unit sampling**
b) **Age and storage condition of SRW units, if known**
c) **Location of coupon extraction from units (provide sketch)**
d) **Types of specimen damage during testing (cracking, scaling, aggregate popouts, etc)**
e) **Percent weight loss at each residue collection interval, *n***
f) **Moisture content and percent**

moisture gain at each residue collection interval, *n* (optional)

NOTE ~~9~~ **17**—If compressive strength and absorption test results (determined in accordance with Test Methods C 140) from representative specimens are available, it is recommended that these values be reported for reference purposes.

10. Precision and Bias

10.1 Precision and bias data for freezing–and–thawing durability is not available.

11. Keywords

11.1 absorption; compressive strength; freezing–and–thawing durability; manufactured concrete units

ANNEX: RECOMMENDED PROCEDURE FOR SURVEY OF INTERNAL TEMPERATURE DISTRIBUTION OF FREEZE-THAW CHAMBER

This section covers procedures for conducting a thermal survey of the freezer. The purpose is to characterize the internal temperature distribution of the freezing environment (consisting of the freezer and the specimens inside it) in terms of *Temperature vs Time* (T-t) and *Standard Deviation vs Time* (σ-t) functions. This survey can be treated as a pre-test mock up, and the information drawn from this survey (such as *Reliability curves* or *R-curves*) assist the planning and execution of eventual tests. As such, this survey must be conducted in an environment that reproduces the environment that will exist in actual tests.

Definitions

In reference to the freezer air cooling curve shown in Figure A.1, the following terms are defined:

- **Cold soak** is the time period during which the air temperature is between –18 ± 5°C (0° ± 10°F), and ASTM C 1262 Clause 8.2.1 requires that cold soak be maintained for 4 to 5 hours.
- **Cooling ramp** is the portion of the curve between the points at which the temperature starts falling until it reaches –13°C (0°F). Together, the cooling ramp and cold soak comprise what is shown as the **Cooling branch** of the curve.
- **Warm soak** is the time period during which the air temperature is between 24 ± 5°C (75 ± 10°F); and ASTM C 1262 Clause 8.2.2 requires that warm soak be maintained for 2.5 to 96 hours.
- **Warming ramp** is the portion of the curve between the end of cold soak and 19°C (65°F). Together, the warming ramp and warm soak comprise what is shown as the **Warming Branch** of the curve.

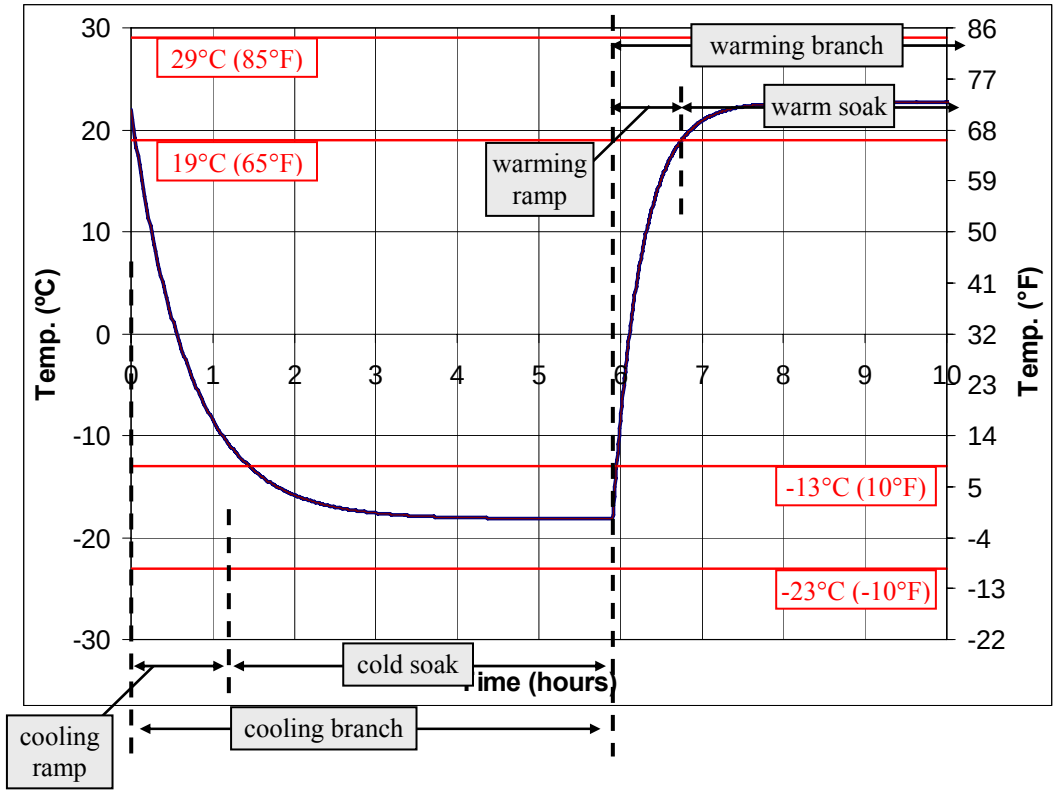

Figure A.1 Freezer air cooling curve definitions.

Initial planning

The overall goal of this initial planning is to identify as many variables as possible that will affect test conditions in actual tests and ensure that these conditions are reproduced during survey of the freezer. Variables that must be first identified include:

- Freezer to be used
- Size and shape of test containers. These may in turn depend on geometry of specimens to be tested.
- Number of specimens to be tested.
- Proposed arrangement of specimens in the freezer, which depends on various factors such as total number of specimens, shape of containers and available space or shelving units in the freezer. Also, the arrangement of specimens must also consider the ASTM C 1262 requirements that a minimum 13 mm (½ in) space separate specimens in the freezers.

Dummy specimens

Dummy specimens to be used for the freezer survey shall be of the same shape and mass as the actual test specimens that will be tested. Although specimens of the same SRW mix may not be necessary for the survey, it is important however that similar geometries be used. These specimens are to be placed in the same containers that will be used in the actual tests. Following this, the dummy specimens shall be placed in the freezer in the exact same arrangement as will be used in actual tests (specimen arrangement as

determined from initial planning) and filled with the same volume of test solution (water or saline) as will be used in actual tests.

Temperature sensors

The temperature sensors to be used such as thermometers or thermocouples must be calibrated to improve the precision as well as accuracy of temperature measurements. Hance (2005) investigated thermocouple calibration in detail and determined that when uncalibrated type T thermocouples were used, any given measurement could be within ±1.3°C (2.3°F) of a reference thermometer at the 95 percent confidence level and within ±2.0°C (3.6°F) at the 99 percent confidence level. Calibration decreases the spread of values registered by the sensors and thus allows for more precise measurements of variations of temperatures within a freezer.

On a separate issue, since the T-t and σ-t characteristics are of interest, these temperature sensors must be connected to a data acquisition system capable of recording and storing multiple measurements over a specified time period (at 5-minute intervals or less). For this purpose, thermocouples connected to data acquisition computer are preferred, although other data logging alternatives may be used.

Placement of temperature sensors

As a general guide, temperature sensors shall be strategically placed in such manner that the recorded temperatures are representative of the conditions *surrounding* the specimens (note that it is this *surrounding condition* that needs to be as uniform as possible to reduce variability arising from freezer internal variation). Sensors shall therefore be placed on each shelf where specimens are located to capture variations at each of the different levels. Within each shelf, sensors shall also be placed around the perimeter of the specimen group, say at the corners of the shelf. In this manner, the sensors placed at each shelf level capture overall temperature variations in the vertical direction, while sensors placed within each shelf capture front-back and left-right variations. In addition, sensors shall also be placed in between specimens on each shelf to capture the conditions in this region. Examples of container and external temperature sensor placement on a given shelf of a freezer are shown in Figure A.2. Other considerations for external temperature sensor placement include:

a) Ensuring that the sensors are not in contact with any other part of the freezer (e.g. wall or shelf) as it is the freezer air temperature that is sought. Thus, sensors shall be placed about 25 mm (1 in) off the shelf level, and
b) Ensuring that the sensors are not in contact with the specimens, especially the bottom part of the container where the solution is, since the latent heat liberated by the solution during freezing can lead to misleading sensor measurements. Again, sensors shall be kept at least 25 mm (1 in) away from container surfaces.

In addition to these sensors, it is recommended that external temperature sensors be placed in the vicinity of the freezer internal (built-in) temperature sensors (specifically, the freezer sensor whose temperature is used by the freezer controller to run the cycle). This enables verifying the validity of the freezer's own sensors.

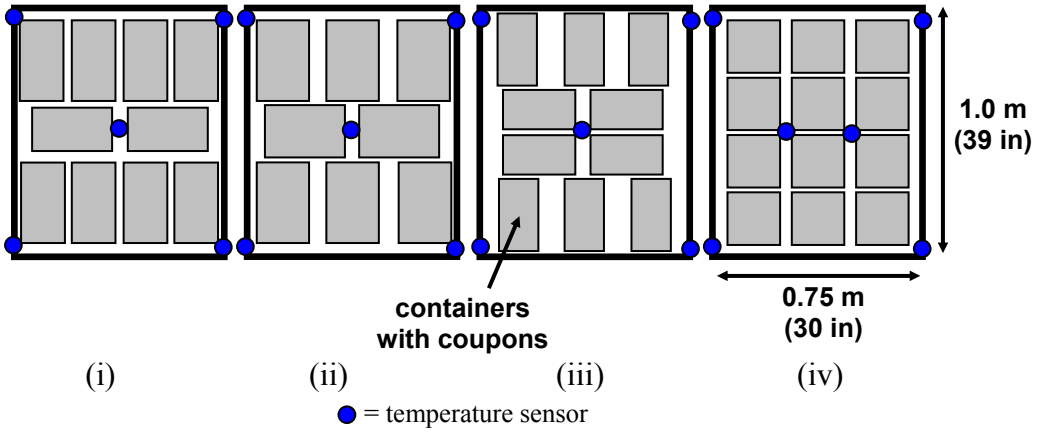

Figure A.2 Examples of container and sensor placement on freezer shelf.

Cycles

It is recommended that at least 3 full freeze-thaw cycles be run to ensure consistency between cycles. For the survey, the duration of cooling ramp may be kept the same as that used in actual tests. However, the total length of the cooling branch in each cycle shall be at least equal to (length of cooling ramp + 5 hours), to ensure that data is collected for the entire cold soak period. From studies at Cornell University, the length of cooling ramp was about 1 hour for a chest freezer, < 2 hours for a Tenney freezer and up to 2.5 hours for a walk-in chamber loaded with 40 specimens. As such, the cooling branch for these freezers under the conditions tested would then need to be at least 6, 7 and 7.5 hours respectively. A trial run shall be carried out to determine this cooling ramp length. Temperature data shall be continuously collected either using a dedicated computer with data acquisition system or through other data loggers. Data shall be collected at intervals of not more than 5 minutes. The graphs shown throughout this annex were based on data collected at 1 minute intervals.

Data processing

The results for the various cycles collected shall be treated separately and independently. The cycles shall not be averaged together (i.e. $T_{\text{location X}}$ = average ($T_{\text{location X, cycle 1}}$ + …+ $T_{\text{location X, cycle n}}$), as this may mask any cycle-to-cycle variations. The various cycles shall be examined for cycle-to-cycle consistency, which is a requirement in ASTM C 1262 (Clause 5.1.1). For each cycle, the following steps shall then be performed:

a) Plot graphs of the T-t, T_{avg}-t and σ-t.
The T-t graph is simply the collection of Temperature vs. Time data for all available sensors.
The T_{avg}-t graph is a plot of *Average Temperature* vs. *Time* where T_{avg} is the average temperature of all sensors at any given time.
The σ-t graph is a plot of *Standard Deviation* vs. *Time* where σ is the temperature standard deviation of all sensors at any given time.
Examples of these plots for measurements in a Tenney freezer are shown in Figure A.3.

b) The T-t plots for all locations shall be scrutinized for any particular pattern in the spatial variation (i.e. Are locations near the fan colder? Are there any locations which did not get cold enough (i.e. stagnant locations)? How big is the temperature spread from front-back, left-right or top-down?) Knowledge of these types of variations may help decide the frequency and pattern of specimen rotation. For example, if front-back variations are observed to be more pronounced than left-right variations, it will then be necessary to rotate specimens more frequently in which front and back specimens are switched around every 10 cycles.

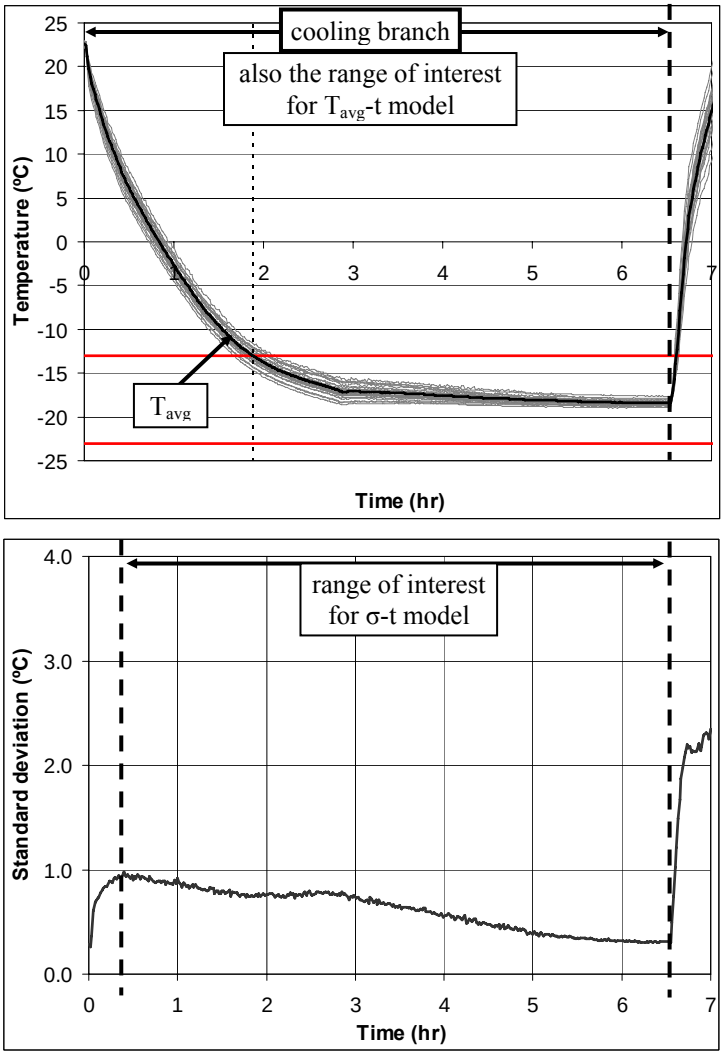

Figure A.3 Sample T-t, T_{avg}-t and σ-t graphs for Tenney freezer.

c) The T_{avg}-t and σ-t responses for the cooling branch shall then be modeled using best fit relationships. For the work conducted here, the software TableCurve 2D, version 4, from AISN Software Inc., copyright 1989-1996 was employed, and in general, it was determined that the exponential function

best described the measured data for both T and σ. This relationship was of the form:

$$T_{avg} = a_1 + b_1 \exp(-t / c_1) \quad \text{(Equation A.1)}$$

and

$$\sigma = a_2 + b_2 \exp(-t / c_2) \quad \text{(Equation A.2)}$$

Examples of curve fits for the graphs in Figure A.3 are shown in Figure A.4. For the T_{avg}-t graph, two separate fits were actually performed for the data before 2.9 hrs and for the data after 2.9 hrs. This is because the T_{avg}-t measurements performed in the Tenney freezer typically displayed a "kink" (in this particular case at 2.9 hrs) which prompted the use of two curves for the model. This bilinear response may not occur in other freezers as shown by the T_{avg}-t response for a walk-in freezer in Figure A.5 where a single curve fit was sufficient to model the entire range of interest (i.e. the cooling branch). In the σ-t response of the Tenney freezer (Figure A.4), data before about 0.3 hrs was truncated for the curve fit.

d) Using these relationships, R-curves can then be constructed as follows[1]:
   i. Select a trial length for the cooling branch, t_{trial}
   ii. Compute $t_{4\,hr} = t_{trial} - 4$
   iii. Compute $t_{5\,hr} = t_{trial} - 5$
   iv. At $t_{4\,hr}$, compute $T_{avg}(t_{4\,hr})$ and $\sigma(t_{4\,hr})$ using Equations A.1 and A.2 respectively.
   v. At $t_{5\,hr}$, compute $T_{avg}(t_{5\,hr})$ and $\sigma(t_{5\,hr})$ using Equations A.1 and A.2 respectively.
   vi. From the values at $t_{4\,hr}$, compute *Proportion of under cooled locations (P_U)* as follows:

$$x = \frac{(T_{cold\ soak\ start}) - T_{avg}(t_{4\,hr})}{\sigma(t_{4\,hr})} \quad \text{(Equation A.3)}$$

where $T_{cold\ soak\ start}$ is –13°C (10°F)

$$P_U = \frac{1}{\sqrt{2\pi}} \exp(-x^2/2) \left\{ \frac{0.436}{(1+0.333x)} - \frac{0.120}{(1+0.333x)^2} + \frac{0.937}{(1+0.333x)^3} \right\} \quad \text{(Equation A.4)}$$

[1] The concepts of reliability and methods of analysis were developed with the assistance of Prof. Mark Turnquist, School of Civil and Environmental Engineering, Cornell University, to whom the authors are grateful.

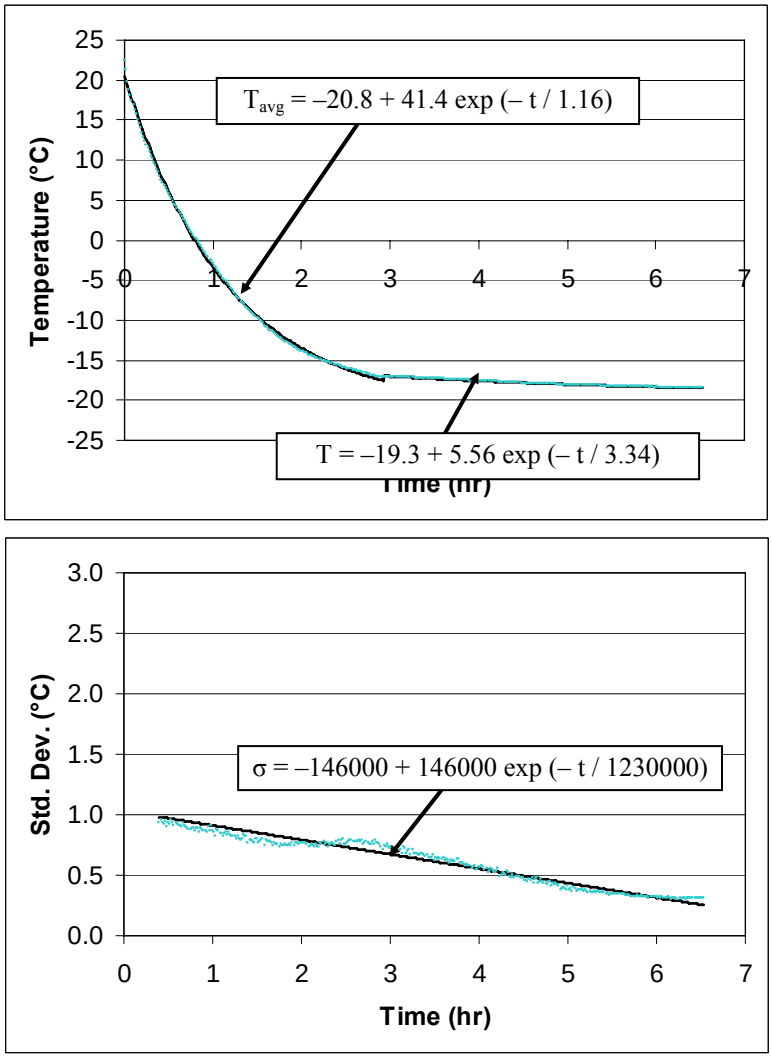

Figure A.4 Curve fits to T_{avg}-t and σ-t graphs of Figure A.3 for Tenney freezer.

vii. From the values at $t_{5\ hr}$, compute *Proportion of overcooled locations (P_O)* as follows:

$$z = \frac{T_{avg}(t_{5\,hr}) - (T_{cold\ soak\ start})}{\sigma(t_{5\,hr})} \qquad \text{(Equation A.5)}$$

where $T_{cold\ soak\ start}$ is –13°C (10°F)

$$P_O = \frac{1}{\sqrt{2\pi}}\exp(-z^2/2)\left\{\frac{0.436}{(1+0.333z)} - \frac{0.120}{(1+0.333z)^2} + \frac{0.937}{(1+0.333z)^3}\right\} \qquad \text{(Equation A.6)}$$

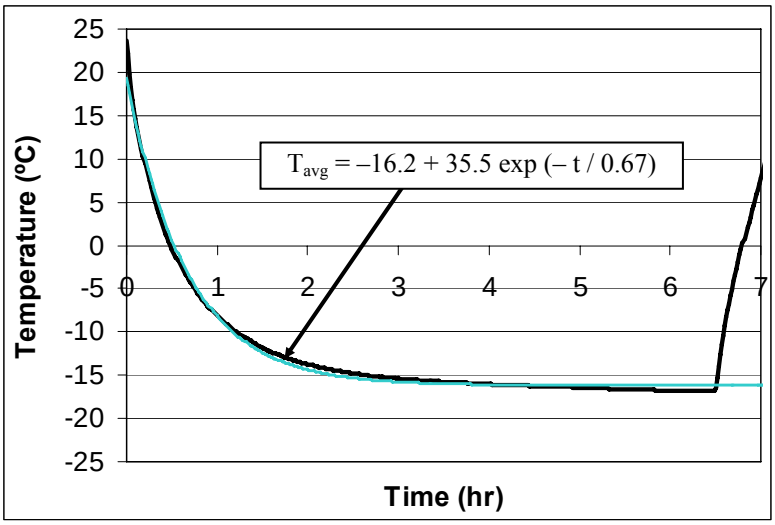

Figure A.5 Curve fit to T_{avg}-t response of walk-in freezer (single curve).

viii. The total Proportion of non-compliant locations (P_{NC}) is thus:

$$P_{NC} = P_U + P_O \qquad \text{(Equation A.7)}$$

ix. The Reliability (R) is then given by:

$$R = (1 - P_{NC}) \times 100 \text{ percent} \qquad \text{(Equation A.8)}$$

x. Repeat steps i to ix for various values of t_{trial}, and plot R versus t_{trial}. This curve is the R-curve which for the T_{avg}-t and σ-t graphs in Figures A.3 and A.4 is shown in Figure A.5.

EXAMPLE R-CURVE CALCULATIONS

The T_{avg}-t and σ-t response from the Tenney freezer shown in Figure A.3 will be used to illustrate the calculations of Reliability following the steps outlined above. The curves in Figure A.3 are modeled by exponential equations shown in Figure A.4.

i. Select $t_{trial} = 6.0$ hrs
ii. $t_{4\ hr} = 6 - 4 = 2$
iii. $t_{5\ hr} = 6 - 5 = 1$
iv. Using the curve fits equations,

$$T_{avg}(t_{4\ hr}) = T_{avg}(2) = -20.8 + 41.4 \exp(-2 / 1.16) = -13.5 \qquad \text{[Equation A.9]}$$

(Note that the curve fit to the region before 2.9 hrs was used in this case.)

$$\sigma (t_{4\ hr}) = \sigma (2) = -146000 + 146000 \exp (-2 / 1230000) = 0.79$$

[Equation A. 10]

v. Using the curve fits equations,

$$T_{avg}(t_{5\ hr}) = T_{avg}(1) = -20.8 + 41.4 \exp (-1 / 1.16) = -3.3$$

[Equation A.11]

(Note that the curve fit to the region before 2.9 hrs was used in this case.)

$$\sigma (t_{5\ hr}) = \sigma (1) = -146000 + 146000 \exp (-1 / 1230000) = 0.92$$

[Equation A.12]

From the values at $t_{4\ hr}$:

$$x = \frac{(-13) - (-13.5)}{(0.79)} = 0.63$$

[Equation A.13]

$$P_U = \frac{1}{\sqrt{2\pi}} \exp(-0.63^2/2) \left\{ \frac{0.436}{(1 + 0.333 \times 0.63)} - \frac{0.120}{(1 + 0.333 \times 0.63)^2} + \frac{0.937}{(1 + 0.333 \times 0.63)^3} \right\} = 0.26$$

[Equation A.14]

vi. From the values at $t_{5\ hr}$:

$$z = \frac{(-3.3) - (-13)}{(0.92)} = 10.5$$

[Equation A.15]

$$P_O = \frac{1}{\sqrt{2\pi}} \exp(-10.5^2/2) \left\{ \frac{0.436}{(1 + 0.333 \times 10.5)} - \frac{0.120}{(1 + 0.333 \times 10.5)^2} + \frac{0.937}{(1 + 0.333 \times 10.5)^3} \right\} = 0$$

[Equation A.16]

vii. $P_{NC} = 0.26 + 0 = 0.26$

viii. $R = (1 - 0.26) \times 100$ percent = 74 percent

ix. Repeating steps i to ix for various values of t_{trial}, the values in Table A.1 are obtained which are then used to plot R curve shown in Figure A.6.

Table A.1 R values for t_{trial}

t_{trial} (hr)	R (Percent)
5.7	0
5.8	12
5.9	42
6.0	74
6.1	92
6.2	99
6.3	100
6.4	100
6.5	100
6.6	100
6.7	98
6.8	86
6.9	58
7.0	26

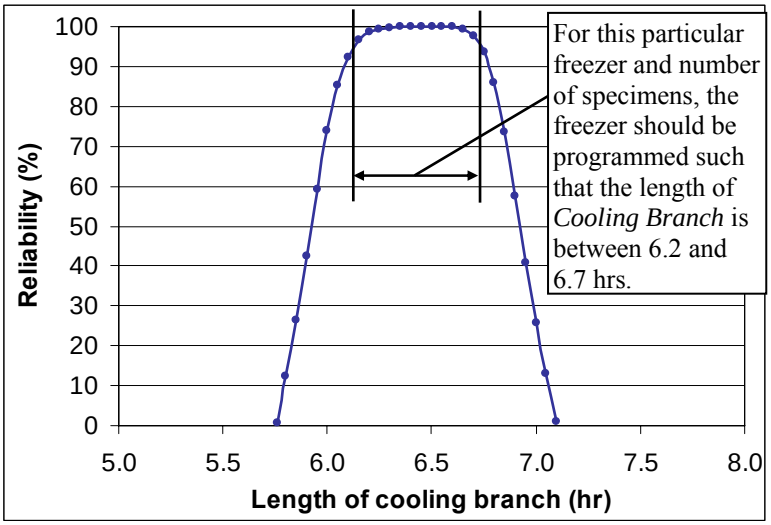

Figure A.6 Reliability (R) curve for the T_{avg}-t and σ-t graphs shown in Figure A.3.

Interpretation of R-curve

R-curves are guides to understand freezer behavior and to help plan cycle times. Figure A.6 shows an R-curve that is "flat topped." Actual freeze-thaw tests shall be run in the region where R is maximum, which for the curve in Figure A.6 would be in the "flat topped" region between 6.2 and 6.7 hours. It is generally recommended to operate the freezer in the middle of this "flat topped" region, i.e. about 6.4 to 6.5 hrs. Operating near the end of this "flat topped" zone, i.e. either at 6.2 or 6.7 hrs, is not advisable since fluctuations in freezer performance may cause R to suddenly drop. For example, if the freezer were set for 6.2 hrs cooling branch and a fluctuation in freezer performance

resulted in the cooling branch ending prematurely by 10-minutes (0.2 hrs); R would drop from 99 to 74 percent.

When the results of a freezer survey indicate that certain variables need to be changed (e.g., reduce number of specimens or change freezer control program) to obtain higher R values, these changes must be improvised and be followed by another survey with the new set of conditions. The data acquired with the new set of conditions shall be analyzed in the manner described above and R-curves be produced to determine optimum cycle lengths.

The R-curve can also be used to determine the proportion of compliant locations had the cycle been operated using a different "control temperature." In the Tenney freezer used for the NCMA studies, the freezer internal sensor used to control the cycle length was located at the coldest measured location in the freezer. From the T-t graphs in Figure A.3, it is seen that the coldest location reached –13ºC at 1.7 hrs. If cold soak were set for 4.0 hrs starting from this point, the cooling branch would only be 5.7 hrs long. In reference to Figure A.6, the corresponding R is about 0 percent. This means that all specimen locations in the freezer are under cooled (i.e. receive less than the minimum 4-hr cold soak required by ASTM C 1262).

Overall, freezer surveys shall precede actual freeze-thaw testing. While the information obtained from the surveys may assist planning actual tests, surveys shall be conducted in any of the following situations:

- Changing specimen conditions including: a) changes in total specimen quantity (either by removing "failed" specimens or adding new test specimens), b) change of containers used or c) changes in the spatial arrangement of the specimens in the freezer.
- Changing freezer conditions such as for maintenance or if the freezer is moved to a different environment (e.g. temperature controlled room or room with variable temperature conditions)

Even if none of the above changes occurred, there is no guarantee that cycles will be identical over say 100 cycles, and thus surveys shall also be periodically conducted. Preferably 5 cycles of every 25 cycles shall be surveyed to ensure that the performance is as expected or if not, that modifications in the programmed cycle length can be improvised. If possible, it is strongly recommended that dedicated temperature logging equipment be maintained for the duration of the actual freeze-thaw tests. In this manner, the actual cycles can be compared to the R-curves determined from the cycle data, thus ensuring that the actual performance is compliant with test standard requirements.

References

Hance, R.M., *Studies of the Frost Resistance of Segmental Retaining Wall Units*, Master's Thesis, School of Civil and Environmental Engineering, Cornell University, May 2005.

Fagerlund, G., "The Significance of Critical Degrees of Saturation at Freezing of Porous and Brittle Materials," *ACI Special Publication*, SP-47, American Concrete Institute, Detroit, MI, pp. 13-65, 1975.

Fagerlund, G., "An Introduction to RILEM Methods of Testing Resistance of Concrete to Freezing and Thawing and the International Cooperative Tests on the Critical Degree of Saturation Method," *Materials and Structures*, Vol. 10, No. 58, pp. 217-230, 1977.

Scherer, G.W. and Valenza II, J.J., "Mechanisms of Frost Damage," *Materials Science of Concrete VII* (eds. J. Skalny), The American Ceramic Society, 2005.

APPENDIX B:
NEWLY PROPOSED VERSION OF ASTM C 1372 (2003)—SPECIFICATIONS FOR SRW BLOCKS

Designation: C 1372 - 01 a
Standard Specification for Segmental Retaining Wall Units[1]

This standard is issued under the fixed designation C 1372; the number immediately following the designation indicates the year of original adoption or, in the case of revision, the year of last revision. A number in parentheses indicates the year of last reapproval. A superscript epsilon (e) indicates an editorial change since the last revision or reapproval.

ASTM C 1262 CLAUSES	COMMENTARY
1. Scope*	
1.1 This specification covers segmental retaining wall units of concrete, machine-made from portland cement, water, and suitable mineral aggregates with or without the inclusion of other materials. The units are intended for use in the construction of mortarless segmental retaining walls.	
NOTE 1-When particular features are desired, such as weight classification, higher compressive strength, surface texture, finish, color, or other special features, such properties should be specified separately by the purchaser. Local suppliers should be consulted as to availability of units having the desired features.	
1.2 The text of this standard references notes and footnotes which provide explanatory material. These notes and footnotes (excluding those in tables and figures) shall not be considered as requirements of the standard.	
1.3 The values stated in inch-pound units are to be regarded as the standard. The values given in parentheses are for information only.	
2. Referenced Documents	
2.1 *ASTM Standards*:	*C 2.1 – A new version of the*
C 33 Specification for Concrete	*ASTM C 1262 may be on the*

Aggregates[2]

C 140 Test Methods for Sampling and Testing Concrete Masonry Units and Related Units [3]

C 150 Specification for Portland Cement[4]

C 331 Specification for Lightweight Aggregates for Concrete Masonry Units[2]

C 595 Specification for Blended Hydraulic Cements[4]

C 618 Specification for Coal Fly Ash and Raw or Calcined Natural Pozzolan for Use as a Mineral Admixture in Concrete[2]

C 989 Specification for Ground Granulated Blast-Furnace Slag for Use in Concrete and Mortars[2]

C 1157 Performance Specification for Hydraulic Cement[4]

C 1209 Terminology of Concrete Masonry Units and Related Units[3]

C 1232 Terminology of Masonry [3]

C 1262 Test Method for Evaluating the Freeze-Thaw Durability of Manufactured Concrete Masonry Units and Related Concrete Units[3]

C XXXX Test Method for Evaluating the Freeze-Thaw Durability of Segmental Retaining Wall (SRW) Units[3]

3. Terminology

3.1 Terminology defined in Terminology C 1209 and Terminology C 1232 shall apply for this specification.

4. Materials

4.1 *Cementitious Materials*– Materials shall conform to the following applicable specifications:

4.1.1 *Portland Cements*– Specification C 150.

horizon exclusively for testing SRW units.

4.1.2 *Modified Portland Cement*–Portland cement conforming to Specification C 150, modified as follows:

4.1.2.1 *Limestone*–Limestone, with a minimum 85 percent Calcium Carbonate ($CaC0_3$) content, shall be permitted to be added to the cement, provided these requirements of Specification C 150 as modified are met:

(1) Limitation on Insoluble Residue–1.5 percent

(2) Limitation on Air Content of Mortar–Volume percent, 22 percent max.

(3) Limitation on Loss of Ignition–7 percent.

4.1.3 *Blended Hydraulic Cements*–Specification C 595.

4.1.4 *Hydraulic Cement*–Specification C 1157.

4.1.5 *Pozzolans*–Specification C 618.

4.1.6 *Blast Furnace Slag Cement*–Specification C 989.

4.2 *Aggregates*–Aggregates shall conform to the following specifications, except that grading requirements shall not necessarily apply:

4.2.1 *Normal Weight Aggregates*–Specification C 33.

4.2.2 *Lightweight Aggregates*–Specification C 331.

4.3 *Other Constituents*–Air-entraining agents, coloring pigments, integral water repellents, finely ground silica, and other constituents shall be previously established as suitable for use in segmental retaining wall units and shall conform to applicable ASTM standards or shall be shown by test or experience to be not detrimental to the durability of the segmental retaining wall units or any material customarily used in segmental retaining wall

construction.

5. Physical Requirements

5.1 At the time of delivery to the work site, the units shall conform to the physical requirements of Table 1 when tested in accordance with 8.2.

TABLE 1 Strength and Absorption Requirements

Minimum Required Net Average Compressive Strength, psi (MPa)		Maximum Water Absorption Requirements lb/ft^3 (kg/m^3)		
		Weight Classification Oven-Dry Density of Concrete lb/ft^3 (kg/m^3)		
Average of 3 Units	Individual Unit	Lightweight: Less than 105 (1682)	Medium Weight: 105 (1682) to less than 125 (2002)	Normal Weight: 125 (2002) or more
3000 (20.7)	2500 (17.2)	18 (288)	15 (240)	13 (208)

5.2 *Freeze-Thaw Durability*–In areas where repeated freezing and thawing under saturated conditions occur, freeze--thaw durability shall be demonstrated by test or by proven field performance that the segmental retaining wall units have adequate durability for the intended use. When testing is required by the specifier to demonstrate freeze-thaw durability, the units shall be tested in accordance with 8.3.

5.2.1 Specimens shall comply with either of the following: (1) the weight loss of each of five test specimens at the conclusion of 100 cycles shall not exceed 1 percent of its initial weight; or (2) the weight loss of each of four of the five test specimens at the conclusion of 150 cycles shall not exceed 1.5 percent of its initial weight. **In either case, RDM shall not be less than 60 percent.**

C 5.2 – All SRW units tested in the FHWA study (obtained from major block plants and from a local plant) complied with compressive strength, water absorption and oven-dry density as per Table 1 in this standard. A number of these units did not, however, meet the freeze-thaw durability requirements of 5.2.1. This confirms that compliance with Table 1 requirements does not imply adequate freeze-thaw requirements. This issue is also pointed out in ASTM C 1262 (Note 3).

C 5.2.1a – While this specification standard concerns freeze-thaw durability in water, there is substantial evidence that saline conditions exacerbate freeze-thaw damage. In the NCMA study, it was also demonstrated that at 1 percent mass loss many specimens had already suffered loss internal damage as indicated by resonant frequency and pulse velocity measurements. Further field studies are required to determine appropriate specification values for mass loss and resonant frequency.

C 5.2.1b –RDM is more sensitive to specimen internal damage compared to mass loss (ref. NCMA study). The

reference value of 60 percent employed here reflects values typically used for testing of ordinary concrete, as found in ASTM C 666 and C 260.

6. Permissible Variations in Dimensions

6.1 Overall dimensions for width, height, and length shall differ by not more than ± t/8 in. (3.2 mm) from the specified standard dimensions.

NOTE 2-The term "width" refers to the horizontal dimension of the unit measured perpendicular to the face of the wall from the exposed surface of the unit to the back of the unit. The term "height" refers to the vertical dimension of the unit as placed in the wall. The term "length" refers to the horizontal dimension of the unit measured parallel to the running length of the wall.

6.1.1 Dimensional tolerance requirements for width shall be waived for architectural surfaces.

NOTE 3-Split-faced surfaces are the most common surfaces used to provide an architectural appearance to segmental retaining walls. However, other means could be used to obtain similar architectural effects like tumbling, grinding, and slumping.

7. Finish and Appearance

7.1 All units shall be sound and free of cracks or other defects that interfere with the proper placement of the unit or significantly impair the strength or permanence of the construction. Minor cracks incidental to the usual method of manufacture or minor chipping resulting from customary methods of handling in shipment and delivery, are not grounds for rejection.

7.2 Where units are to be used in exposed wall construction, the face or faces that are to be exposed shall not show chips or cracks, not otherwise permitted, or other imperfections when viewed from a distance of not less than 20 ft (6.1 m) under diffused lighting.

7.2.1 Five percent of a shipment

containing chips not larger than 1 in. (25.4 mm) in any dimension, or cracks not wider than 0.02 in. (0.5 mm) and not longer than 25 percent of the nominal height of the unit is permitted.

7.3 The color and texture of units shall be specified by the purchaser. The finished surface that will be exposed in place shall conform to an approved sample consisting of not less than four units, representing the range of texture and color permitted.

8. Sampling and Testing

8.1 The purchaser or authorized representative shall be accorded proper facilities to inspect and sample units at the place of manufacture from the lots ready for delivery.

8.2 Sample and test units for compressive strength, absorption, and dimensional tolerances in accordance with Test Methods C 140.

8.3 When required, sample and test five specimens for freeze-thaw durability in water in accordance with Test Method C 1262. Freeze-thaw durability shall be based on tests of units made with the same materials, concrete mix design, manufacturing process, and curing method, conducted not more than 24 months prior to delivery.

9. Compliance

9.1 If a sample fails to conform to the specified requirements, the manufacturer shall be permitted to remove units from the shipment. A new sample shall be selected by the purchaser from remaining units from the shipment with a similar 'configuration and dimension and tested at the expense of the manufacturer. If the second sample meets the specified requirements, the remaining portion of the shipment represented by the sample meets the specified requirements. If the second sample fails to meet the specified

requirements, the remaining portion of the shipment represented by the sample fails to meet the specified requirements.

NOTE 4-Unless otherwise specified in the purchase order, the cost of tests is typically borne as follows: (1) if the results of the tests show that the units do not conform to the requirements of this specification, the cost is typically borne by the seller; (2) if the results of the tests show that the units conform to the specification requirements, the cost is typically home by the purchaser.

10. Keywords

10.1 absorption; aggregates; cementitious materials; compressive strength; concrete masonry units; dimensions; durability; weight classification

REFERENCES

ASTM C 78-02, "Standard Test Method for Flexural Strength of Concrete (Using Simple Beam with Third-Point Loading)," *Annual Book of ASTM Standards 2002, Volume 04.02*, ASTM International, West Conshohocken, PA, pp. 35–37, 2002.

ASTM C 140-99b, "Standard Test Methods for Sampling and Testing Concrete Masonry Units and Related Units," *Annual Book of ASTM Standards 2000, Volume 04.05*, ASTM International, West Conshohocken, PA, pp. 99–109, 2000.

ASTM C 215-97, "Standard Test Method for Fundamental Transverse, Longitudinal, and Torsional Frequencies of Concrete Specimens," *Annual Book of ASTM Standards 2002, Volume 04.02*, ASTM International, West Conshohocken, PA, 1997.

ASTM C 457-98, "Standard Test Method for Microscopical Determination of Parameters of the Air-Void System in Hardened Concrete," *Annual Book of ASTM Standards 2004, Volume 04.02*, ASTM International, West Conshohocken, PA, pp. 242–255, 2004.

ASTM C 597-02, "Standard Test Method for Pulse Velocity Through Concrete," *Annual Book of ASTM Standards 2004, Volume 04.02*, ASTM International, West Conshohocken, PA, pp. 310–313, 2004.

ASTM C 642-97, "Standard Test Methods for Density, Absorption, and Voids in Hardened Concrete," *Annual Book of ASTM Standards 2002, Volume 04.02*, ASTM International, West Conshohocken, PA, pp. 334–336, 2002.

ASTM C 666-03, "Standard Test Method for Resistance of Concrete to Rapid Freezing and Thawing," *Annual Book of ASTM Standards 2004, Volume 04.02*, ASTM International, West Conshohocken, PA, pp. 337–342, 2004.

ASTM C 671-94, "Standard Test Method for Critical Dilation of Concrete Specimens Subjected to Freezing," *Annual Book of ASTM Standards 2002, Volume 04.02*, ASTM International, West Conshohocken, PA, pp. 351–356, 2002.

ASTM C 672 / C 672 M-03, "Standard Test Method for Scaling Resistance of Concrete Surface Exposed to Deicing Chemicals," *Annual Book of ASTM Standards 2004, Volume 04.02*, ASTM International, West Conshohocken, PA, pp. 353–355, 2004.

ASTM C 1262-98, "Standard Test Method for Evaluating the Freeze-Thaw Durability of Manufactured Concrete Masonry Units and Related Concrete Units," *Annual Book of ASTM Standards 2003, Volume 04.05*, ASTM International, West Conshohocken, PA, pp. 829–832, 2003.

ASTM C 1372-01, "Standard Specification for Segmental Retaining Wall Units," *Annual Book of ASTM Standards 2003, Volume 04.05*, ASTM International, West Conshohocken, PA, pp. 898-900, 2003.

Bathurst, R., Simac, M., and Berg, R., "Review of NCMA Segmental Retaining Wall Design Manual for Geosynthetic-Reinforced Structures," *Transportation Research Record*, No. 1414, Washington, DC, pp. 16–25, 1993.

Chan, C., Hover, K.C., and Folliard, K. J., "Spatial Variations in Material Properties of Segmental Retaining Wall (SRW) Units, Part I: Observed Variations," *Journal of ASTM International, Civil Engineering and Building Materials*, February 2005 (2005a).

Chan, C., Hover, K.C., and Folliard, K. J., "Spatial Variations in Material Properties of Segmental Retaining Wall (SRW) Units, Part II: Sampling Considerations for Absorption Tests," *Journal of ASTM International, Civil Engineering and Building Materials*, February 2005 (2005b).

Chan, C., Hover, K.C., and Folliard, K.J., "Performance of Segmental Retaining Wall (SRW) Units: from Laboratory to Field," *Construction Materials, Proceedings of CONMAT 05 and Mindess Symposium* (eds. N. Banthia, T. Uomoto, A. Bentur and S.P. Shah), Vancouver, Canada, Aug. 21–24, 2005 (2005c).

Chan, C., Hover, K.C., Folliard, K.J. and Trejo, D., "Frost Durability Indices of Segmental Retaining Wall (SRW) Units," manuscript submitted to *ACI Materials Journal*, November 2005 (2005d).

Chan, C., *Freeze-Thaw Durability and ASTM C 1262 Testing of Segmental Retaining Wall (SRW) Units*, Ph.D. Dissertation, Cornell University, 2006.

Chan, C., Hover, K.C., and Folliard, K.J., "Segmental Retaining Wall (SRW) Split Face Delaminations and Practical Implications," submitted to *Construction and Building Materials Journal*, April 2006 (2006a).

Chan, C, Hover, K.C., and Folliard, K., "Durability of Segmental Retaining Wall (SRW) Concretes to Different Deicing Salt Types," manuscript submitted to Transportation Research Board, August 2006 (2006b).

Chan, C., Hover, K.C., and Folliard, K.J., "Comparison of Distribution of Properties in Segmental Retaining Wall Units between Manufacturers" (in progress) 2006c.

Charola, E., "Salts in the Deterioration of Porous Materials: An Overview," *Journal of the American Institute for Conservation*, JAIC 2000, Vol. 39, No. 3, Article 2, pp. 327–343, 2000.

Chatterji, S., "Aspects of the Freezing Process in a Porous Material-Water System. Part 1. Freezing and the Properties of Water and Ice," *Cement and Concrete Research*, Vol. 29, Issue 4, pp. 627–630, 1999 (a).

Chatterji, S., "Aspects of the Freezing Process in a Porous Material-Water System. Part 2. Freezing and Properties of Frozen Porous Materials," *Cement and Concrete Research*, Vol. 29, Issue 5, pp. 781–784, 1999 (b).

Cordon, W.A., "Freezing and Thawing of Concrete – Mechanisms and Control," *ACI Monograph No. 3*, American Concrete Institute, 1966.

Embacher, R. A., Snyder, M. B. and Shultz, A. E., "Condition and Durability of Segmental Concrete Block Retaining Walls Along Roadways in Minnesota." Final Report to Minnesota Department of Transportation. University of Minnesota Department of Civil Engineering, Minneapolis, MN, 2001.

Fagerlund, G., "The Significance of Critical Degrees of Saturation at Freezing of Porous and Brittle Materials," *ACI Special Publication, SP-47*, American Concrete Institute, Detroit, MI, pp. 13–65, 1975.

Fagerlund, G., "An Introduction to RILEM Methods of Testing Resistance of Concrete to Freezing and Thawing and the International Cooperative Tests on the Critical Degree of Saturation Method," *Materials and Structures*, Vol. 10, No. 58, pp. 217–230, 1977.

Fagerlund, G., "Frost Resistance of High Performance Concrete—Some Theoretical Considerations," *Durability of High Performance Concrete*, Proceedings of the RILEM International Workshop (ed. H. Sommer), Vienna, February 12–15, pp. 112–140, 1994.

Ghafoori, N. and Mathis, R., "Prediction of Freezing and Thawing Durability of Concrete Paving Blocks," *ASCE Journal of Materials in Civil Engineering*, Volume 10, Issue 1, pp. 45–51, February 1998.

Haisler, J., *Freeze-Thaw Durability of Segmental Retaining Wall Blocks,* Master of Science thesis, The University of Texas at Austin, 2004.

Hance, R., *Studies of the Frost-Resistance of Segmental Retaining Wall Units*, Master of Science thesis, Cornell University, 2005.
Harnik, A.B, Meier, U., and Ŝösli, A.R., "Combined Influence of Freezing and Deicing Salt on Concrete—Physical Aspects," *Durability of Building Materials and Components*, Proceedings of the First International Conference (eds. Sereda and Litvan), ASTM STP 691, Ottawa, Canada, 21–23 August, 1978, pp. 474–484 (proceedings published 1980).
Hazrati, K., "Efficacité des scellants face au problème d'écaillage des bétons en presence de sels fondants," Master's degree thesis, Department of Civil Engineering, Laval University, Ste-Foy, Québec, 110 pp., 1993.
Hazrati, K. and Kerkar, A.V., "Freeze-Thaw Durability of Dry Masonry Concrete," *12th International Brick / Block Masonry Conference*, Madrid, Spain, 2000.
Hover, K.C., "Air Content and Density of Hardened Concrete," *Significance of Tests and Properties in Concrete and Concrete-Making Materials*, (eds. J. Klieger and J.F. Lamond), ASTM STP 169C, American Society for Testing and Materials, 1994.
Kaufmann, J.P., "A Qualitative Sequential Frost Deicing Salt Damage Model Based on Experimental Data," *Frost Resistance of Concrete*, Proceedings of the International RILEM Workshop (eds. M.J. Setzer, R. Auberg and H.-J. Heck), RILEM Publication PRO 24, Essen, Germany, pp. 197–204, April 18–19, 2002.
Kosmatka, S. and Panarese, W., *Design and Control of Concrete Mixtures*, 13th ed., Portland Cement Association, Skokie, IL, 1994.
Kukko, H., *Frost effects on the microstructure of high strength concrete, and methods for their analysis*, VTT Publications 126, Technical Research Centre of Finland, Espoo, 1992.
Lohr, S.L., *Sampling: Design and Analysis*, Duxbury Press, Pacific Grove, CA, 1999.
MacDonald, K.A., Lukkarila, M.R., "Freezing and Thawing Resistance of Dry Compacted Segmental Retaining Wall Units," *Frost Damage in Concrete*, Proceedings of the International RILEM Workshop (eds. D.J. Janssen, M.J. Setzer and M.B. Snyder), RILEM Publication PRO 25, Minneapolis, MN, pp. 53–64, 28–30 June 1999.
Marchand, J., Pigeon, M., Isabelle, H.L., and Boisvert, J., "Freeze-Thaw Durability and Deicer Salt Scaling Resistance of Roller Compacted Concrete Pavements," *Paul Klieger Symposium on Performance of Concrete* (ed. D. Whiting), American Concrete Institute, SP-122, pp. 217–236, 1990.
Marchand, J., Boisvert, L., Tremblay, S., Maltais, J., and Pigeon, M., "Air Entrainment in No-Slump Mixes," *Concrete International*, Vol. 20, Issue 4, pp. 38–44, April 1998.
Michel, B., *Ice Mechanics*, Les Presses de L'Université Laval, Québec, Canada, 1978.
Mn/DOT, Minnesota Department of Transportation Program Support Group, Technical Memorandum No. 01-05-MRR-01, February 8, 2001.
Morgan, D.R., "Special Sprayed Concretes," *Sprayed Concrete: Properties, Design and Application* (eds. S. Austin and P. Robins), McGraw-Hill, Inc., New York, pp. 229–265, 1995.
National Concrete Masonry Association (NCMA), NCMA "TEK 15-8: Guide to Segmental Retaining Walls," *NCMA E-TEK Manual*, 2002.
National Concrete Masonry Association (NCMA), Internet site: http://www.ncma.org/use/srw.html, 2005a.
National Concrete Masonry Association (NCMA), Private communication, May 2005b.
Neville, A.M., *Properties of Concrete*, John Wiley & Sons, Inc., New York, NY, 1996.

Ott, R. L., *An Introduction to Statistical Methods and Data Analysis*, 4th ed, Duxbury Press, Belmont, CA, pp. 564–646, 1993.

Penttala, V., "Freezing-Induced Strains and Pressures in Wet Porous Materials and Especially in Concrete Mortars," *Advanced Cement Based Materials*, Vol. 7, Issue 1, pp. 8–19, January 1998.

Personal communication with National Concrete Masonry Association (NCMA), May 2005 (2005b).

Personal communication with Prof. G. Scherer, Dept. of Civil and Environmental Engineering, Princeton University, March 2005.

Petersson, P.E. and Utgenannt, P., "Parameters Influencing the Results When Testing the Scaling Resistance of Concrete," *Frost Damage in Concrete*, Proceedings of the International RILEM Workshop (eds. D.J. Janssen, M.J. Setzer and M.B. Snyder), RILEM Publication PRO 25, Minneapolis, MN, 28–30 June 1999, pp. 233–242.

Pigeon, M. and Pleau, R., *Durability of Concrete in Cold Climates*, E&FN SPON (an imprint of Chapman & Hall), London, UK, first edition, 1995.

Powers, T.C., "The Air Requirement of Frost-Resistant Concrete," *Proceedings of the Highway Research Board*, Vol. 29, pp. 184–211, 1949.

Powers, T.C., "Freezing Effects in Concrete," *Durability of Concrete, SP-47*, American Concrete Institute, Detroit, MI, pp. 1–11, 1975.

Powers, T.C. and Helmuth, R.A., "Theory of Volume Changes in Hardened Portland Cement Paste During Freezing," *Proceedings of Highway Research Board*, 32nd Annual Meeting, pp. 285–297, 1953.

Sahagian, M.E. and Goff, H.D., "Fundamental Aspects of the Freezing Process," *Freezing Effects on Food Quality* (ed. L.E. Jeremiah), Marcel Dekker, Inc., New York, 1996.

Scherer, G.W., "Freezing gels," *Journal of Non-Crystalline Solids*, Elsevier, Vol. 155, Issue 1, pp. 1–25, March 1993.

Scherer, G.W., "Crystallization in Pores," *Cement and Concrete Research*, Vol. 29, Issue 8, pp. 1347–1358, August 1999.

Scherer, G.W., "Stress from Crystallization of Salt," *Cement and Concrete Research*, Vol. 34, Issue 9, pp. 1613–1624, September 2004.

Scherer, G.W. and Valenza II, J.J., "Mechanisms of Frost Damage," *Materials Science of Concrete, Vol. VII* (eds. J. Skalny and F. Young), The American Ceramic Society, 2005.

Scherer, G.W., Private communication, March 2005.

SEM (Service d'Expertise en Matériaux Inc.), *Literature Survey*, SEM Project 200110, submitted to National Concrete Masonry Association, August 2001.

SEM (Service d'Expertise en Matériaux Inc.), *Preliminary Report, Task 3—Frost Durability Index*, SEM Project 200110, submitted to National Concrete Masonry Association, May 2004.

Setzer, M.J., "Micro Ice Lens Formation and Frost Damage," *Frost Damage in Concrete*, Proceedings of the International RILEM Workshop (eds. D.J. Janssen, M.J. Setzer and M.B. Snyder), RILEM Publication PRO 25, Minneapolis, MN, June 28–30, 1999, pp. 1–15.

SHRP-S/FR-92-110, Cady, P. and Gannon E., *Condition Evaluation of Concrete Bridges Relative to Reinforcement Corrosion—Volume 8: Procedure Manual*, "Standard Test Method for Chloride Content in Concrete Using the Specific Ion Probe," Strategic Highway Research Program, Washington, DC, pp. 85–105, 1992.

Siebel, E. and Gräf, "Standard Methods for Testing the Resistance of Concrete to Freezing and Thawing—Internal Deterioration," *European Research Project No. 3085, Reference MAT1-CT9-0055*, (Project leader: Eberhard Siebel), Commission of the European Communities Directorate General XII, Science, Research and Development Directorate C: Industrial and Materials Technologies, Synthesis Report (Be-TB-1489-5/1998), 1995.

Thomas, R., "Discussion on Freeze-Thaw Durability of SRWs," presented at *FHWA pooled fund research meeting and workshop*, Minneapolis, MN, March 10, 2003.

Van Vlack, L. H., *Elements of Materials Science*, 2nd edition, Addison-Wesley Publishing Company, Reading, MA, 1967.

Venečanin, S.D., "Experimental Study of Thermal Incompatibility of Concrete Components," *3rd International Conference on the Durability of Building Materials and Components*, Vol. 3, VTT Symposium 50, Espoo, Finland, August 12–15 1984, pp. 510–520, 1984.

Verbeck, G.J. and Klieger, P., "Studies of Salt Scaling of Concrete," *Highway Research Board Bulletin No. 150*, pp. 1–13, 1956.

Whiting, D., "Air Contents and Air-Void Characteristics in Low-Slump Dense Concretes," *ACI Materials Journal*, Vol. 82, No. 5, pp. 716–723, Sept.–Oct. 1985.

Wisconsin Department of Transportation, "Mechanically Stabilized Earth Modular Block Wall, Item 90031," 2000.

HRDI-06/04-07(500)E